Virginia Center *for* Transportation
INNOVATION & RESEARCH

Differential Settlement of a Geosynthetic Reinforced Soil Abutment: Full-Scale Investigation

http://www.virginiadot.org/vtrc/main/online_reports/pdf/15-r3.pdf

ANDREW KOST, E.I.
Graduate Student

GEORGE M. FILZ, Ph.D., P.E.
Professor

THOMAS E. COUSINS, Ph.D., P.E.
Professor

The Charles E. Via, Jr. Department of Civil and Environmental Engineering

Virginia Tech

Final Report VCTIR 15-R3

VIRGINIA CENTER FOR TRANSPORTATION INNOVATION AND RESEARCH
530 Edgemont Road, Charlottesville, VA 22903-2454

www.VTRC.net

Standard Title Page - Report on Federally Funded Project

1. Report No.: FHWA/VCTIR 15-R3	2. Government Accession No.:	3. Recipient's Catalog No.:
4. Title and Subtitle: Differential Settlement of a Geosynthetic Reinforced Soil Abutment: Full-Scale Investigation		5. Report Date: May 2015 6. Performing Organization Code:
7. Author(s): Andrew Kost, George M. Filz, Ph.D., P.E., and Thomas E. Cousins, Ph.D., P.E.		8. Performing Organization Report No.: VCTIR 15-R3
9. Performing Organization and Address: The Charles E. Via, Jr. Department of Civil and Environmental Engineering Virginia Polytechnic Institute and State University 200 Patton Hall Blacksburg, VA 24061-0105		10. Work Unit No. (TRAIS): 11. Contract or Grant No.: 101796
12. Sponsoring Agencies' Name and Address: Virginia Department of Transportation 1401 E. Broad Street Richmond, VA 23219 Federal Highway Administration 400 North 8th Street, Room 750 Richmond, VA 23219-4825		13. Type of Report and Period Covered: Final Contract 14. Sponsoring Agency Code:
15. Supplementary Notes:		

16. Abstract:

The Geosynthetic Reinforced Soil Integrated Bridge System (GRS-IBS) uses alternating layers of closely spaced geosynthetic reinforcement and well-compacted granular fill to support the bridge superstructure and form an integrated roadway approach. This system offers simple and rapid construction, lower costs than traditional alternatives, and reduction or elimination of the bump at the end of the bridge. However, like all shallow foundations, GRS-IBS can be vulnerable to differential settlements beneath the foundation.

This report describes research into the behavior of GRS abutments subjected to differential settlements, which may be due to compressible soils beneath the foundation or to scour undermining. A field-scale model was constructed and subjected to carefully controlled differential settlements, and a comprehensive instrumentation program monitored the response of the abutment. The robust response of the abutment under the large differential settlements imposed in these tests indicated that GRS abutments will perform well under the smaller levels of differential settlement that would be expected in field applications. However, if large enough differential settlements occur such that the facing blocks separate, then hydraulic forces could pose a significant hazard to the abutment if the reinforced fill is not adequately protected. Three measures to reduce the vulnerability of the reinforced fill are presented, and a predictive equation was developed to estimate the settlement of the abutment's facing blocks in response to differential foundation settlement. The predictive equation is specific to the conditions of the field-scale test.

The authors recommend that the Virginia Department of Transportation's Structure and Bridge Division consider GRS-IBS as a viable bridge technology. For crossings over water, the authors agree with the recommendation of Adams et al. (2011) that GRS-IBS should be considered only if scour concerns can be adequately addressed. In addition, the authors suggest that GRS-IBS designers consider additional measures to protect the reinforced fill in the event of unanticipated settlements.

17 Key Words:	18. Distribution Statement:
Geosynthetic Reinforced Soil Integrated Bridge System, GRS-IBS, geosynthetic reinforcement, differential settlement	No restrictions. This document is available to the public through NTIS, Springfield, VA 22161.

19. Security Classif. (of this report):	20. Security Classif. (of this page):	21. No. of Pages:	22. Price:
Unclassified	Unclassified	140	

FINAL REPORT

DIFFERENTIAL SETTLEMENT OF A GEOSYNTHETIC REINFORCED SOIL ABUTMENT: FULL-SCALE INVESTIGATION

Andrew Kost, E.I.
Graduate Student

George M. Filz, Ph.D., P.E.
Professor

Thomas E. Cousins, Ph.D., P.E.
Professor

The Charles E. Via, Jr. Department of Civil and Environmental Engineering
Virginia Tech

VCTIR Project Manager
Michael C. Brown, Ph.D., P.E., Virginia Center for Transportation Innovation and Research

In Cooperation with the U.S. Department of Transportation
Federal Highway Administration

Virginia Center for Transportation Innovation and Research
(A partnership of the Virginia Department of Transportation
and the University of Virginia since 1948)

Charlottesville, Virginia

May 2015
VCTIR 15-R3

DISCLAIMER

The project that is the subject of this report was done under contract for the Virginia Department of Transportation, Virginia Center for Transportation Innovation and Research. The contents of this report reflect the views of the authors, who are responsible for the facts and the accuracy of the data presented herein. The contents do not necessarily reflect the official views or policies of the Virginia Department of Transportation, the Commonwealth Transportation Board, or the Federal Highway Administration. This report does not constitute a standard, specification, or regulation. Any inclusion of manufacturer names, trade names, or trademarks is for identification purposes only and is not to be considered an endorsement.

Each contract report is peer reviewed and accepted for publication by staff of Virginia Center for Transportation Innovation and Research with expertise in related technical areas. Final editing and proofreading of the report are performed by the contractor.

ABSTRACT

The Geosynthetic Reinforced Soil Integrated Bridge System (GRS-IBS) uses alternating layers of closely spaced geosynthetic reinforcement and well-compacted granular fill to support the bridge superstructure and form an integrated roadway approach. This system offers simple and rapid construction, lower costs than traditional alternatives, and reduction or elimination of the bump at the end of the bridge. However, like all shallow foundations, GRS-IBS can be vulnerable to differential settlements beneath the foundation.

This report describes research into the behavior of GRS abutments subjected to differential settlements, which may be due to compressible soils beneath the foundation or to scour undermining. A field-scale model was constructed and subjected to carefully controlled differential settlements, and a comprehensive instrumentation program monitored the response of the abutment. The robust response of the abutment under the large differential settlements imposed in these tests indicated that GRS abutments will perform well under the smaller levels of differential settlement that would be expected in field applications. However, if large enough differential settlements occur such that the facing blocks separate, then hydraulic forces could pose a significant hazard to the abutment if the reinforced fill is not adequately protected. Three measures to reduce the vulnerability of the reinforced fill are presented, and a predictive equation was developed to estimate the settlement of the abutment's facing blocks in response to differential foundation settlement. The predictive equation is specific to the conditions of the field-scale test.

The authors recommend that the Virginia Department of Transportation's Structure and Bridge Division consider GRS-IBS as a viable bridge technology. For crossings over water, the authors agree with the recommendation of Adams et al. (2011) that GRS-IBS should be considered only if scour concerns can be adequately addressed. In addition, the authors suggest that GRS-IBS designers consider additional measures to protect the reinforced fill in the event of unanticipated settlements.

FINAL REPORT

DIFFERENTIAL SETTLEMENT OF A GEOSYNTHETIC REINFORCED SOIL ABUTMENT: FULL-SCALE INVESTIGATION

Andrew Kost, E.I.
Graduate Student

George M. Filz, Ph.D., P.E.
Professor

Thomas E. Cousins, Ph.D., P.E.
Professor

The Charles E. Via, Jr. Department of Civil and Environmental Engineering
Virginia Tech

INTRODUCTION

Geosynthetic reinforced soil (GRS) consists of alternating layers of well-compacted granular fill and closely spaced geosynthetic reinforcement. While GRS systems share many similarities with more familiar mechanically stabilized earth (MSE) systems, proponents of GRS highlight differences between the two systems and provide separate guidelines for design and construction of GRS systems. In particular, Adams et al. (2011) emphasize: (1) composite action of the compacted fill and closely spaced geosynthetic reinforcement layers in GRS systems and (2) frictional connections between the reinforcement and facing elements in GRS walls versus structural connections between the reinforcement and facing elements in most MSE walls.

GRS systems have been utilized in retaining structures since the 1970s. More recently, researchers at the Federal Highway Administration (FHWA) (Adams et al., 1999), the Colorado Department of Transportation (Abu-Hejleh et al., 2002), and the University of Colorado (Wu et al., 2006) have explored applications for bridge abutments. The result has been the development of the GRS Integrated Bridge System, or GRS-IBS. The system consists of a reinforced soil foundation (RSF), a GRS abutment, and an integrated approach (Adams et al., 2011). The bridge superstructure is supported directly on the reinforced soil abutment, without utilizing any deep foundations.

GRS-IBS technology offers a number of advantages over traditional pile-supported bridges, including lower cost, simple and rapid construction, and reduced environmental impact (Adams et al., 2011). The abutment supports both the superstructure and approach and allows these two components to settle uniformly, reducing or eliminating the bump that often forms at the end of the bridge. However, the absence of deep foundations has contributed to a perceived vulnerability of the system to changes in the support condition at the foundation level. Differential settlements have the potential to negatively impact any type of shallow foundation,

including GRS abutments. In particular, because many GRS-IBS bridges are placed along waterways, the possibility of scour-induced settlement must be considered.

While reinforced soil structures are widely considered to possess inherent flexibility, the authors are not aware of any research examining the behavior of a load-bearing GRS structure subjected to variable support conditions at its base. Like all shallow foundations, GRS-IBS structures are designed with the assumption that the structure will not experience detrimental differential settlements. The designer will conduct sub-surface explorations, require excavation and replacement of soft soils beneath the RSF, and provide compaction specifications for the subgrade beneath the RSF in an effort to minimize settlements due to compressible soils beneath the foundation (Adams et al., 2011). Likewise, the designer will assess hydraulic flow, scour potential, and channel instability; place the top of the RSF beneath the calculated scour depth; and employ scour countermeasures, as appropriate, to guard against scour-induced settlements (Adams et al., 2011a). However, it is helpful for both the designer and the owner to understand the potential consequences for the structure if these measures fall short. Additionally, investigating the response of GRS abutments subjected to large differential settlements provides unique insight into the behavior of these structures that could not be gained from observations of the structures under normal operating conditions.

PURPOSE AND SCOPE

This project began as a collaboration between the Virginia Department of Transportation (VDOT) and Virginia Tech to provide design support and monitoring for the first GRS-IBS bridge in Virginia. A crossing along Towlston Road near McLean, Virginia was selected for the pilot project. However, a number of extenuating circumstances, including the washout of the existing structure in September 2011, contributed to significant delays for the project. When it became evident that much of the original scope of work would occur outside of the schedule for this research project, Virginia Tech proposed modifications to the scope to examine the effects of differential settlements on GRS-IBS structures.

The purpose of this research was to address a lack of knowledge regarding the performance of GRS-IBS in response to differential settlements, whether these settlements result from the presence of compressible soils beneath the foundation or are due to scour of the subgrade material. This knowledge will help policy-makers, owners, and designers make informed decisions regarding implementation of GRS systems. To this end, a field-scale investigation was carried out at Virginia Tech. The field-scale experiment examined the response of one GRS abutment to differential settlements represented by two different areas and two different depths, for a total of four support-loss conditions. Because the field-scale model lacked an integrated approach, the term “GRS abutments” is used in place of “GRS-IBS” throughout this report when referring to observations specific to the experimental abutment. However, the experimental GRS abutment did include a reinforced soil foundation, a load-bearing GRS fill, and an equivalent bridge load, so the test was representative of a GRS-IBS installation in most respects.

Nine project tasks were established:

1. Develop a test concept to induce carefully controlled settlements beneath a field-scale GRS abutment.

2. Design the field-scale model to adequately represent an in-service abutment while ensuring measurable abutment response and remaining within the constraints of the testing site.

3. Select materials that are representative of materials commonly used for GRS-IBS.

4. Construct the field-scale abutment using techniques and methods representative of typical GRS-IBS construction.

5. Instrument the abutment to observe key indicators of structural response during testing, including settlement of the fill and facing blocks, stress changes within the reinforced fill, and strain changes in the reinforcement.

6. Subject the abutment to differential settlements of carefully controlled magnitude and area, and measure the abutment's response.

7. Reduce and interpret data collected during testing, identifying important trends and behavior of the abutment.

8. Develop a predictive equation to estimate the settlement of the abutment as a function of area of support removed, depth of support removed, and height above the foundation.

9. Develop conclusions and recommendations for VDOT regarding the implementation of GRS-IBS based on the results of this study and the authors' experience in designing and constructing the test abutment, and provide recommendations for future research.

This report describes the results of these project tasks. Design and construction procedures (Tasks 1 through 4) are summarized in the "Methods" section. The extensive instrumentation effort (Task 5) and testing procedures (Task 6) are also summarized in the "Methods" section. Data were collected during testing and reduced. Reduced data are presented and interpreted, along with the predictive equation, in the "Results and Discussion" section (Tasks 7 and 8). The "Conclusions" and "Recommendations" sections (Task 9) follow, and the report concludes with "Benefits and Implementation Prospects."

METHODS

A field-scale testing program was carried out to investigate the response of GRS abutments to differential settlements. The following sections describe the experimental concept and design, materials, testing site, construction, instrumentation, and testing procedures.

Experimental Concept

A method of simulating settlement beneath a column-supported embankment using geofoam was developed by Sloan et al. (2013). This method was modified to simulate differential settlements beneath a GRS abutment. A field-scale abutment was constructed over a subgrade in which the support conditions were carefully controlled. The primary subgrade material was a well-compacted crushed rock fill. However, in regions where differential settlements would be induced, a portion of the crushed rock was replaced with a stiff, expanded polystyrene (EPS, commonly referred to as geofoam) inclusion. This foam was stiff enough to support the abutment without excessive deformations, and it could later be dissolved using an environmentally friendly solvent to simulate settlement in these regions.

Experimental Design

Thorough consideration was given to appropriate dimensioning of the experimental abutment and the regions from which support would be removed. The objectives throughout the design process were to model reasonable abutment geometry, to ensure that settlements induced at the foundation level would be large enough to produce measureable deformations at the surface, and to minimize the influence of tests at one corner of the abutment on results observed at the opposite corner. The following paragraphs detail the design of the abutment and reinforced soil foundation, the location of the geofoam inclusions, and a protective wrap that was included behind the facing elements at one level of the abutment.

Abutment and Reinforced Soil Foundation

The test abutment, including its reinforced soil foundation (RSF), was designed and detailed in accordance with FHWA guidelines (Adams et al., 2011). This design procedure is most reflective of the current state of the practice. Figure 1 shows a front view of the abutment configuration with the relevant dimensions marked, and Figure 2 shows a side view of the abutment with the internal reinforcement layout. Consistent with the terminology used in the FHWA guidelines, this report will use the term “length” to refer to the abutment dimension in the horizontal plane of the abutment face, transverse to a non-skewed bridge alignment. The term “width” will refer to the abutment dimension in the horizontal plane of the wing walls, parallel to a non-skewed bridge alignment. The overall dimensions of the abutment, about 10 ft high by 24.5 ft long, represent a geometry that is reasonable for a relatively small full-scale bridge—for example, a one-lane bridge over a small to moderately sized stream.

When possible, the most critical case was selected in designing the abutment. For example, the base width of the abutment was set to 5 ft, the minimum allowed by the FHWA guidelines for small spans. However, many of the dimensions were also constrained by the testing location. For example, the length of the abutment was limited by the size of the concrete mat foundation of the testing facility. The height was limited both by site constraints and by the need to ensure surface expression of the differential settlements at the base (i.e., measureable deformations at the surface of the GRS abutment).

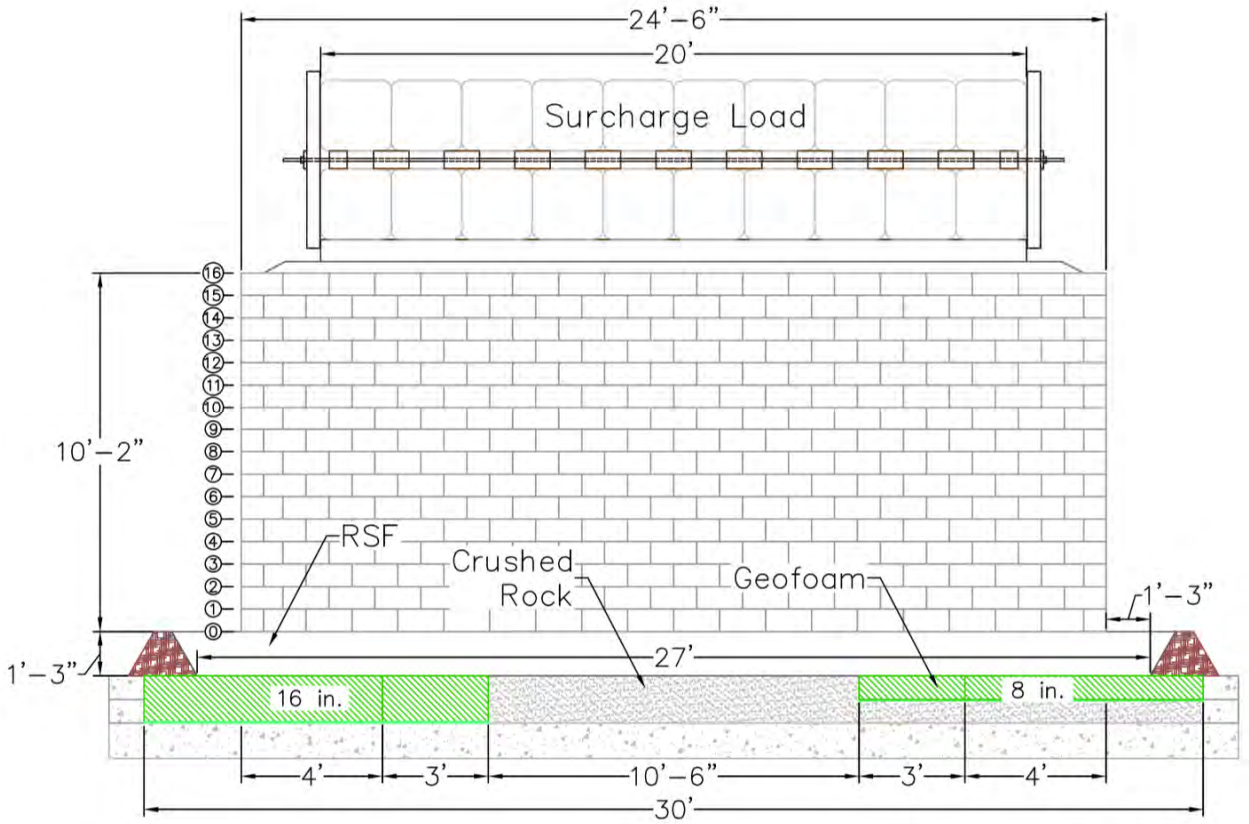

Figure 1. Front View of Abutment Configuration

The width of the abutment increased at a constant 1H:1V slope over the entire height of the abutment. Because the base of the abutment was placed above the surrounding grade, a ramp of compacted, crushed rock was placed as construction progressed to support the abutment at this 1H:1V slope. This ramp also served to simulate the cut or fill slope behind the abutment, to apply horizontal earth pressures to the back of the abutment, and to permit delivery of materials to the top of the abutment throughout construction.

Primary reinforcement was spaced at 8-in vertical intervals throughout the abutment. Secondary reinforcement was placed in the upper five levels at the midpoint of primary reinforcement, resulting in a combined spacing of 4 in for the primary and secondary reinforcement, as shown in Figure 2. The secondary reinforcement spacing and bearing bed for the surcharge load were detailed in accordance with FHWA guidelines, although some non-structural detailing was omitted. The integrated approach was also omitted from the test abutment.

The RSF extended a minimum of 0.25 times the base width, or 15 in, from the abutment at the face and both wing walls and was 15 in deep. Adams et al. (2011a) indicate that reinforcement is commonly spaced at 12 in within the RSF. In order not to exceed this recommendation, one sheet of primary reinforcement was placed within the RSF at a distance of 7.5 in from the bottom and top of the RSF.

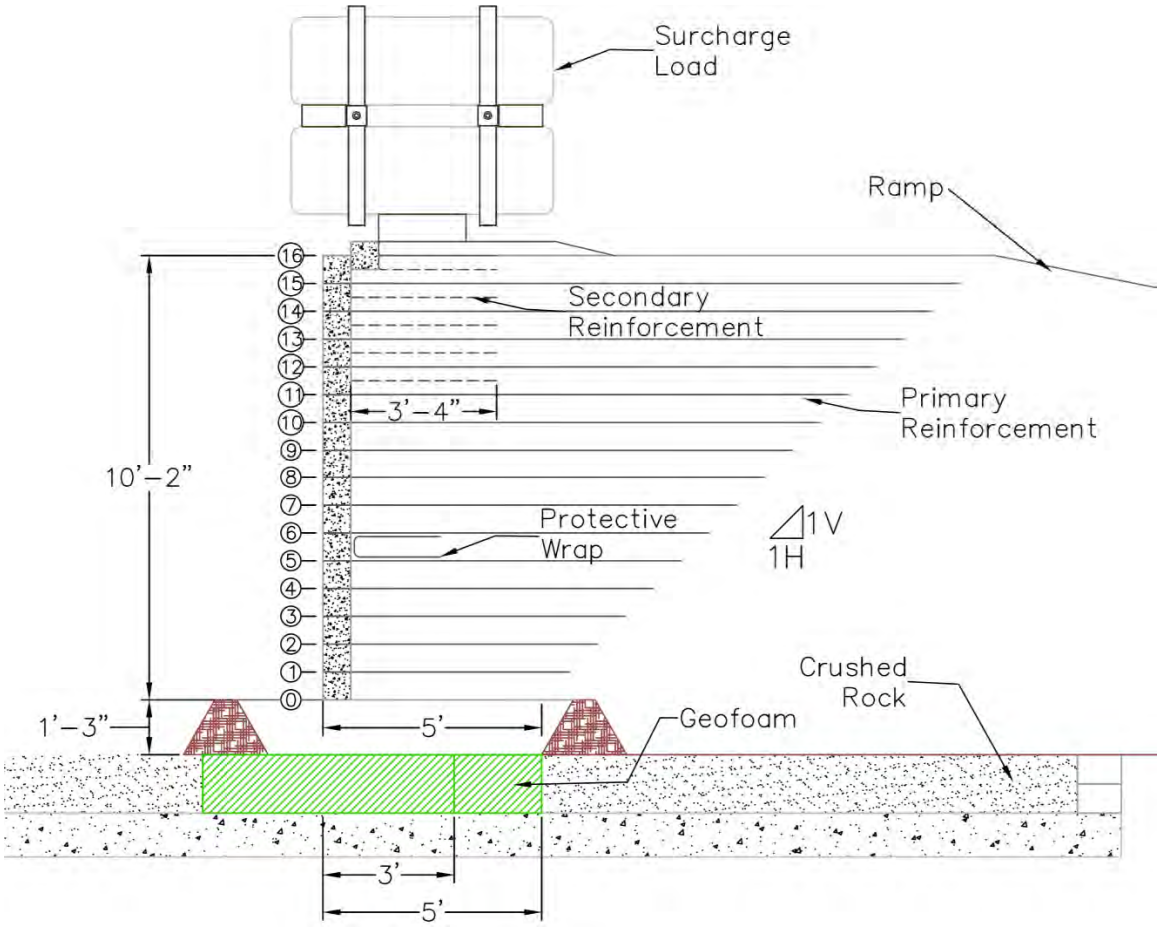

Figure 2. Side View of Abutment Configuration, Showing Reinforcement Spacing

Surcharge Load

A surcharge load consisting of large, precast concrete blocks was applied to the top of the abutment to simulate a bridge dead load. Twenty blocks measuring 2 ft wide by 2 ft high by 6 ft long were stacked on top of a foundation measuring 2 ft wide by 20 ft long, resulting in a bearing pressure of approximately 1750 psf. This load represents the maximum load that the researchers believed could safely be applied during testing while maintaining a low risk of toppling of the concrete blocks. The applied bearing pressure is within the range of design values for small GRS-IBS systems (M. Adams, personal communication).

In most GRS-supported bridges, the superstructure is comprised of precast, prestressed concrete box beams that are transversely post-tensioned together. In order to simulate this composite stiffness, and to improve the stability of the surcharge load, the concrete blocks were tensioned together following placement. The tensioning process is described later in this report.

Geofoam Inclusions

Geofoam inclusions were placed within the subgrade beneath the abutment and RSF to serve as temporary support. These inclusions were later dissolved to induce controlled

settlements beneath the abutment, and therefore their dimensions represent the variables investigated in this research. Consequently, considerable care was taken in selecting the dimensions of these inclusions. Figure 3 shows a plan view of the geofoam inclusions.

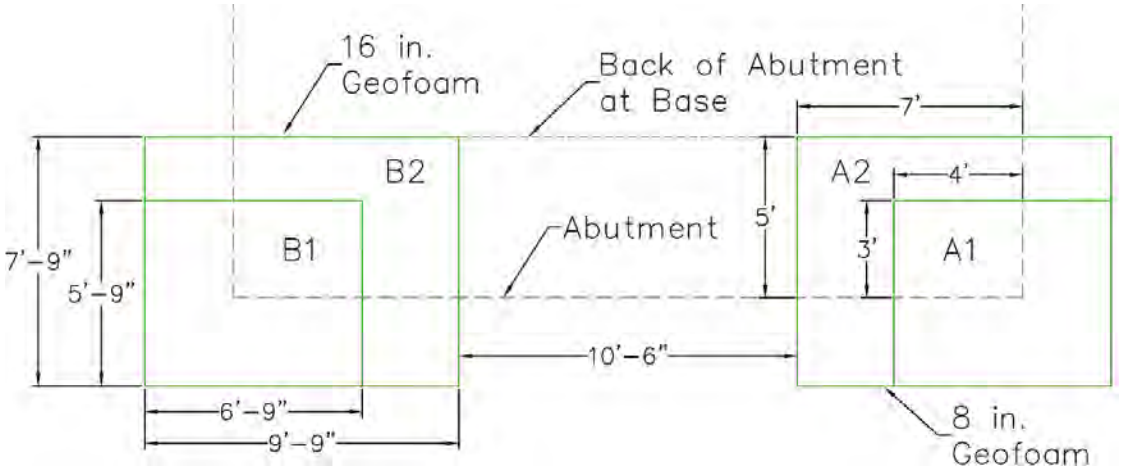

Figure 3. Location of Geofoam Inclusions

The thickness of the geofoam inclusions was selected to ensure that settlement at the base was large enough to result in measureable deformations at the surface of the abutment. The testing site could accommodate geofoam up to 16 in thick, and therefore this thickness was selected for the inclusions on one side (Side B) of the abutment. The inclusions on the opposite side (Side A) were half the thickness of Side B at 8 in thick.

The area in plan of the geofoam inclusions for each testing increment was also selected in an effort to create measureable deformations while minimizing the influence of the tests at one side of the abutment on the tests at the opposite side. After considering a number of possible configurations, an area of 3 ft by 4 ft beneath the abutment was selected for the first test on each side (i.e., Test A1 and Test B1), and an area of 5 ft by 7 ft was selected for the second test on each side. The actual dimensions of the geofoam inclusions were larger in order to completely undermine the RSF that extended beyond the GRS fill and to allow access to the geofoam after construction of the RSF. Table 1 shows the area of base support and the percentage of the base area that was removed during each individual test, as well as the cumulative total of support removed. By the end of testing, large settlements had been induced beneath nearly 60% of the abutment, which represents an extreme loading condition.

Table 1. Percentage of Abutment Base Area Removed During Each Testing Sequence

Test	Area of Abutment Base Support Removed (ft^2)		Percentage of Abutment Base Support Removed	
	Individual	Cumulative	Individual	Cumulative
A1	12	12	9.8%	9.8%
A2	23	35	18.8%	28.6%
B1	12	47	9.8%	38.4%
B2	23	70	18.8%	57.1%

Note: The total base area of the abutment is 122.5 ft^2.

Protective Wrap

During the experiment's design, a suggestion was provided to the researchers by Andy Zickler of VDOT to explore the effectiveness of a wrap behind the facing units to prevent erosion of the fill material in case gaps were to form between the facing units. The researchers incorporated this suggestion at one level of the abutment, Level 6, as shown in Figure 2. The wrap was designed to be one continuous length behind the abutment face and both wing walls. A 7.5-ft-wide roll of fabric was used for the wrap, resulting in an embedded length of approximately 3 ft 4 in.

In deciding to incorporate this suggestion, the researchers considered that including additional reinforcement at this level may alter the stiffness of the reinforced fill and therefore influence the stress distribution within the reinforced fill. The geotextile selected for this application was very lightweight in order to minimize this effect, and unnecessary material where the geotextile was folded behind the corners of the abutment was removed. The researchers were also concerned that the interface friction angle between the two geotextiles may be less than the interface friction angle between the primary reinforcement and the fill. Consequently, a very thin layer of aggregate was placed between the two geotextiles. The procedure for installing this protective wrap is described later in this report.

Materials

This section describes the materials that were used in the construction and testing of the GRS abutment. Materials were selected that are typical of in-service GRS-IBS bridges.

Fill

A crushed rock fill is the primary structural component of a GRS system. The FHWA guidelines allow for use of either a well-graded fill or an open-graded fill. To date, the vast majority of GRS-IBS projects have used an open-graded fill, and therefore an open-graded fill (ASTM No. 8) was also selected for this project. The No. 8 fill has a maximum particle size of 0.5 in and less than 5% passing the No. 16 sieve. The gradation of the fill used for these experiments is shown in Figure 4. Figure 5 shows the moisture-density relationship for this fill, as determined by AASHTO T 99.

A well-graded fill must be used for the RSF, according to the FHWA guidelines. For this project, VDOT No. 21A crushed rock, which has a maximum particle size of 2 in and fines content between 6% and 12%, was selected for the RSF. The gradation of the fill used for these experiments is shown in Figure 4. Figure 6 shows the moisture-density relationship for this fill, as determined by AASHTO T 99, plotted with the zero air voids (ZAV) curve. Steven Smith of Acco Stone provided the authors with the results of VDOT quality assurance tests on coarse aggregates from the quarry (personal communication). Using the dry bulk specific gravity and absorption from these tests, the apparent specific gravity (G_a) was calculated to be 2.86. A small measurement error may be observed in either the highest-moisture-content compaction point of the curve in Figure 6 or the G_a value.

Both fills were provided by Acco Stone in Blacksburg, Virginia.

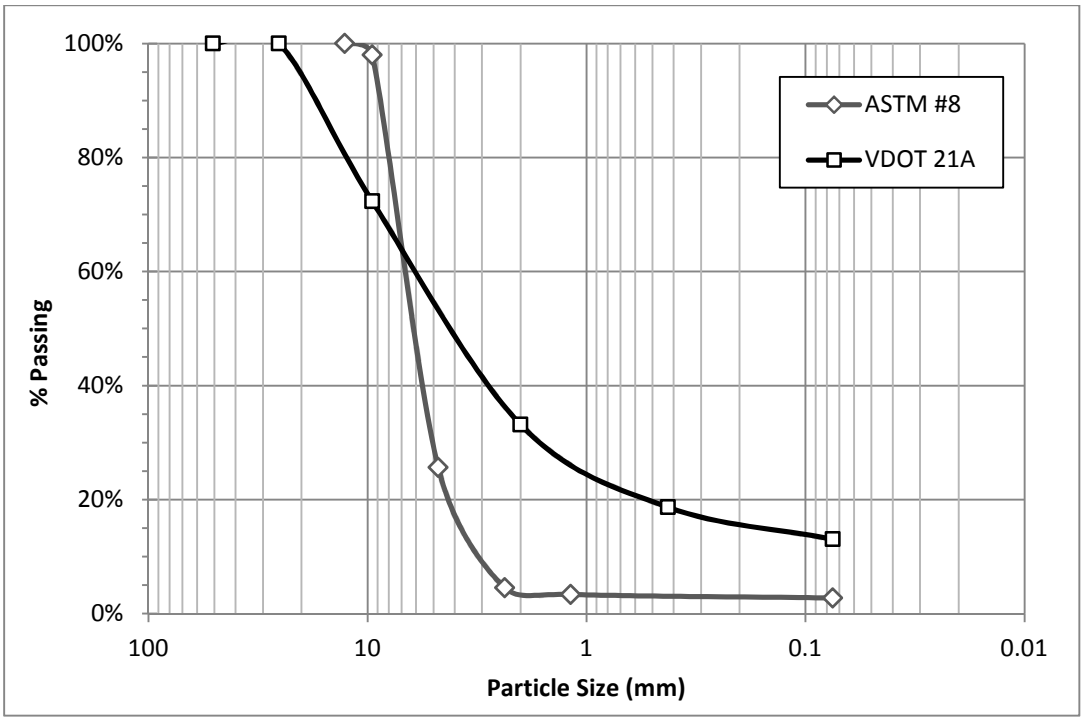

Figure 4. Gradation of Crushed Rock Fills

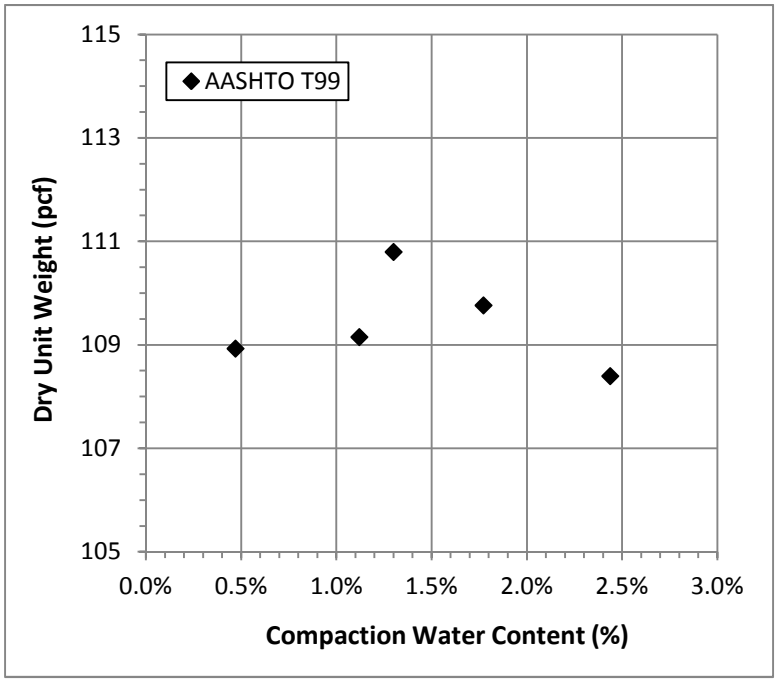

Figure 5. Moisture-Density Compaction Curve for ASTM No. 8

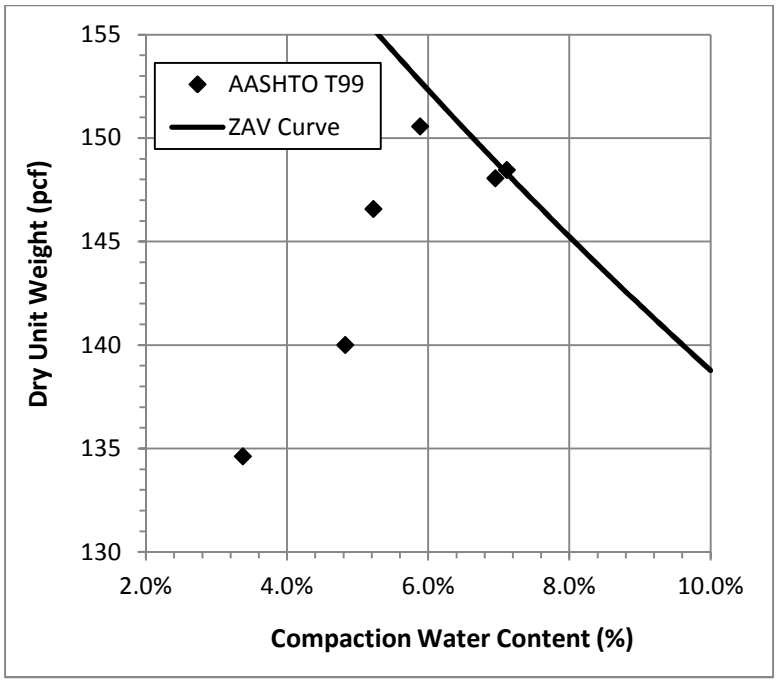

Figure 6. Moisture-Density Compaction Curve for VDOT No. 21A, With ZAV Curve Shown for $G_a = 2.86$

Geotextiles

Two geotextiles were used in the construction of the abutment, and a third geotextile was used to protect the geofoam. The geotextile used for fill reinforcement was a TenCate Mirafi HP570, which is a biaxial, woven polypropylene geotextile. The manufacturer reports a minimum average roll value (MARV) for the ultimate tensile strength of 4800 lb/ft in both directions, and a MARV for the tensile strength at 2% strain of 960 lb/ft in the machine direction and 1320 lb/ft in the cross-machine direction. Although the strength of this geotextile significantly exceeds the required strength for this abutment configuration, it was selected for two reasons. First, fabric strength of 4800 lb/ft is the minimum allowed by the FHWA design guidelines, and therefore this fabric represents the most critical case for this structure. Second, the majority of GRS-IBS structures to date have been constructed with 4800 lb/ft biaxial, woven polypropylene geotextile. The HP570 was used for both the primary and secondary layers of reinforcement in the abutment, and also for the RSF.

The second geotextile was used to create the protective wrap behind the Level 6 facing units. The Tencate Mirafi 140N, a very lightweight geotextile for filtration, was selected for this application. The 140N is a needle-punched, non-woven geotextile with an apparent opening size (AOS) of 0.212 mm and a permittivity of 1.7 sec^{-1}, according to the manufacturer.

The third geotextile was used to wrap the geofoam inclusions beneath the abutment, preventing the fill material from puncturing the plastic wrap that isolated the geofoam in the different testing regions. This geotextile was a thick needle-punched, non-woven geotextile that was surplus from a previous experiment.

Facing Units

While a variety of materials can be used for the facing units of a GRS system, concrete masonry units (CMUs) are the most common. This project used nominal 8 in by 8 in by 16 in hollow-core CMUs with a compressive strength of 4000 psi. The project duration was less than six months and occurred in the summer and fall; therefore, resistance to freeze-thaw cycles was not considered.

Geofoam

An Insulfoam EPS39 geofoam was selected for the geofoam inclusions beneath the abutment. In general, geofoam should have a large enough stiffness to ensure that its strain does not exceed 1%, or creep behavior may result. According to the manufacturer, the EPS39 experiences 1% strain at a compressive stress of 15 psi, which is considerably larger than the estimated 11.6 psi of stress applied to the subgrade.

Geonet

A geonet was used as part of the solvent delivery system to evenly distribute the solvent beneath the geofoam inclusions. The geonet used for this project was a SynTec UBXC, which has a thickness of 200 mils and a transmissivity of 2×10^{-3} m^2/s in the machine direction, according to the manufacturer.

Solvent

EPS can be readily dissolved using a variety of agents. For this project, a biodegradable, non-caustic solvent known as d-Limonene was used. d-Limonene is derived from concentration of citric oils and is commonly used in the recycling industry to reduce the volume of EPS packaging.

Testing Site

The abutment was constructed at Virginia Tech's Kentland Farm, located about 10 miles west of the Blacksburg campus. At the farm, the researchers have access to a 30-ft-square, 12-in-thick concrete mat foundation. The mat is enclosed by a 16-in-high CMU wall, with the top of the wall at grade with the adjacent ground surface. Figure 7 shows the concrete mat foundation in the winter prior to construction. The mat provides a stable foundation for the abutment and ensures that all measured deformations are the result of the induced differential settlements rather than consolidation of the underlying natural soils.

A large quantity of crushed rock was also present on-site from previous experiments. While this rock could not be used for the abutment or RSF fill, it was compacted around the geofoam inclusions to complete the subgrade, and it was used to construct the ramp behind the abutment as construction of the abutment progressed.

Figure 7. Testing Site Prior to Construction

Construction

Construction of the test abutment utilized a crew of two or three students who did not have prior experience with GRS construction. Even so, the crew found that they were able to carry out the construction operation without undue difficulty. Construction equipment was generally small and hand-operated and is described in greater detail in the following sections. A small Bobcat utility vehicle was also used to move fill and other materials during construction.

Construction proceeded according to the guidelines established by the FHWA (Adams et al., 2011), which are generally described in the following sections. The experimental setup and circumstances that required different construction techniques are described in greater detail.

Subgrade, Geofoam Inclusions, and Solvent Delivery System

Construction of the subgrade underlying the test abutment comprised the first phase of construction. First, the geofoam was trimmed to the appropriate dimensions. Next, each region of geofoam was packaged in plastic in order to contain the solvent and eventually the dissolved EPS, as well as to isolate each testing region. In order to wrap the L-shaped foam regions for Tests A2 and B2, the foam was divided into two rectangular shapes and wrapped independently. The process of packaging each testing region is shown in Figure 8.

First, a large section of 6-mil plastic was spread on the concrete foundation. Care was taken not to step on the plastic to prevent puncturing or tearing the material. Next, a section of geonet that was approximately 1 in less than the geofoam dimensions in all directions was placed on top of the plastic. The edges of the geonet were covered with duct tape to prevent them from tearing the plastic. The geofoam was then placed on top of the geonet so that it overhung the geonet by approximately 0.5 in on each side. At the corner of the geofoam where the solvent would be introduced, approximately 1 in of foam was trimmed to provide a path for the solvent to reach the geonet.

Figure 8. (a) Placing Geofoam on Top of Geonet and Plastic; (b) Wrapping Geofoam in Plastic; (c) Wrapping Geofoam and Plastic in Non-Woven Geotextile; (d) Arranging Packaged Geofoam in Testing Configuration

The plastic was then wrapped around the geonet and geofoam and secured such that the bottom and sides of the foam had no seams or other avenues for the solvent to escape. The two pieces of foam on each side that comprised the L-shaped region for Tests A2 and B2 were each wrapped with a second layer of plastic to ensure that no solvent that might escape from Test A1 and Test B1 would induce premature settlement in these regions. After the plastic had been wrapped and secured, duct tape was used to encircle the perimeter of the plastic, about halfway up the sides of the foam. The tape provided some structure to the plastic and allowed the plastic to maintain a shape that contained the solvent and dissolved EPS. The plastic-wrapped geofoam was then placed on a thick non-woven geotextile and wrapped such that the geotextile covered the bottom and sides of the geofoam package. Finally, a small hole was trimmed in the plastic and geotextile at one of the upper corners as a delivery point for the solvent.

On the side of the foundation located beneath Side B of the abutment, a large piece of 6-mil plastic was placed in the location of the geofoam regions. This barrier served as an additional line of defense against both groundwater intrusion and escape of the solvent and dissolved EPS. The packaged geofoam blocks were carefully arranged on top of the plastic in their final configuration, the plastic was folded up to cover the sides of the geofoam, and the geofoam was secured with CMUs. The crushed rock for the subgrade, a VDOT 21B stone, was placed over the concrete mat foundation at a water content near its optimum and compacted to a lift thickness of 8 in using a hand-operated, vibratory plate compactor. As the fill was being placed, posts were also placed for later use in securing instrumentation.

On the side of the foundation located beneath Side A of the abutment, considerable effort was made to ensure that the top of this lift was level, smooth, and at the correct elevation. Then, similar to the process on Side B, a large piece of 6-mil plastic was placed, the packaged geofoam blocks were carefully arranged, the plastic was folded up to cover the sides of the geofoam, and the blocks were secured in placed with CMUs. Fill was then placed and compacted to the top of the geofoam at both sides.

Finally, 1-in PVC pipes for delivering the solvent were positioned at the delivery points. The geofoam packages were covered with a final sheet of 6-mil plastic and secured to prevent infiltration by rainwater. A section of non-woven geotextile was placed over the plastic and geofoam packages as a final protective layer. Figure 9 shows the foam regions beneath Side B ready for construction of the RSF.

Figure 9. Fill Compacted Around Geofoam on Side b, Solvent Delivery System in Place, and Foam Covered With Protective Non-Woven Geotextile

Reinforced Soil Foundation (RSF)

The GRS test abutment and retained soil were constructed from the ground surface upward, rather than the usual scenario of constructing the GRS from the bottom of an excavation upward. Consequently, in order to represent a normal RSF geometry, a berm of fill was first placed to create a compaction form for the RSF, as shown in Figure 10. Prior to placing the berm, which covers the solvent delivery tubes shown in Figure 9, the valves to the delivery points were closed and covered with a piece of non-woven geotextile for protection.

Figure 10. Berm to Construct RSF

Following placement of the berm, lengths of HP570 reinforcement were cut for the exterior of the RSF and placed such that they would wrap from the bottom heel of the RSF around the front and back to the upper heel. A minimum of 3 ft of overlap was provided between adjacent sheets. Sufficient material was left at the edges of the RSF so that the reinforcement could be wrapped around the edges and secured at the top of the RSF, enclosing it on five sides. The VDOT No. 21A crushed rock was placed evenly and compacted such that the compacted lift thickness was slightly less than 4 in. The fill was compacted to at least 95% of maximum dry density per AASHTO T 99 at a water content within 2% of optimum using a hand-operated, vibratory plate compactor.

Two lifts were placed, resulting in a total lift thickness of 7.5 in. A single sheet of reinforcement was placed with the cross-machine direction oriented perpendicular to the plane of the abutment face, and two more lifts of fill were placed. While the surface of the RSF was constructed nearly level in all locations, additional effort was made to level the fill in the locations that would support the first course of CMU facing units. The remaining tail of the reinforcement was then folded over the compacted fill to complete the wrap.

Abutment

General Procedure

In general, construction of a GRS system is relatively straightforward. First, the facing units are placed in the appropriate configuration. Second, fill is placed behind the facing units and compacted. Third, a sheet of geosynthetic reinforcement is placed over the fill and facing units. This process is repeated until the abutment reaches the design height. Details for the

bridge bearing zone and other details specific to this project are discussed further in the following sections.

Leveling the Facing CMUs

Because the facing CMUs are dry-stacked, it is critical that the first row of blocks be carefully leveled. Considerable effort was devoted to this task, and a thin layer of fine aggregate was used as necessary to facilitate leveling. As the abutment was constructed, small strains in the geofoam beneath the corners of the abutment required that some CMU blocks be ground to avoid rocking and points of stress concentration.

Block Alignment

At each level, the CMUs were aligned using a string line and subsequently set back 0.25 in to allow for small displacements during compaction. The compaction process usually did not return the blocks completely to their original position, and so a hand tamper was then used on the fill behind the face to nudge the CMUs back into a flush alignment. The corner blocks were clamped together to prevent a gap from opening between these two blocks during compaction.

Fill Placement and Compaction

The ASTM No. 8 fill was placed from the face towards the rear of the abutment, and from the wing walls inward. This process worked any slack that may have existed in the underlying reinforcement toward the center rear of the abutment. Beginning approximately at Level 4 of the abutment, the reinforcement was long enough that the loader could no longer place the fill directly behind the face without driving over the reinforcement. Rather than risk damaging the reinforcement by doing so, some of the rear CMUs for the wing wall were removed, and the reinforcement was rolled toward the face to allow the loader to reach the front of the abutment. In this process, care was taken to avoid turning the loader on the compacted fill of the underlying level so that the fill was not disturbed. As the fill was placed, the fabric was unrolled back into position, and the wing wall CMUs were repositioned.

When the GRS fill had been placed nearly to the back of the abutment, a well-graded fill was used to construct a small berm across the back of the abutment, creating the rear boundary that is normally provided by the cut or fill slope. The remainder of the fill for that level of the abutment was then placed within the confines of the berm. At this time, additional material was added to the ramp to raise it to the same height as the berm and permit delivery of the material for the following level of the abutment.

After the fill had been placed, it was compacted at a water content near optimum using a hand-operated, vibratory plate compactor until there was no visible displacement of the fill. Trials were performed on a test compaction pad before the start of the project to determine if sand cone testing might prove to be a feasible option to evaluate compacted dry density. Ultimately, it was determined that compaction to no visible displacement was the most consistent compaction objective for this open-graded fill. Generally, three to four passes with the vibratory tamper were sufficient to meet this criterion, which is the same number of passes that was

generally used in compaction of the VDOT No. 21A fill. Although the lift thickness was larger for the No. 8 fill (8 in vs. 4 in), the ease of compacting the No. 8 fill and the weight of the vibratory tamper give the authors confidence that the relative compaction of the fill met or exceeded the 95% minimum set out in the FHWA guidelines.

Reduced compaction effort was used immediately behind the CMU facing units. Through construction of Level 12, the vibratory plate compactor was used to compact the fill to within 6 in of the face and wing walls. Repeated passes with a hand tamper were used to compact the fill within 6 in of the face. Beginning at Level 13, a lightweight, vibratory plate asphalt compactor was procured. The heavier vibratory plate compactor was used to compact the fill to within 1 ft of the face and wing walls, and subsequently the lighter asphalt compactor was used to compact the fill to with 2 in of the face and wing walls. The hand tamper was used to compact the final two inches.

Reinforcement Placement

After compacting the fill, a sheet of reinforcement was placed over the fill and the facing CMUs with the cross-machine direction oriented perpendicular to the plane of the abutment face. A single, continuous sheet of reinforcement was used to reinforce the abutment and the wing walls. Following FHWA guidelines, the reinforcement covered at least 80% of the CMU area to ensure adequate frictional strength. Any slack in the reinforcement was removed to the extent possible.

Protective Wrap

As discussed previously, the researchers integrated a trial of a protective wrap behind the facing units, intended to prevent the loss of fill should any gaps form between the CMUs. To install this wrap, the facing blocks for Level 6 were first positioned as normal. A thin layer of the ASTM No. 8 fill, no more than one particle thick, was spread over the underlying reinforcement to create adequate friction between the two geotextiles. The lightweight filtration fabric was cut long enough to wrap the fill behind the abutment face and both wing walls with one length of fabric, and the fabric was positioned behind the CMUs with a tail length of slightly less than 3.5 ft. Behind the corners, the material was carefully folded, and extra material was trimmed away to minimize the change in stiffness created by the addition of the geotextile.

The fill was then placed and compacted as normal. The remaining geotextile was folded over the top of the compacted fill, with its tail also slightly less than 3.5 ft. Again, the fabric at the corners was carefully folded and trimmed to remove bulky excess material. Finally, a thin layer of aggregate was placed over the filtration geotextile to create adequate friction between it and the overlying reinforcement. This installation process is illustrated in Figure 11.

Secondary Reinforcement

In the upper five levels of the abutment, Levels 12 through 16, layers of secondary reinforcement were included in compliance with FHWA recommendation. Secondary reinforcement was placed at the midpoint of primary reinforcement, resulting in a combined

spacing of 4 in for the primary and secondary reinforcement, and it extended back 3 ft 4 in from the back of the CMU facing blocks. The lower four layers of secondary reinforcement are simply single sheets that are placed at the midpoint of the lift, behind the facing CMUs. The uppermost layer, at the midpoint of Level 16, wraps around a 4-in-thick lift of compacted fill immediately below the bearing bed. Figure 12 illustrates these details.

When installing the secondary reinforcement, fill was placed and compacted to a thickness of 4 in for a distance of approximately 4 ft behind the CMUs. The secondary reinforcement was placed, and additional fill was placed over the secondary reinforcement and compacted to the top of the CMUs. Subsequently, the remainder of the fill for the level was placed and compacted.

Figure 11. Placing the Protective Wrap. (a) Thin Layer of Aggregate Placed Over Primary Reinforcement; (b) Placing Protective-Wrap Geotextile and Fill; (c) Fill Compacted and Wrap Completed; (d) Thin Layer of Aggregate Placed Over Protective-Wrap Geotextile, Prior to Placement of Next Level of Primary Reinforcement

Bearing Bed Detailing

The load supported by the abutment (in this case, a surcharge load simulating the weight of the bridge superstructure) was set back from the face of the wall. The FHWA guidelines provide recommendations for detailing in order to provide this setback distance and to maintain clear space between the bridge superstructure and the top of the facing units. Since no clear space concerns existed for this experiment, the setback distance was created using a row of CMUs, as illustrated in Figure 12.

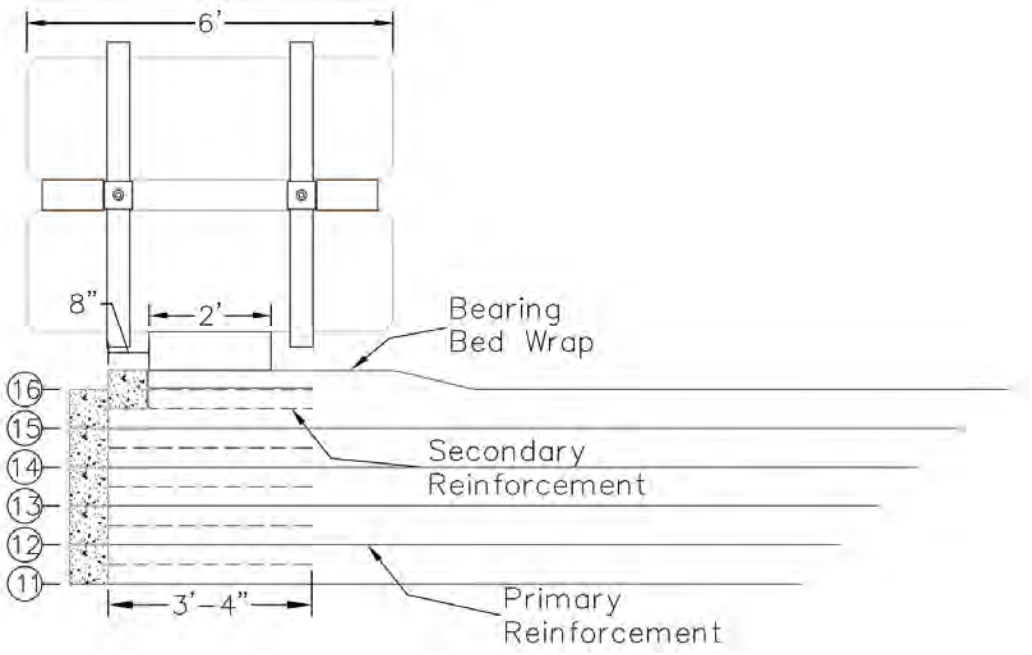

Figure 12. Secondary Reinforcement and Bearing Bed Detailing

After placing and compacting the initial 4-in lift for Level 16, a row of CMUs was placed on the fill directly behind the facing CMUs, such that the blocks creating the setback distance extended approximately 4 in above the abutment face. The secondary reinforcement was then placed behind the setback CMUs, an additional 4 in of fill was placed and compacted, and the secondary reinforcement was wrapped over this compacted fill. The remainder of the fill for Level 16 was placed and compacted as usual.

Finally, an additional 4-in lift was constructed to serve as the bearing bed. A thin layer of aggregate was placed over the Level 16 secondary reinforcement wrap, and the reinforcement was positioned to form the bottom of the bearing bed wrap. The No. 8 fill was placed and compacted to a final lift thickness of 4 in over an area extending 1 ft beyond the width and length of the surcharge foundation. Beyond 1 ft, the fill was graded down at a slope of about 3H:1V until it was at the level of Level 16. The fill in the location of the surcharge foundation was carefully leveled, and the reinforcement was wrapped over the top of the fill to complete the bearing bed. A thin layer of aggregate was placed over the tail of the wrap to secure it.

Pinning the Upper CMUs

The frictional connection between the CMUs and the reinforcement is quite strong when there is sufficient normal stress between the two components. Near the top of the wall, the self-weight of the blocks does not provide for sufficient connection strength. Consequently, the top three courses of CMUs are filled with concrete or grout and pinned together with vertical lengths of rebar.

To allow the concrete and rebar to pass through the reinforcement, "X"-shaped slits were cut in the reinforcement at Levels 14 and 15 over the hollow cores of the CMUs during

construction, as illustrated in Figure 13. Following completion of the bridge bearing bed, the hollow cores of the upper three levels of CMUs were filled with a high-slump 4,000 psi concrete, which was rodded into place. A 20-in-length of No. 4 rebar was vertically inserted into each hollow core to pin the CMUs together.

Figure 13. "X"-Shaped Slit in Reinforcement at Level 15

Surcharge Foundation

The 2-ft-wide by 20-ft-long surcharge foundation was constructed of six 8 in by 8 in by 10 ft pieces of lumber, arranged as shown in Figure 14. Joints were offset, and the wood was bolted together with sections of 1-in-diameter threaded rod spaced at 2.5 ft.

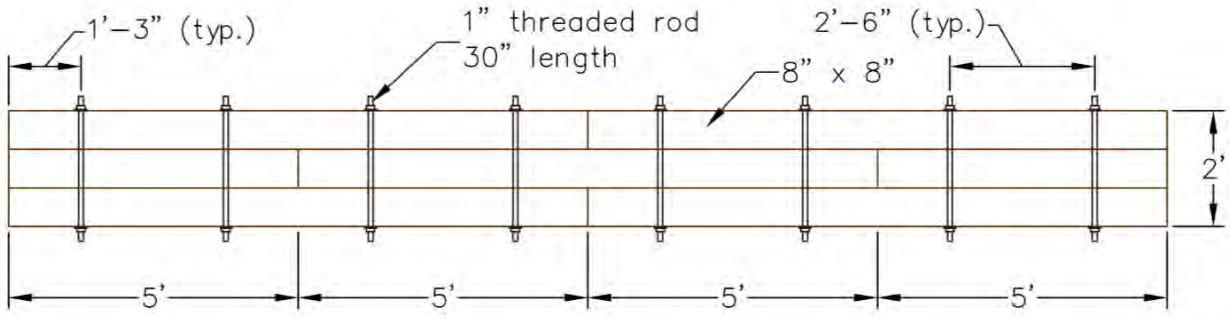

Figure 14. Surcharge Foundation Detailing

Surcharge Load

The surcharge load consisted of twenty 2 ft by 2 ft by 6 ft concrete blocks, arranged in two levels of ten blocks each. The blocks were placed by crane, beginning with the two blocks

at the center of the abutment and moving outward, placing one block at a time on alternating sides. The blocks were placed such that the middle 2 ft of the 6 ft length was centered over the 2-ft-wide surcharge foundation.

After the first level of surcharge blocks had been placed, 6 in wooden spacing blocks were added prior to placing the second level of concrete blocks. Shims were added where necessary to level these concrete blocks. Two 25 ft lengths of 1-in-diameter, A36 threaded rod were placed over the first level of surcharge blocks in preparation for horizontally tensioning the surcharge load. The second level of surcharge blocks was then placed, following the same sequence as the first level.

Following placement of the surcharge load, the blocks were tensioned together to add restraint and create a composite stiffness for the surcharge load. Square steel HSS sections were used as side restraints. Holes were drilled in the HSS sections, the HSS sections were placed over the A36 threaded rod, and a 0.5-in-thick bearing plate, washer, and nut were threaded onto the rod and tightened by hand. This process was repeated for both threaded rods at each end of the surcharge load. After the HSS sections had been brought into snug contact with the end surcharge blocks, a doughnut hydraulic jack was used to tension each rod. In the process of tensioning the rod, small amounts of space that remained between individual surcharge blocks were eliminated as the blocks were pulled closer together. The doughnut jack had a small amount of travel and therefore had to be locked off and reset several times. Once no additional displacement of the surcharge blocks was observed, the tension in the rod was increased to the desired load and locked off. The process was then repeated for the other rod. Irregularity in the horizontal dimensions of the surcharge blocks resulted in an offset between the ends of the two levels, requiring the use of steel shims to achieve a good contact area with the HSS sections. These shims were not available at the site the evening that the concrete surcharge blocks were placed. Consequently, the rods were tensioned sufficiently to ensure stability of the surcharge load overnight. The following morning, the tension in the rods was released, the shims were inserted, and the rods were re-loaded to approximately 24 kips each and locked off.

Following placement of the surcharge blocks, several CMUs were placed on top of the Level 16 facing CMUs and beneath the front end of the surcharge blocks. Across the top of these blocks were placed lengths of 2 in by 6 in dimensional lumber. This system had between 1 and 2 in of clearance between the top of the lumber and the bottom of the surcharge blocks and was intended to reduce the chance of the blocks tumbling from the top of the abutment if they tilted towards the face during testing. Two additional surcharge blocks were placed at the rear of the abutment and secured to the surcharge load with 5/16-in braided wire and tensioned with 2-ton-capacity come-alongs to provide additional stability to the load. During testing, the surcharge blocks experienced virtually no rotation, and clearance between the surcharge blocks and the 2 in by 6 in lumber was maintained.

In total, construction and instrumentation of the abutment, including placement of the surcharge load, took 35 days of work. A photograph of the completed abutment is shown in Figure 15.

Figure 15. Completed Abutment

Instrumentation

During construction, five types of instrumentation were installed to monitor the behavior of the abutment. Instrumentation included survey targets, PVC tubing for settlement measurements, earth pressure cells, draw-wire extensometers, and resistance strain gages. With the exception of the survey targets, the location of each instrument is shown in Figures 16 and 17.

The identification number for each instrument begins with a three-letter code identifying the type of instrumentation—e.g., "EPC" identifies an earth pressure cell. The codes are provided in a legend with each figure. The three-letter code is followed by a dash, a letter, a number, a second dash, and a final number. The letter identifies whether the instrument is on Side A (A), Side B (B), or in the center of the abutment (C). For the settlement profiling tubes that run the length of the abutment, this letter is omitted altogether. The subsequent number identifies the abutment level where the instrument is located. This number is followed by a dash and a final number, which identifies the particular instrument at the indicated level. Instruments are numbered from the face toward the back of the abutment, or from the wing wall toward the center of the abutment, depending on the configuration. As an example, EPC-B1-2 denotes the earth pressure cell located on Side B of the abutment, within the Level 1 fill, second instrument from the wing wall.

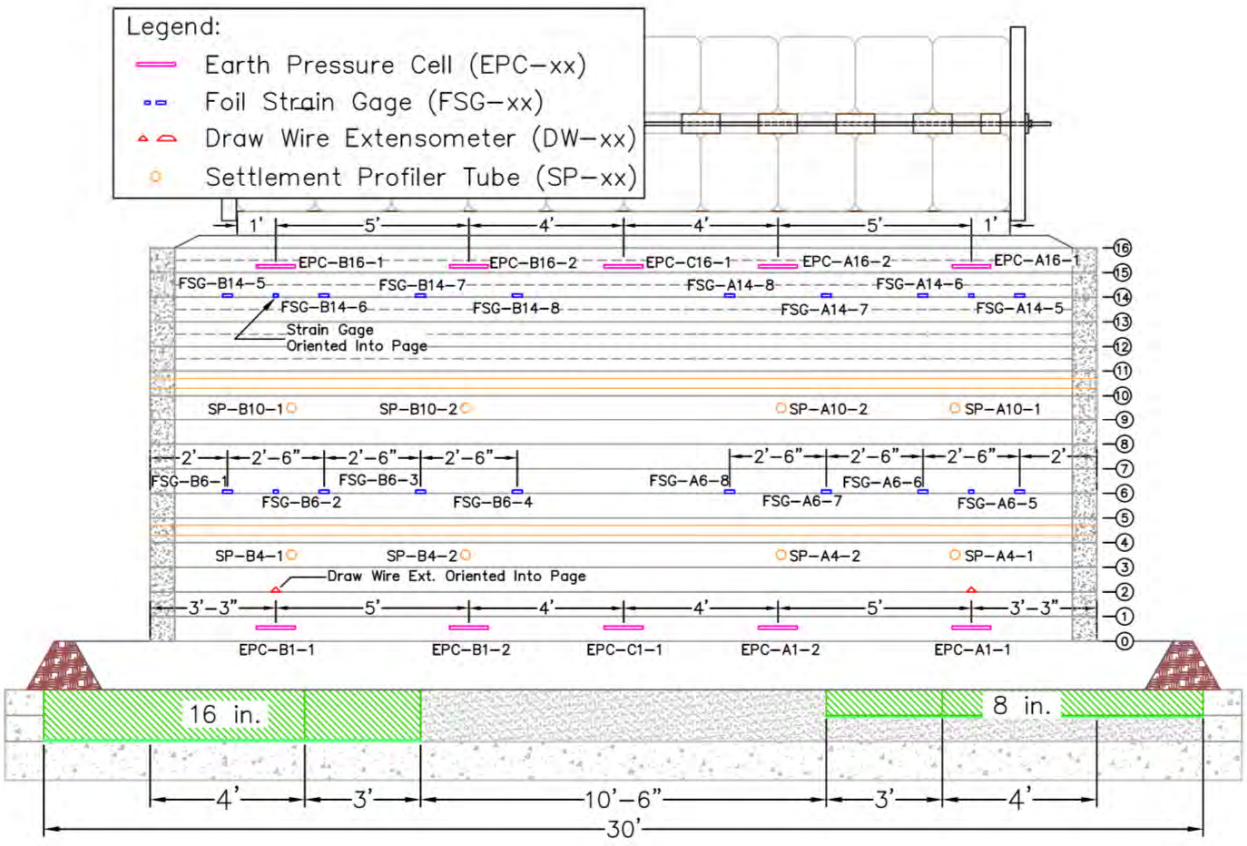

Figure 16. Front View of Instrumentation Configuration

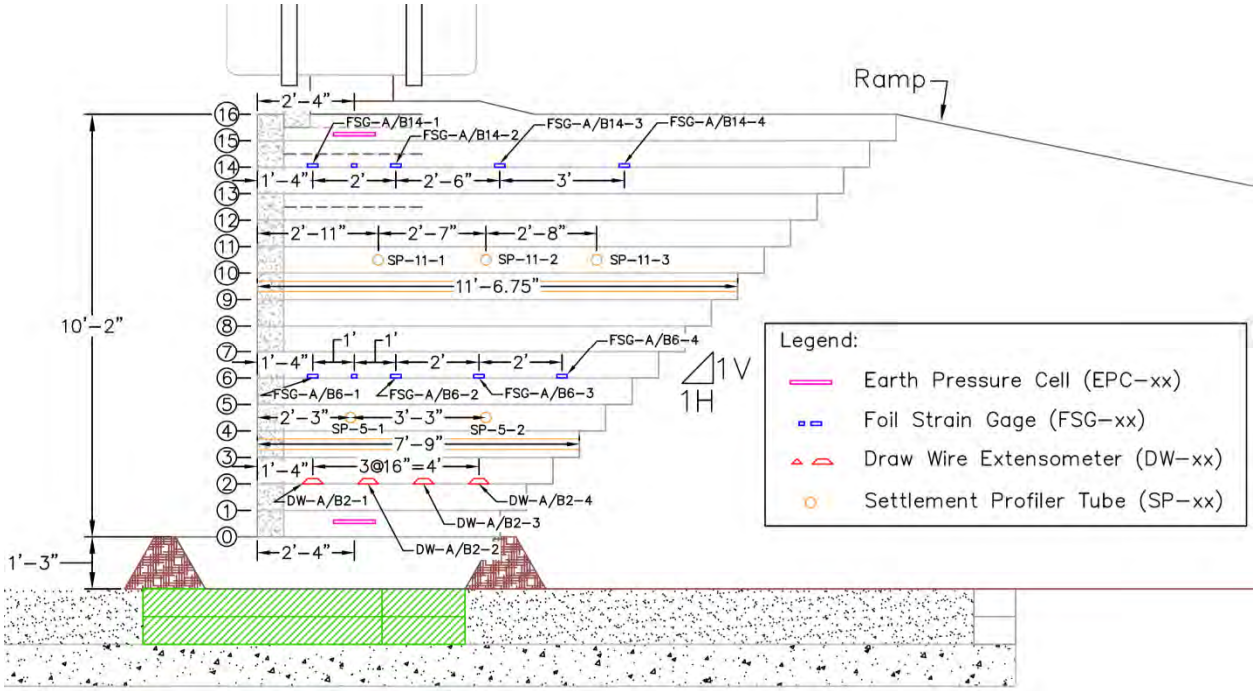

Figure 17. Side View of Instrumentation Configuration

Survey Targets

Reflective survey targets were placed on the facing CMUs to monitor three-dimensional displacements using a total station. Targets were also placed on the wooden surcharge foundation and on the large concrete surcharge blocks, and points were marked on the surface of the abutment and the RSF to survey using a handheld rod. The locations of these survey points are shown in Figures 18 through 20. Targets were placed symmetrically on the wing walls of the abutment; only one of the wing walls is shown in Figure 20. Where survey targets and settlement profiling tubes are shown at the same location in these figures, the survey target was placed on the CMU facing block directly above the profiling tube. In total, 214 survey points on the abutment were monitored throughout the testing sequences. Three benchmarks were established around the abutment from which to take survey measurements.

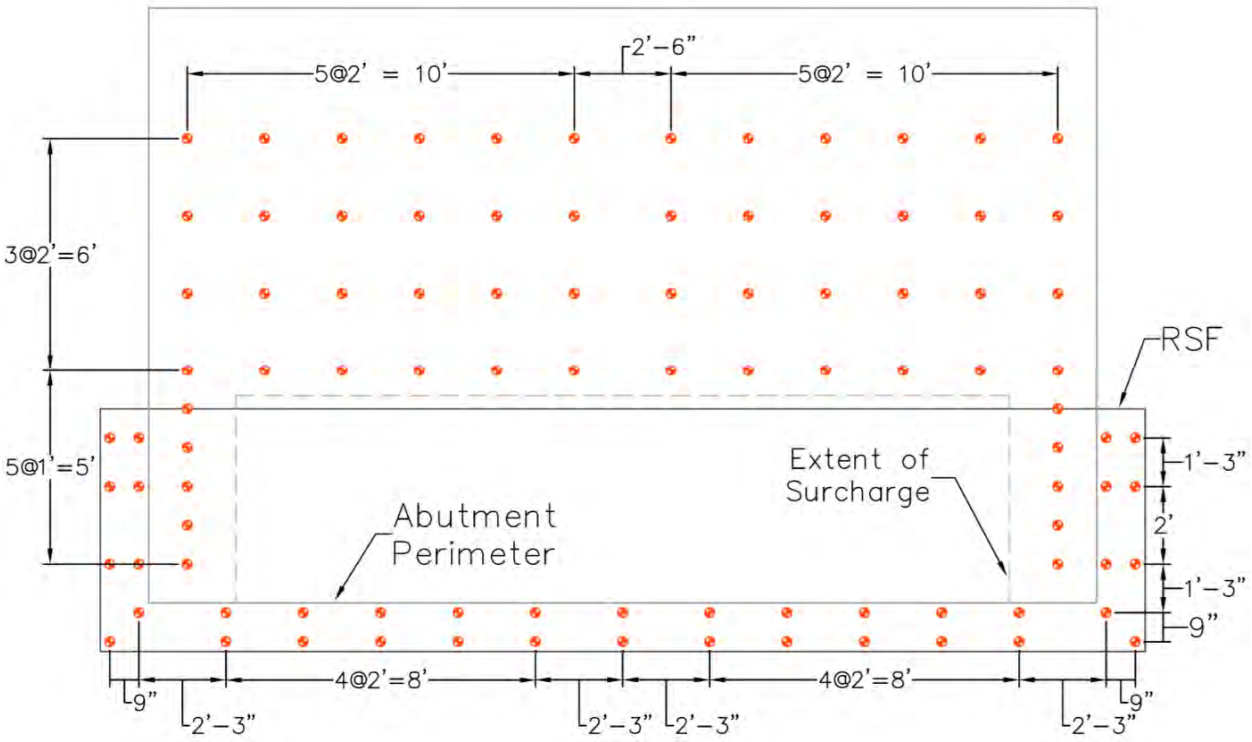

Figure 18. Plan View of Survey Points on Top Surface of Abutment and RSF

Settlement Profiling Tubes

To monitor the settlement of the reinforced fill within the abutment, 2-in-diameter PVC pipes were placed within the fill at Levels 4, 5, 10, and 11, at the locations shown in Figures 16 and 17. The 2-in inside-diameter is large enough to allow the profiling instrument to pass even after experiencing significant deflections. The pipes were placed approximately level in the middle of the fill prior to compaction. Holes were drilled through the facing CMUs to allow the pipes to pass through. An example of one of these settlement profiling tubes is shown in Figure 21.

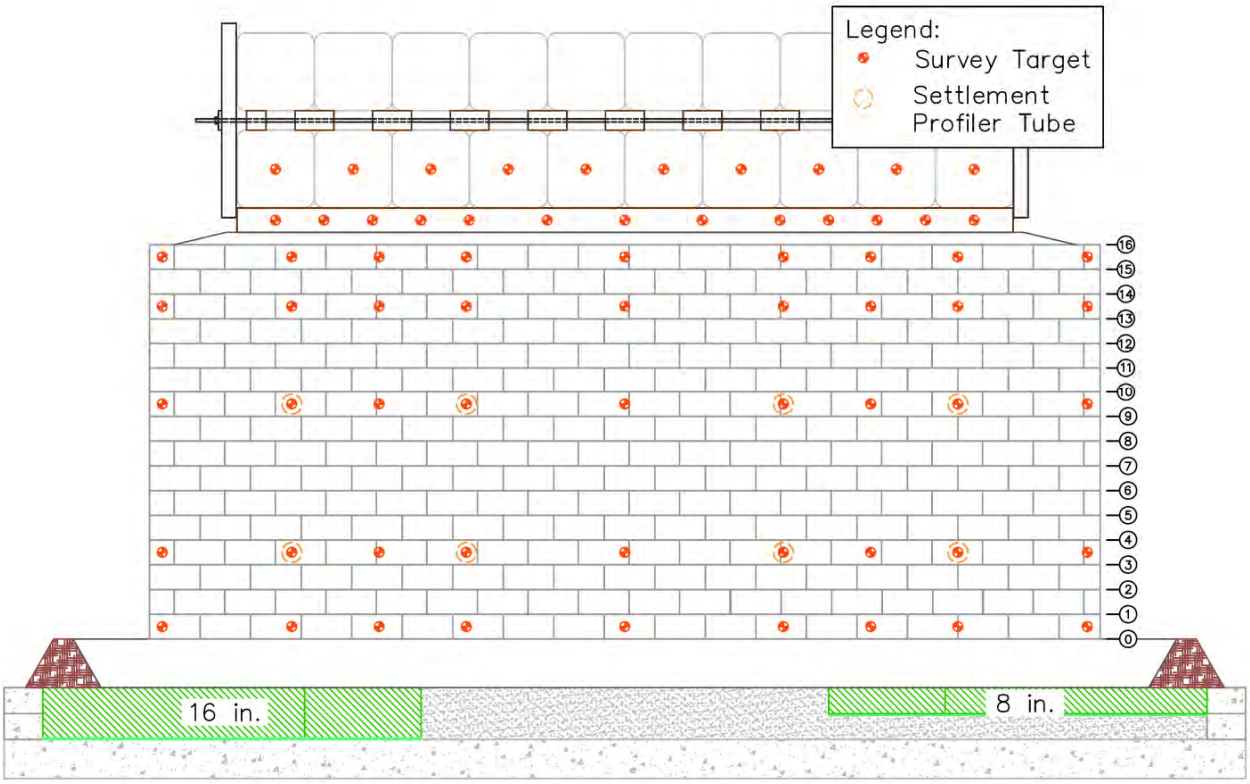

Figure 19. Profile View of Survey Target Locations on Front of Abutment

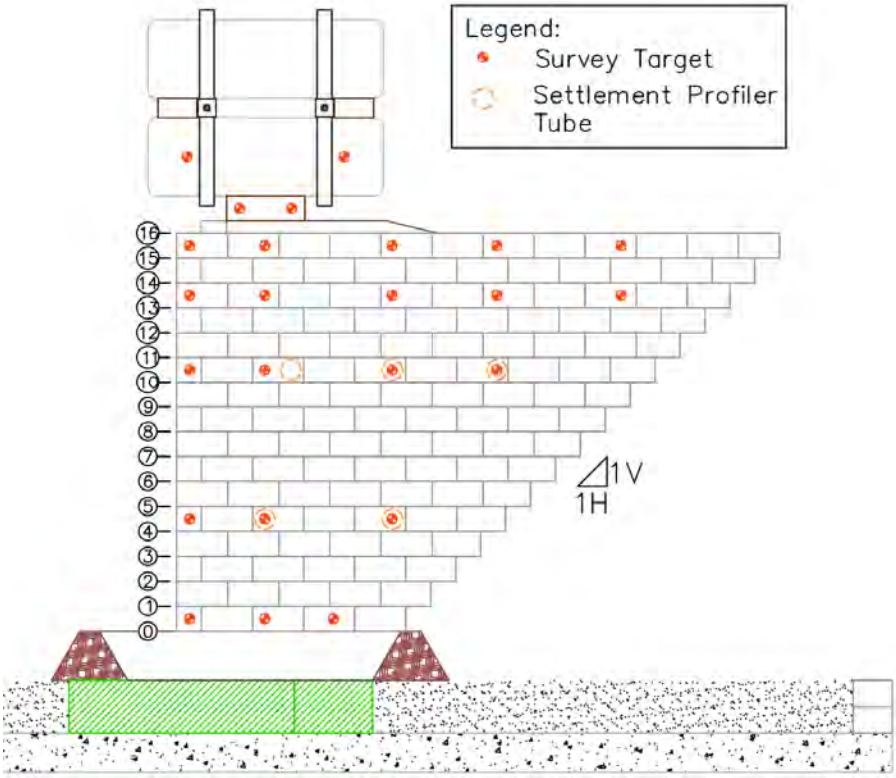

Figure 20. Profile View of Survey Target Locations on Side of Abutment

Figure 21. Example of Settlement Profiling Tube

The settlement profiling instrument is a vibrating wire piezometer connected to a length of flexible plastic tubing that is filled with a mixture of water and antifreeze. The tubing is connected to a container placed above the elevation of the PVC pipes to maintain a constant elevation head. As the profiling device is pulled through the settlement profiling tubes, any changes in elevation are recorded by the piezometer as changes in fluid pressure. The instrument used for these experiments was a Geokon 4651-1-170KPA.

Earth Pressure Cells

Earth pressure cells (EPCs) were employed to monitor changes in the stress distribution within the fill. An EPC consists of two circular, stainless steel plates that are welded together around the perimeter. The thin chamber between the plates is filled with de-aired oil and connected to a vibrating wire pressure transducer. External pressures induce an equal pressure in the oil medium and can be measured by the pressure transducer. For this application, ten Geokon 4800-1-170KPA pressure cells were embedded in the abutment fill. These cells are 6 mm thick and 230 mm in diameter (0.24 in by 9.06 in) and can accommodate pressures as high as 170 kPa (24.7 psi) with an accuracy of ±0.12 psi and a resolution of 0.006 psi. Five were placed at the midpoint of the lowest lift (Level 1), and five were placed in the highest lift (Level 16) at the midpoint between the primary reinforcement and the secondary reinforcement. The location of the cells is depicted in Figures 16 and 17. An example of an EPC within the Level 1 fill is shown in Figure 22.

Figure 22. Example of Earth Pressure Cell in Level 1 Fill

Draw Wire Extensometers

A draw wire extensometer (DWE) generally consists of a retractable stainless steel wire that is connected to a rotating potentiometer. Draw wire extensometers can also be referred to as string potentiometers, or "string pots." As the wire is extended or retracted, the potentiometer registers a change in voltage, which can be calibrated to a change in position. Eight Micro-Epsilon WPS-1000-MK6-P25 extensometers with a resolution of 0.3 mm were selected and divided into two groups of four. Each set of four sensors can measure the average strain of three regions by determining the relative displacement of two points and dividing by the distance between these points.

The DWEs were used to measure the relative displacements of eight points on the reinforcing fabric at Level 2 (four near each corner), as shown in Figures 16 and 17. Larger strains were anticipated at the lower levels of the abutment, and it was unclear if strain gages would be able to accommodate these strains. However, the geometry of the abutment required that the sensor be able to retract the wire to measure displacements of the fabric towards the face of the abutment. The manufacturer publishes a wire retraction force of only 1 N, and therefore the ability of the gage to retract the wire against frictional forces was questioned. The field performance of the DWEs ultimately showed that this concern was unfounded.

This installation process generally followed the recommendations provided by Cuelho et al. (2008) and is illustrated Figure 23. The sensors were connected to the geotextile reinforcement using a 0.020-in-diameter, stainless steel wire with a spring temper, similar in stiffness to a piano wire. The wire was passed through the fibers of the geotextile from top to bottom, then from bottom to top such that it spanned four fibers. The wire was bent 180 degrees, and the free end was secured by sliding a piece of plastic sheathing of an 18-gauge wire over both the wire and its free end. At each connection point, an area of the geotextile about the size of a penny was then treated with an epoxy to stiffen the fibers.

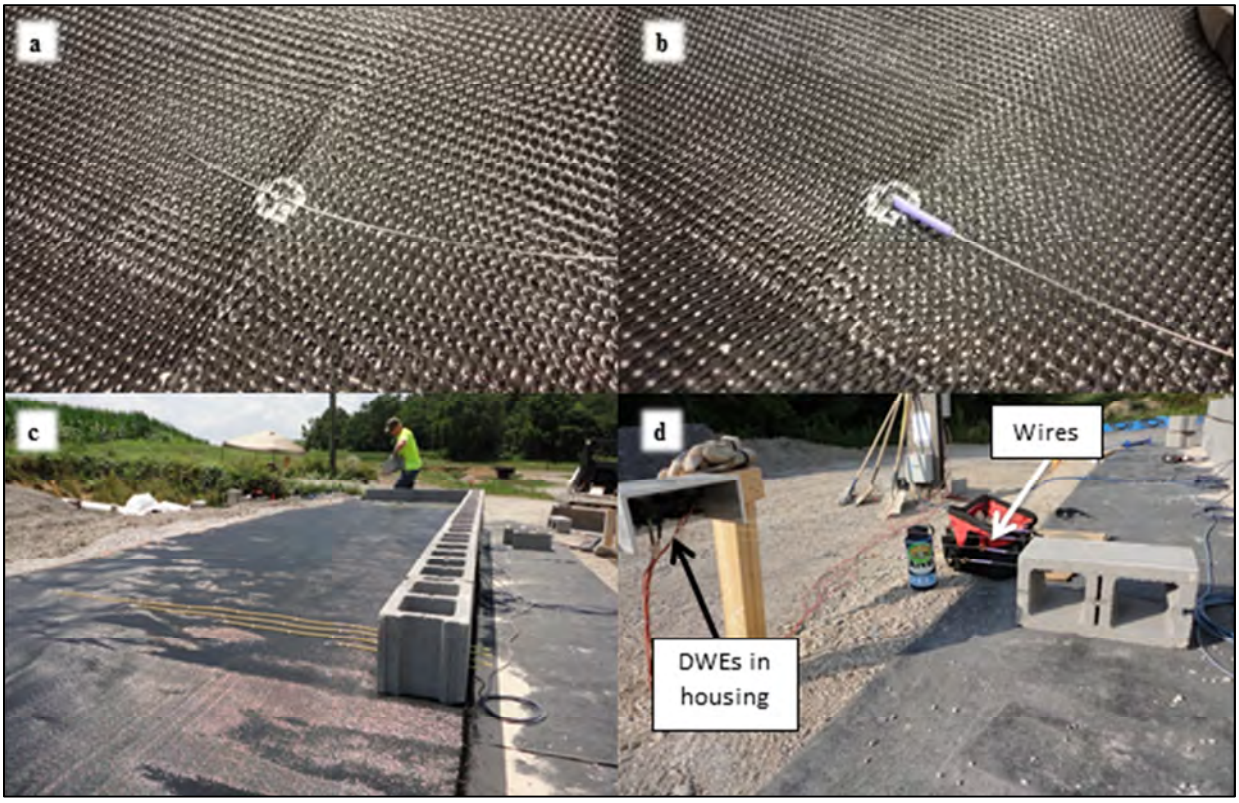

Figure 23. Installing DWE in Lab and Field. (a) Passing Stainless Steel Wire Through Geotextile; (b) Bending the Wire 180° and Securing It; (c) Protecting the Wire With Nylon Tubing and Installing in Field; (d) Stainless Steel Wire Connected to Instrument (Located in Weather-Resistant Housing)

To allow the wire to translate freely after placement of the fill, a section of 0.106-in inside-diameter nylon tubing was placed over the wire from the front of the geotextile up to 0.5 in from the connection point to the geotextile. This gap was provided to allow the fabric to move towards the DWE sensor without catching on the tubing. Graphite lubrication was used to minimize friction between the inside of the tubing and the wire. The tubing was secured in a straight line to the geotextile using wire ties. During installation in the field, grooves were cut in bottom of the CMUs to allow the wire and tubing to pass freely through the facing units. The stainless steel wires were then connected to the draw wire sensors, which were housed beneath an aluminum cover to shield the sensors from the elements.

Resistance Strain Gauges

Resistance strain gages, also known as foil strain gages, were also employed to monitor strains in the geosynthetic reinforcement. A resistance strain gage consists of a grid of annealed constantan foil on a tough, polyimide backing. A known voltage can be passed through the foil grid, and the resistance of the gage is measured. As the gage elongates or contracts, the foil is stretched or compressed, causing a change in the resistance of the gage.

Vishay Micro-Measurements EP-08-10CBE-120 gages were selected for this application. These gages are designed for high elongation, although most gages in the lab failed between 3%

and 4% strain. Strains measured in the field were generally less than 1%, and therefore gage elongation was not a limitation. The gages were installed on the reinforcement for Levels 6 and 14, at the locations shown in Figures 16 and 17. On each side of the abutment at each level of reinforcement, four gages were installed perpendicular to the abutment face, and four gages were installed parallel to the abutment face. In total, 32 gages were installed within the abutment. Because the multiplexor could only read 16 gages at one time, only the gages on the tested side were monitored during testing. The gages on Side A were monitored during construction.

The process of attaching a strain gage to the geotextile is somewhat involved. Therefore, the laboratory installation, calibration, and field installation procedures are documented in the Appendix. The gages were wired in a quarter Wheatstone bridge configuration with three lead wires. This wiring system is simple and eliminates the thermally induced error caused by changes in the resistance of the lead wires due to temperature fluctuations. The gage itself remains sensitive to temperature changes, although these effects were minimal once a cover of fill was placed over the gages. The lead wires were connected to a full bridge completion module at the multiplexor, as the datalogger could only read full Wheatstone bridge circuits.

Although resistance strain gages can provide highly accurate readings, installing these gages on a geosynthetic material requires a calibration between the global strain of the material and the strain recorded by the gage. This calibration procedure is described in the Appendix. Due to this calibration, the accuracy of the gages in this setting is difficult to quantify. Calibration figures presented in the Appendix suggest that the accuracy is good at the strain levels of interest for this project.

Data Acquisition System

A Campbell Scientific CR1000 datalogger was used to record instrument readings for the EPCs, DWEs, and strain gages during construction and testing. Three Geokon 8032 multiplexors were used to accommodate the large number of instruments, one each for the EPCs, DWEs, and strain gages, respectively. An AVW-200 signal analyzer pre-processed the signal from the vibrating wire pressure cells before it was recorded by the datalogger.

Survey data were stored in the total station instrument and transferred to a laptop computer. The settlement profiler was monitored using a Geokon GK-404 handheld readout device, and the data were recorded by hand.

Testing Procedures

The abutment was tested by introducing the solvent to one region of geofoam and monitoring the resulting changes. Testing was performed in the following order: Region A1, Region A2, Region B1, and Region B2 (see Figure 3 for illustration of these regions). The following paragraphs provide additional details on the general testing procedure and the differences in the testing procedure for Test B1.

General Procedure

Prior to each test, the soil berm used in construction of the RSF was excavated and removed from the perimeter of the area where support would be removed. The intent of removing this berm was to account for the loss of this additional support to the RSF that would occur in some cases of differential settlement, such as scour-induced settlements. Figure 24 shows this berm removed prior to Test A1.

Figure 24. RSF Berm Removed for Test A1

After removing the berm, the valve(s) regulating the flow of solvent to the foam region were opened, and solvent was pumped into the packaged foam region using a hand-operated pump at a rate of approximately six gallons per minute. From the volume of solvent used by Sloan et al. (2013), it was calculated that 12 gallons of solvent would be adequate to dissolve each of the foam regions, regardless of the thickness of the foam. Due to uncertainty in the actual pumping rate, the target volume was increased to 18 gallons to promote complete dissolution of the foam.

Following introduction of the solvent, the geofoam dissolved over a period of several hours. Data from total station surveys and earth pressure cells were monitored as the primary indicator of the progress of the test. Once the earth pressure cell readings showed no significant stress changes within the fill and the survey data indicated settlements of less than 0.003 ft over 24 hours, the test was considered complete. Data from the strain gages did not always demonstrate asymptotic trends by the end of testing, but testing could not be prolonged indefinitely to attain this result. The length of each test is given in Table 2. Very shortly before the beginning of Test B1, the signal analyzer for the vibrating wire instruments failed. Test B1 was initiated due to schedule constraints while the replacement part was ordered and installed. The test was allowed to run long enough for the replacement part to be installed and final readings to be obtained, leading to a longer test duration.

Table 2. Test Durations

Test	Duration (days)
A1	5
A2	13
B1	23
B2	14

Test B1

Test B1 proceeded with some slight differences from the other three tests. After introducing the solvent, it was noticed that the dissolution of the geofoam was occurring more slowly than usual and progressing from the corner where the solvent was introduced inward, rather than evenly across the entire area. A hypothesis was formed that water had infiltrated the solvent containment system and filled the geonet. The solvent, which is lighter than water, would float on top of the water and be unable to spread uniformly through the geonet located beneath the foam. This hypothesis accounted for the high level of solvent observed near the insertion point and the progression of dissolution from the insertion point laterally towards the opposite corner. Over the course of that afternoon and the following morning, an access channel was excavated through the RSF and the intact foam to access the geonet. The fluid in the bottom of the pit was removed, first by pumping and then using a sponge. In addition to the volume of solvent pumped in, approximately 10 additional gallons of fluid were removed. This fact supports the water infiltration hypothesis.

After removing as much fluid as possible, the disturbed area was reconstructed, and new solvent was introduced at this location. The test proceeded in the usual manner from that time forward, with evenly distributed settlements. The condition of the abutment at the end of Test B1 appeared to be in consistent proportion to the other test areas and did not appear to reflect differences resulting from the different testing procedure.

RESULTS AND DISCUSSION

This section presents data and observations from construction and the four testing sequences performed on the experimental abutment. The observations and conclusions from these tests reflect the behavior of one abutment geometry subjected to four specific combinations of area and depth of support removal.

This section begins with construction and general testing observations that include photographs of the abutment after each testing sequence. Subsequently, instrumentation data are presented and analyzed for each type of instrumentation, beginning with construction observations and then sequentially examining the results of each test. Next, based on the observations of abutment performance, three potential methods of mitigating the vulnerability of the reinforced fill are presented. A discussion of the authors' investigation into repair methods for the abutment follows, and the section concludes with recommendations for future research.

Construction Observations

Although construction of the test abutment utilized a crew of two or three students who did not have prior experience with GRS construction, the crew found that they were able to carry out the construction operation without undue difficulty. In total, construction and instrumentation of the abutment, including placement of the surcharge load, took 35 working days. A photograph of the completed abutment was presented previously in Figure 15. Instrumentation data were collected during construction and are discussed later in this report.

The FHWA manual by Adams et al (2011) was consulted as the primary reference for construction. The authors found the construction guidance in the manual to be accessible and generally easy to reference, with a number of helpful photographs.

General Testing Observations

Post-testing deconstruction of the abutment revealed that the geofoam inclusions had been fully dissolved during the testing process. Figure 25 shows the abutment prior to testing. The RSF at Region A1 has been dug out prior to testing, but no solvent had been introduced at that time. Black lines can be noticed between some of the CMU courses; these lines are short lengths of reinforcement extending past the front of the CMUs and are not gaps. On the left side of the abutment, coiled gray wires from the strain gages on Side B can be seen. The wires were waterproofed and were connected to the multiplexor prior to testing on Side B.

Figure 25. Front View of Abutment Before Testing, RSF Removed Around Region A1

Photographs documenting the performance of the abutment through all four stages of testing are presented in Figures 26 through 33. While viewing the photographs, it should be remembered that the area and magnitude of settlements induced on the structure represent very extreme loading conditions for this abutment geometry. Two photographs are shown of the abutment following each test. One photograph shows the abutment from the front, and the other shows a close-up view of the affected corner. Photographs of the corners of the abutment often show white lines painted on the RSF; these lines mark the lateral extent of each geofoam region. Recall that the upper three courses were filled with concrete and pinned together, which caused them to behave similar to a cantilevered beam. While difficult to identify in these photographs, vertical cracks formed through the concrete-filled CMUs, which led to small settlements. The vertical cracks were most noticeable following Tests A2 and B2 directly above the interface between the compacted fill subgrade and the geofoam dissolved in Tests A2 and B2.

The blocks at and near the corners of the abutment appear vulnerable after they have experienced settlements. This observation is particularly apparent following tests on Side B, as shown in Figure 31 and Figure 33. This experiment tested only the response of the abutment to differential settlements. If water action were introduced, as would occur in a scenario of scour-induced settlement or of heavy stream flow after large differential settlements due to foundation compression, it is quite conceivable (and perhaps likely) that the combined effects of buoyant and viscous water forces could remove some of these blocks and expose the fill to erosion. This scenario could lead to serious damage or failure of the abutment. Some considerations to mitigate this potential hazard are discussed later in this report.

Figure 26. Front View of Abutment After Test A1

Figure 27. Corner a of Abutment After Test A1

Figure 28. Front View of Abutment After Test A2

Figure 29. Corner a of Abutment After Test A2

Figure 30. Front View of Abutment After Test B1

Figure 31. Corner B of Abutment After Test B1

Figure 32. Front View of Abutment After Test B2

Figure 33. Corner B of Abutment After Test B2

The deformation pattern of the facing blocks demonstrates a predictable, stair-step pattern that begins at the edge of the region where support is removed. Particularly for smaller regions of support removal, the CMUs are able to bridge over the region of support loss and minimize settlements of the overlying CMUs. This pattern is similar to the support condition within the reinforced fill, which is able to support the full width of the surcharge load even after support beneath a large portion of the foundation has been removed. On Side A, the deformation patterns induced by Test A1 are erased by the patterns of Test A2, suggesting that the same deformation pattern would be seen if the support of Regions A1 and A2 had been removed at one time rather than in two steps. The behavior on Side B suggests similar trends, although the larger magnitude of settlement increases the extent to which Test B1 influenced the final settlement pattern following Test B2.

Additionally, these figures show that the facing blocks rotated outward and away from the center of the abutment as they settled. During all tests, but particularly after removal of the larger area of support on both sides, the rotation was more pronounced toward the face than toward the wing walls. Movement of the fill behind these blocks during settlement is believed to have followed a similar pattern. This behavior is believed to result from three-dimensional effects of the abutment configuration, including the dimensions in plan of the support removal, the additional restraint provided by the ramp to the abutment fill and wing wall CMUs, and the longer embedment length of the reinforcement in the direction parallel to the abutment face than in the direction perpendicular to the abutment face.

Figure 34 presents a side-by-side comparison of the abutment prior to and after all testing sequences. The figure is not intended to show the details of the deformation patterns, but rather to demonstrate that, despite removing support beneath much of the foundation area, the abutment was still able to adequately support the surcharge load. Clear space was maintained between the surcharge load blocks and the front safety blocking through all tests.

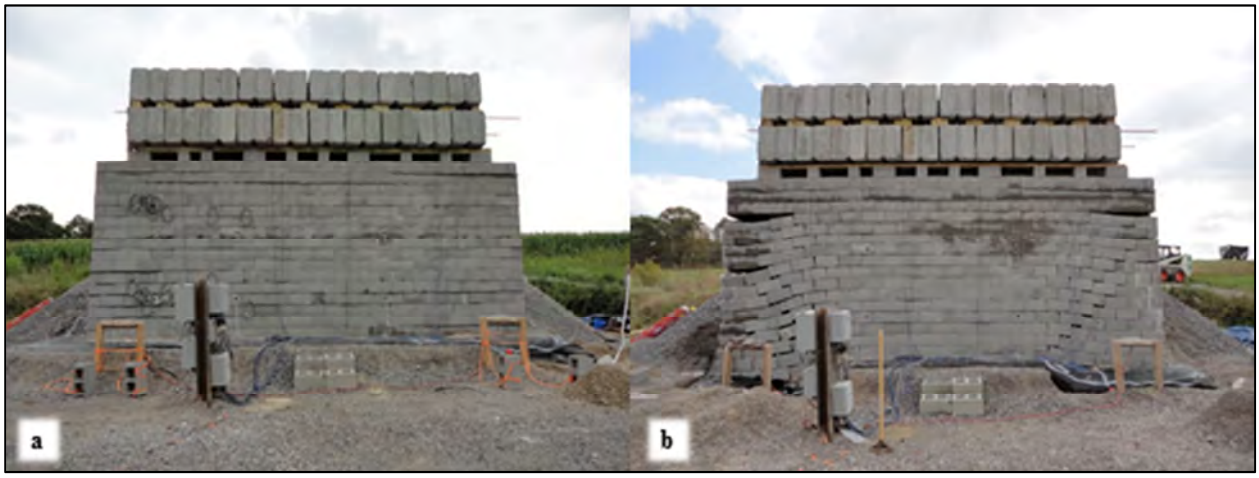

Figure 34. Comparison of Abutment (a) Before and (b) After All Testing Sequences

Instrumentation Data

In the following five sections, the observations captured by the many types of instrumentation during testing are presented, analyzed, and discussed. Settlements of points on the surface and face of the abutment are discussed first, followed by settlement of the fill as captured by the settlement profiling tubes. Earth pressure cell data are discussed next. Strain data captured by the draw wire extensometers and foil strain gages are discussed in the final two sections, respectively.

Survey Targets

A full survey of the abutment was completed before and after each testing sequence. This section briefly discusses the important trends observed in the survey data for each of the four testing sequences and compares data from Sides A and B. Survey data were primarily used as a reference when analyzing data collected by other instruments, although important trends are discussed in the following sections. If details of the CMU settlement pattern are desired, the photographs presented in Figures 26 through 34 may prove helpful. A predictive equation to estimate settlement of the facing CMUs is presented, and the key observations of the survey data are summarized.

General

Targets placed on the CMUs were shot directly with the total station, and targets on the surface of the RSF and abutment were shot using a handheld rod and prism. The total station could measure position in three dimensions with an accuracy of 0.005 ft, or 0.06 in. For targets

measured using the handheld rod, the variations were slightly larger due to the challenge of placing the rod in exactly the same position, setting the rod height precisely, and keeping the rod plumb for each measurement. During all tests, the settlement of the surcharge load was closely monitored to anticipate any potential instability of the load. No differential settlement was measured between the targets on either end of the surcharge load, indicating that the load did not tip towards the face of the abutment. Visual inspection and survey data indicated that the load remained stable throughout all testing sequences.

Figures 18 through 20, presented earlier in this report, show the location of the survey targets on the abutment. Figure 35 shows the baseline survey data for the abutment prior to any testing, viewed from the perspective of Side A of the abutment. Corresponding survey data were also obtained for Wing Wall B of the abutment but are not visible from the perspective of the figure. The survey targets on the front and the ends of the surcharge load have been omitted from this figure for clarity. In Figure 35, the single line of targets on the surface that runs the length of the abutment is the line of targets located on the front of the surcharge load foundation. On either end of the surcharge load is a short line of five survey points. Behind the surcharge load is a 4 by 12 grid of survey points at 2 ft spacing. The points in the row closest to the abutment face are located on the surface of the bearing bed and are approximately 4 in above the other three rows of points.

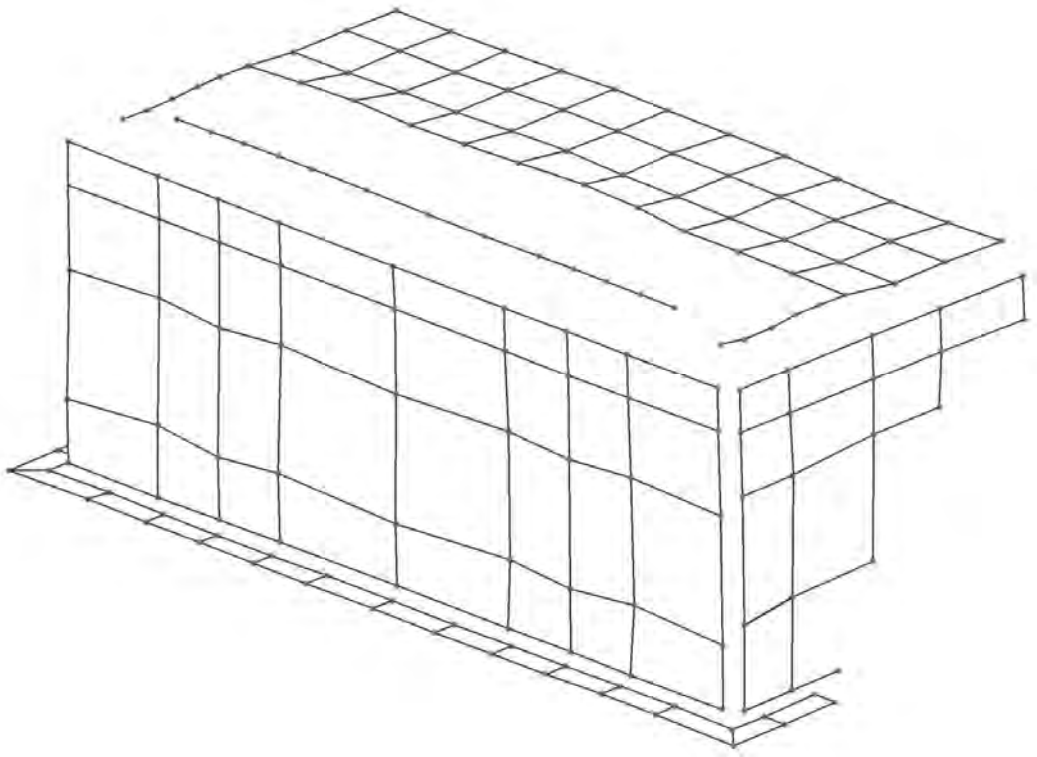

Figure 35. Baseline Survey Data for Abutment, From Perspective of Side A

Tests A1 and A2

Survey data collected after Test A1 and Test A2 are presented in Figure 36. In the figure, the lightest gray lines represent the baseline data. The darker gray lines represent data collected after Test A1, and the black lines represent data collected after Test A2. Settlements of less than 1 in are difficult to distinguish at this scale, but the overall trends are clear and logical. Settlements decreased with increasing height and with distance from the corner of the abutment.

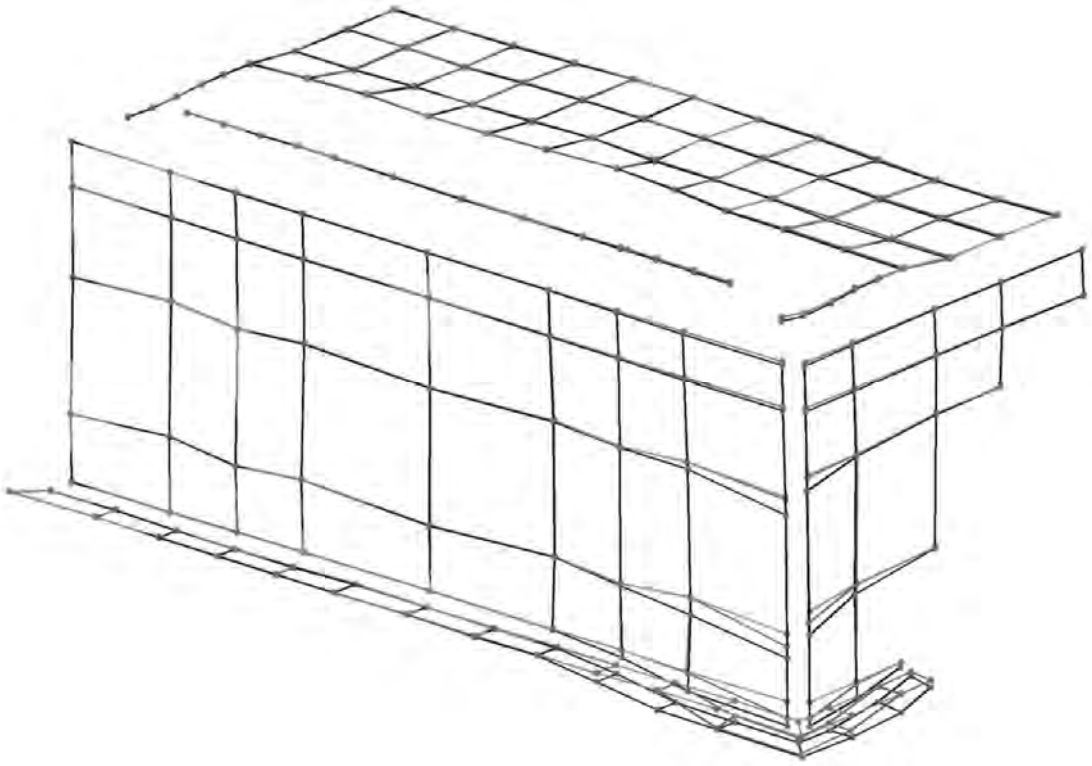

Figure 36. Deformations of Side A of Abutment From Survey Data

The settlement of the foundation for the surcharge load in response to dissolving the geofoam is shown in Figure 37. Data for the targets on the surcharge blocks are not plotted but follow the same trends as the foundation. During Test A1 and Test A2, the foundation rotated downward on Side A as the fill beneath it settled. Settlement in Test A1 was 0.08 in at the right-most target, and the left-most target moved up 0.07 in during rotation of the foundation. Test A2 resulted in a settlement of 0.58 in at the right-most target, the largest settlement of the foundation observed during any test. Small settlements continued at the right end of the foundation after the completion of Test A2. Because Test A2 induced small settlements at the left side of the foundation, it is possible that these additional settlements on the right hand side after completion of Test A2 are the result of testing on Side B. However, small settlements of the CMUs on Side A also continued after the completion of Test A2, and the magnitude of the CMU settlement is very similar to the magnitude of the foundation settlement. Therefore, it is more likely that the continuing settlements of the foundation on the right hand side resulted from continued settlement of the fill on the right hand side and would have occurred even if no testing had occurred on Side B.

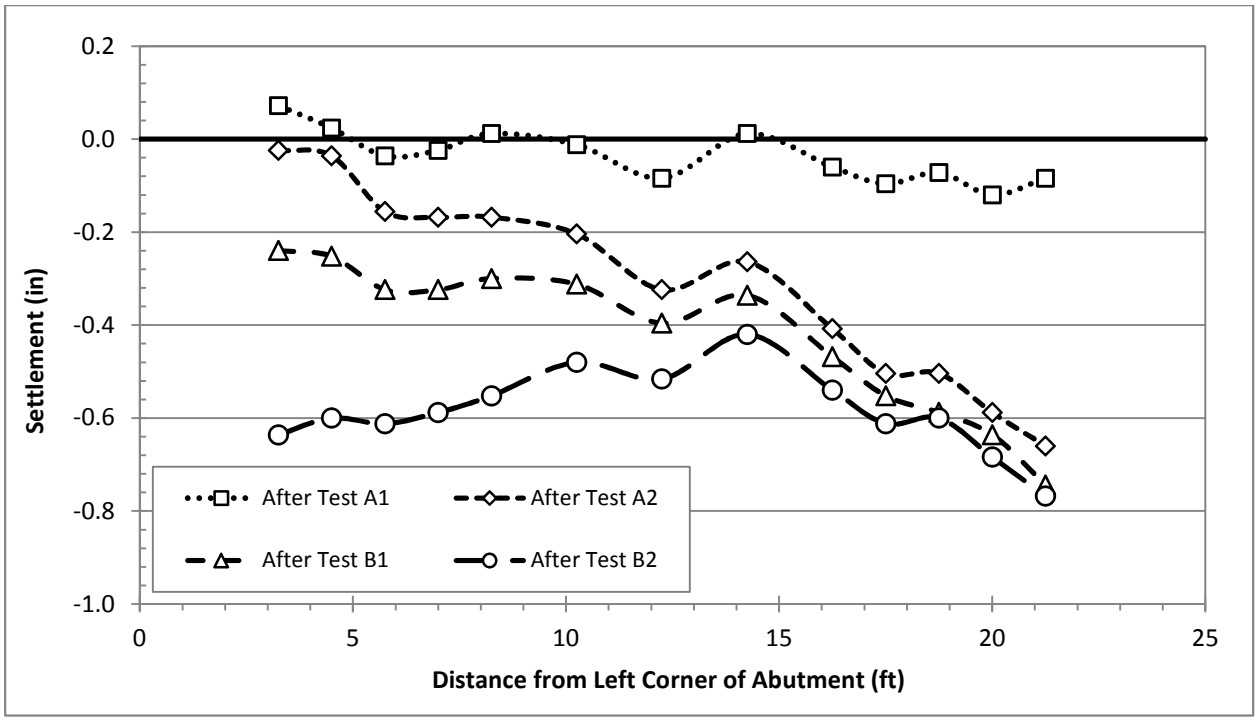

Figure 37. Settlement of Surcharge Foundation

Survey points on the surface of the abutment fill generally exhibited minimal settlements of less than 0.10 in during Test A1 and settlements between 0.10 and 0.30 in during Test A2. The five survey points located between the surcharge load and Wing Wall A were the only points to show settlements outside this range. Settlements at these points were as high as 0.30 in during Test A1 and 1.09 in during Test A2. Settlements decreased with distance from the region of support loss.

Tests B1 and B2

Survey data collected after Test B1 and Test B2 are presented in Figure 38. In the figure, the lightest gray lines represent the baseline data, collected after Test A2. The darker gray lines represent data collected after Test B1, and the black lines represent data collected after Test B2. Again, settlements less than 1 in are difficult to distinguish at this scale, but the overall trends are clear and logical. Blocks at Level 1 near the corner settled slightly in excess of 16 in, indicating complete geofoam dissolution and shifting of the RSF backfill during settlement that allowed the blocks to settle more than the amount of support removed. Settlements decreased with increasing height and with distance from the corner of the abutment.

Figure 37 shows the settlement of the surcharge foundation during Test B1 and Test B2. As with the tests on Side A, the foundation settled and rotated toward the side where support was removed. The far left target on the foundation settled 0.22 in during Test B1 and 0.40 in during Test B2. However, the data show less free rotation; rather, the wood foundation was subjected to flexure, with the point of maximum curvature at a position of approximately 14 ft from the left corner of the abutment.

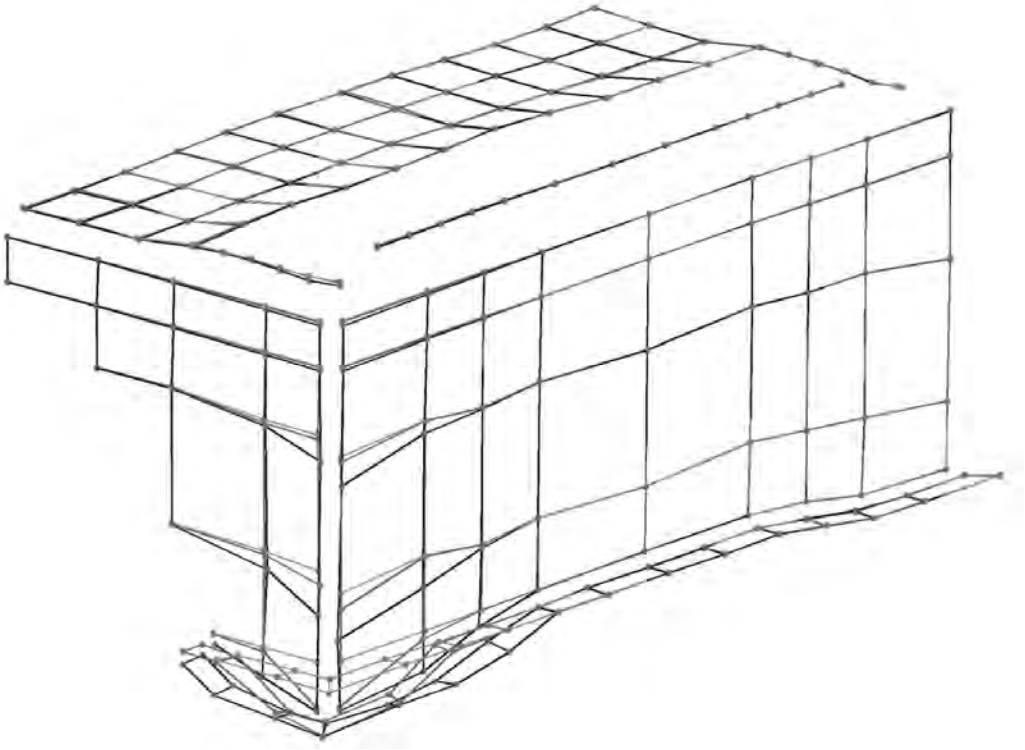

Figure 38. Deformations of Side A of Abutment From Survey Data

The flexural resistance of the tensioned surcharge blocks and the wood beams, which were 8-in-square timbers, likely contributed to a smaller observed settlement of the surcharge load during Test B1 and Test B2 than during Test A1 and A2.

Survey points on the surface of the abutment generally saw minimal settlements of less than 0.10 in during Test B1, although some settlements were as high as 0.20 in. Settlements during Test B2 generally ranged from 0.10 in to 0.40 in. The five survey points located between the surcharge load and Wing Wall A were the only points to show settlements outside this range. Settlements during Test B1 were approximately 0.20 in, and settlements during Test B2 were as high as 1.35 in. Settlements decreased with distance from the region of support loss.

Comparison of Results from Side A and Side B

As expected, settlements of the CMUs were greater on Side B. CMUs on Side B that were located over the region of support loss and low enough to lose support generally settled about twice as much as the corresponding CMUs on Side A. When the CMUs were high enough relative to the area of support loss that the underlying CMUs could offer some support, following the stair-step pattern described previously, the settlements tended to be only slightly higher on Side B than on Side A.

The surcharge foundation settled more on Side A than on Side B, for reasons previously outlined. However, five survey points were located on the surface of the abutment adjacent to each end of the surcharge load. These points revealed that the reinforced fill settled about 15%

more on Side B than on Side A in the 2 ft closest to the abutment face. Survey points on the surface of the abutment behind the surcharge load showed small increases in settlement on Side B compared to Side A. These differences were reduced or eliminated as the distance from the region of support loss increased.

The maximum angular distortion of the surcharge foundation, which is the ratio of the differential settlement of two adjacent points to the distance between these points, was 0.008 and occurred during Test A2. Coduto (2001) notes that an angular distortion of 0.008 is the maximum allowed for bridges with simply supported spans when designing to meet serviceability criteria. If the angular distortion is instead measured between the center and the edge of the surcharge load, the resulting average distortion may provide a better indication of the potential distress to the superstructure. Using this approach, the maximum average angular distortion observed during any test was 0.003, which is not likely to cause severe distress. Overall, the abutment maintained acceptable performance with respect to angular distortion of the superstructure.

Development of Predictive Equation

The survey data collected during testing were used to develop a predictive equation that described the settlement of the CMUs observed during the testing sequences. The following paragraphs discuss the development of the predictive equation and the goodness of fit to the data. Although an attempt was made to formulate the predictive equation in normalized terms, it is not yet known if this normalization would apply to other configurations. So, at present, the predictive equation is specific to the conditions of this test set-up.

Only the settlements of targets located above the region of support removal were considered in developing the equation. In addition, the top three courses of CMUs were filled with concrete, which resulted in different settlement patterns for these CMUs. Consequently, the settlements of targets on the upper three levels of CMUs were not considered in determining the coefficients of the fitted equation. These selection criteria resulted in 12 data points each for Test A1 and Test B1 and 15 data points each for Test A2 and Test B2, for a total of 54 data points considered.

A functional form of the equation was developed, which is discussed further in the following paragraphs. Coefficients for the functional form were calculated using the Solver function of Microsoft Excel. The resulting predictive equation is presented in Equation (1). Figure 39 illustrates the *XYZ* coordinate system employed in the equation.

$$\frac{S}{S_b} = \left(\frac{X}{0.5S_b + 2.55t_{RSF}}\right)^{1.07} \left(\frac{Y}{0.5S_b + 2.85t_{RSF}}\right)^{1.09} \left[1 - \left(\frac{Z}{1.04(X+Y)}\right)^{1.22}\right] \quad \text{Equation (1)}$$

where: S = settlement at the desired point

S_b = magnitude of support loss beneath RSF

t_{RSF} = thickness of the RSF

X = horizontal distance from edge of support loss to desired point, measured in the plane parallel to abutment face

Y = horizontal distance from edge of support loss to desired point, measured in the plane perpendicular to abutment face

Z = vertical distance from top of RSF to desired point

All terms raised to a power are restricted to a maximum value of 1.

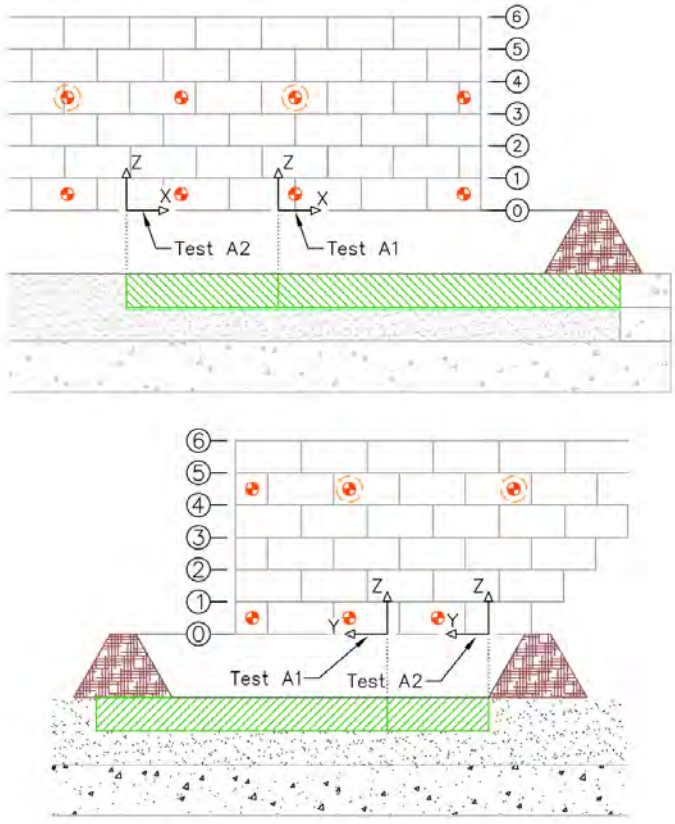

Figure 39. Coordinate System for Predictive Equation

The equation estimates the settlement of a point located over the region of support loss, normalized by the magnitude of support loss beneath the RSF. Therefore, values of S/S_b can range from 0 to 1. The first two terms on the right side of the equation reflect the influence of horizontal distance from the edge of support loss to the point of interest. When this distance is zero, the point is located at the edge of support loss, and the settlement would be expected to be very near zero. As this distance increases, the settlement will increase until it reaches a maximum, which is equal to the magnitude of support lost at the base (S_b). The first two terms reflect this increase with distance in the X and Y directions until reference distances are reached, at which the value of each term is set to 1. The reference distance is a function of the magnitude of support loss at the base and the thickness of the RSF, and it is slightly different in the X and Y

directions. The RSF is much longer than it is wide, and some difference is to be expected in the flexural behavior in these two directions.

The third term on the right side of the equation reflects the influence of height above the top of the RSF. As previously noted, settlements decreased with increasing height above the RSF due to increased support from underlying blocks, extending in a stair-step pattern back to the region of consistent support. The equation defines a critical height, *1.04(X + Y)*, above which the settlement of the CMUs is essentially zero. Therefore, the term raised to the power of 1.22 is also limited to 1. The 1.04 factor suggests that this height is approximately twice the arithmetic average of the X and Y distances to the edge of support loss. This approximation is reasonable, although small settlements are still likely at this height. When the X and Y distances are greater than their respective reference distances and the height above the RSF is zero, the settlement is simply equal to magnitude of support loss.

A comparison of the observed settlement and the settlement predicted by this equation is shown in Figure 40. A quick visual assessment reveals that the fit generally is good, although there are a few outliers. The R^2 value is 0.9223, indicating that about 92% of the data variability is predicted by this equation. The mean of the residuals (the difference between the predicted and observed values) is -0.008, which shows that this estimation is relatively unbiased. Likewise, a histogram of the residual values, shown in Figure 41, closely approximates a normal distribution. This trend suggests that the errors in the predictive equation are randomly distributed about the mean.

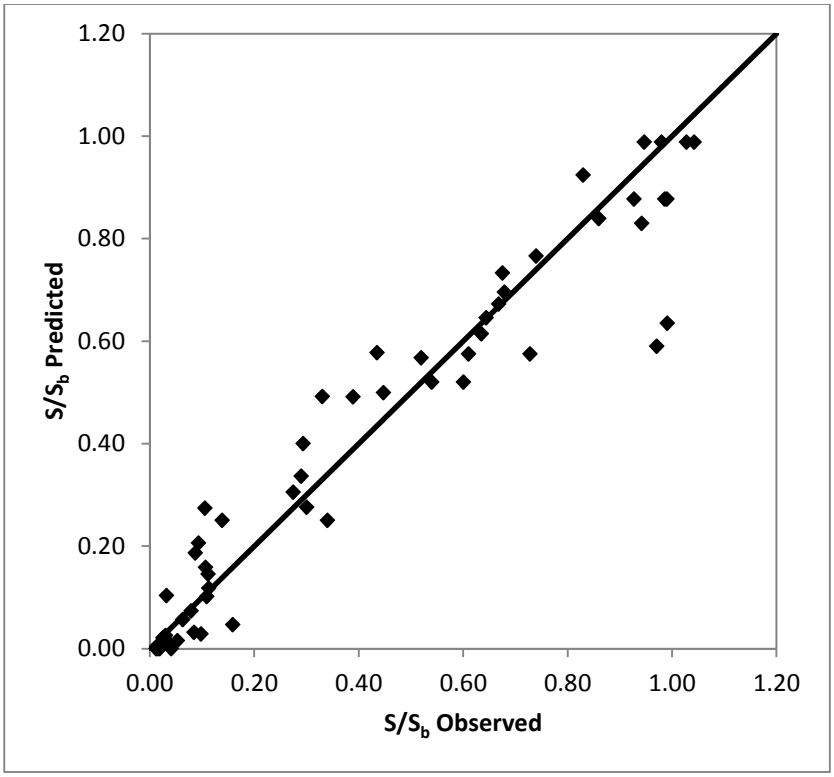

Figure 40. Comparison of Observed and Predicted Settlements

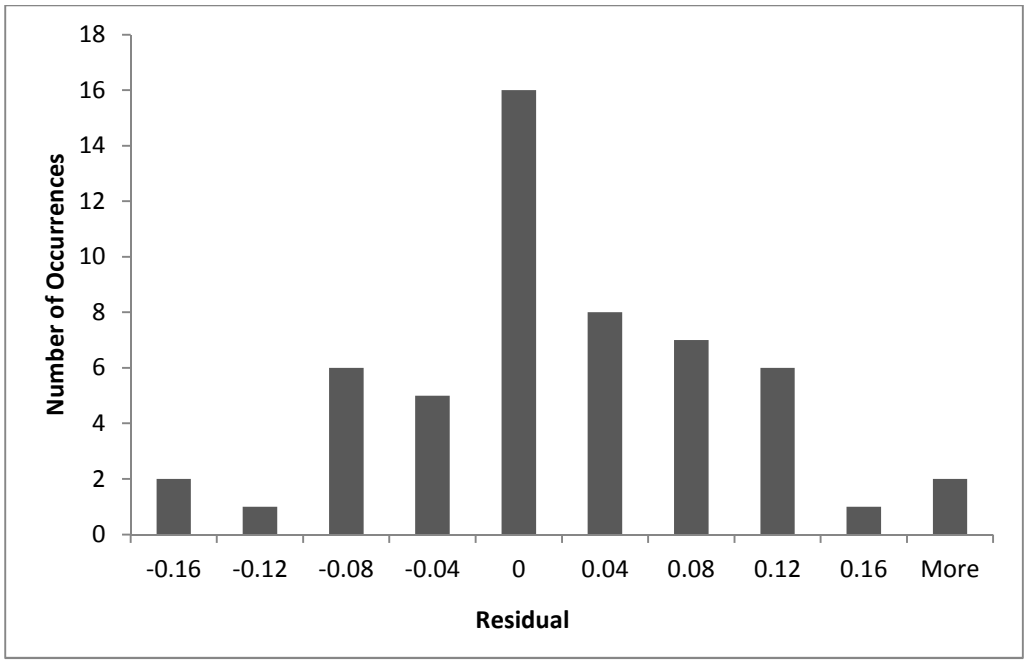

Figure 41. Histogram for Distribution of Residual Values

This predictive equation generally provides reasonable estimates for the settlements observed for the CMUs in the lower two thirds of the abutment. It may be used to obtain an estimate of the settlement that would occur if the abutment were subjected to a support loss of known magnitude and geometry. Larger predicted settlements imply larger gaps between adjacent CMUs, which would result in greater exposure to the fill. The estimate may not be as accurate for the upper third of the abutment, since there are no data with which to calibrate the predictive equation. For example, the predictive equation only predicts settlements at the highest level of CMUs when the X and Y values are large. However, it is expected that some settlement, albeit small, would occur at these CMUs even if the X and Y values are small. While the support of underlying CMUs greatly reduces the settlement of overlying CMUs, the height expected for the settlements to fully reach zero is anticipated to be large.

Key Points

- The surcharge load remained stable throughout all testing sequences.
- Settlements at the surface decreased with distance from the region of support loss.
- The maximum angular distortion of the surcharge load in the plane parallel to the abutment face was 0.008, and the maximum average angular distortion between the center and edge of the surcharge load was 0.003. Both measures are within the range of acceptable serviceability values for simply supported spans.
- The reinforced fill significantly reduced the settlements observed at the surface compared to the base of the abutment and provided acceptable performance for the surcharge load.

- A predictive equation was developed to estimate the settlement of the CMUs if the geometry and magnitude of the region of support loss is known.

Settlement Profiling Tubes

Settlement data were collected using the profiling instrument and tubes before and after each test. This section briefly discusses the data collection procedure and sources of data variability, examines important trends from the settlement profiling data for each of the four testing sequences, and compares the data with survey data for the surcharge load. Subsequently, the dimensions of the regions experiencing settlements are compared using the settlement profiling data and survey data from the surface of the abutment. Finally, key points are summarized.

General

Readings were taken before and after each test for the tubes running through the abutment parallel to the face. Tubes running into the abutment perpendicular to the face on Side A were read before and after Test A1 and Test A2, as well as after the completion of all tests. Tubes running into the abutment perpendicular to the face on Side B were read before and after Test B1 and Test B2.

Data readings were taken using a handheld readout and recorded manually. While the principles on which the settlement profiling instrument operates are straightforward, a number of sources of potential errors are present. The reservoir of the profiler is open to the atmosphere through a small bleed-screw hole, which is intended to maintain a constant head. However, barometric pressure variations with changing weather patterns, which are common in southwest Virginia during the summer, can affect this constant head. Wind that passes over the bleed-screw hole can induce pressure changes according to Bernoulli's principle. Both the vibrating wire piezometer and the readout, which powers the piezometer, also demonstrated sensitivity to temperature changes. Each of these effects is a potential source of variation in the data. In general, the quality of the readings appeared to improve with time as the authors learned measures to take to diminish the effect of these factors. In a few instances, the readings seemed to indicate movement of the tubes that would appear to be physically impossible. However, when these movements are viewed in the context of the overall scale of the measurements, they generally are not significant.

The configuration of the profiling tubes is presented in Figures 16 and 17. The subsequent analyses refer to these previous figures as necessary. The data collected following each of the testing sequences are presented in Figures 42 through 48. In these figures, the individual graphs are arranged in the same configuration as the settlement profiling tubes when looking at the abutment face. All figures use a consistent vertical axis to facilitate comparisons of settlement magnitudes at various locations. Additionally, the horizontal axis scales are consistent for all similarly oriented tubes.

Profiling tubes were oriented along both horizontal axes of the abutment. For each side of the abutment, these tubes overlapped at ten locations. Settlement data for each of the tests can

be compared at these ten locations. It is reasonable to expect these data to vary slightly since they are located in different levels of the abutment. In most cases, the points of overlap record settlements that are within 0.2 in of each other, and the smaller settlement is usually the overlying tube. Of the cases in which the difference is larger than 0.2 in, nearly all of these tubes are located directly over the region of support removal, where the reduction in settlement at each successive level is more significant. In these situations, the settlement of the overlying tube was smaller than that of the underlying tube. Therefore, the settlement profiling observations appear to be consistent with each other.

The settlement trends of the tubes can also be projected to the face and compared with the optical survey data measured at nearby targets. In most cases, the two types of survey data are also consistent with each other.

Test A1

Figure 42 shows the settlement of the four tubes oriented perpendicular to the abutment face on Side A. During Test A1, settlements at these locations were small (less than 0.4 in). Tubes SP-A4-2 and SP-A10-2 are located over the compacted fill subgrade. Settlements at these locations result from fill redistribution within the abutment to compensate for the loss of support near the corner and are not expected to be large. The small settlements at SP-A4-1 and SP-A10-1, which are located over the region where support was removed, indicate that the abutment was able to bridge over the region of support loss. This bridging action begins at the edge of the region of support loss and extends out over the region of support loss, with each successive lift of reinforced soil supporting more of the overlying lift than the lift below, thereby reducing the settlement at higher-elevation lifts.

Figures 44 through 48 show the settlement of the five tubes oriented parallel to the abutment face. Figures 44 and 45 show a maximum settlement of about 0.5 in at SP-11-1 and SP-5-1, respectively. Trends in Figures 46 and 48 show essentially no settlements at SP-11-2 and SP-11-3, respectively. In Figure 47, data for Test A1 at SP-5-2 show variations in tube elevation where there should be very little or none. The authors suspect that the Test A1 variations in SP-5-2 readings were due to the sources of error described above.

Comparing the settlement data with the survey data shows that the reinforced fill settled more than the facing CMUs at all locations where the settlement of the fill was measured during Test A1. When this scenario occurs, the slope of the settlement line reverses at the point of maximum deflection of the settlement tube. This trend is difficult to distinguish in the data for Test A1 due to the small settlements of both the CMUs and the fill, but it is easier to identify in the data for later tests. When this trend is present, the location of maximum settlement of the fill is generally between 2 and 3 ft behind the wall face. The end of the tube is relatively fixed where it passes through the CMU at the face, and therefore this offset represents the distance required for the tube to deflect downward and reach the point of maximum settlement of the fill. In reality, the location of maximum settlement is likely much closer to the back of the CMUs.

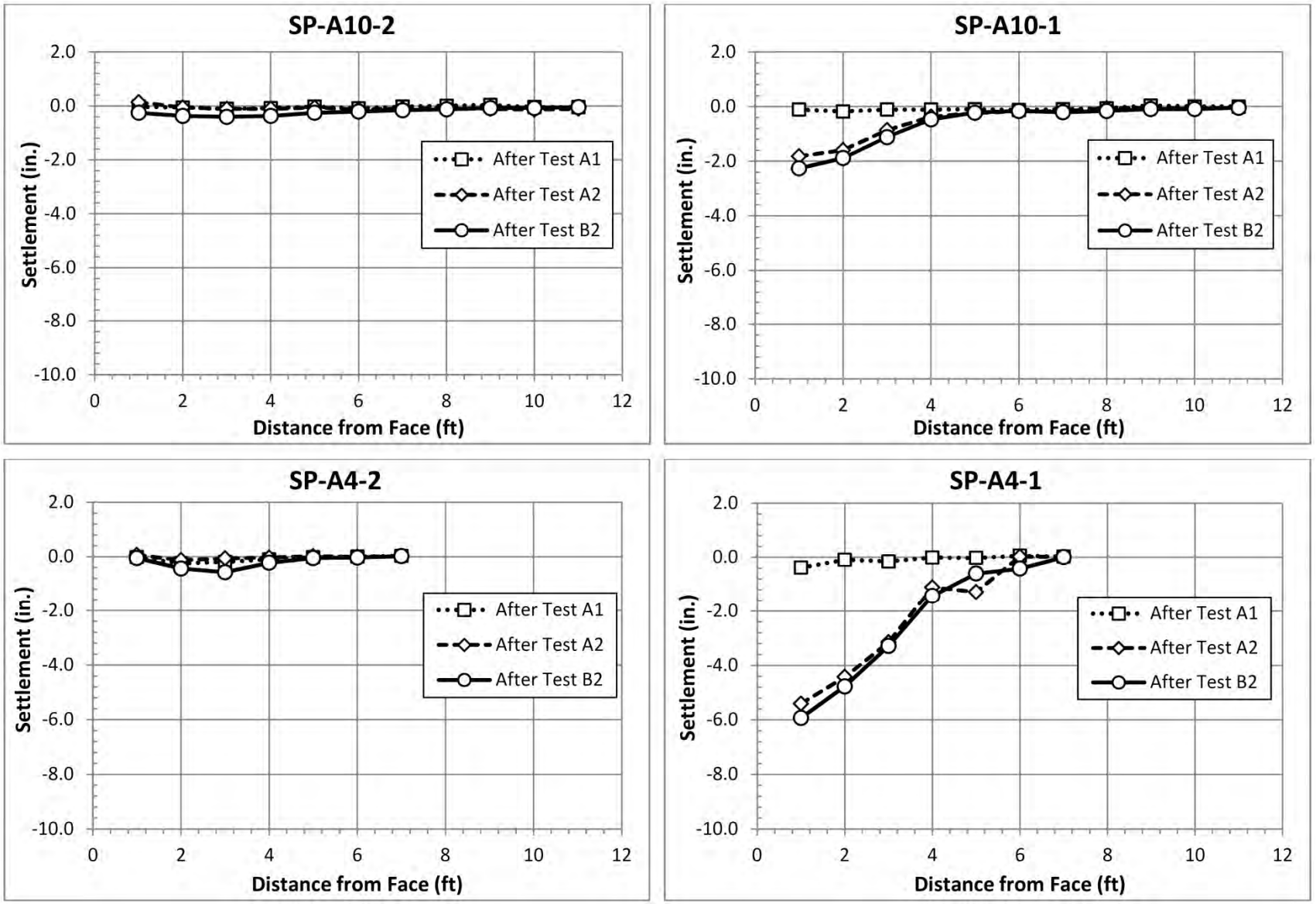

Figure 42. Settlement Profiler Data for Tubes Perpendicular to Abutment Face on Side A

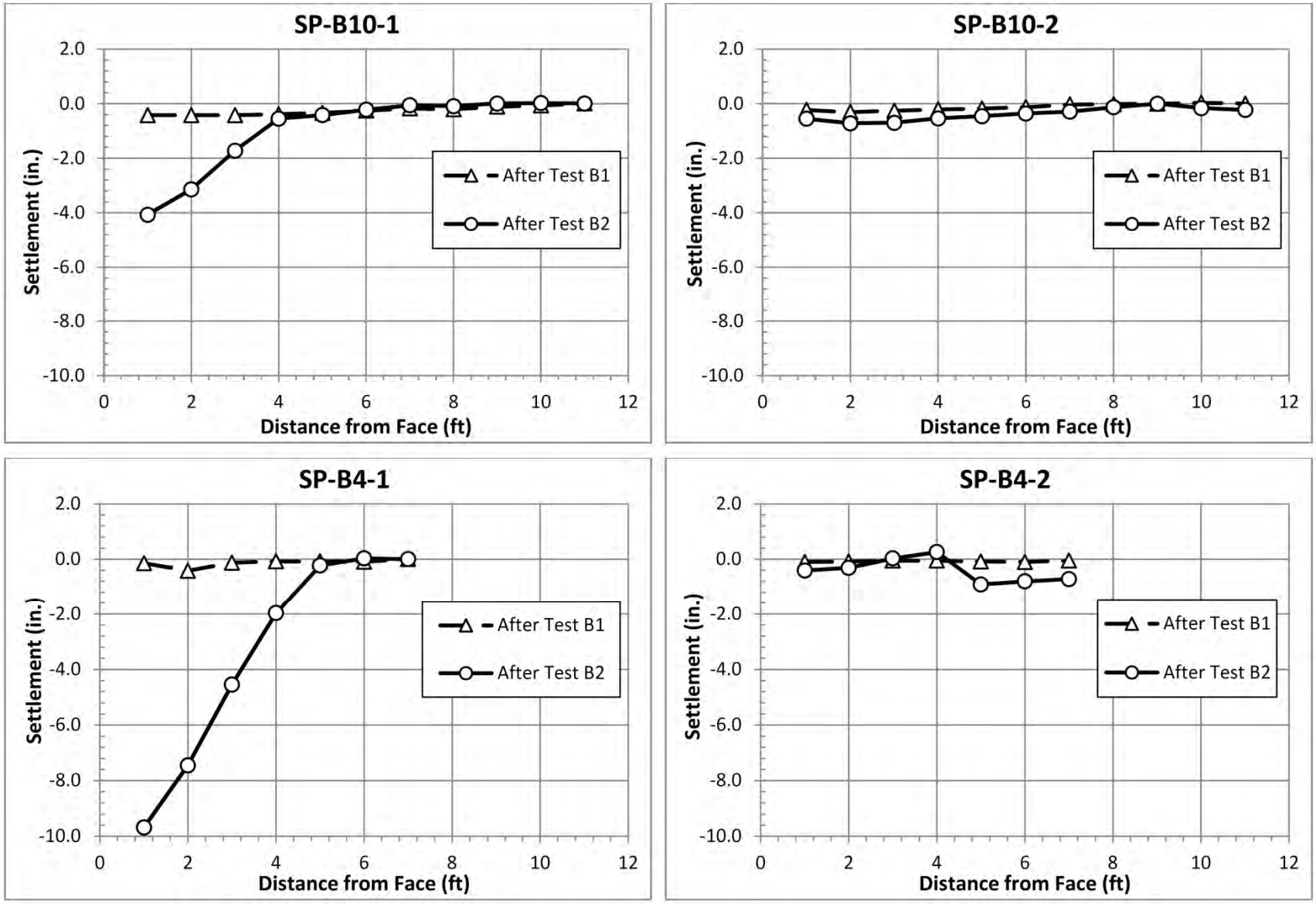

Figure 43. Settlement Profiler Data for Tubes Perpendicular to Abutment Face on Side A

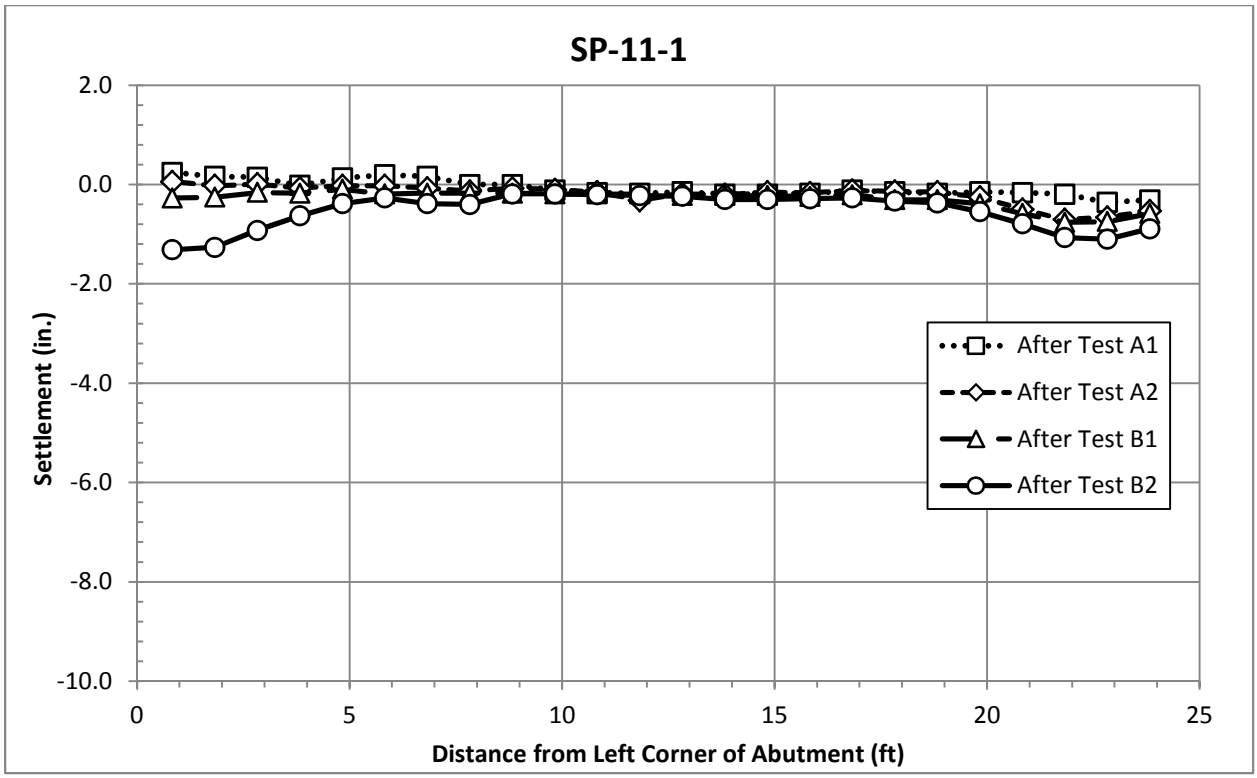

Figure 44. Settlement Profiler Data for SP-11-1

Figure 45. Settlement Profiler Data for SP-5-1

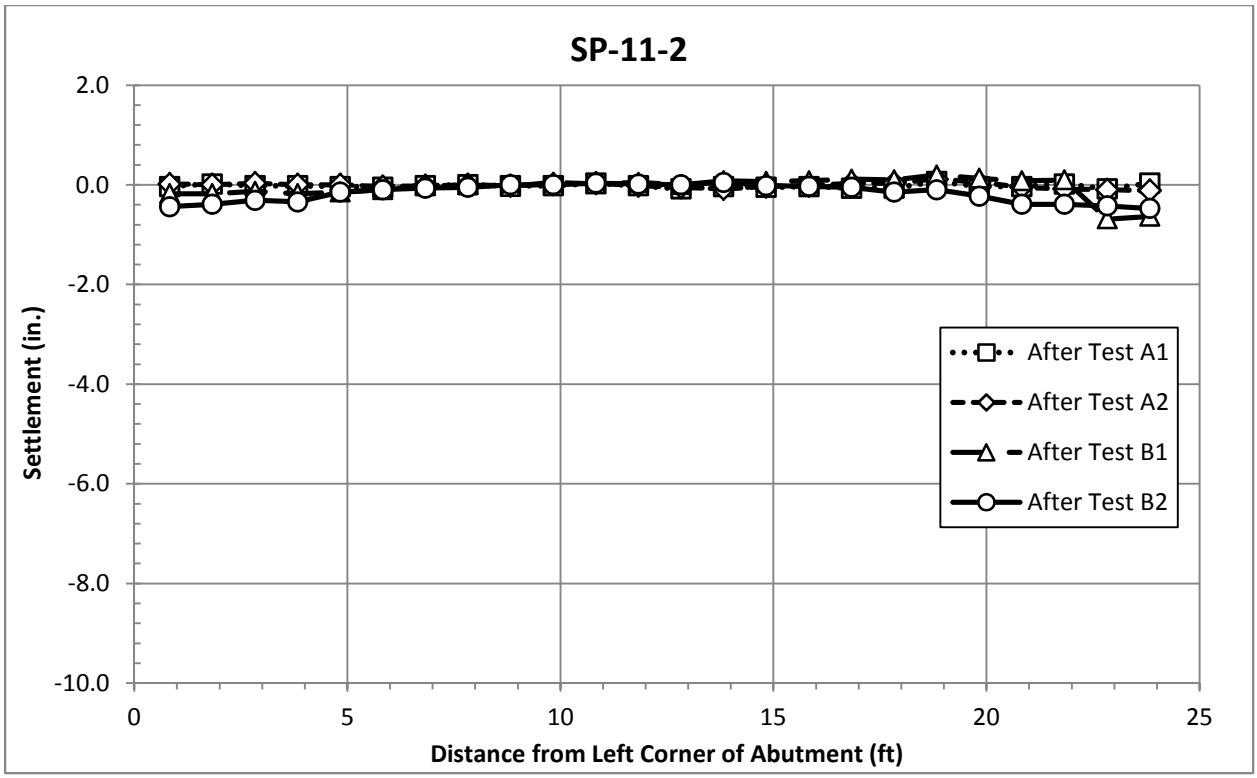

Figure 46. Settlement Profiler Data for SP-11-2

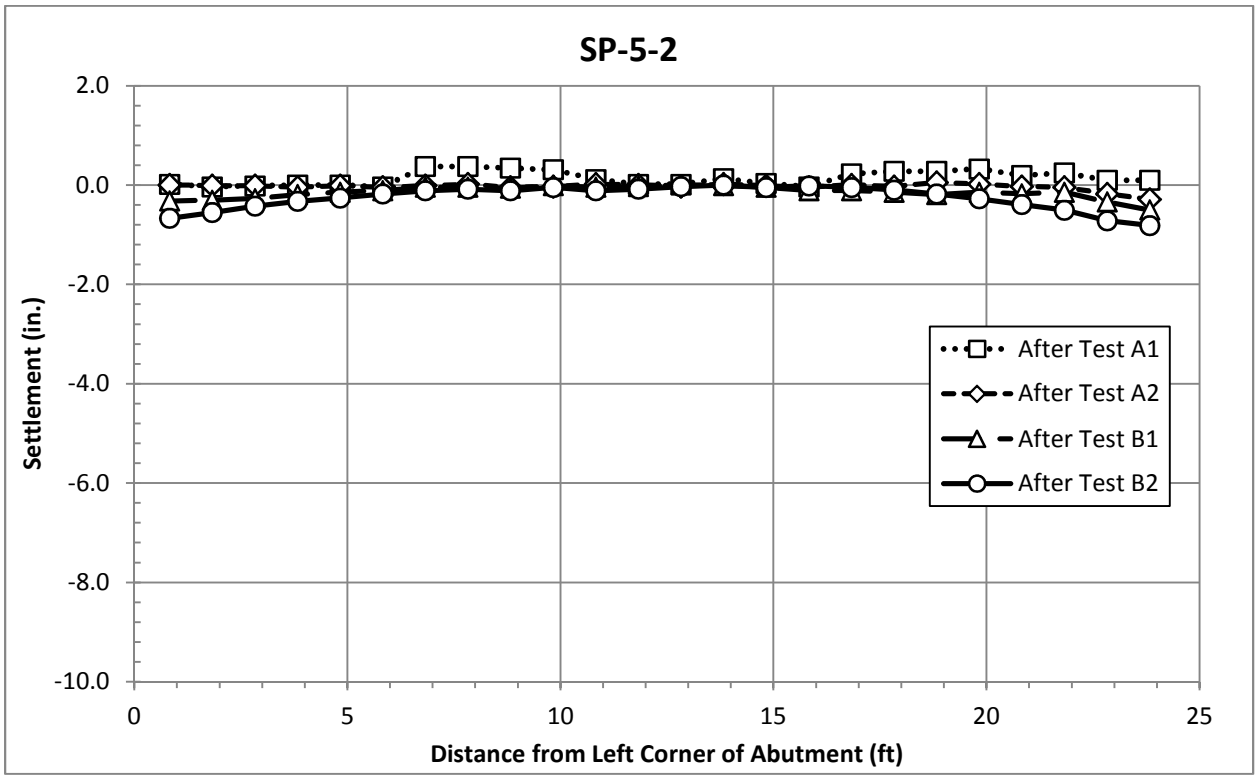

Figure 47. Settlement Profiler Data for SP-5-2

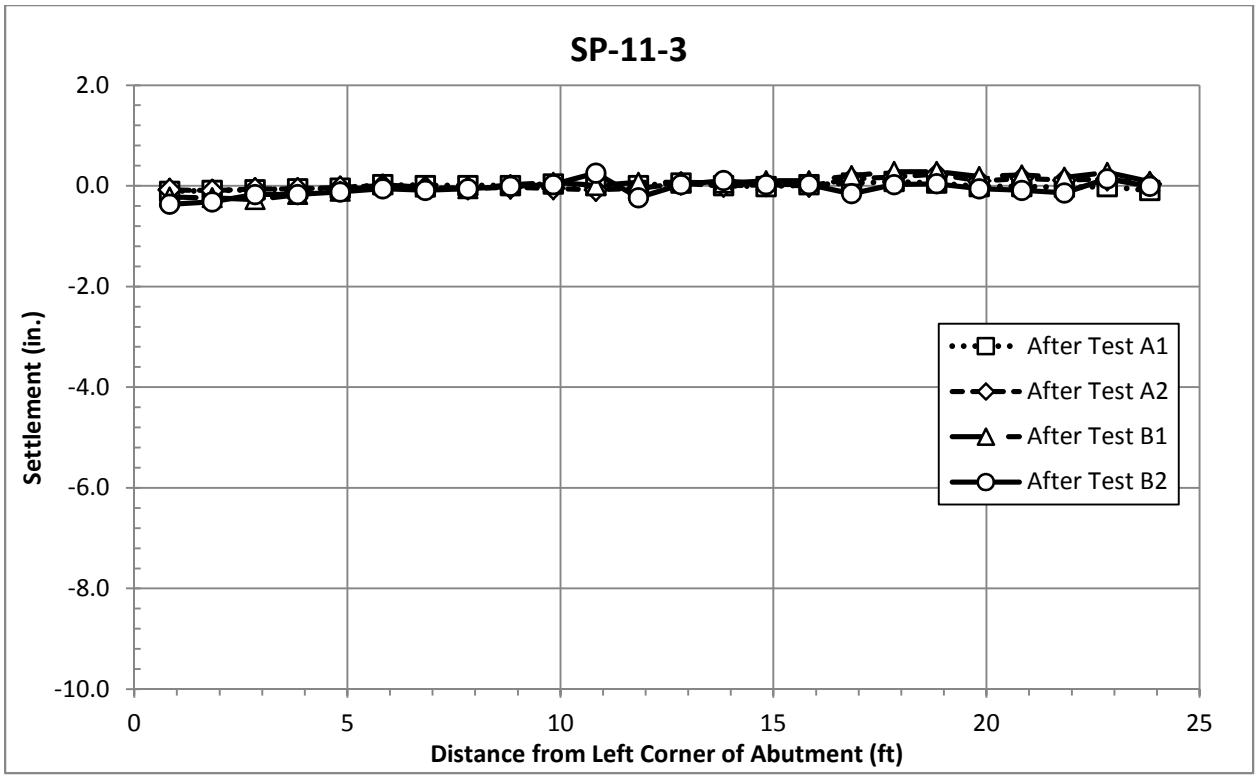

Figure 48. Settlement Profiler Data for SP-11-3

Test A2

Figure 42 shows that the settlement of the fill was generally larger for the four tubes oriented perpendicular to the abutment face after Test A2 than the settlement after Test A1. The two tubes located over the region of support removal (SP-A4-1 and SP-A10-1) settled significantly more during Test A2 than Test A1. The data for SP-A4-2 show that the elevation of the tube increased approximately 0.10 in at many locations after Test A2. These are small amounts compared to many of the other settlement readings shown in Figure 42, but they are believed to be incorrect because an elevation increase at this location does not seem to be a reasonable response to dissolving the geofoam in Region A2. The settlement recorded after the conclusion of all tests, i.e., after Test B2, can be considered as an upper bound to the settlement after Test A2. Therefore, SP-A4-2 settled no more than 0.5 in.

Figures 44 through 48 show the settlement of the five tubes oriented parallel to the abutment face. Tubes SP-5-1 and SP-11-1, located over the area of support removal and beneath the surcharge load, show that the maximum recorded settlement of the fill (between 2 and 3 ft behind the face) exceeds the settlement of the CMUs at the same elevation. However, even the largest settlement of 4.8 in is substantially less than the 8 in of support that was removed. No settlements were noticeable near the upper back of the abutment at SP-11-3. When the data for all tubes in both orientations are considered, the settlement decreased with height and with distance from the region of support removal.

Test A2 was considered complete when the rate of settlement of the CMUs had slowed to less than 0.003 ft in 24 hours and pressure cell data had effectively stabilized. Comparing these data with the data taken after the completion of all tests 37 days later, it is clear that settlements of the fill continued beyond the time when Test A2 was terminated. These trends are supported by survey data for the CMUs. The continued settlements affected all tubes except SP-11-3, suggesting that the settlement process required a long time to fully complete. The outside edge of the influence of the reinforced fill's bridging action may be susceptible to gradual sloughing of the fill, which would allow additional settlement of the overlying fill at this location.

It is not immediately clear what the effect of dynamic loads on the abutment, such as traffic loads, may be on the durability of this bridging action. If these dynamic loads are small in comparison to the static load, the effect should be small. However, if these loads are large in comparison to the static load, it may contribute to a more rapid breakdown of the bridging action and increase the differential settlements expressed at the surface.

Test B1

Figure 43 shows the settlement of the four tubes oriented perpendicular to the abutment face on Side B. The individual graphs within the figure are arranged according to the position of the settlement tubes when viewed from the face of the abutment; this configuration is a mirror image of the configuration for Side A in Figure 42. Figure 43 shows that while the settlements were small, the settlement patterns of the fill during Test B1 are consistent with the trends in Figure 42 for Test A1. The Level 4 tubes exhibited approximately equal magnitude of settlement during both Test A1 and B1. However, Test B1 induced noticeably larger settlements at Level 10 tubes than Test A1 at the corresponding tubes on Side A. Near the face, these settlements are approximately the same magnitude as those at Level 4, indicating that the influence of a larger depth of support removal extended to a greater height at this location. Settlement of the tubes decreases with increasing distance from the region of support loss.

Figures 44 through 48 show the settlement of the five tubes oriented parallel to the abutment face. As with tubes SP-B4-1 and SP-B4-2, the settlement of SP-5-1 during Test B1 was similar to the settlement of the opposite end of the tube during Test A1. Data from SP-5-2 on Side A were erratic for Test A1, preventing a comparison at this tube. Settlement at Level 11was less than the settlement at Level 5 at all tubes. When compared with the corresponding tubes for Test A1, settlements from the tubes oriented parallel to the abutment face were again larger for Test B1. SP-11-1 was an exception to this trend, but data for this tube for Test A1 were of questionable accuracy. After showing no discernible settlement during Tests A1 and A2, SP-11-3 settled just over 0.1 in during Test B1. For all tubes oriented parallel to the abutment face, settlements decreased rapidly with distance from the region of support loss.

Test B2

Figure 43 shows that the settlement of the fill was generally larger for the four tubes oriented perpendicular to the abutment face after Test B2 than the settlement after Test B1. Readings taken after Test B2 for SP-B4-2 were somewhat erratic and are not considered in the following analysis. The two tubes that are located over the region of support removal, SP-B4-1

and SP-B10-1, showed significantly larger settlements following Test B2 than occurred during Test B1. The portion of the tube toward the rear of the abutment showed upward movement of the tube, which is presumably a response to the flexure in the pipe and not an error in the readings. SP-B10-2, located over a consistent support condition, showed a small increase in settlement.

The trends of SP-B4-1 and SP-B10-1 are very similar to the trends of the corresponding tubes on Side A after Test A2, which are shown in Figure 42. Magnitudes of settlement on Side B ranged from 1.4 to 2.2 times greater than the settlement on Side A. These values are reasonable for a depth of support removal on Side B that was twice the depth of Side A.

Figures 44 through 48 show the settlement of the five tubes oriented parallel to the abutment face. As expected, the largest magnitude settlements were observed in SP-5-1, which recorded a maximum settlement of 6.6 in. The corresponding tube at Level 11, SP-11-1, recorded a maximum settlement of only 1.3 in, demonstrating how the bridging action of the reinforced fill decreases settlements of the fill with increasing height. SP-5-2 and SP-11-2 show similar trends, although the percentage reduction is not as significant. SP-11-2 and SP-11-3 exhibited nearly identical settlement patterns and magnitudes on Side B during Test B2.

All tubes in both orientations once again show a reduction in settlement as distance from the region of support loss increases.

When compared to the data from Test A2, each of the five tubes oriented parallel to the abutment face settled more in Test B2. For tubes that experienced noticeable settlements during Test A2, the ratio of the maximum settlement after Test B2 to that after Test A2 ranged from 1.4 to 2.3. Although SP-11-1 and SP-11-2 had settled more after Test B2 than after Test A2, the final settlements on both sides are similar after the long-term settlements on Side A are considered.

Comparison with Settlement of the Surcharge Load

The settlement of the fill can be compared with the settlement of the foundation for the surcharge load. Figure 49 compares the settlement of the surcharge foundation with the settlement recorded at the two profiling tubes located beneath the surcharge in the reinforced fill, SP-5-1 and SP-11-1. The relative position of these elements is shown in Figure 17. The figure shows that settlements near the corners of the abutment decreased significantly with increasing height above the foundation, while the settlement near the center of the abutment increased slightly as the pressures in the fill were redistributed within the abutment to compensate for the loss of support near the corner. Settlements higher above the location of support loss were also more uniform than settlements closer to the location of support loss.

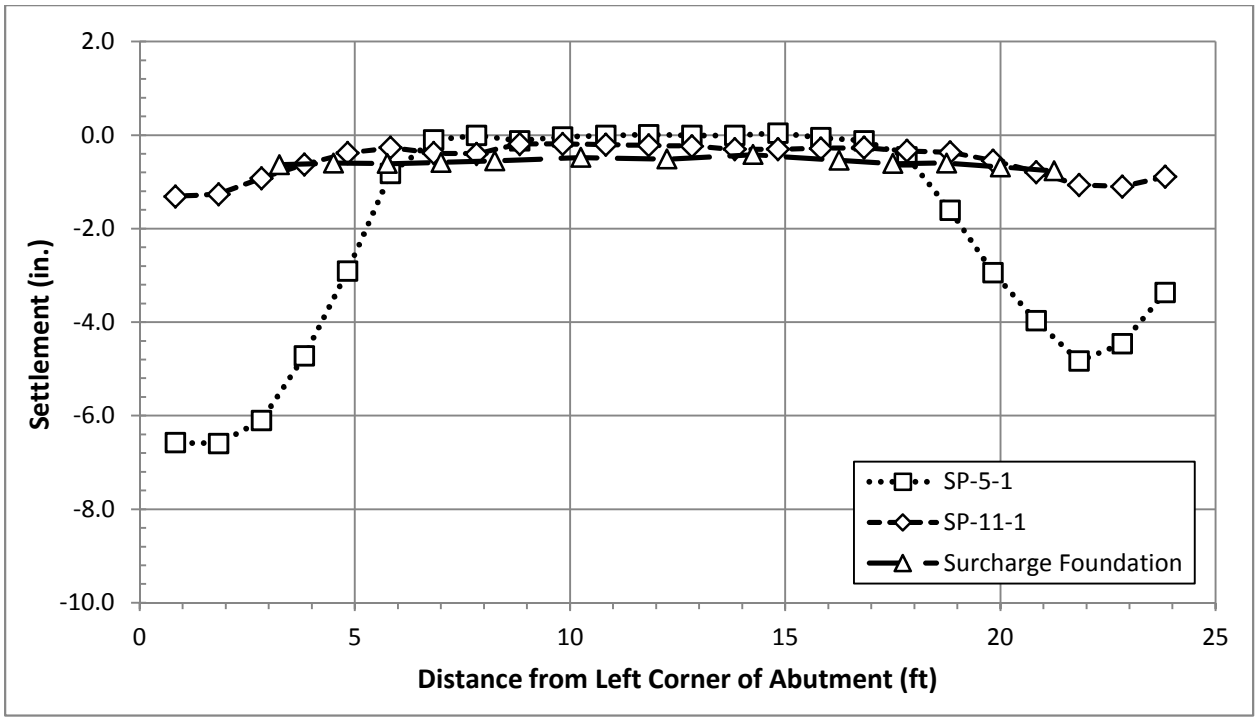

Figure 49. Comparison of Settlement of SP-5-1, SP-11-1, and Surcharge Foundation After Test B2

Comparison of Area Experiencing Settlement

The settlement profiler data were used to estimate the extent of the reinforced fill that experienced settlement as a result of support removal at the base. The data were primarily taken from the tubes located over the regions where support was removed—SP-A4-1, SP-A10-1, SP-5-1, and SP-11-1 for Side A; and SP-B4-1, SP-B10-1, SP-5-1, and SP-11-1 for Side B. If these data were difficult to interpret, data from adjacent tubes were also considered. Two different thresholds were considered for settlement to be considered significant. A small settlement threshold was defined for settlements exceeding 0.1 in, and a larger settlement threshold was defined for settlements exceeding 0.5 in. The results are summarized in Table 3. Although the dimensions are presented in a format that suggests a rectangular area, the geometry of the settlement area varies and is difficult to precisely define with the data available.

Table 3. Approximate Extent of Settlement, by Test

After Test	Dimensions of Support Removal (ft)[a]	Approximate Extent of Settlement (ft)[a]			
		Settlement ≥ 0.1 in		Settlement ≥ 0.5 in	
		Level 4/5	*Level 10/11*	*Level 4/5*	*Level 10/11*
A1	3 x 4	3 x 4	6 x 8	-	-
A2	5 x 7	6 x 7	7 x 8	5 x 6	3 x 4
B1	3 x 4	3 x 5	7 x 6	-	-
B2	5 x 7	5 x 8	8 x 6	4 x 6	4 x 3

[a]Dimensions given in W x L, where W = dimension perpendicular to abutment face, and L = dimension parallel to abutment face.

This table shows that, at low levels of the abutment, the extent of the reinforced fill experiencing settlements of at least 0.1 in is similar to the extent of support removed. At higher levels, the extent of fill experiencing settlements of at least 0.1 in is larger than the extent at lower levels. However, the opposite effect is observed when considering settlements of at least 0.5 in. Neither Test A1 nor Test B1 resulted in settlements larger than this threshold at the levels of the profiling tubes. In Test A2 and Test B2, the area of fill at lower levels experiencing settlements greater than 0.5 in is again similar to the area of support removed. At higher levels, a smaller region of fill experienced settlements in excess of 0.5 in than at lower levels.

These results can also be compared to the survey data recorded at the surface of the abutment. The survey points that settled more than 0.1 in during testing are marked in Figure 50. Very few survey points settled 0.1 in or more during Test A1 or Test B1, but most targets experienced at least 0.1 in of settlement by the end of Test A2 and Test B2. No survey points had settled more than 0.5 in after Test A1 or Test B1. After Test A2 and Test B2, only four targets on each side had settled at least 0.5 in. These targets were the four targets closest to each corner of the abutment, adjacent to the surcharge load. These trends are consistent with the trends observed by the profiling tubes. While it is not immediately clear why more survey points on Side A than on Side B experienced at least 0.1 in of settlement, these observations are consistent with the survey data obtained for the surcharge load. These data, presented in Figure 37, show slightly larger settlements on Side A of the abutment. Pressure cell data, which will be subsequently discussed in the "Earth Pressure Cells" subsection, reveal a slight asymmetry of the surcharge pressure towards Side A. This shift in pressure is believed to be a contributing factor to the larger area of surface settlement of the reinforced fill observed on Side A.

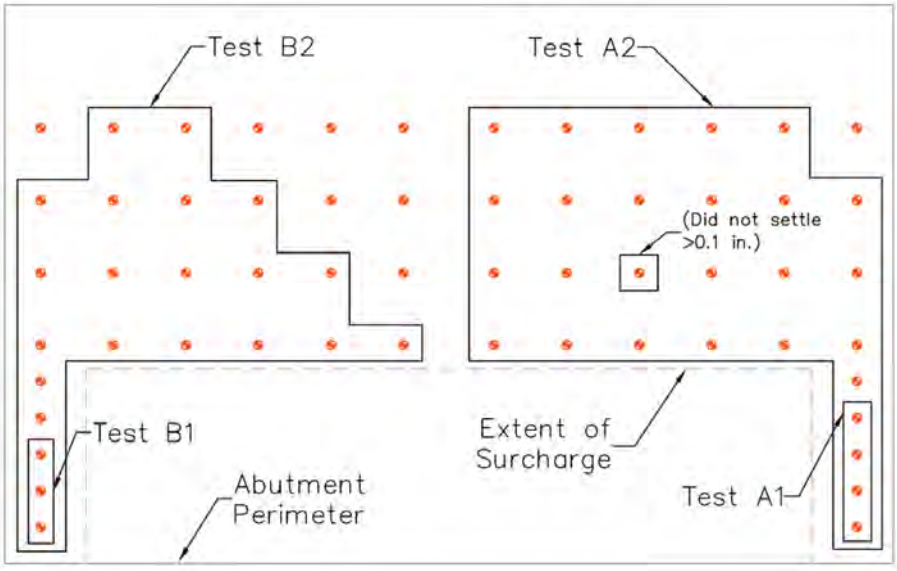

Figure 50. Survey Targets on Surface of Abutment That Settled More Than 0.1 in

Three conclusions may be drawn from these observations. First, settlement at low levels of the abutment affects a region roughly equal in size to the region of support loss. Second, as the height above the region of support loss increases, the extent of the reinforced fill that experiences large settlements decreases, while the extent of fill that experiences small

settlements increases. Third, when these observations are combined with survey observations showing small deformations at the surface of the abutment, it is clear that the reinforced fill of the abutment minimized the surface expression of extreme differential settlement conditions at the base of the abutment. This performance shows an inherent robustness in the GRS abutment's ability to minimize surface expressions of differential settlements beneath its foundation.

Key Points

- In many instances, the maximum settlement of the fill at a given level was greater than the settlement of the facing CMUs at the same level.

- When support is lost beneath part of the foundation, the reinforced fill acted to bridge over the area of support loss. The additional support extends upward and outward from the inside edges of the region of support loss. The effect of support loss diminishes with height above the foundation.

- Settlements within the reinforced fill decreased and the uniformity of settlement increased with height and with distance from the region of support loss due to the effect of the bridging action.

- When the depth of support removal was held constant, settlement of the fill increased with removal of the larger area of support.

- When the area of support removal was small, as in Test A1 and Test B1, the settlements of the fill were relatively similar at the level of the profiling tubes, independent of the depth of support removal.

- When the area of support removal was large, as in Test A2 and Test B2, the settlement of the fill at the levels of the settlement tubes was significantly larger on Side B than Side A, where a larger depth of support was removed on Side B. However, surface expressions of the settlements were not necessarily larger on Side B than Side A.

- The small settlements observed at the surface of the abutment in response to severe differential settlement conditions at the base demonstrate robust performance in the GRS abutment's ability to minimize surface expressions of differential settlements beneath its foundation.

Earth Pressure Cells

The pressure cells were monitored regularly from the time of installation through construction and each of the four testing sequences. Pressure data could not be monitored continuously during Test B1 due to failure of the signal analyzer for the vibrating wire instruments. Baseline readings for the test were known, and final readings were obtained at the end of the test once a replacement signal analyzer had been installed. Replacing the signal analyzer is not believed to have impacted the zero readings of the EPCs. The following sections

discuss temperature effects on gage readings, data trends observed during construction and each of the four testing sequences, the effect of stress increases on strength demand in the reinforcement, and key observations from the EPC data.

Temperature Effects

Earth pressure cells consist of a de-aired fluid (usually oil) that is sealed inside a metal instrument. As the surrounding temperature increases, the fluid expands in volume, increasing the pressure within the cell. This pressure change is also influenced by the level of restraint provided to the cell by the surrounding medium. If the metal plates of the cell are relatively free to deflect as the fluid expands in volume, the pressure change will be much less than what would be observed if the cell is surrounded by a stiff medium, such as the GRS fill under high confining stress. Finally, the vibrating wire instrument itself is affected by temperature changes due to changes in the wire tension.

The manufacturer provides a calibration factor for each cell to account for the temperature effects on the vibrating wire instrument. However, the manufacturer cannot provide a calibration factor for the entire cell because the stiffness of the surrounding medium cannot be known in advance. Studies such as Daigle and Zhao (2003) also note that seemingly identical cells under the same confinement conditions can react very differently to fluctuations in temperature, requiring a separate calibration factor for each cell.

In most cells, a clear cyclic variation can be observed in the pressure readings. The period of these variations is approximately 1 day for all cells, indicating that these effects are most likely due to temperature changes. Additionally, the two outermost cells at each level showed markedly smaller cyclic variations in comparison to the three middle cells at each level. Because these cells are subjected to a lower confining stress during construction and a significantly lower confining stress during testing, it is logical to observe smaller cyclic variations if these variations are temperature-induced. For these reasons, the authors believe that temperature fluctuations are primarily responsible for these variations, although attempts to determine a definitive correlation between temperature and pressure changes proved largely unsuccessful. These efforts are discussed in the following paragraphs.

The authors of this report attempted to determine a temperature calibration specific to each cell in order to demonstrate that the observed variations were indeed temperature-induced. Two cells were initially selected, one from Level 1 and one from Level 16, which exhibited average to high sensitivity to temperature fluctuations. Temperature changes were recorded by a thermistor in each pressure cell. The data for these cells were analyzed over a period from the evening of August 9 through the morning of August 14 (Days 43.8 to 48.2 of construction). This range encompassed the period following construction of the abutment and prior to placement of the surcharge load. While the stresses are somewhat lower than the final stresses following the placement of the surcharge load, it was believed that the geostatic stresses were constant throughout this interval and that the variations recorded were primarily due to temperature effects. If successful, further attempts could then be made to estimate the calibration factor of the cells following placement of the surcharge load.

The pressure data were corrected to account for variations in barometric pressure using weather data recorded at the nearby town of McCoy. The effect of barometric pressure was generally less than 0.05 psi. The corrected pressure was then plotted versus temperature, which is the standard method of determining a temperature correction factor. A typical plot is shown in Figure 51. If time is considered, a trace of the data would begin at the right side of the plot and move towards the left side in a shifting hysteresis type of loop. These data suggest that additional factors besides temperature may be complicating the analysis. It is possible that some very small compressions of the geofoam continued during this period, creating subtle shifts in the stress distribution of the abutment. Subsequently, the change in pressure was plotted versus the change in temperature across each time step. Figure 52 shows that this method at least produces a recognizable trend between temperature and pressure increases, although the ability to fit a regression line is poor. No further attempt was made to correct the data for temperature effects.

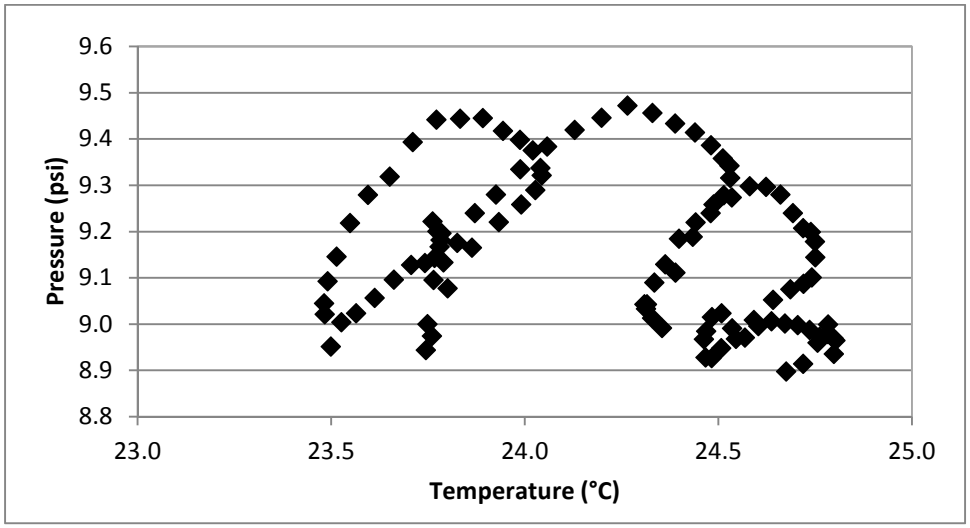

Figure 51. Pressure vs. Temperature for EPC-C1-1

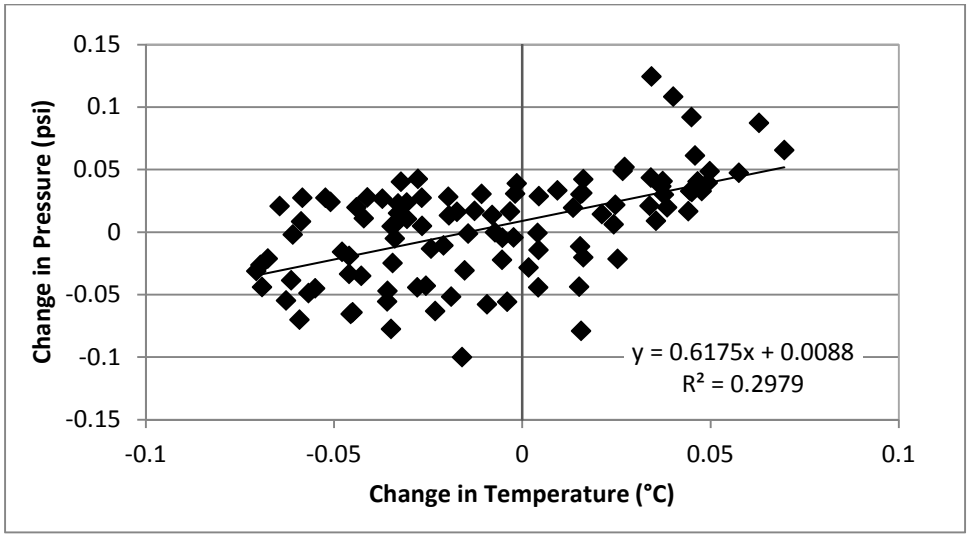

Figure 52. Change in Temperature vs. Change in Pressure for EPC-C1-1

Construction

Figures 53 and 54 present the data collected during construction and compare them to the stress levels that would be expected from the weight of the fill and surcharge load. Stresses due to the weight of the fill were computed using simple geostatic stresses. Stresses induced by the weight of the surcharge load at Level 16 were computed using the Boussinesq equation for a distributed load, since the assumption of elastic half space is reasonable at small distances beneath the surcharge foundation. At Level 1, the face of the abutment introduces a new boundary condition, and therefore a 1H:2V equivalent footing approximation that was truncated at the back of the CMU face was used to calculate the stress at this location.

The pressures recorded by the EPCs initially corresponded well to the expected stress levels. By Level 5 of construction, the pressure recorded by the two outermost cells that are located over the region supported by geofoam, EPC-A1-1 and EPC-B1-1, had dipped below the expected value. The difference between the expected and actual pressures at these cells continued to increase throughout construction. At the same time, the pressure at EPC-A1-2 and EPC-B1-2, which are located over the relatively incompressible compacted fill, show a corresponding increase in recorded stresses above the expected stresses. Cell EPC-C1-1 continues to follow the expected stress levels until Level 11, when the recorded stresses begin to exceed the predicted. These trends indicate that the geofoam underwent small strains during construction. As the geofoam compresses, the reinforced fill attempts to bridge the gap, transferring some of the load to the portion of the abutment where the support condition remains unchanged. Each lift of reinforced fill supports an area larger than that of the lift below, creating the bridging action that previously was discussed.

The effect of placing the surcharge load can be seen in both Figures 53 and 54, but most clearly in Figure 54, which displays the data from the cells immediately beneath the surcharge load. The surcharge load consisted of two rows of 10 concrete blocks, each with a weight of approximately 3500 lb. Together, the blocks comprising the surcharge load weighed approximately 70 kips and resulted in a bearing pressure of about 1750 psf.

The inset in Figure 54 shows the pressure trends for the Level 16 cells during placement and the initial tensioning of the load. As the load was placed, the pressure increased in all cells symmetrically, similar to the behavior observed in the Level 1 pressure cells during construction and placement of the surcharge load. When the surcharge blocks were tensioned, the pressure dropped dramatically at EPC-A16-1 and EPC-B16-1, while it increased at EPC-A16-2, EPC-C16-1, and EPC-B16-2. These trends result from the tensioning process used to secure the blocks together. It appears that small deformations occurred in the corner regions of the abutment above the geofoam support. As the surcharge blocks were placed, the wood foundation on which the blocks sat was flexible enough to deform slightly. As a result, the stresses immediately after the placement of the surcharge load were consistent with the stresses below a somewhat flexible footing and corresponded reasonably well to the expected stress levels. The highest stress levels were observed in the center and decreased slightly near the perimeter of the foundation. As the blocks were tensioned together, the blocks near the edge were pulled into alignment with the center blocks and partially cantilevered, reducing the pressure beneath the ends of the wood foundation and concentrating the load in the middle of the beam seat.

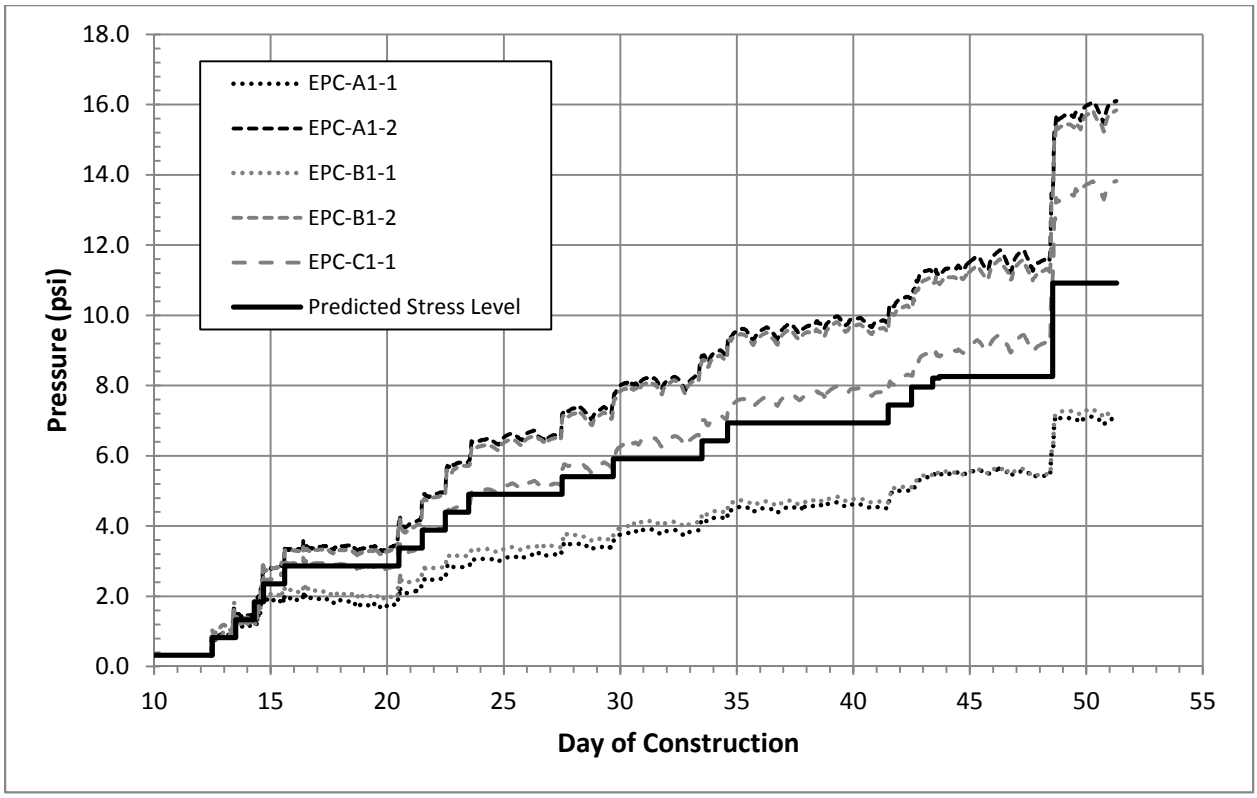

Figure 53. Stress Levels in Level 1 EPCs During Construction

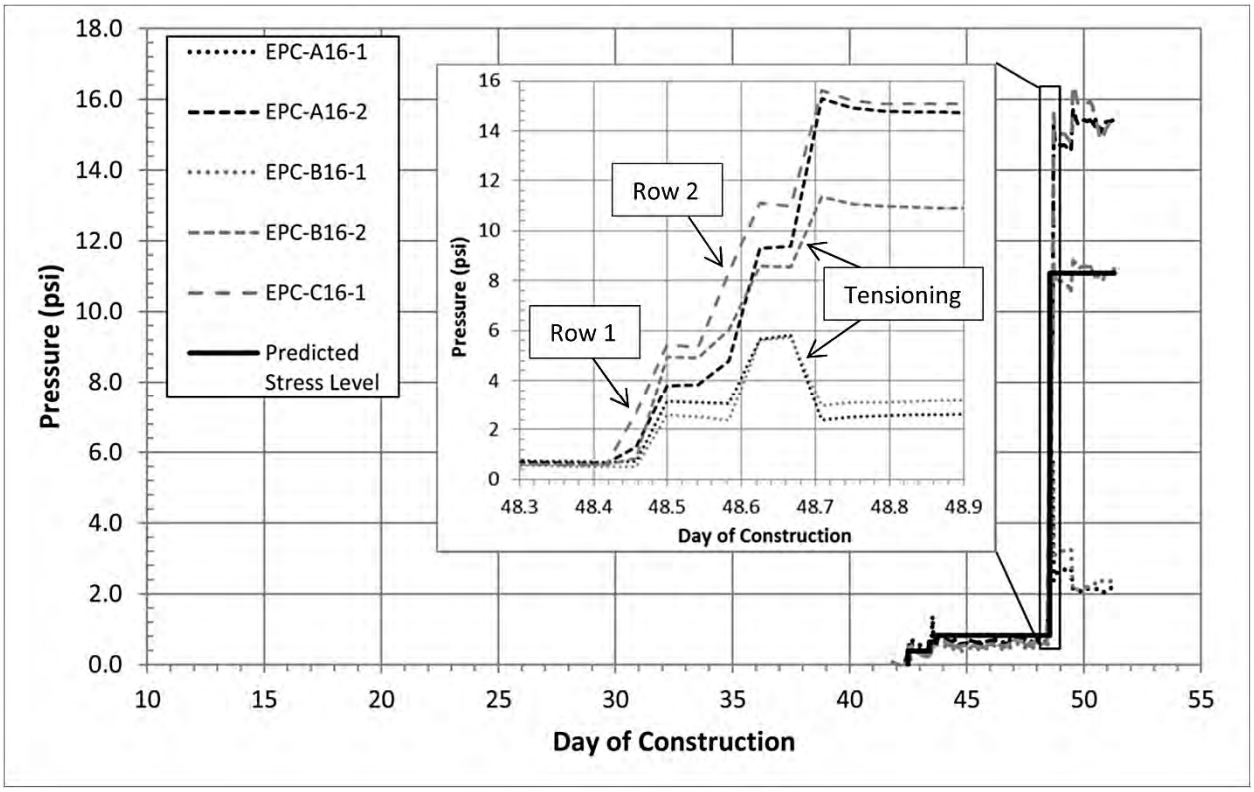

Figure 54. Stress Levels in Level 16 EPCs During Construction

During the tensioning process, steel shims were required to eliminate a gap at the ends of the surcharge blocks but were not available that same day. The inset in Figure 54 shows that, at the end of the tensioning process, the stresses recorded at Level 16 were asymmetrical. The next day, the tensioning system was loosened, the shims were inserted, and the system was re-tensioned, leading to the small peaks and drops in pressure observed on the morning of Day 49 and shown in Figure 54. The stresses remained asymmetrical at the upper levels of the abutment. Cells EPC-A16-2 and EPC-C16-1 recorded the highest stress levels, while EPC-B16-2 recorded a lower level that was very close to the predicted stress level. It appears that additional weight from Side A of the surcharge load was transferred toward the center of the beam seat. The survey data do not suggest that the surcharge load settled non-uniformly during placement. While the exact reasons for the increased pressure concentration at Side A are unclear, the pressure cells located at Level 1 did not record any asymmetrical stresses. This observation indicates that the reinforced fill was able to distribute the stress concentrations evenly at the base of the abutment.

Test A1

Figure 55 present plots of stress versus time from Test A1 at both levels of the abutment where the pressure cells were located. This figure and the following figures that present the stress changes with time are designed to allow the reader to quickly reference the location of the instrument and compare readings between different pressure cells. The vertical and horizontal scales are the same for all graphs in these figures. Figure 56 displays a plot of change in stress versus position for both Test A1 and A2 and is referred to in the discussion of both tests. The changes in stress in this figure are the differences between the stresses at the beginning of the test and at the end of the test.

All of the trends observed in Test A1 are very reasonable. Figure 55 shows that, within the Level 1 pressure cells, the pressure in the cell immediately above Region A1 of support removal (EPC-A1-1) dropped immediately and significantly, and this load was distributed over the adjacent cells. The increased load from this redistribution of stresses to adjacent cells decreased in proportion to distance from the region of support removal until no effect was observed at cell EPC-B1-1. The final stress change at the end of testing is shown in Figure 56.

Figure 55 shows that the Level 16 cells initially responded in a very similar manner to those in Level 1, with the pressure decreasing in EPC-A16-1 and increasing at EPC-A16-2, EPC-C16-1, and EPC-B16-2, although the stress changes were smaller at Level 16 than at Level 1. Over time, the pressure at EPC-A16-1 returned to its initial level, while the pressure at EPC-C16-1 and EPC-B16-2 decreased slightly below their initial levels. EPC-A16-2 held its increased pressure constant throughout the remainder of the test. Meanwhile, the pressure at cell EPC-B16-1 decreased slightly. The final stress changes are shown in Figure 56. These pressure trends correspond to survey data indicating that the surcharge foundation rotated slightly on the beam seat, as shown in Figure 37, reducing the bearing pressure on the left side of the bearing bed and increasing pressure on the right side. The location of zero pressure change at Level 16 is shifted to the right of the centerline of the abutment, consistent with the asymmetrical bearing pressure observed following placement of the surcharge load.

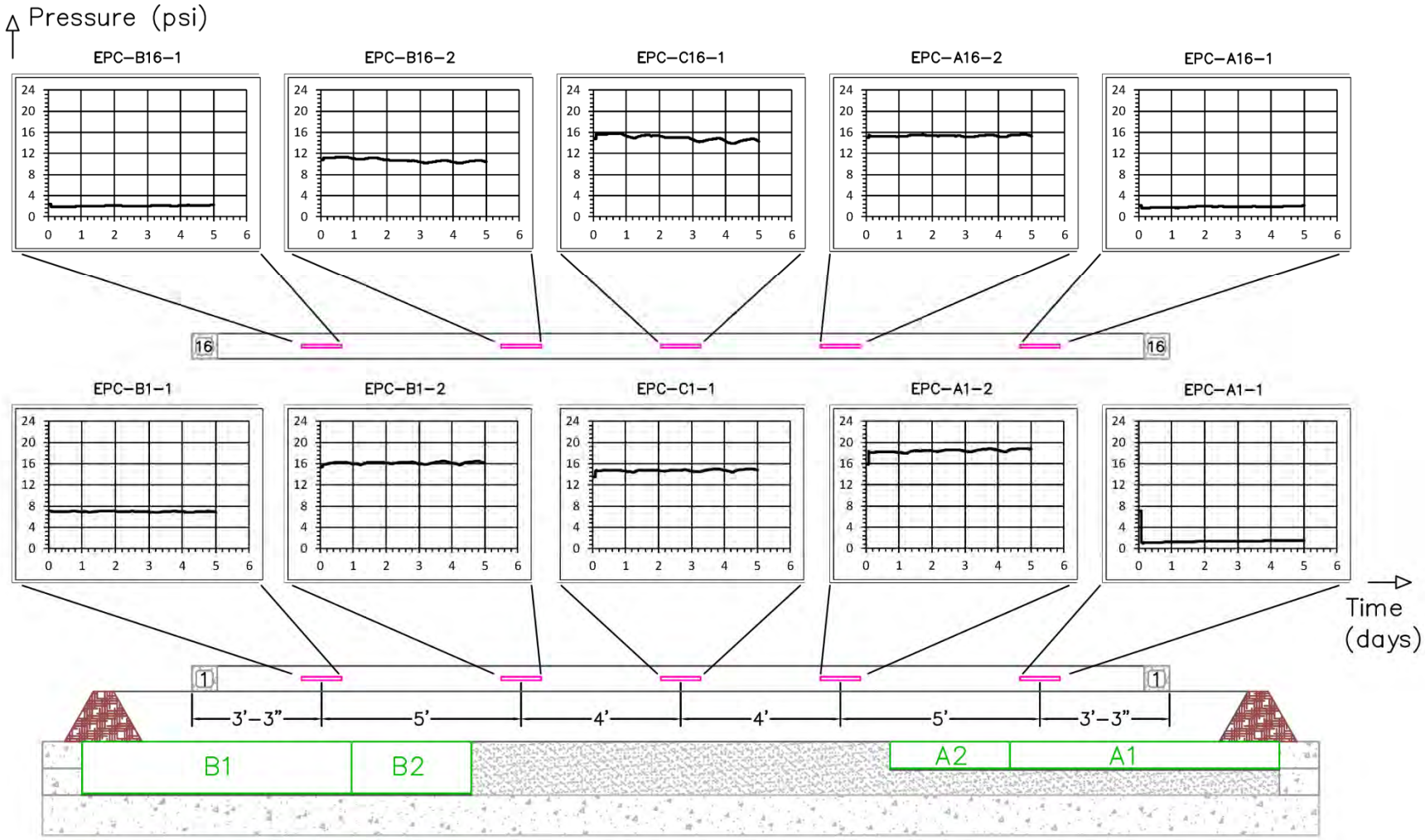

Figure 55. Stresses During Test A1

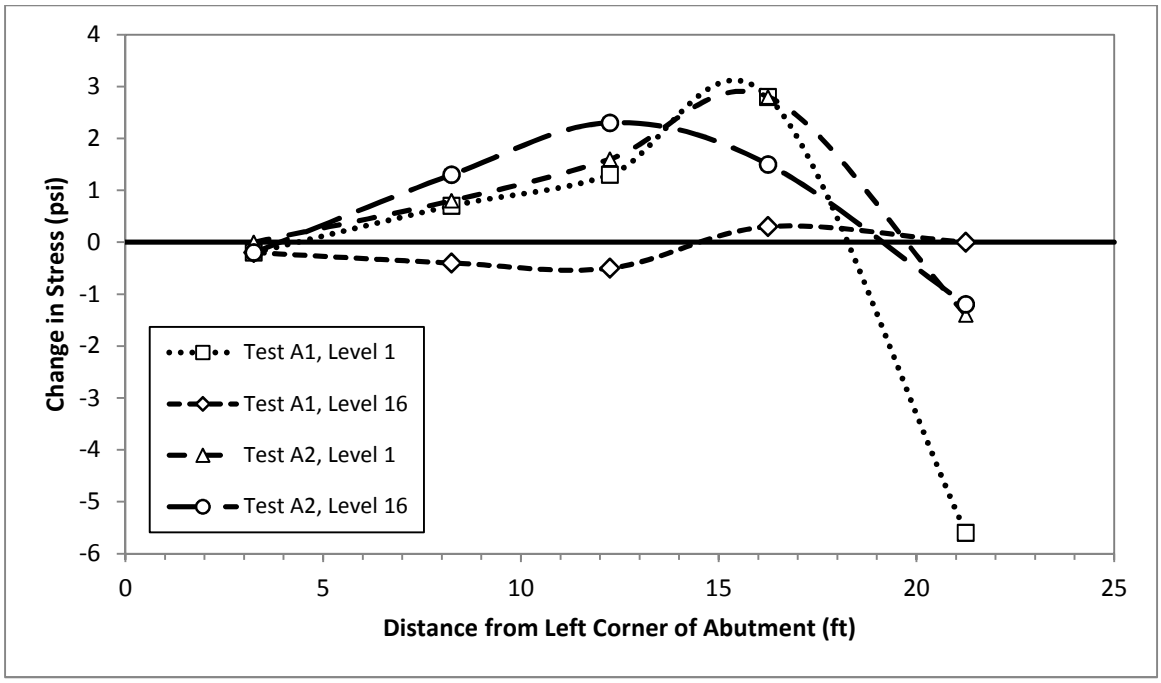

Figure 56. Change in Stress During Tests A1 and A2

The pressure changes that occurred when the solvent was first introduced were too rapid to be fully captured by the 15-minute reading interval. The amount of settlement experienced by Corner A of the abutment within these first 15 minutes was not large. This observation indicates that the initial stress redistribution within the reinforced fill occurred rapidly in response to small deformations. The pressure cell readings essentially stabilized within approximately one day of the start of testing.

Test A2

Figure 57 presents the stress time history from Test A2. This figure and Figure 56 show that the trends at Level 1 for Test A2 are nearly identical to those of Test A1. EPC-A1-1 experienced a significant drop that reduced the pressure at that cell to nearly zero. All other cells recorded pressure changes that are nearly identical to the pressure changes during Test A1. This observation is likely an unintentional consequence of the geometries selected for the abutment and support removal, and a somewhat different outcome would be expected for other geometries.

The pressure cells located in Level 16 exhibited unique trends during this test. Figure 56 shows that the magnitude of the stabilized pressure change is significantly larger than the change during Test A1, which is expected since the support at Level 16 should be affected more by a larger area of support removal at the base. However, the initial impression given by the plot of the data in Figure 56 is that equilibrium is not satisfied. That is, the amount of stress increase far outweighs the amount of stress decrease at Layer 16, which should not occur since no additional force was applied.

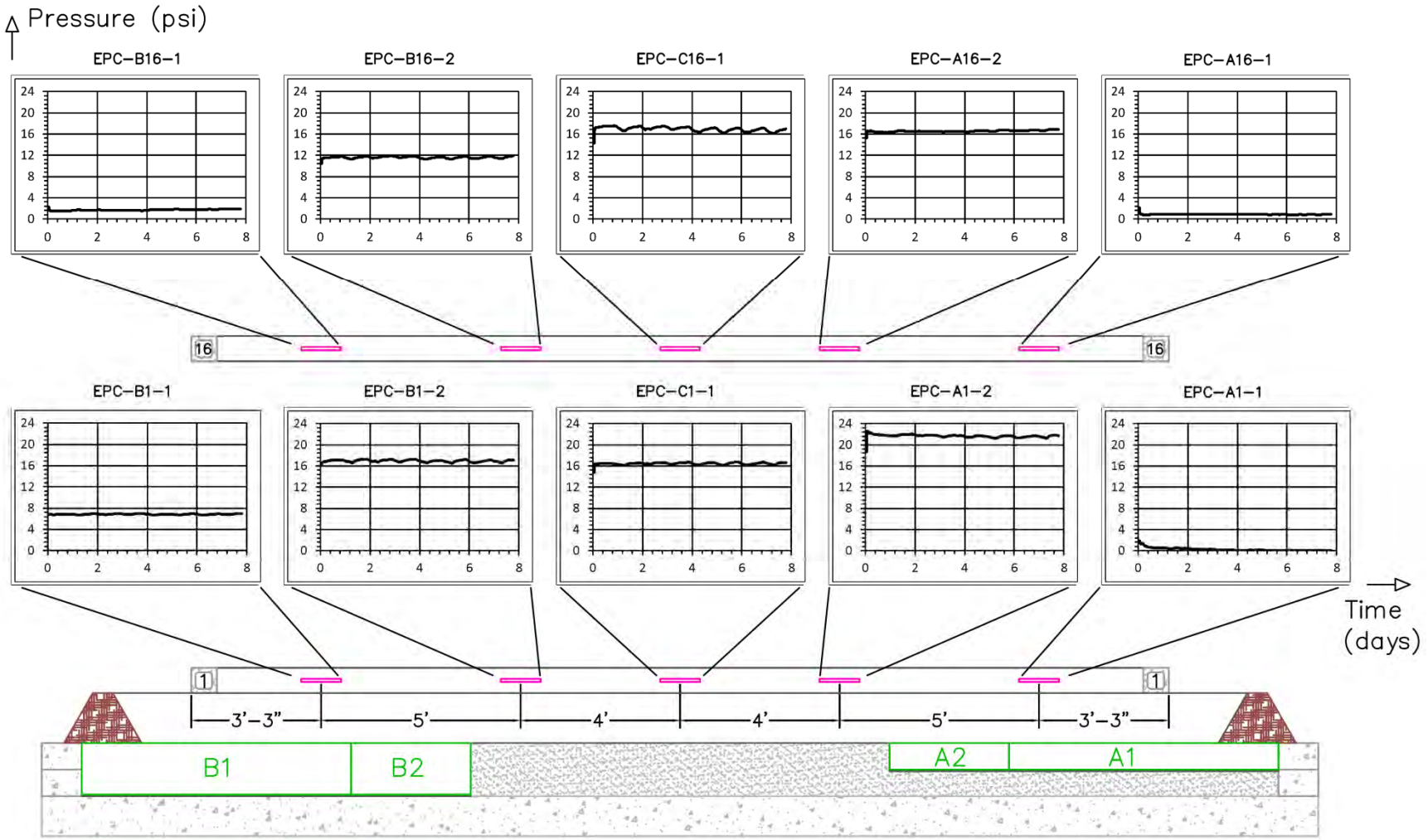

Figure 57. Stresses During Test A2

A similar observation could be made for the pressure cells at Level 1 following Test A2. As shown in Figure 56, the smooth curve would seem to show that the stress increases exceeded the stress decreases. However, the pressure changes at Level 1 are expected to transition abruptly from stress increases over the compacted fill subgrade to stress decreases over the region of support loss. For Test A2, the pressure cell at the corner was relatively far from this transition and therefore the smooth curve shown in the figure does not adequately capture the region over which the stress decreased.

At Level 16, the transition from stress increases to stress decreases is not expected to be as abrupt due to the bridging action of the underlying reinforced fill. Two hypotheses could explain the behavior at Level 16. First, it is possible that the pressure cells were positioned in a configuration that happened to register large stresses without identifying rapid changes in stress levels that may occur near the ends of the surcharge load. In this case, the gradually curving lines used to approximate the stress levels between observations may not be correct; the changes may occur much more suddenly and equilibrium is maintained.

A second hypothesis could be that friction between the fill and the CMUs influenced the observed stress levels. If the fill settled more than CMUs during Test A1, the interface friction would transfer some load to the CMUs and reduce the stress carried by the reinforced fill. During Test A2, many of these CMUs would lose support, transferring some of the load back into the reinforced fill and producing an increase in the pressures recorded at Level 16. There are some data to support this hypothesis. Survey data indicate that the fill settled more than the CMUs at Level 16. Looking at Figure 56, if the smooth curves are assumed to accurately represent the stress distribution, Level 16 showed a net decrease in stress during Test A1. However, while this second hypothesis is plausible, similar behavior was not observed in Test B2, as discussed in later sections.

The reading interval for the beginning of this test was decreased to one minute, which allowed the distinct peaks of the data to be observed. In general, the immediate changes in the stress levels in the abutment occurred within 10 minutes of the solvent's introduction. The pressure cell data effectively stabilized within 1.5 days.

Test B1

Figure 58 plots stress versus time for Test B1. Short-term stress changes could not be observed for Test B1 due to the failure of the vibrating wire instrument signal analyzer. The unit was replaced, and long-term stress levels were monitored. Replacement of the unit is not believed to have had any effect on the baseline levels of the pressure cells. Long-term trends again showed reasonable values compared to initial readings taken before dissolving the geofoam, with stresses dropping at locations over the region of support removal and increasing at locations over a consistent support condition. The stabilized stresses for both Test B1 and Test B2 are plotted in Figure 59, which is referred to in the following discussion of both tests. The change in stress for each test is measured as the difference between the level at the beginning of the test and that at the end of the test; that is, the change in stress for Test B1 is the difference between the stress recorded at the end and the beginning of Test B1, and likewise for Test B2.

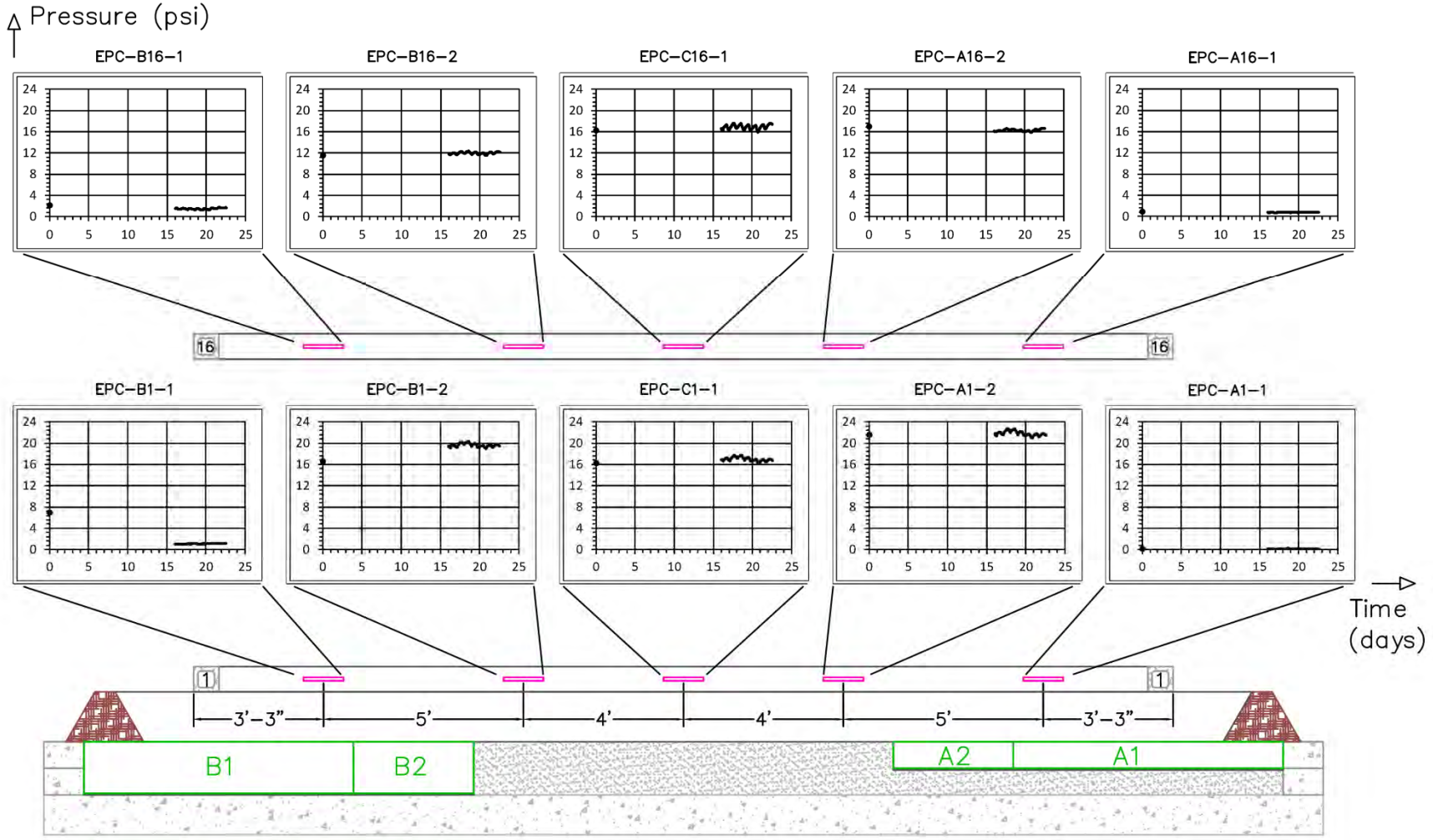

Figure 58. Stresses During Test B1

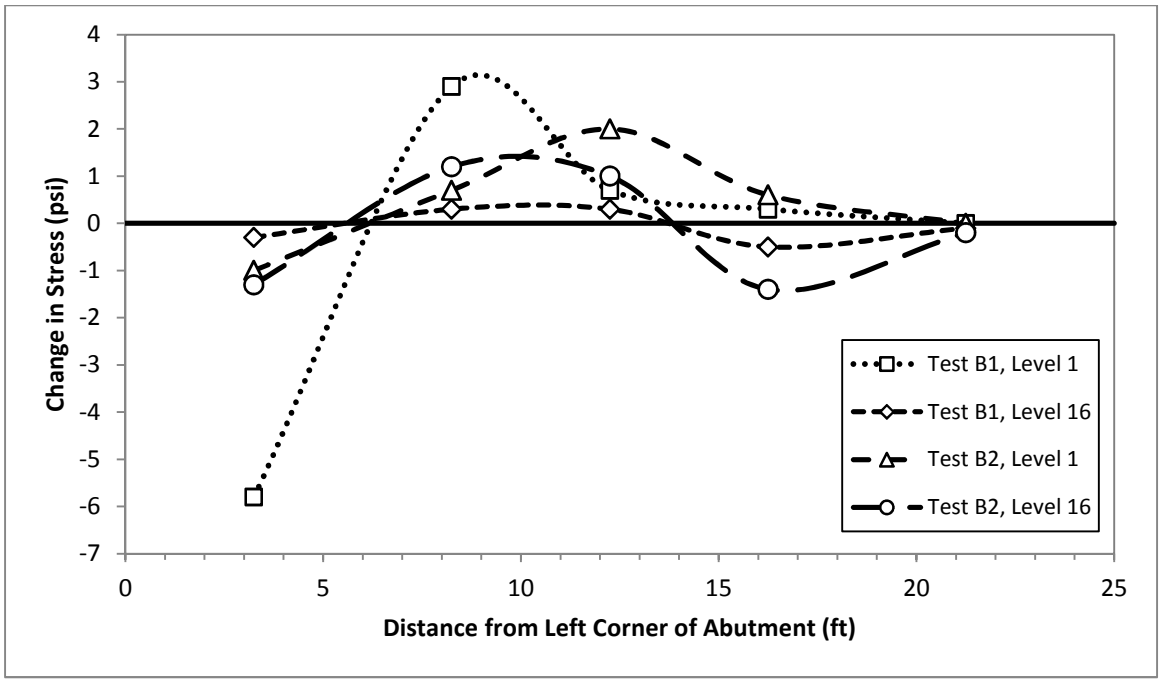

Figure 59. Change in Stress During Tests B1 and B2

In Level 1, the stress again decreased significantly in the pressure cell located over the region of support removal. The corresponding load was shifted to the three pressure cells located over the compacted fill subgrade, with most of the load transferred to the cell located nearest to the area of support removal. In Level 16, the pressure trends correspond to survey data in Figure 37, which indicate that the surcharge foundation rotated slightly on the beam seat, reducing the bearing pressure on the right side of the bearing bed and increasing pressure on the left side. The location of zero pressure change is shifted to the right of the centerline of the abutment, consistent with the asymmetrical bearing pressure observed following placement of the surcharge load.

Test B2

Figure 60 presents the stress time history for Test B2. All cells whose readings were not close to zero exhibited a noticeable, negative trend around Day 10 of testing. It is believed that this is due to temperature effects, as Day 10 was the first day that ambient air temperatures dropped sharply overnight without warming significantly again the following day, leading to the first extended period of consistently cooler weather.

In Test B2, the stress variations at cell EPC-B1-2 deviated from the expected behavior at that location. After rapidly increasing at the start of the test, the pressure decreased over the next day to levels less than the initial value. It eventually stabilized at a pressure slightly higher than the initial pressure. This unexpected decrease occurred over a period of 0.8 days, approximately the same amount of time for the geofoam to fully dissolve.

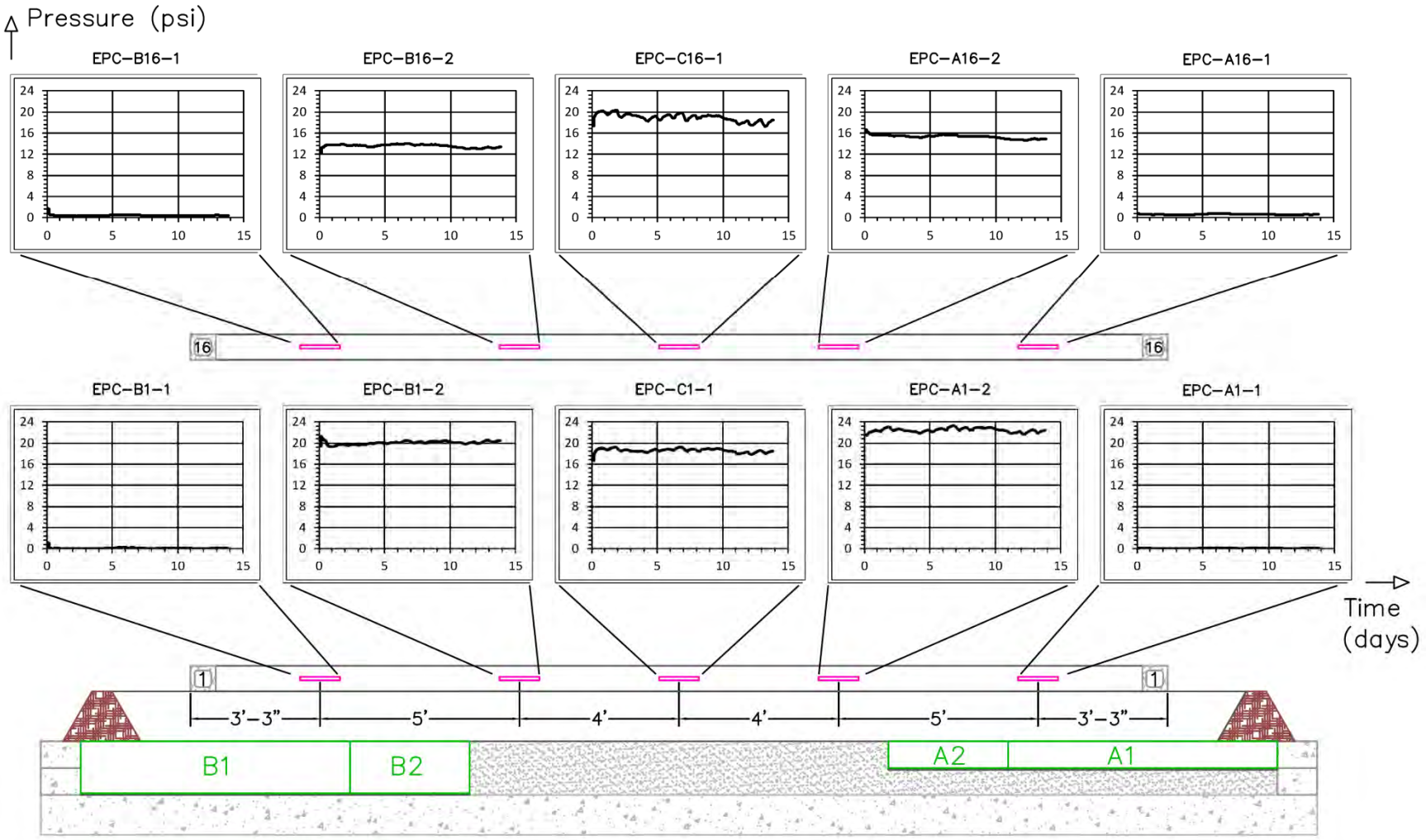

Figure 60. Stresses During Test B2

During deconstruction, vertical tension cracks were observed in the RSF at the edge of the area of support removal for Test B2. The authors believe that these cracks formed as the geofoam dissolved and the RSF settled, creating an unsupported vertical face of the RSF. The adjacent RSF, located over the compacted fill subgrade, had previously experienced increases in vertical stress due to testing sequences A1, A2, and B1. During Test B2, it is believed that the additional concentration of stresses at the corner exceeded the strength of the RSF at the unsupported face, causing a small amount of settlement beneath EPC-B1-2. This settlement relieved some of the vertical stresses at this location and facilitated a further transfer of stresses to the adjacent fill. Only small settlements would be required to cause this variance in stress changes. The resulting stress pattern, shown in Figure 59, shows that the stresses have been transferred further to the middle of the abutment.

The trends at the pressure cells in Level 16 are nearly identical to the trends from Test B1, as shown in Figure 59. The magnitudes of the pressure changes are significantly larger in Test B2, indicating that the upper levels of the abutment are more affected by the larger area of support removal.

Comparison of Results from Side A and Side B

Figure 61 compares the change in pressure during Tests A1 and B1 at Levels 1 and 16. The symmetry of the data is remarkable, showing nearly identical stress changes at both levels for both tests. Although both tests removed support from beneath an equal area of the foundation, Test B1 removed twice the depth of support as Test A1. These results indicate that, for the magnitudes of settlement induced in these tests, the final stress distribution within the abutment is a function of the area of support loss and not magnitude of settlement.

Figure 62 compares the change in pressure during Tests A2 and B2 at Level 1. Data from Test A2 at Level 16 showed unusual trends and did not resemble the data from any other test, as previously discussed. A comparison of Figures 61 and 62 shows that the data collected during Test B2 did not exhibit the same symmetrical behavior observed in Test B1 due to the small stress increase at EPC-B1-2 (at the 8 ft location). The authors believe that the most likely explanation is that dissolving the foam on Side B created a 16-in-high, unsupported vertical face and initially concentrated large stresses at the edge of this unsupported face. The high stress concentration led to local deformations of the subgrade and the RSF that, even if relatively small, prevented the vertical stresses at EPC-B1-2 from increasing significantly.

The authors believe that the observed stresses at Level 1 in Test B2 are valid. However, they also postulate that, had subgrade and RSF deformations not occurred, the observed stress changes would have displayed similar trends to the symmetrical behavior observed during Tests A1 and B1. Previously, Figure 56 showed that the stress changes of the pressure cell nearest the area of support removal had experienced essentially identical pressure changes during Tests A1 and A2. If this trend is assumed to hold true for Tests B1 and B2 as well—and the symmetry displayed in Figure 61 suggests this is a reasonable assumption—then the gray, dashed line in Figure 62 shows an adjusted trend, for which the stress changes during Test B2 would be more comparable to the stress changes during Test A2.

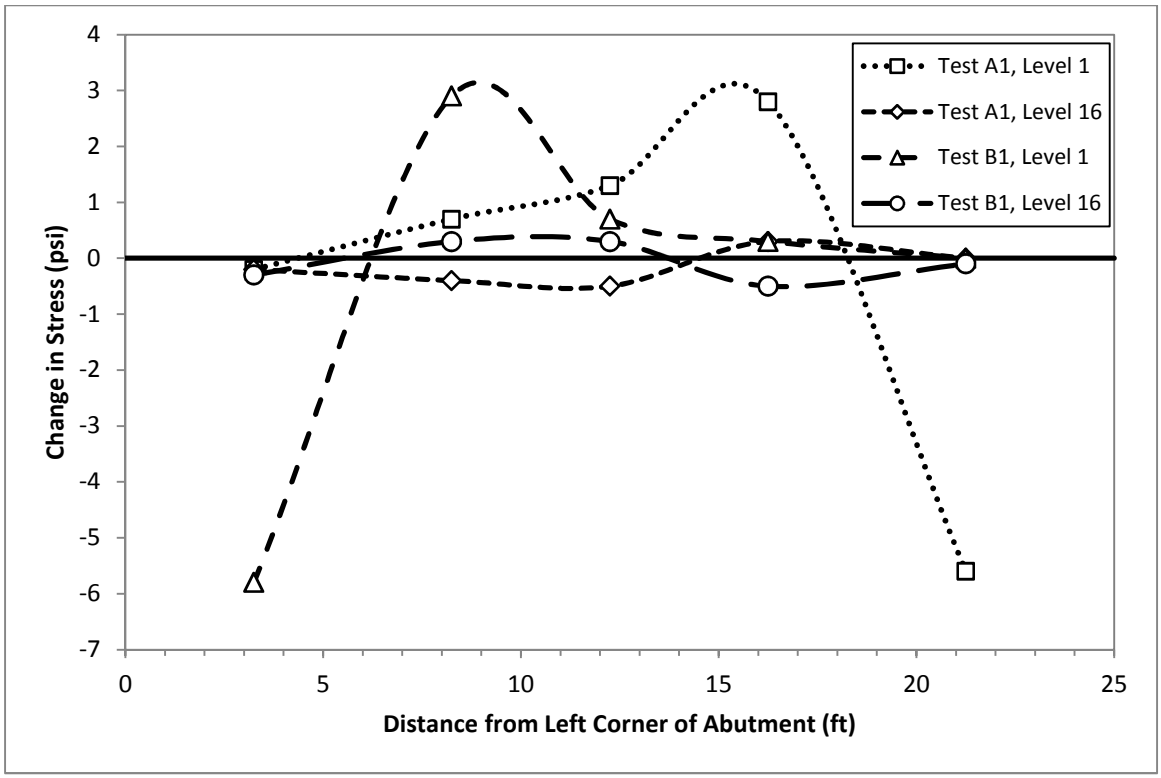

Figure 61. Comparison of Stress Changes During Test A1 and Test B1

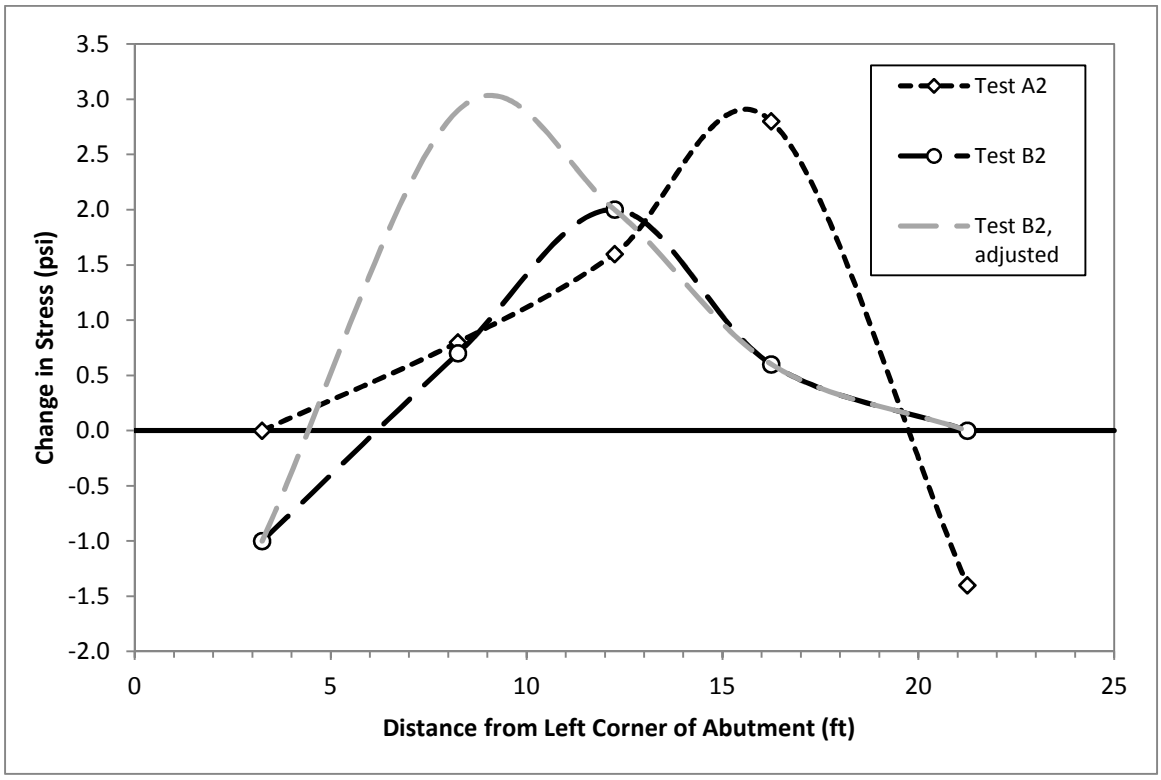

Figure 62. Comparison of Stress Changes at Level 1 Epcs During Test A2 and Test B2

Effect of Stress Changes on Strength Demand in Reinforcement

Vertical stress increased in the reinforced fill located over a consistent support condition during the four testing sequences. These vertical stress increases create an increased strength demand the reinforcement. To illustrate this effect, the increased demand on the Level 1 reinforcement was estimated using the FHWA method (Adams et al., 2011) and the stress data from EPC-C1-1. Equation (2) is used by the FHWA method to estimate T_{req} in the reinforcement.

$$T_{req} = \left[\frac{K_a \sigma_v'}{0.7^{\left(\frac{S_v}{6 d_{max}}\right)}}\right] S_v \qquad \text{Equation (2)}$$

where: T_{req} = required tensile strength of reinforcement
K_a = coefficient of active earth pressure
σ_v' = effective vertical stress
S_v = vertical reinforcement spacing
d_{max} = maximum particle size

The reinforced fill was assumed to have an effective stress friction angle of 44°, which gives $K_a = 0.180$. Vertical reinforcement spacing was 8 in, and the maximum particle size for the fill was 0.5 in. The ultimate strength of the reinforcement is 4800 lb/ft according to the manufacturer, and the factor of safety is determined by dividing the ultimate strength by the required strength, without applying any partial factors of safety. The FHWA method considers a factor of safety of 3.5 or greater to be acceptable. The results are presented in Table 4. This table only presents an estimate of strength demand based on one method of calculation and does not represent measured values.

Table 4. Effect of Stress Changes on Strength Demand in Level 1 Reinforcement, Based on Data From EPC-C1-1

Phase	$\sigma'_{v,f}$ (psi)	T_{req} (lb/ft)	% Increase in T_{req}	F.S.	% Decrease in F.S.
EOC	13.5	603.9	-	7.95	-
Test A1	14.8	662.0	9.6%	7.25	8.8%
Test A2	16.4	733.6	21.5%	6.54	17.7%
Test B1	17.0	760.4	25.9%	6.31	20.6%
Test B2	18.8	841.0	39.3%	5.71	28.2%

Key Points

- The above discussion has included explanations of unexpected pressure cell response that occurred in a few instances, and in one case even speculated about what the quantitative response of a pressure cell should have been. Despite occasional irregularities, the earth pressure cells provided useful information and identified several important and logical trends.

- When support is lost beneath part of the foundation, the reinforced soil transfers load to the portion of the foundation where the support conditions are unchanged. Vertical stresses in the fill directly above the region of support loss drop substantially, although this effect diminishes with increasing height above the foundation.

- Only small deformations are required to cause a re-distribution of stresses within the reinforced fill.

- Removing a larger area of support results in larger stress changes at upper levels of the abutment but in similar stress changes at lower levels. The first observation is expected to hold true for any scenario of support loss; the second observation may be a function of the geometry of support removal selected for these tests.

- For the magnitudes of foundation settlement investigated in these tests, stress changes in the reinforced soil depend primarily on the area of support removed and not the depth of support removed.

- Stress increases in the regions of the reinforced fill to which load is transferred imply increased tensile demand in the reinforcement at these locations.

Draw Wire Extensometers

The draw wire extensometers (DWEs) at Level 2 of the abutment were monitored from the time of their installation through construction and all testing sequences. This section describes the general approach to data interpretation, examines the data trends for construction and each of the testing sequences, and presents key points. The extensometer data are considered further in the discussion of the strain gage data in the following section.

General

The attachment points for the extensometers are shown in Figures 16 and 17. Displacements were monitored at four points of the reinforcement on each side of the abutment. The relative displacement between two adjacent points was used to determine the average strain over this length of the reinforcement, resulting in three readings of strain versus time on each side of the abutment. The average strain between the closest and farthest draw wire attachment points can be determined by averaging the three individual components of strain in the strain plots that are presented in this discussion of the DWE data.

During the experiment design process, the authors questioned the ability of the DWEs to exert enough force to retract the draw wire against the forces applied by the overlying fill. The wires had been protected by nylon tubing and lubricated to reduce the sliding resistance as much as possible. Data recorded by the sensors appear to show that this concern was not substantiated. The sensors showed some variations due to temperature fluctuations, but these variations do not obscure the displacement trends. The manufacturer states that the sensors have a resolution of 0.3 mm, although the sensors appeared to record values with a smaller resolution. Nevertheless, some of the figures that follow show the limitations of the sensor resolution.

The DWE data are presented sequentially in the subsequent paragraphs, and each figure is discussed in the following subsections. In all graphs, positive displacements indicate movement away from the sensor (toward the rear of the abutment), and negative displacements indicate movement toward the sensor (toward the face of the abutment). Positive strains denote elongation, while negative strains denote contraction. In many figures, similar levels of displacement or strain can make it difficult to differentiate individual readings. In these cases, captions were added to help distinguish these readings. The exception to this practice was for figures that show minimal changes in displacement over the course of a test. In these cases, it is not important to identify individual trends.

Construction

Figure 63 shows the displacements recorded by the sensors on Side A during construction, which indicate that the DWEs are functioning properly. The sudden spike noted in the middle of construction resulted from a temporary railing post falling across the wires overnight. Once corrected in the morning, no residual effects were observed. While it may be difficult to distinguish individual readings within some time intervals, the overall trends of the data clearly show movement of all points toward the face of the abutment. Two conclusions can be made from this movement. First, the sensors were able to retract the draw wire despite the increasing overburden. Second, strains in the reinforcement developed primarily as a result of displacement of elements of the fabric toward the face. However, this trend should not be mistaken for pullout of the reinforcement. Calculations of pullout resistance during construction show that the fabric had very high factors of safety against pullout, and the magnitude of the displacements is small. Because the reinforced fill is placed and compacted tightly against the ramp at the rear of the abutment, it is only free to displace toward the front of the wall as the fabric strength is mobilized. Therefore it is reasonable to believe that placing and compacting this fill would result in strain toward the face.

These displacements were converted into strains, which are shown in Figure 64. Strains measured at (A2-1→A2-2) and (A2-2→A2-3) increase slowly to approximately 0.1% and then remain relatively constant. Strain measured between (A2-3→A2-4) decreases suddenly and then slowly increases. This decrease may be due to slack introduced to the rear portion of the fabric during the construction process. The method for placing fill near the back of the abutment, described in the "Methods" section, was developed first for Level 2, and some slack may have been introduced.

On Side B, extensometer DW-B2-1 was damaged during installation and was replaced as soon as a new gage could be delivered; extensometer DW-B2-4 recorded invalid data initially due to a loose electrical connection. Both issues were resolved, and displacements were monitored from that time forward, as shown in Figure 65. Displacement trends were similar to those on Side A, with all sensors showing movement toward the abutment face. When these displacements were converted to strains, as shown in Figure 66, the strains tended to be small. However, because two of the sensors could not record the first week of readings, the data for (B2-1→B2-2) and (B2-3→B2-4) do not show any strains that occurred over this time period.

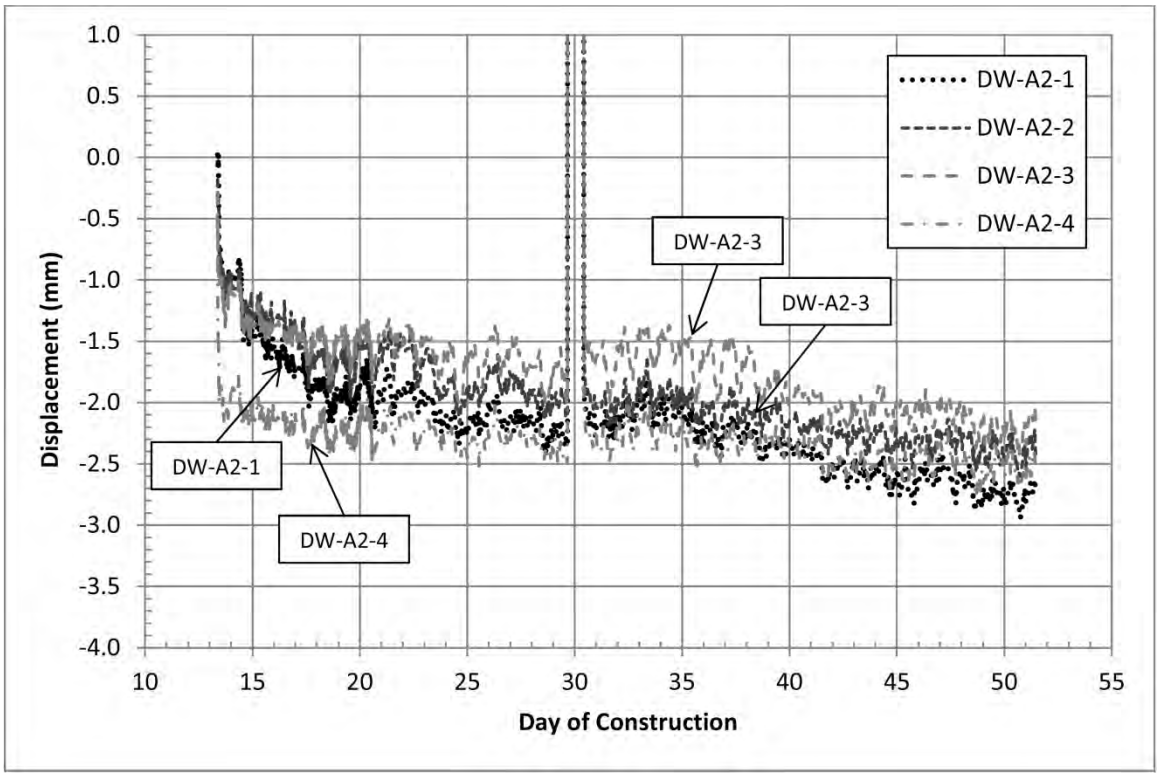

Figure 63. Displacement of DWEs on Side A During Construction

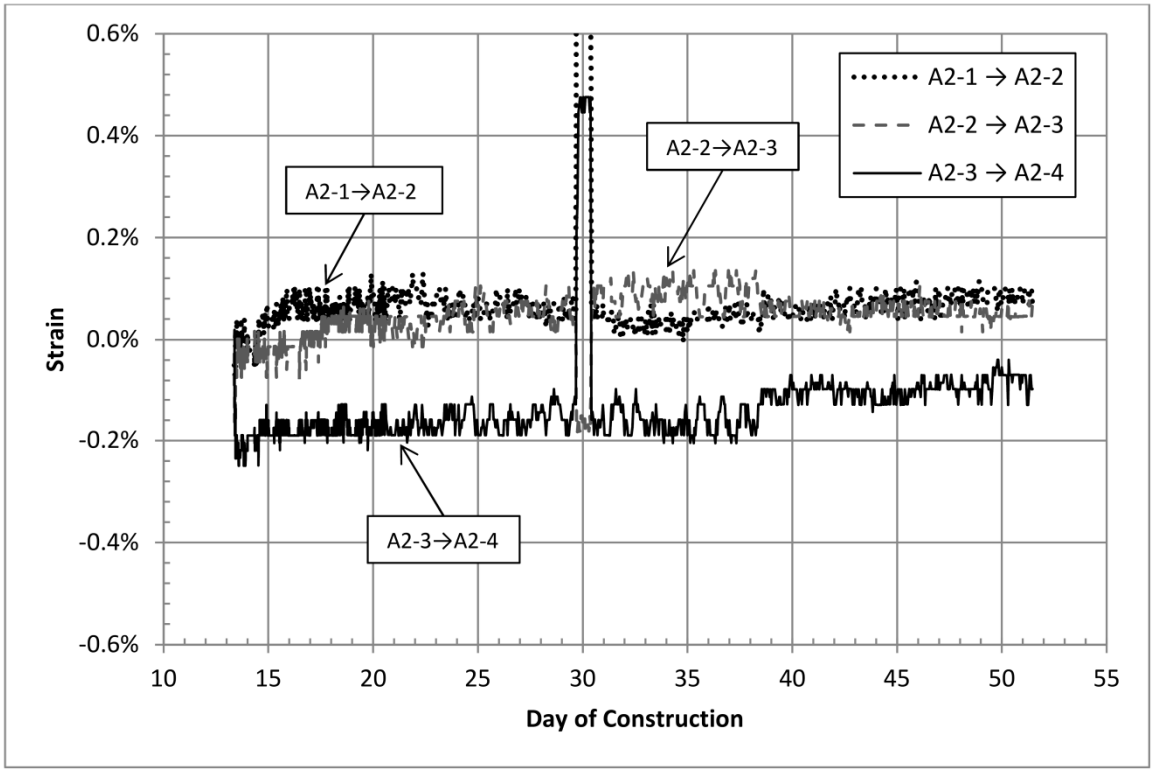

Figure 64. Strain From DWEs on Side A During Construction

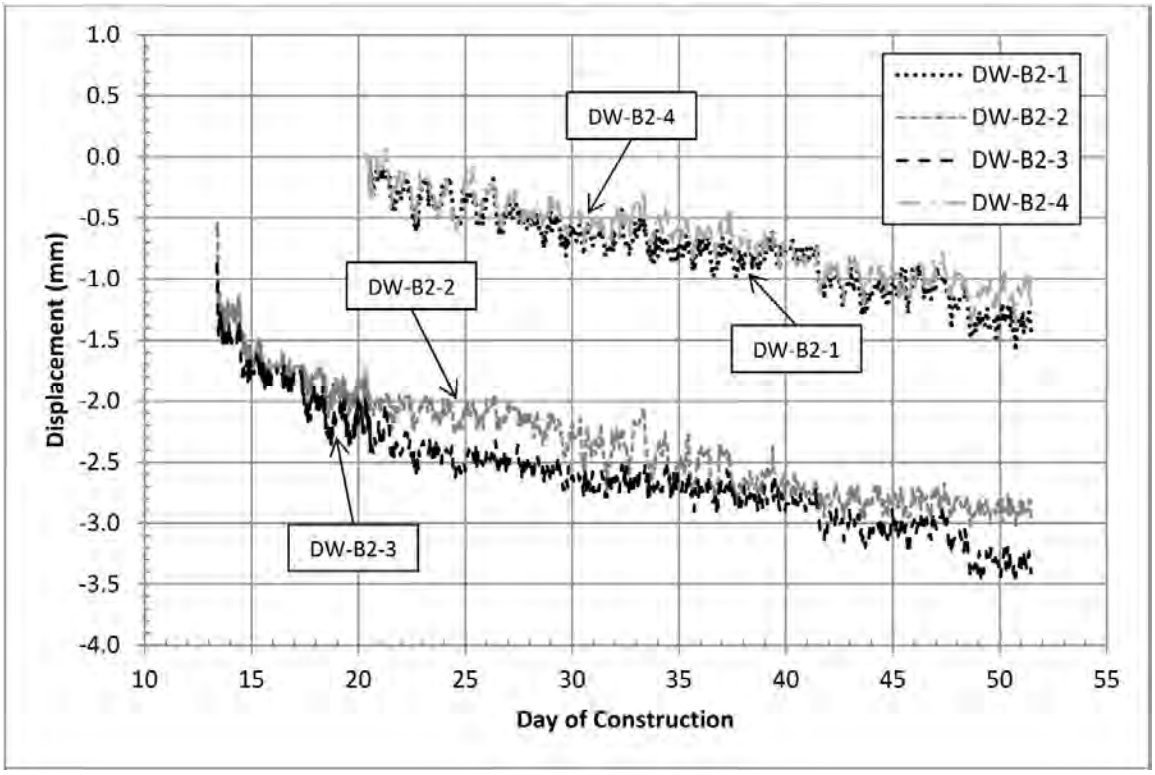

Figure 65. Displacement of DWEs on Side B During Construction

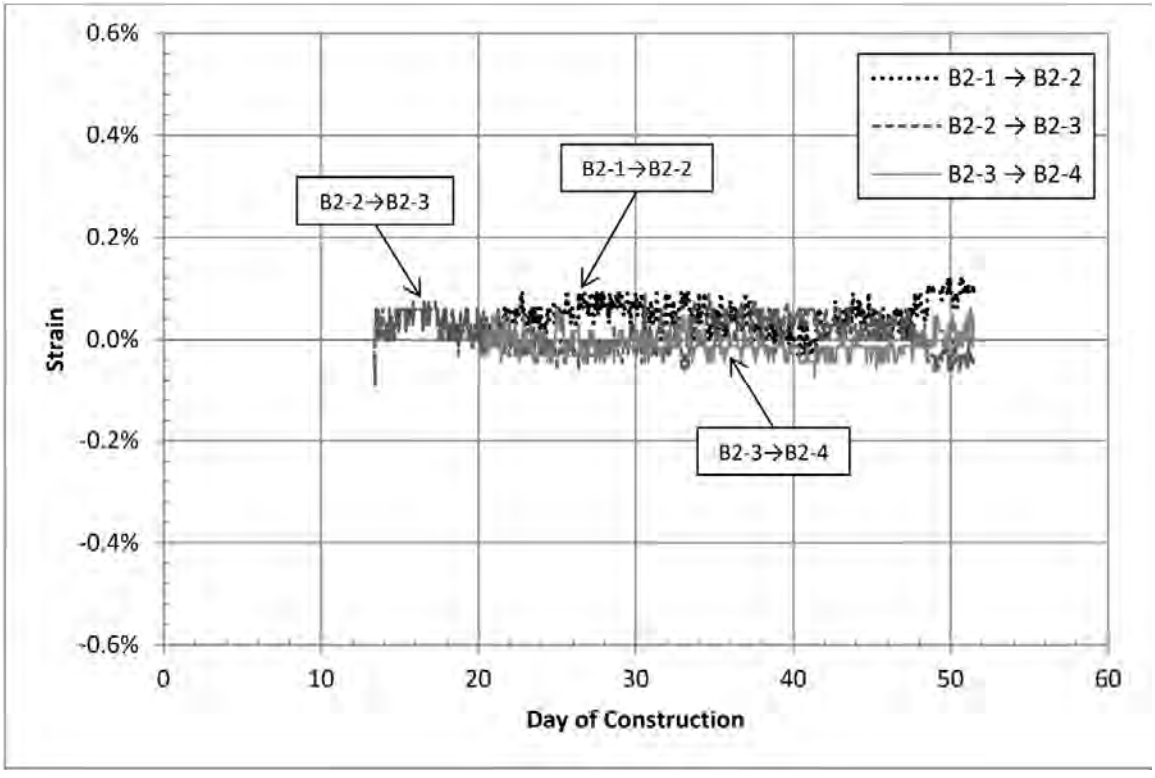

Figure 66. Strain From DWEs on Side B During Construction

On Side A, Figure 64 shows that a significant portion of the final strain occurred within the first week. Consequently, the end-of-construction strains shown in Figure 66 likely do not reflect the actual strain in the reinforcement. Subsequent observations for the testing sequences are based on change in strain during the test and are not influenced by any differences between the end-of-construction readings and actual strains.

The surcharge load was placed on the abutment on Day 47 of construction. The strain data on Side A, shown in Figure 64, do not show any distinguishable response to this event. The strain data on Side B, shown in Figure 66, show a small increase in strain at (B2-1→B2-2) near the end of Day 48, which may be in response to the surcharge placement.

Test A1

Settlement of the facing blocks and reinforcement can influence the displacement readings by lengthening the draw wire. Consequently, for each test, the extensometer data and photographs of the settlement patterns of the CMUs were examined to determine whether the recorded trends were dominated by actual response of the reinforcement or by the influence of settlement. Displacements during Test A1 are presented in Figure 67. The trends show all points moving slightly (about 1 mm) toward the face of the abutment. This behavior is believed to reflect the actual response of the reinforcement. The strains represented by these displacements are shown in Figure 68. Strains were about 0.1% at (A2-1→A2-2) and (A2-2→A2-3) and approximately 0.0% for (A2-3→A2-4). These trends are all very reasonable. The displacements on Side B were zero, as shown in Figure 69.

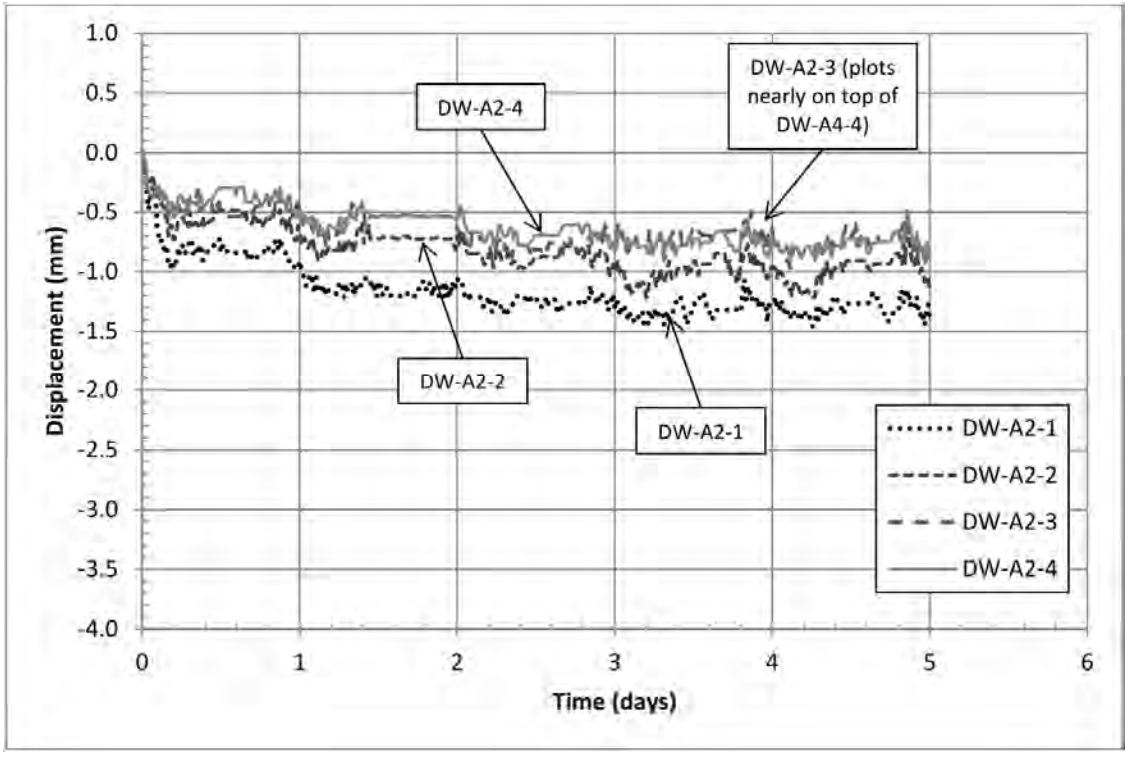

Figure 67. Displacement of DWEs on Side A During Test A1

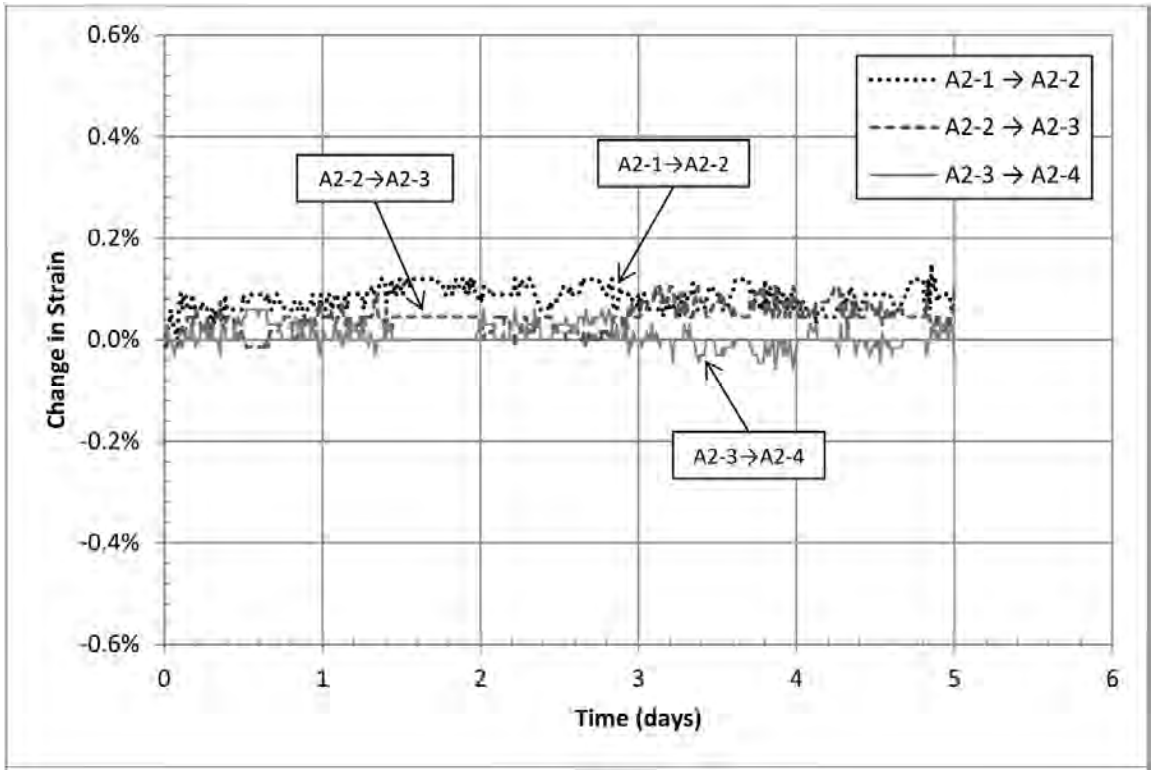

Figure 68. Change in Strain From DWEs on Side A During Test A1

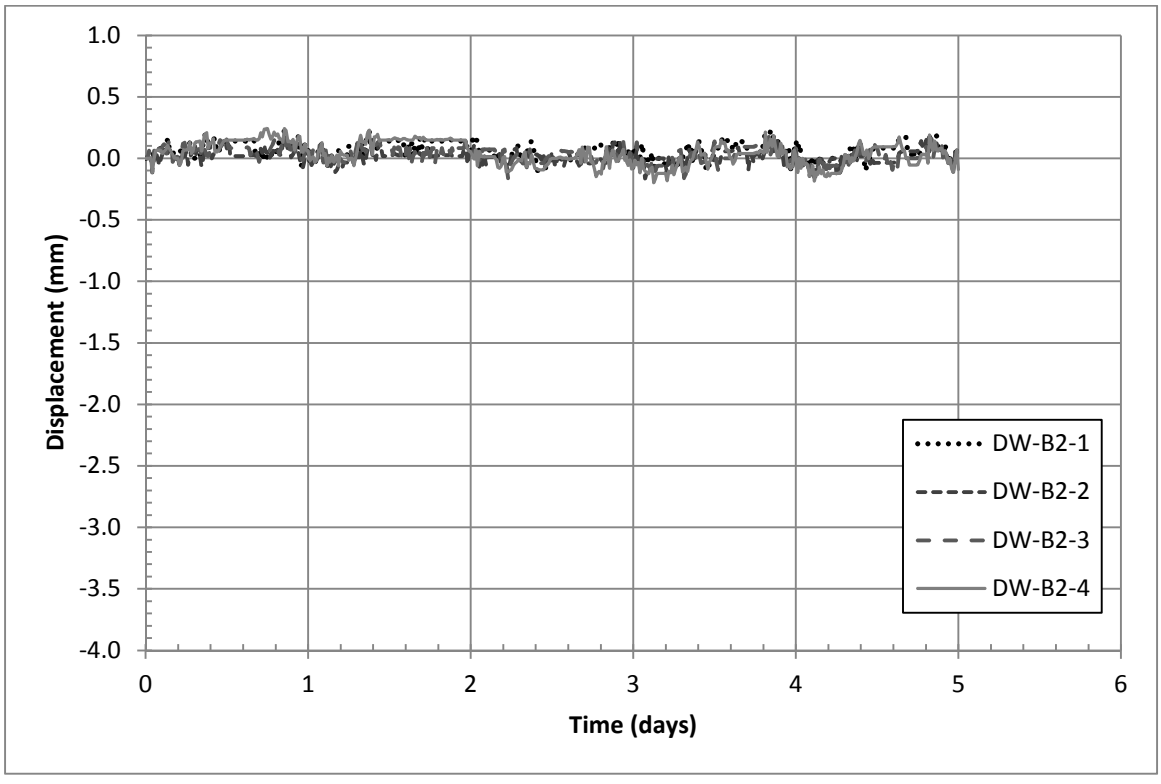

Figure 69. Displacement of DWEs on Side B During Test A1

Test A2

Photographs of the facing CMUs following Test A2 showed that settlement significantly influenced the displacements recorded during the test. Displacements recorded by the extensometers are presented in Figure 70 and generally range between 18 and 20 mm. Survey data can be used to estimate the settlement of the CMU in contact with the draw wires. Knowing the settlement and distance from the CMU to the DWE, the expected positive displacement of the wire from this settlement is estimated to be approximately 10 mm. The observed positive displacement is greater by a factor of two, suggesting that additional settlement of the fill behind the CMUs also contributed to the observed displacements.

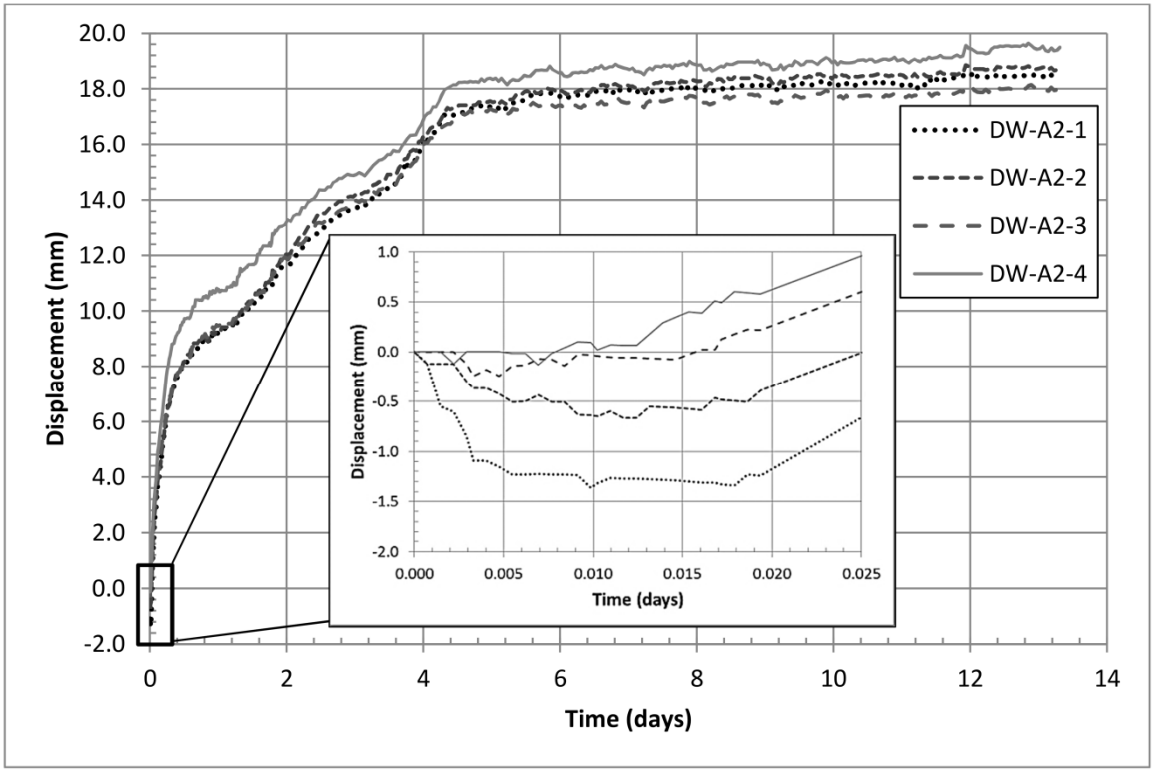

Figure 70. Displacement of DWEs on Side A During Test A2

Immediately following introduction of the solvent to begin Test A2 and before the CMU had settled enough to contact the nylon sleeves around the wires, small negative displacements were observed. These displacements are shown in the insert in Figure 70. It is believed that the overlying CMU contacted the wires at a time of approximately 0.019 days (27 min). The changes in strain corresponding to this time period are shown in Figure 71. The immediate response to the support removal of Test A2 was an increase in strain of approximately 0.1% to 0.2% for all three reinforcement regions. These strains presumably do not represent final values, as settlement and system distortion continued well beyond this time. Subsequent calculations of strain from the extensometers would be obscured by large movements of the CMU blocks. Displacements of Side B during Test A2 are shown in Figure 72 and are once again zero.

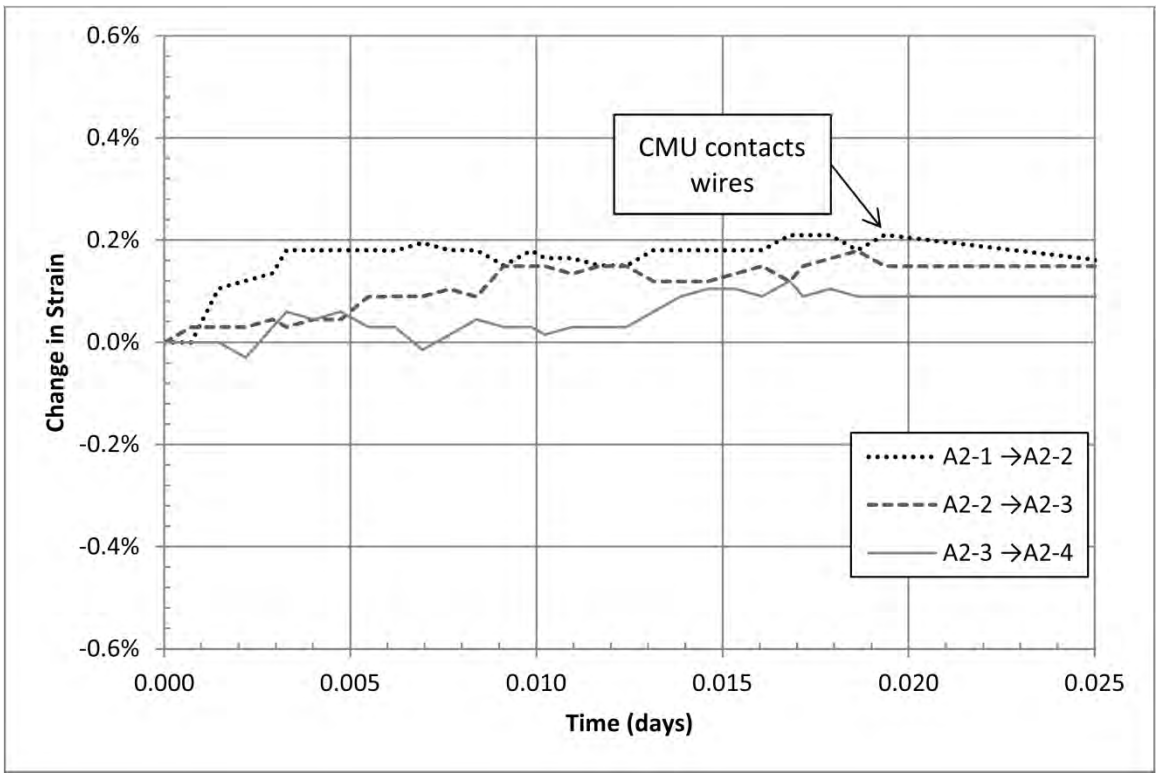

Figure 71. Change in Strain From DWEs on Side A During Initial 0.025 day of Test A2

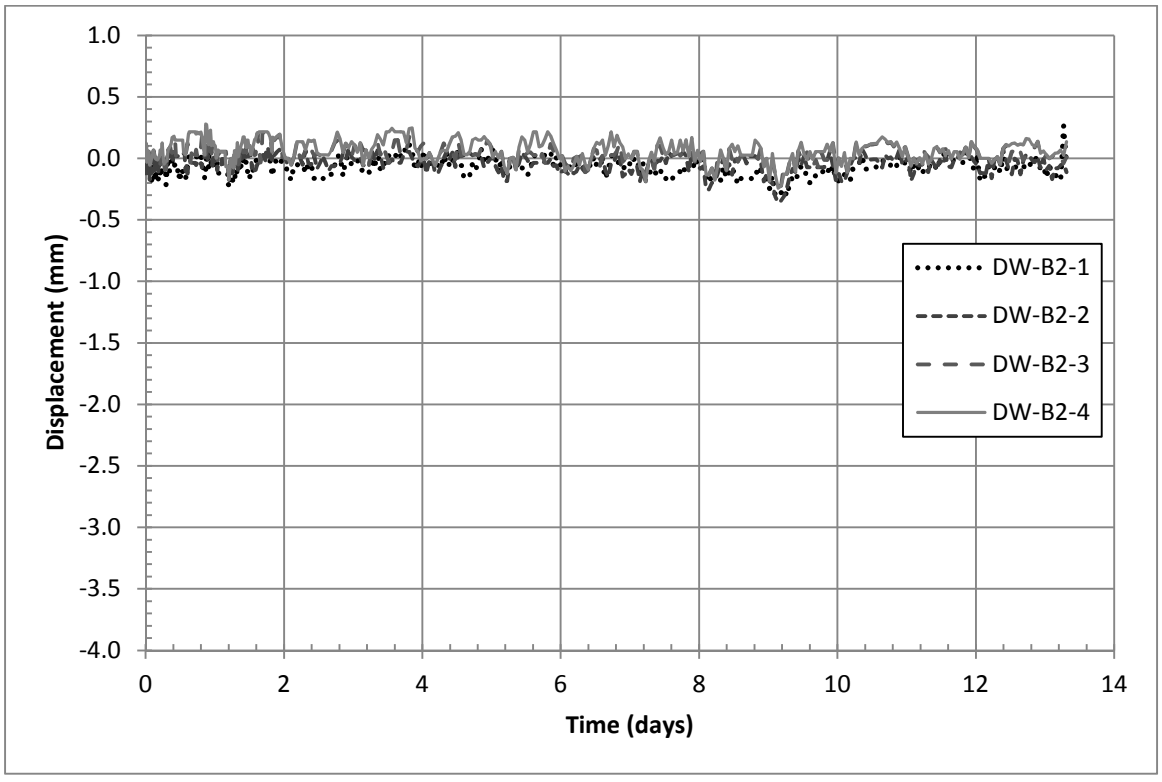

Figure 72. Displacement of DWEs on Side B During Test A2

Test B1

The displacement data on Side B from Test B1 are shown in Figure 73. The displacement data for DW-B2-1 and DW-B2-2 appear to show influence of settlements after the re-start of Test B1 at Day 1.4. However, the subsequent negative displacements may reflect actual strains in the reinforcement. The displacement data for DW-B2-3 and DW-B2-4 indicate movement of the reinforcement toward the face and do not reflect significant settlement influence.

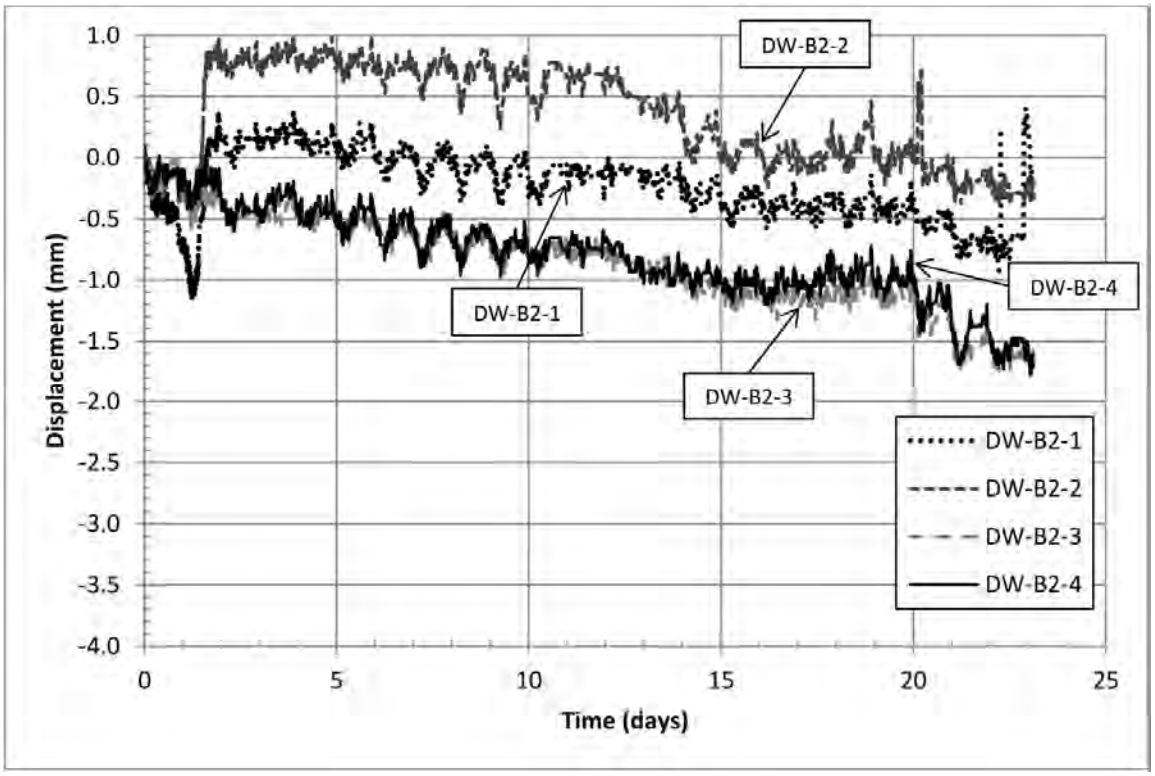

Figure 73. Displacement of DWEs on Side B During Test B1

Figure 74 shows the strains calculated from these displacements. Strain at (B2-3→B2-4) is approximately 0.08% at the end of the test and appears to be a reliable value. The initial large increase of (B2-1→B2-2) strain and the initial large decrease of (B2-2→B2-3) strain are believed to be the result of settlement. The subsequent decrease of (B2-1→B2-2) strain and increase of (B2-2→B2-3) strain around Day 13 may reflect actual changes in the strain of the reinforcement. After having received minimal rainfall since the beginning of Test A1, the test site received 1.95 in of rainfall over these two days, which may have caused the reinforced fill to shift slightly.

Displacements of Side A during Test B1 are shown in Figure 75. A small increase in displacements is visible toward the end of the test, which is believed to be the result of small continued settlements of the facing CMUs at Side A.

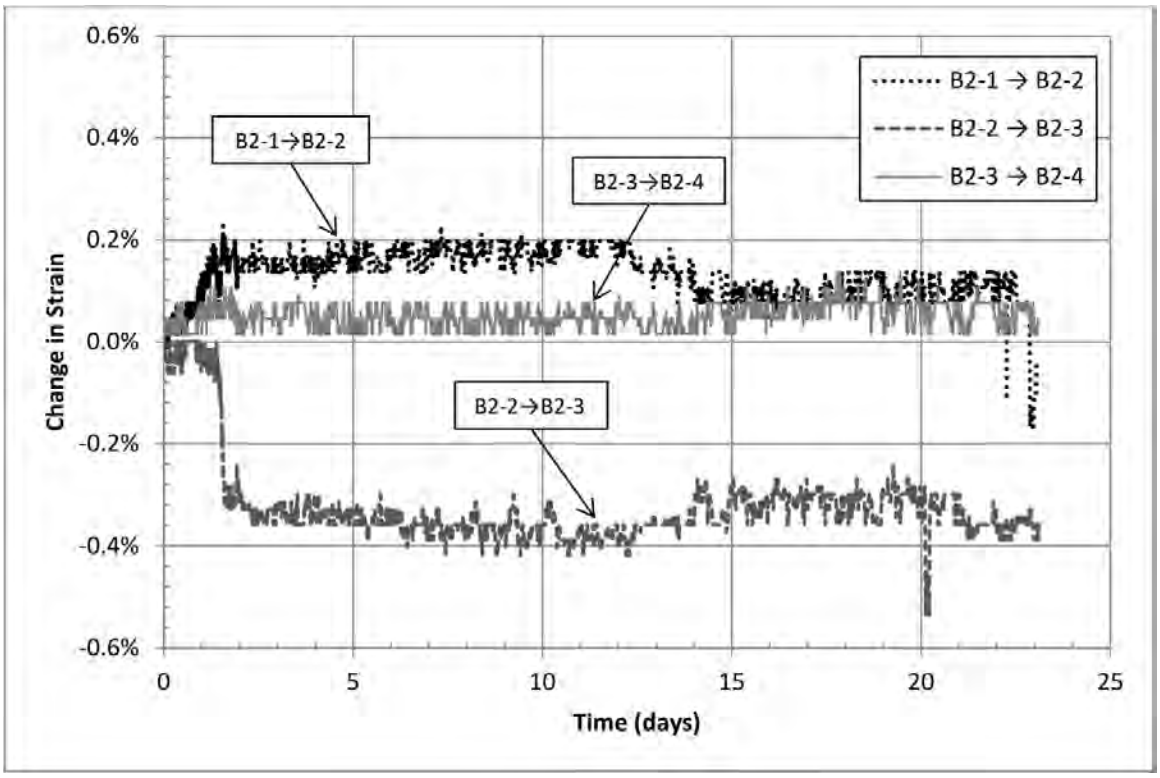

Figure 74. Change in Strain From DWEs on Side B During Test B1

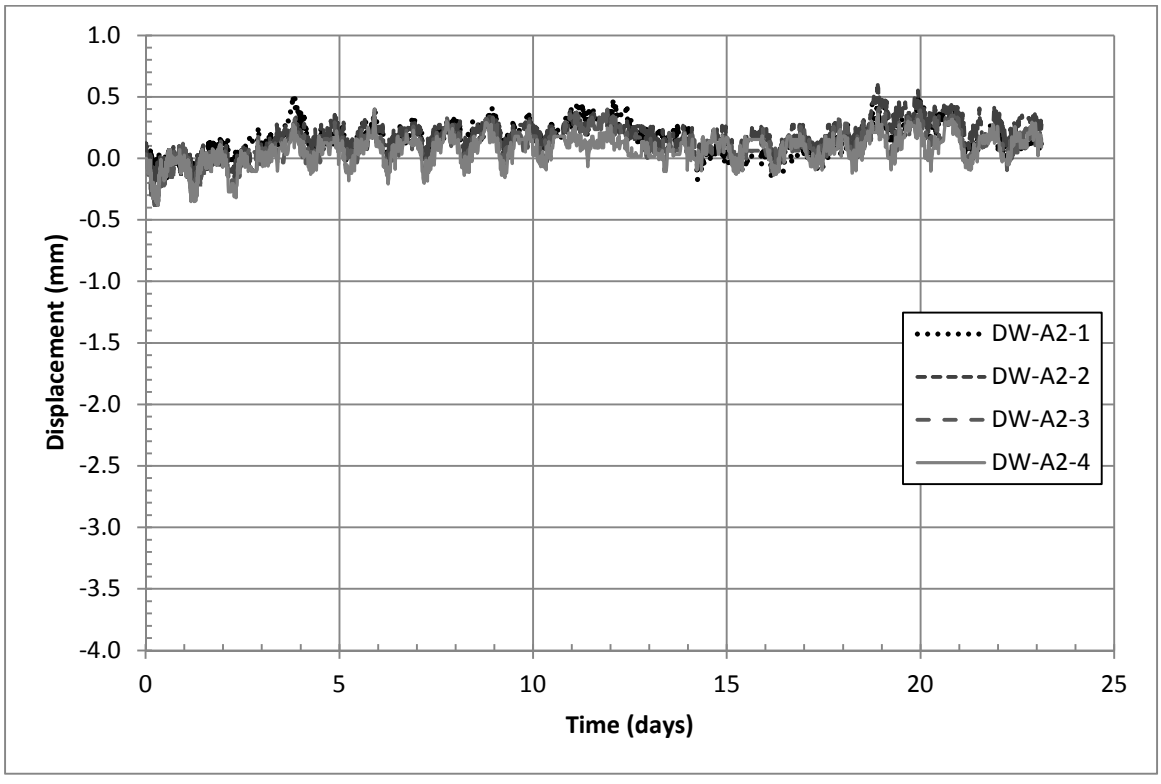

Figure 75. Displacement of DWEs on Side A During Test B1

Test B2

Figure 76 presents the displacement data for the extensometers on Side B during Test B2. These displacements resulted from settlement of the overlying CMU facing block and the reinforcement. At the completion of the test, the relative displacement between adjacent pairs of draw wires was nearly identical, due to the combined settlement and rotation of the overlying CMU. Figure 77 shows a diagram of the location where the draw wires pass through the CMU and the direction of rotation of the CMU during Test B2, which resulted in incrementally larger displacements moving from DW-B2-4 outward to DW-B2-1. In Figure 76, DW-B2-1 initially increased significantly more than the adjacent extensometers but then dropped suddenly to a level consistent with the behavior of other extensometers. This initial increase is believed to have resulted from the wire catching on the edge of the groove in the CMU through which it passes before eventually coming loose.

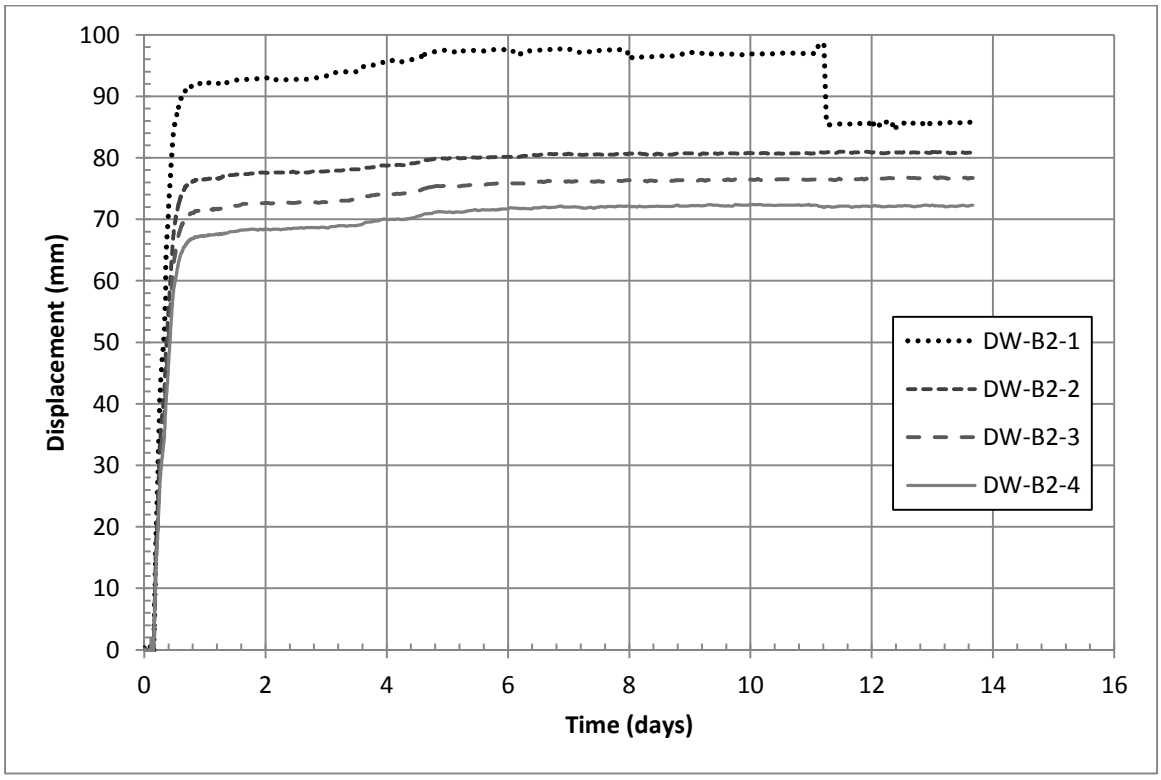

Figure 76. Displacement of DWEs on Side B During Test B2

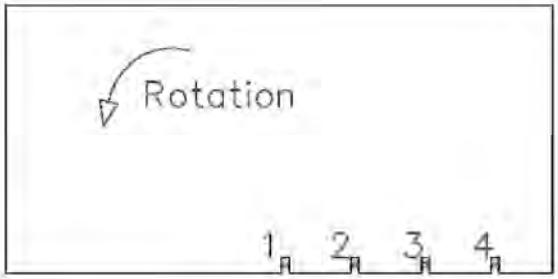

Figure 77. Rotation of CMU Over Side B DWEs During Test B2

Corresponding strains are not presented for the DWEs on Side B for Test B2 since these strains are not considered meaningful due to the large influence of the CMU movement on the measured displacements. Figure 78 shows the displacement of the DWEs on Side A during Test B2. The displacements at this side were essentially zero.

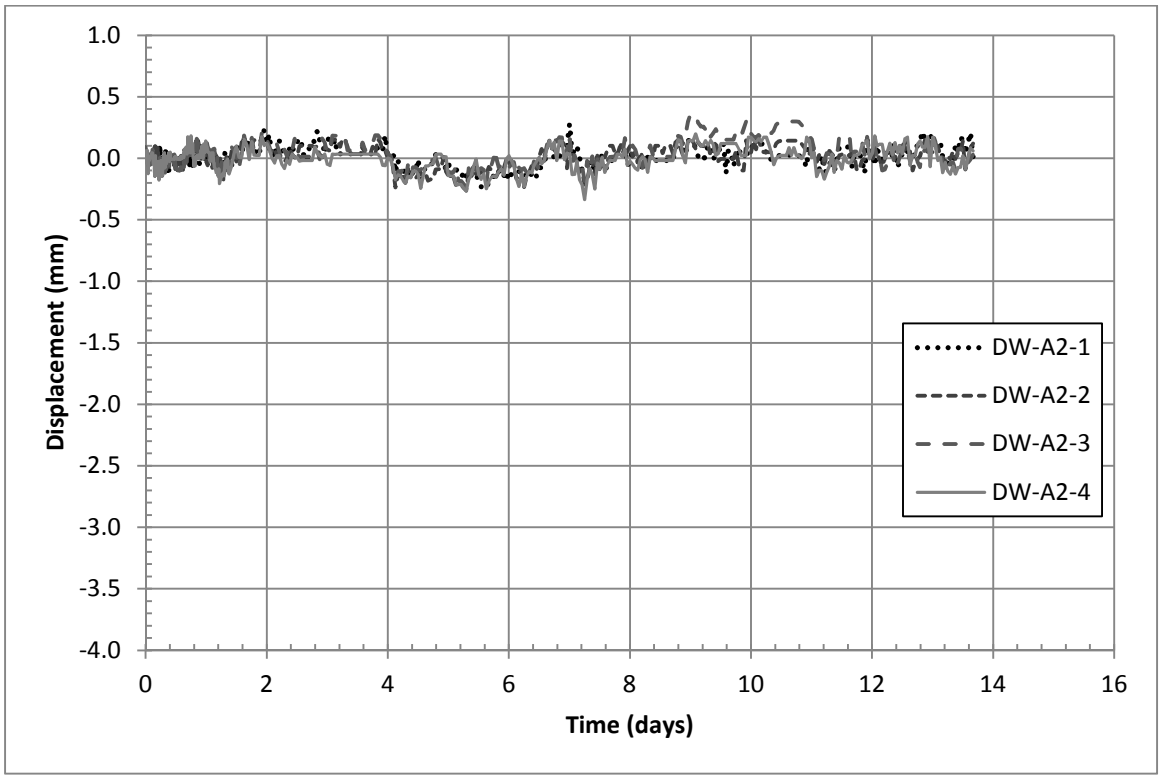

Figure 78. Displacement of DWEs on Side A During Test B2

Key Points

- Strains observed at Level 2 during construction were small, generally less than 0.1%.
- During construction, all measured displacements showed that these strains were directed toward the abutment face.
- Strains during Test A1 and Test B1 were small and generally resulted from displacements toward the face.
- Strains during Test A2 were difficult to identify because large settlement of the facing CMUs and reinforcement controlled the observed displacements; strains during Test B2 were completely obscured by settlements.

Resistance Strain Gauges

Strain gages on Side A were monitored continuously from the time of installation through both testing sequences on Side A. Following the completion of Test A2, these gages were

disconnected, and the gages on Side B were connected. The Side B gages were then monitored through the completion of testing. This section presents general background information for the interpretation of the strain data and discusses the effects of temperature variations and reinforcement curvature on the data. Data collected during construction are discussed, followed by data from each of the four testing sequences. Finally, data from tests on Sides A and B are compared, and key points are presented for this section.

General

Resistance strain gages are an excellent tool to measure small strains of many materials, including geosynthetics. However, their limitations should be recognized. Based on laboratory calibrations, the authors noted that small initial strains of the fabric are not always captured by the strain gages due to differences between the global stiffness of the fabric and the local stiffness in the region of the gage, which is inevitably higher as a result of the adhesive used to apply the gage. Also, some uncertainty exists in the calibration factor used to relate the strain measured by the gage to the strain experienced by the geotextile. Further details on the calibration procedure can be found in the Appendix.

The locations of the gages within the abutment are shown in Figures 16 and 17. All gages survived construction, and all gages performed well for the duration of the tests with the exception of gage FSG-B6-6, which began providing only intermittent readings approximately one week into Test B1. The data that were recorded from FSG-B6-6 appeared reasonable and consistent with general strain trends, and therefore it is included in these figures and the following analysis, although it is not assigned the same level of confidence as data from other gages. The top three courses of the facing CMUs were pinned together using vertical pieces of rebar and concrete, which passed through slits cut in the reinforcement. The CMUs at Level 14 were therefore secured to the reinforcement throughout testing, while the CMUs at Level 6 had the potential to slip at the frictional connection with the reinforcement. However, no trends could be directly attributed to these differences.

Temperature Effects

The wiring configuration used for this project eliminates thermally induced errors due to temperature changes in the lead wires connecting the gages to the datalogger, although the gage itself remained sensitive to temperature fluctuations. Because these wires were exposed to direct radiation from sunlight throughout the summer, this was anticipated to be the primary thermally induced error. Once the gages were covered with the fill, thermally induced strain variations were small, generally less than 0.02% as determined from the trends of the data.

Curvature Effects

Some gages, particularly those closest to the corners of the abutment, recorded negative strains during testing. Two possible reasons were identified for these observations: (1) the reinforcement experienced relaxation, and (2) the gage readings were influenced by curvature of the reinforcement.

In support of factor (1), the earth pressure cell readings at Levels 1 and 16 indicated that vertical pressures dropped in the regions of the reinforced fill above the area of support removal. As vertical pressures dropped and compaction-induced horizontal stresses were lost due to rearrangement of the fill particles, the tension in the reinforcement may have decreased. However, it could also be argued that the tension in the reinforcement may actually increase even though the vertical pressures were decreasing. Vertical pressures decreased due to the bridging action of the reinforced fill, which requires the reinforcement to carry additional load. It is not known whether this increased demand extended completely to the corners when the area of support loss is small. In such cases, the facing blocks remained self-supporting at the level of the strain gages and did not require additional support from the reinforcement. However, the dead weight of the fill alone could still result in an increase in strain at the gage locations. Particularly during removal of the smaller area of support on each side, the frictional connection between the facing CMUs and the reinforcement remained strong. Comparison of the survey and settlement profiling data shows that the fill settled more than the CMUs, and the magnitude of settlement decreased with height. The reinforcement then must carry the weight of a portion of this fill lift, a force that was previously carried by the underlying lift. Consequently, it is not likely that the fabric experienced relaxation at the location of the strain gages.

Settlement data and post-testing deconstruction both suggest that the curvature is primarily responsible for the negative strains observed during some tests. In describing the shape of the curvature, the terms "upward" and "downward" are used as illustrated in Figure 79. Because the gages were placed only on the upper side of the reinforcement, upward curvature will cause the gage to shorten, and downward curvature will cause the gage to extend. The settlement profiler data reveal that, when the fill settled more than the facing blocks, the profiling tubes experienced an upward bend behind the face. Farther from the face, the tube formed a downward bend. A similar trend would be expected of the reinforcement, and in fact was observed during deconstruction of the abutment.

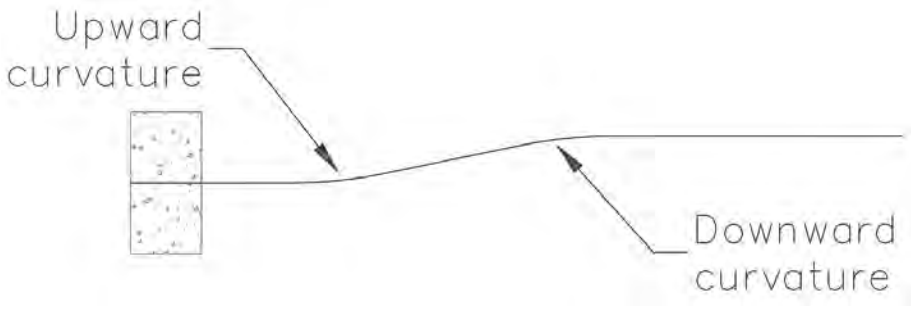

Figure 79. Illustration of "Upward" and "Downward" Curvature

Figures 80 and 81 provide visual confirmation that the curvature of the reinforcement follows these patterns. Disturbance has likely altered the exact deformation patterns to some extent, but the overall trends should be consistent with the post-testing state. Therefore, the authors believe that, in most cases, strain decreases during testing are the result of reinforcement curvature rather than relaxation.

Downward fabric curvature may also have contributed to strain readings that are higher than the true strain in the fabric. This influence is more difficult to identify in the strain readings.

Figure 80. Side A, Level 5 During Deconstruction

Figure 81. Side B, Level 5 During Deconstruction

Construction

Only the gages on Side A could be monitored during construction due to the limited number of channels on the multiplexor. The data are presented in Figures 82 and 83. These figures present the strain versus time plots for each of the gages on Side A, shown according to the position of the gage on the reinforcement. Both the horizontal and vertical scales are identical for all graphs during the construction period to permit easy comparison between the strain levels at various locations. The strains at all gages increased non-linearly with time. This trend is the result of two factors. First, the lower levels of the abutment required less fill and less work to raise the support ramp, and therefore were constructed more rapidly.

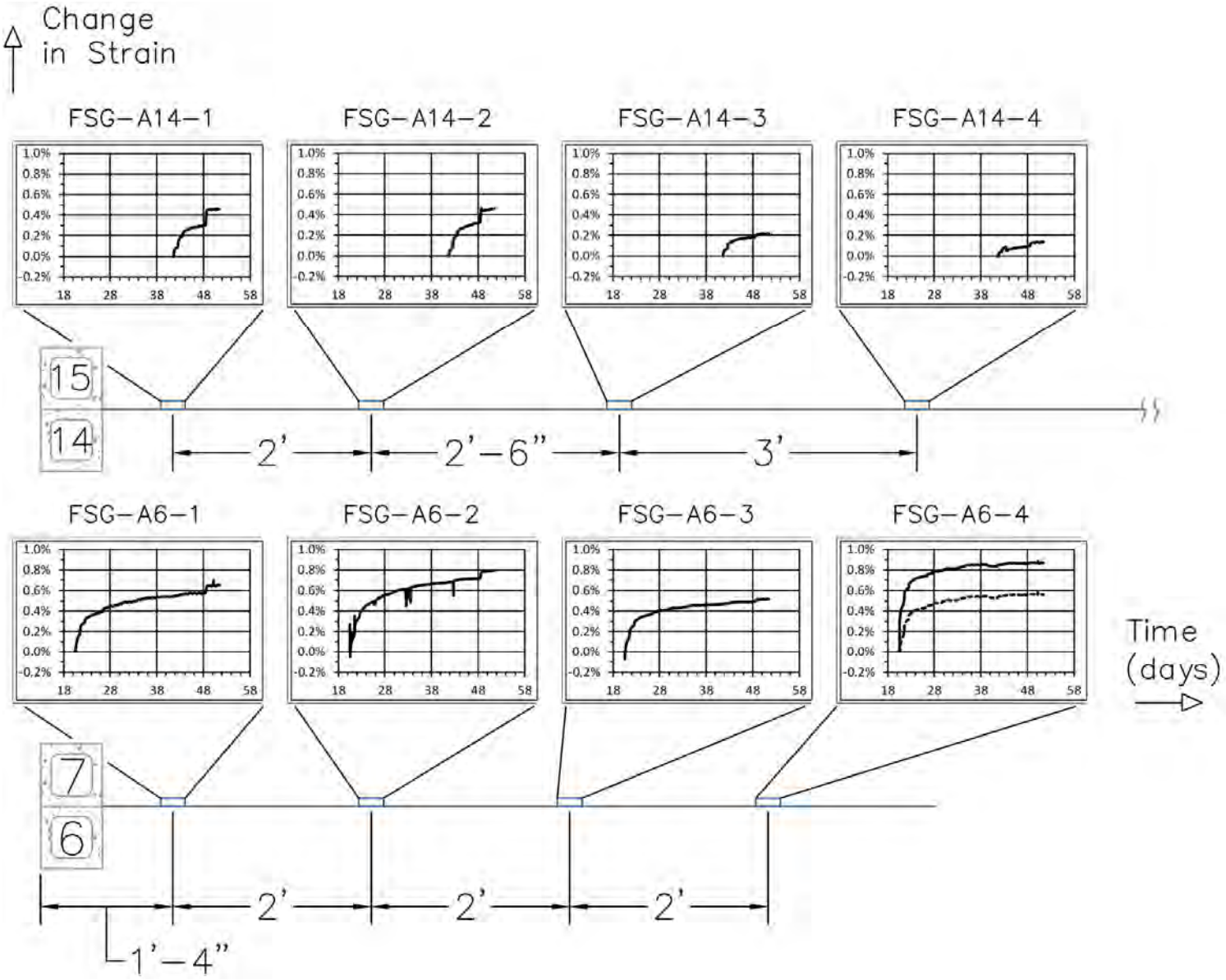

Figure 82. Strain Data for Side A Gages Oriented Perpendicular to the Wall Face During Construction

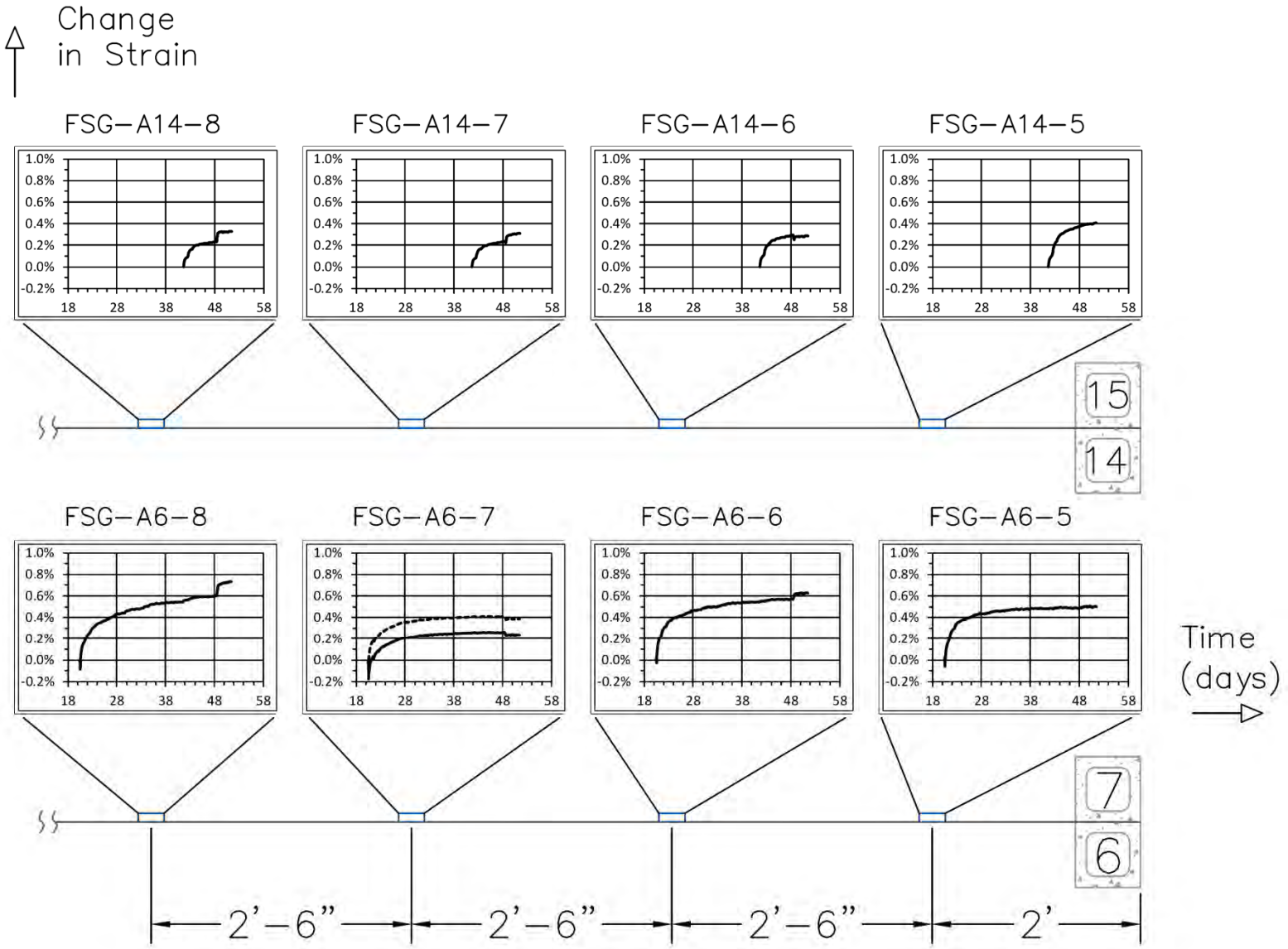

Figure 83. Strain Data for Side A Gages Oriented Parallel to the Wall Face During Construction

Construction of the upper levels required more fill and time to raise the ramp. Vertical stresses therefore increased at a nonlinear rate, as shown by the pressure cell data in Figures 53 and 54. Second, the geosynthetic reinforcement possesses nonlinear stress-strain behavior, displaying a lower elastic secant modulus at low strains than at moderate strains.

In the early stages of construction, most of the gages at Level 6 recorded a brief period of small, negative strain. Because this behavior was not observed at any of the gages in Level 14, it is believed to have occurred due to small amounts of slack introduced at this level when placing the fill and not from any effect of the geotextile's Poisson ratio, which is believed to have a low value. The behavior of FSG-A6-7 in particular showed a sharp decrease of -0.2% in this time interval. If this negative strain is removed from the data, the trend would follow the dashed line overlaid on the same graph in Figure 83. Because all of the gages at Level 6 oriented parallel to the abutment face showed small negative strains shortly after placement of the fill, a more representative strain value for this gage location likely falls between these two lines.

Near the end of construction, on Day 48, the effect of the placement of the surcharge load is visible. Most gages recorded an effect of the placement of the surcharge load. On average, the placement of the surcharge load induced strains in Level 14 that were twice the strains induced in Level 6. Two gages, FSG-A6-7 and FSG-A14-6, showed small decreases in strain when the surcharge load was placed. The reasons for this response are not immediately clear but are presumed to be the result of shifting stress distribution patterns within the reinforced fill.

At the end of construction, gages at Level 6 displayed larger strains than the gages at Level 14. This result is expected. While the horizontal stresses in the fill are expected to be larger beneath the surcharge load at Level 14, additional layers of secondary reinforcement were placed at 4-in spacing in the upper five levels of the abutment. Without these additional layers, the method presented in the FHWA manual (Adams et al., 2011) predicts that the tensile demand in Level 14 will be higher than that of Level 6. With the secondary reinforcement, the predicted demand at Level 14 is only about 40% of the demand at Level 6.

It is interesting, and perhaps surprising, that of all the gages in Level 6, FSG-A6-4 recorded the highest level of strain. However, the slope of the initial portion of the strain versus time plot is very steep, suggesting that minimal tensile force was developed in the reinforcement over these strains. If the initial 0.3% of strain is discounted, the strain follows the trend shown by the dashed line overlaid on the same graph in Figure 82. These trends are comparable to the levels at FSG-A6-3.

Gages FSG-A14-1 and FSG-A14-2 display almost identical behavior. Both gages would have experienced a similar compaction effort, and the gages are spaced symmetrically about the centerline of the surcharge load. Therefore, similarity of strains observed during construction and placement of the surcharge load is reasonable. Gages FSG-A6-1 and FSG-A6-2 also display similar trends, although the strain levels at FSG-A6-1 are lower than those at FSG-A6-2. This may indicate that compaction immediately behind the face was not as effective as at other regions in this lift, or it may indicate that the facing CMUs were carrying some of the load from the overlying fill, reducing the demand on the fabric near the face. Upon placement of the surcharge load, the strain increased equally at both gages.

The woven geotextile used as reinforcement possesses different stiffness properties in the two planes of the fabric. The stiffness in the machine direction is lower than the stiffness in the cross-machine direction of the roll, and this would result in larger strains at the same tensile force in the reinforcement. During construction, strains observed in the machine direction (parallel to the abutment face) were generally not larger than those in the cross-machine direction (perpendicular to the abutment face), which suggests that the forces in the direction perpendicular to the abutment face were larger than in the direction parallel to the abutment face.

Comparison of Observed and Predicted Strains during Surcharge Placement

Adams et al. (2011) provide a procedure, referred to here as the FHWA procedure, for calculating the maximum lateral strain of the abutment due to the application of the bridge load. First, the vertical strain of the reinforced soil mass under the bridge load must be estimated, either by conducting a full-scale, stress-strain performance test or by using a stress-strain curve given by Adams et al. (2011). As shown in Table 5, the materials used in the FHWA performance test are very similar to those used in the Virginia Tech test abutment, and therefore it is reasonable to use this stress-strain curve. For a surcharge load of 1750 psf, the estimated vertical strain is 0.18% from the FHWA performance test.

Table 5. Comparison of materials for FHWA performance test and VT test abutment.

	FHWA Performance Test Adams et al. (2011)	**VT Test Abutment (this report)**
Fill	ASTM No. 89	ASTM No. 8
Max Particle Size	0.5 in	0.5 in
Passing No. 16 Sieve	0 – 10%	0 – 5%
Friction Angle	48°	44° (assumed for design)
Reinforcement Type	Woven polypropylene, biaxial	Woven polypropylene, biaxial
Reinforcement T_{ult}	4800 lb/ft	4800 lb/ft

The FHWA procedure then assumes that no volume change has occurred and that a plane strain condition exists – that is, all lateral strains are in the direction of the abutment face. Both of these assumptions are conservative with respect to the strain magnitude. The procedure also assumes that the lateral strain follows a triangular profile, such as the profile shown for the Virginia Tech test abutment in Figure 84. The maximum lateral strain occurs at an unknown height, *a*H, above the foundation. The FHWA procedure does not give specific guidance on determining *a*, but it does note that *a* is generally larger than 0.67. The value of *a* does not influence the calculated magnitude of the maximum strain, although it does influence the strain distribution. Using these assumptions, the FHWA procedure then calculates the maximum lateral strain to be twice the vertical strain of the abutment. For this case, this maximum lateral strain is 0.35%.

The strain gages recorded the increase in strain due to the application of the surcharge load at Levels 6 and 14. For the purpose of comparison, the point of maximum lateral strain was assumed to occur at a height of 0.75H, as shown in Figure 84. The triangular profile was then used to determine the predicted strain increases at Levels 6 and 14 due to application of the surcharge load according to the FHWA procedure.

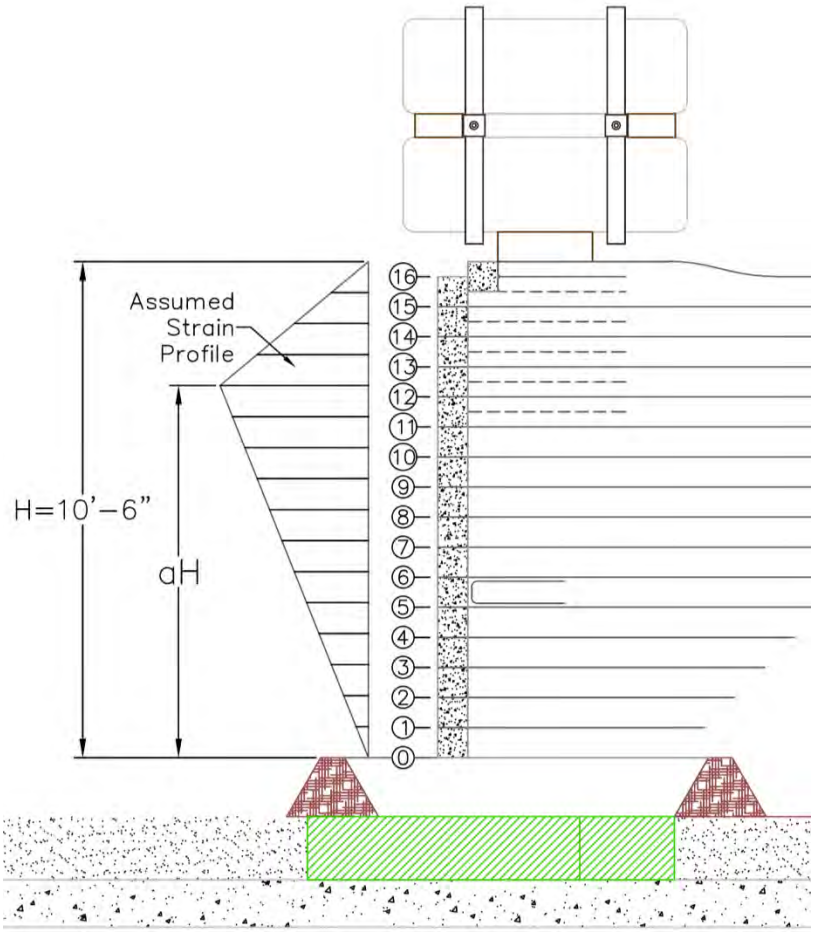

Figure 84. Lateral Strain Profile Assumed in FHWA Procedure, With *a* = 0.75

Table 6 compares the observed and predicted strain increase at each level. For this table, the observed strains were calculated as the average of readings from FSG-A6-1 and FSG-A6-2 for Level 6, and the average of readings from FSG-A14-1 and FSG-A14-2 for Level 14. This approach gives a good average of the strains directly below the surcharge foundation, which is consistent with the conditions under which the FHWA procedure was developed.

Table 6. Comparison of Observed and Predicted Strains With Surcharge Placement

Level	Height Above Foundation (ft)	Strain Increase with Surcharge Placement	
		Observed	Predicted
6	3.81	0.07%	0.17%
14	8.90	0.14%	0.21%

Table 6 shows that the predicted strains were slightly conservative. Several assumptions are incorporated in the FHWA procedure and this comparison, which may have contributed to this over-prediction. In particular, the assumption of plane strain may be inaccurate at the location of the strain gages, which are closer to the wing walls than the center of the abutment. However, the values in Table 6 indicate that the FHWA procedure does provide a reasonable estimate of lateral strains in this case.

Test A1

The change in strain at each gage location for Test A1 is plotted as a function of time in Figures 85 and 86. The vertical axis scale is consistent for all plots, and this scale is maintained for the results of all future testing sequences. In the discussion of future tests, the horizontal scale changes according to the length of the test since the length of tests can vary significantly.

Many of the gages stabilized within five days after testing commenced, but many also showed small continued increases in strain through the duration of testing. Testing was terminated when the observed settlements of the facing blocks were less than 0.003 ft in 24 hours and pressure cell data demonstrated asymptotic trends. However, it is known that small settlements of the facing blocks and fill continued after this time. It is therefore reasonable to observe small continued increases in strain.

In the direction perpendicular to the face, the gage at each level closest to the face demonstrated negative strain changes. In the direction parallel to the face, the gage at each level closest to the wing wall demonstrated no change in strain. These readings are believed to be influenced by upward curvature of the fabric. In future discussions of testing, these four gages and the corresponding four gages on Side B often display strain patterns different from other gages and are referred to as the "corner gages." All other strains were positive, indicating that the reinforcement helped to bridge the area where support was lost and transfer load from both the self-weight of the abutment and the surcharge load toward the center of the abutment. The magnitude of strain changes during Test A1 was small (less than 0.10%), with the exception of FSG-A6-1.

In Figure 85, the trends at Level 6 and Level 14 for gages perpendicular to the abutment face are consistent with each other, and the magnitude of strain is generally larger at Level 6. At Level 14, the strain in the three rear gages is nearly identical by the end of testing. At Level 6, the strain in the middle two gages is nearly identical, and the strain at the rear gage is very small. These trends show a larger area of influence at Level 14 than Level 6, although the magnitude of that influence is larger at Level 6.

In Figure 86, the trends at Level 6 and Level 14 for gages parallel to the abutment face are again consistent. The magnitude of strain is nearly identical for each corresponding Level 6 and Level 14 gage. The exception is at the gage closest to the centerline of the abutment at each level, where FSG-A6-8 shows a significantly larger increase in strain than FSG-A14-8.

The strain data in Figure 85 can also be compared with the extensometer data collected at Level 2 of the abutment, which are shown in Figure 68. The extensometer data show strains of approximately 0.10% in the front two thirds of the reinforcement and minimal strains in the rear third of the reinforcement. These trends compare well with the strain gage data, and the strain magnitudes from the extensometers at Level 2 are slightly higher than from the strain gages at Level 6, which is consistent with the strain reduction observed when moving from Level 6 to Level 14.

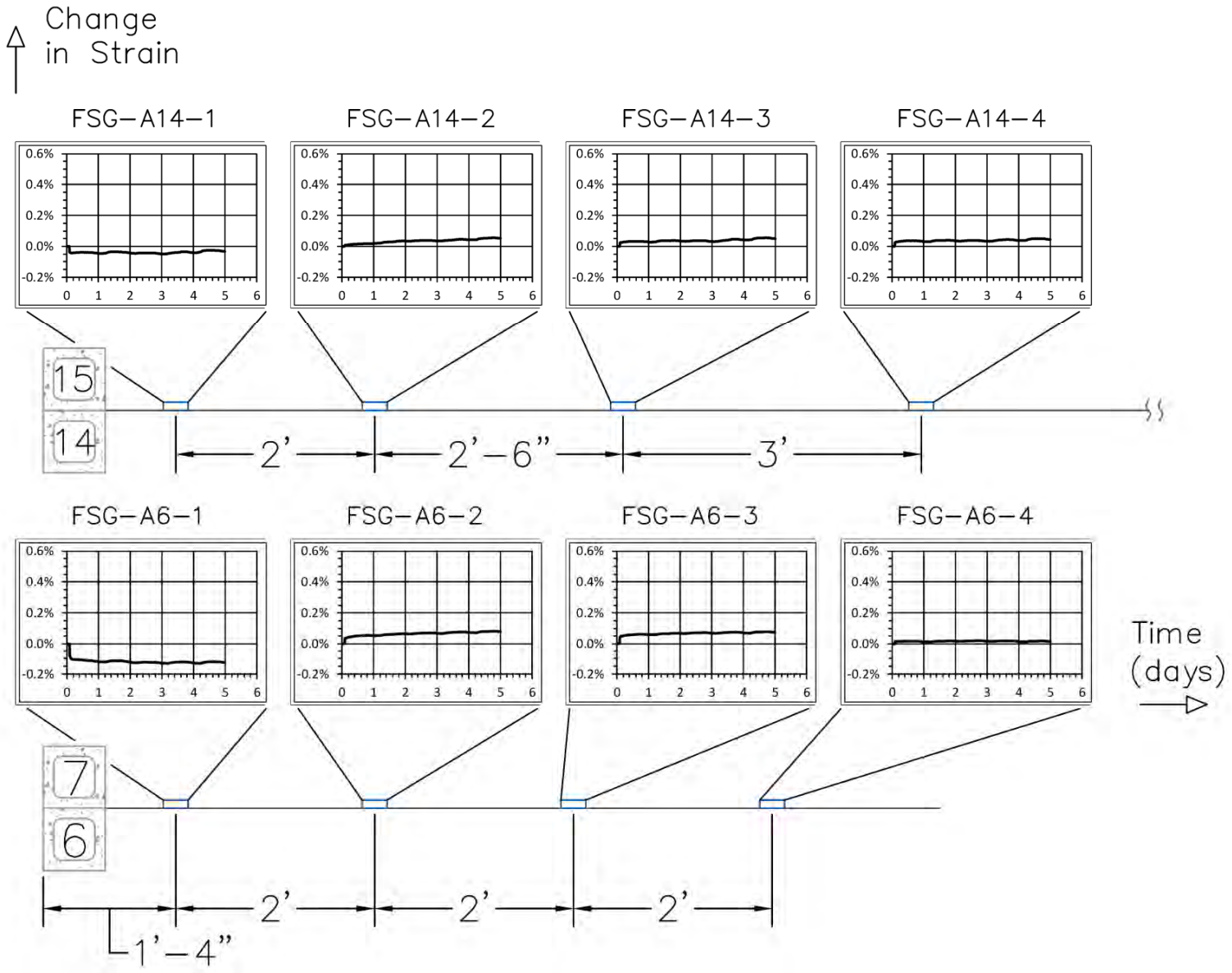

Figure 85. Strain Data for Side A Gages Oriented Perpendicular to the Wall Face During Test A1

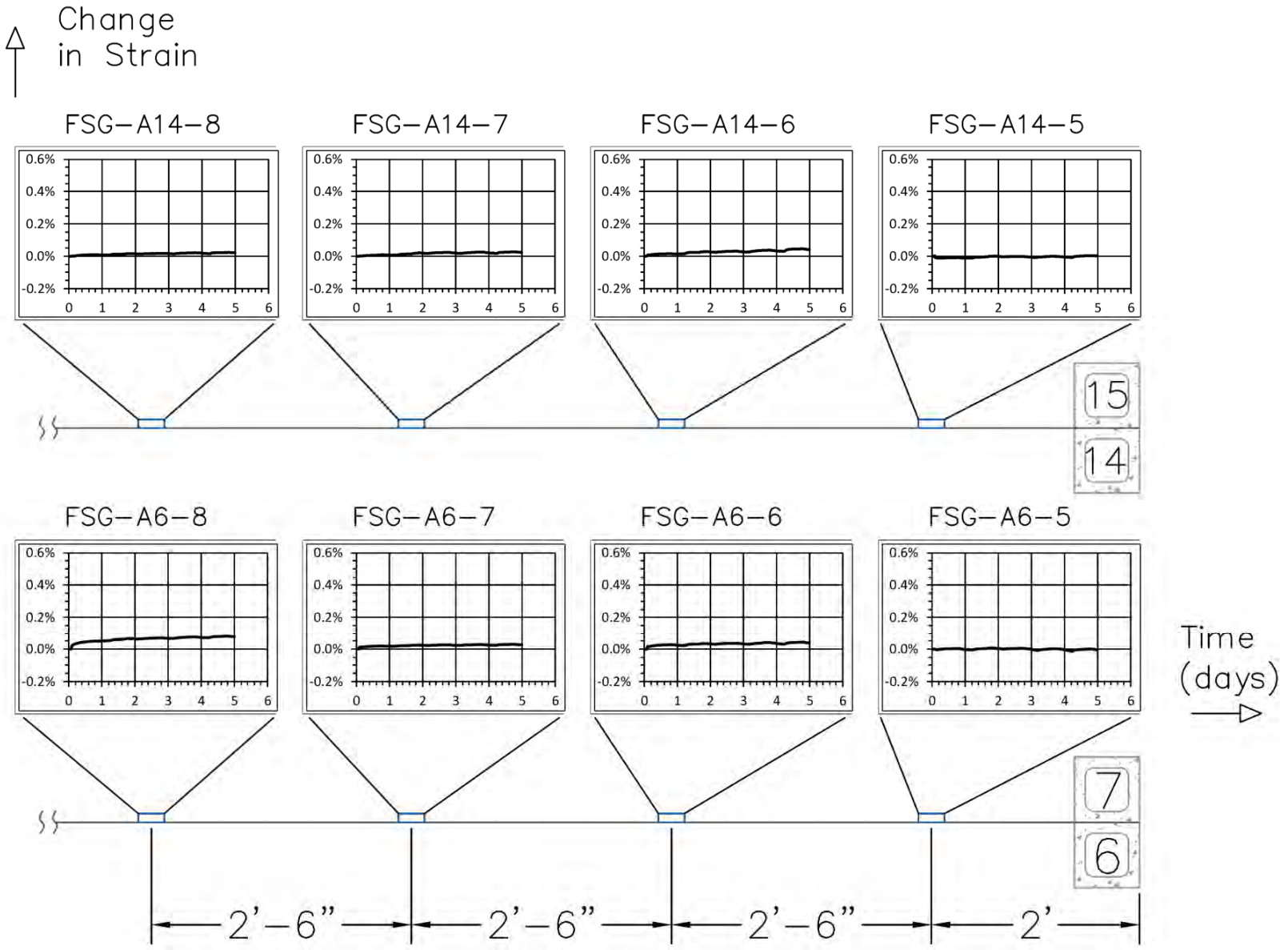

Figure 86. Strain Data for Side A Gages Oriented Parallel to the Wall Face During Test A1

Test A2

The change in strain at each gage location for Test A2 is plotted as a function of time in Figures 87 and 88. Strains measured in Test A2 tended to be larger than the strains measured in Test A1, as expected, but nearly all strain increases were still less than 0.3%. Strains continued to increase at most gages over the duration of the test. Survey data continued to show small settlements of the abutment for several weeks after the completion of testing, leading to increased strains in the reinforcement. It is also possible that the increasingly downward curvature of the fabric induced by these settlements had an influence on these strain values. However, it is believed that the strain increases recorded represent actual increases in the tensile forces in the reinforcement.

In Figure 87, the gages at Level 6 perpendicular to the face showed a variety of trends. FSG-A6-1 showed a large increase in strain (in fact, the largest strain observed during any testing sequence) that resulted in a net positive strain for Tests A1 and A2. For this test, FSG-A6-2 exhibited negative strains, again attributed to upward curvature of the fabric. The area of support removal has increased, and it is logical that the settlement causes the inflection point of the reinforcement to shift farther from the corner of the abutment. These two gages also show an apparent shift in the reinforced fill approximately two days into testing. The strain at FSG-A6-3 follows the expected trend and is similar to its behavior in Test A1. The strain at FSG-A6-4 initially increases slightly (0.02%) and then returns to zero net change for the test. The gages at Level 14 all showed positive strains during the test. All magnitudes were larger than the corresponding values for Test A1, and the strains were relatively uniform at the three rear gages.

In Figure 88, the gages at Level 6 parallel to the face generally displayed trends corresponding well with the trends at Level 14. FSG-A6-5 and FSG-A6-6 also indicate the apparent shift in the fill approximately two days into testing, with the reinforcement at FSG-A6-5 transferring some of its tension to the reinforcement at FSG-A6-6. Particularly at the two gages closest to the center of the abutment at each level, the strain distribution is uniform. Level 6 strains are approximately twice the strains at Level 14. When compared with Test A1 strains in Figure 86, strains are significantly larger during Test A2 at all locations.

A lack of reliable DWE data for this test makes a comparison with the DWE data difficult. Figure 71 shows that strains in the fabric during the first 0.019 day (27 min.) of testing were approximately 0.2% near the front of the abutment and 0.1% near the rear. When compared with Figure 87, these trends appear reasonable.

The total strain levels at the end of construction (EOC), after Test A1, and after Test A2 are plotted for the gages perpendicular to the face in Figure 89 and for the gages parallel to the face in Figure 90. The changes in strain for each test are equal to the distance between the curves. However, the primary observation from these graphs is that the maximum strain in the fabric remains relatively small. After constructing the abutment, applying the surcharge load, and incrementally removing 8 in of support from beneath a large area on this side of the abutment, the maximum strain observed at these two levels of the abutment was still only around 1%. The FHWA method requires the abutment to be designed such that the required tensile demand is less than the reinforcement strength at 2% strain, and these observations fall well within this criterion, even after the severe loading condition imposed on the abutment.

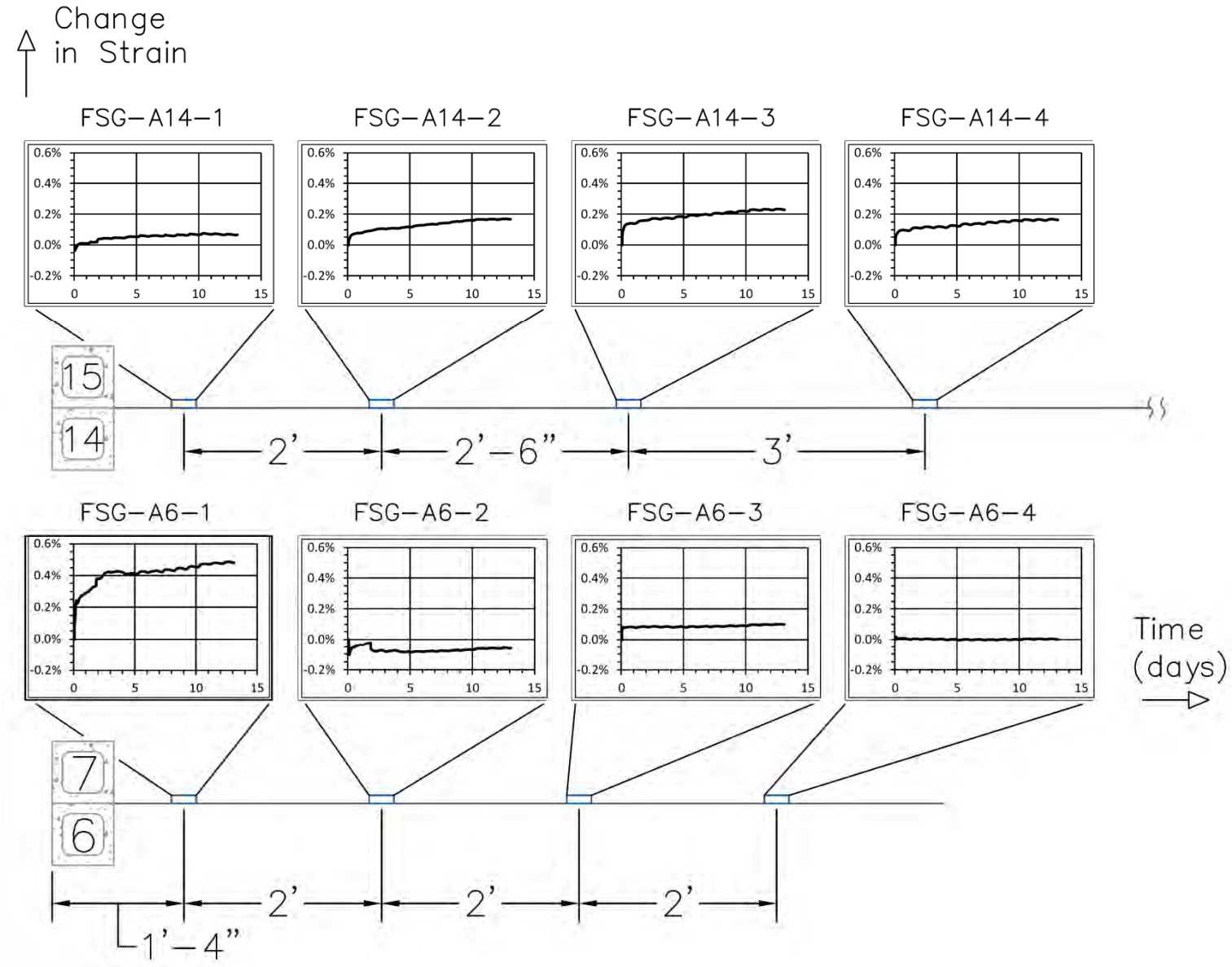

Figure 87. Strain Data for Side A Gages Oriented Perpendicular to the Wall Face During Test A2

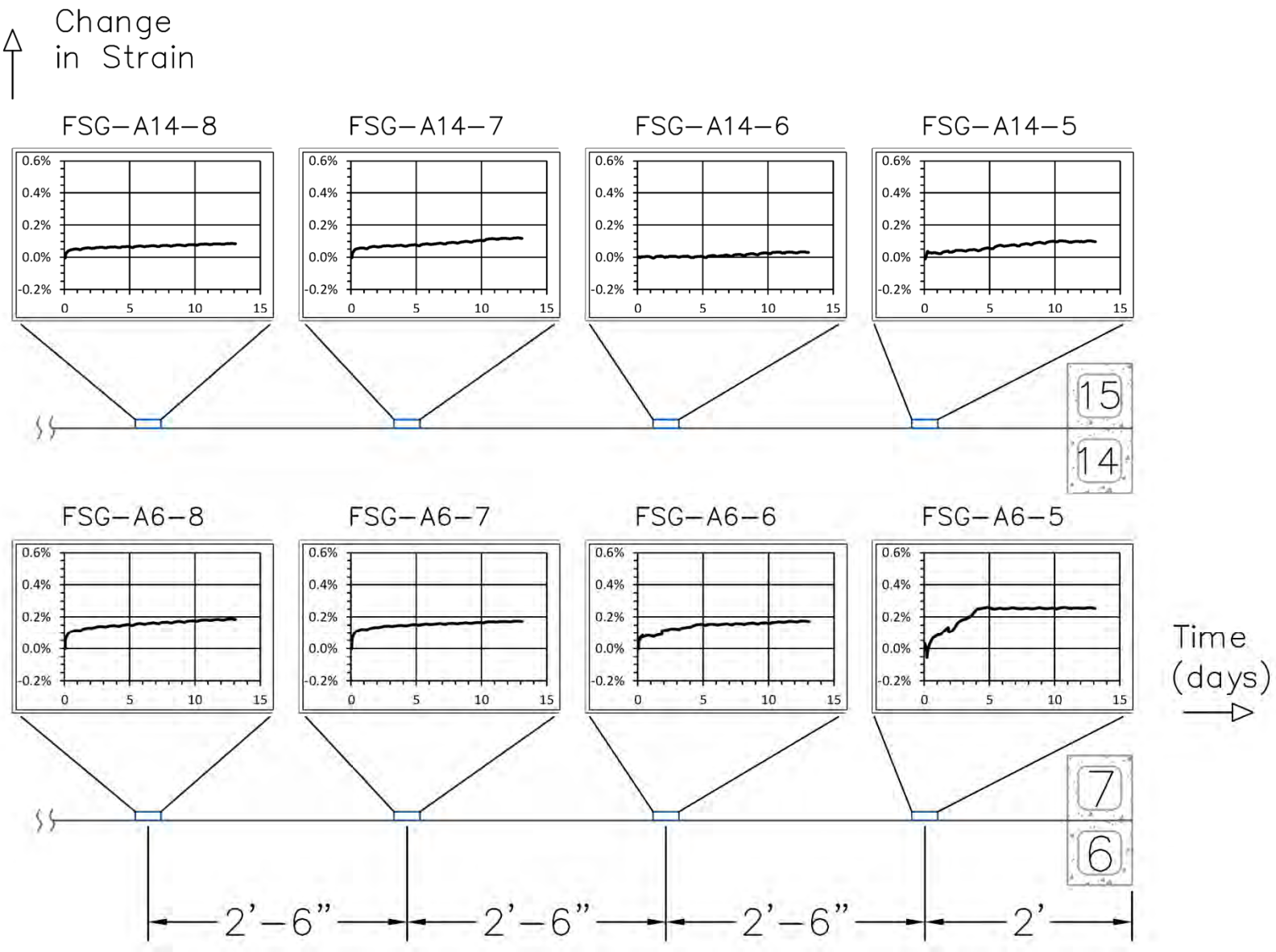

Figure 88. Strain Data for Side A Gages Oriented Parallel to the Wall Face During Test A2

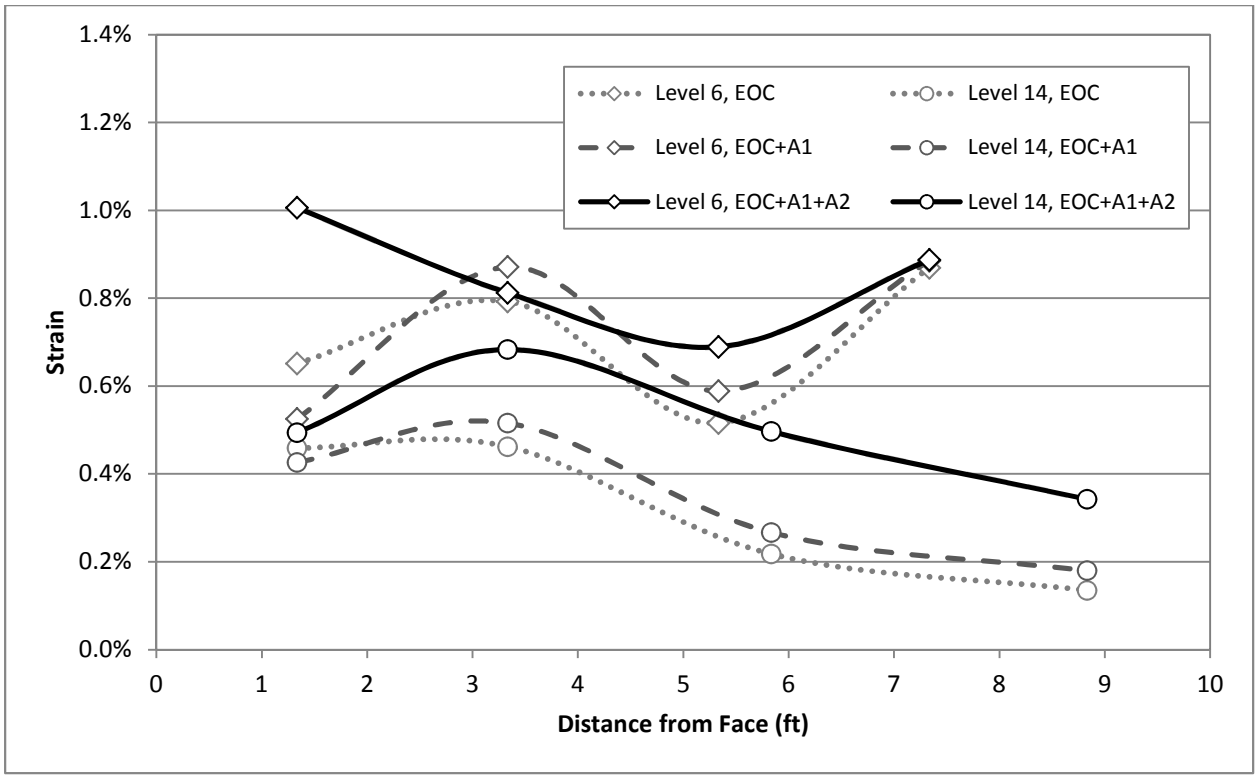

Figure 89. Strain Levels for Gages Perpendicular to the Wall Face on Side A After Construction and Testing

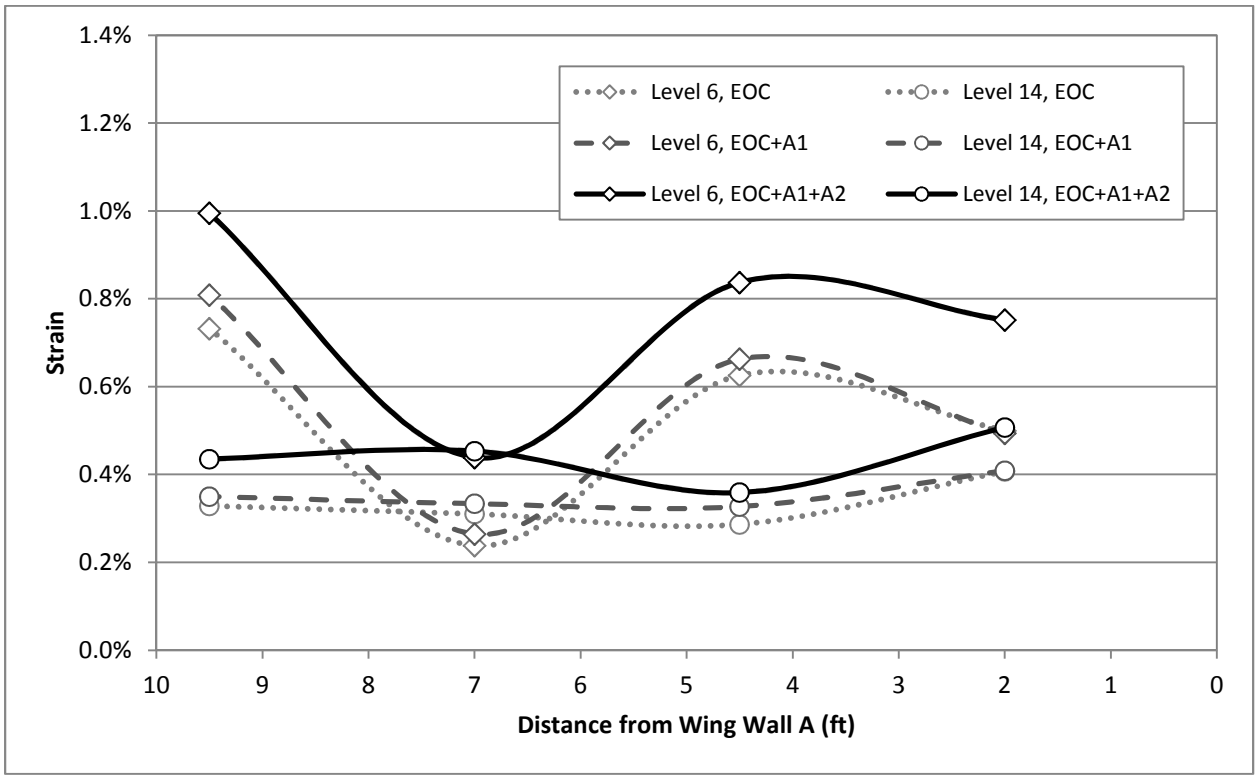

Figure 90. Strain Levels for Gages Parallel to the Wall Face on Side A After Construction and Testing

Test B1

The change in strain at each gage location for Test B1 is plotted as a function of time in Figures 91 and 92. As noted in the "Methods" section, Test B1 proceeded differently from the other three testing sequences. The infiltration of water into the solvent containment system prevented the solvent from flowing evenly under the geofoam blocks. As a result, the solvent began to dissolve the foam from the corner of the geofoam where it was introduced. The side of the geofoam that was placed against the perimeter wall of the concrete mat foundation was not subjected to high lateral stresses, which allowed the solvent to seep along this edge between the plastic barrier and the geofoam. In contrast, the other three sides of the geofoam blocks were surrounded by well-compacted fill, which formed a much tighter seal between the foam and the plastic barrier. Consequently, when Side B of the abutment is viewed from the front, the initial dissolution of the foam began at the left side of the geofoam and progressed toward the center of the abutment. This irregular progression was eventually terminated by excavating into the foundation region and pumping out the solvent and water, and subsequently re-introducing new solvent. This process of removing the old solvent and water was completed approximately 30 hours after the start of testing. By this time, some support had been removed from beneath the left side of the abutment, and the resulting deformations caused the lower levels of the abutment to lean to the left. New solvent was re-introduced approximately 1.4 days after the initial introduction of solvent, and settlements then proceeded as normal.

This sequence and the resulting settlement pattern provide insight into the behavior of FSG-B6-5, shown in Figure 92. The three other corner gages on Side B, as well as the four corner gages on Side A during Test A1, consistently showed strain decreases or no strain increases. However, FSG-B6-5 exhibits a linear increase followed by a small plateau. The linear increase follows the anticipated increase in strength demand in this plane as the lower levels of the abutment tilted towards the left. The plateau begins at approximately the time when the solvent was removed, and the end of the plateau corresponds to the time when new solvent was introduced. From this point forward, the behavior of gage B6-5 shows trends similar to the behavior of other gages located near the corner of the abutment.

Test B1 was allowed to continue for 23 days while a replacement part for the vibrating wire instrument data acquisition system was obtained. Despite the extended test length, many of the gages oriented parallel to the abutment face did not stabilized by the end of testing. Although difficult to recognize in some graphs at this scale, most of the gages show a distinctive shift of about ±0.02% strain during Days 12 and 13. After having received minimal rainfall since the beginning of Test A1, the test site received 1.95 in of rainfall over these two days. The rainfall may have prompted a slight shift in strength demand that was recorded by the strain gages. The EPCs were not functional at this time, so the pressure data could not be cross-checked to see if a corresponding stress change was observed.

Figure 91 shows that, for the strain gages oriented perpendicular to the abutment face, the gage nearest the face at each level recorded negative strains or no change in strain and are believed to be influenced by fabric curvature. The six other gages showed trends and magnitudes for strain change that are very similar to each other over the course of the test.

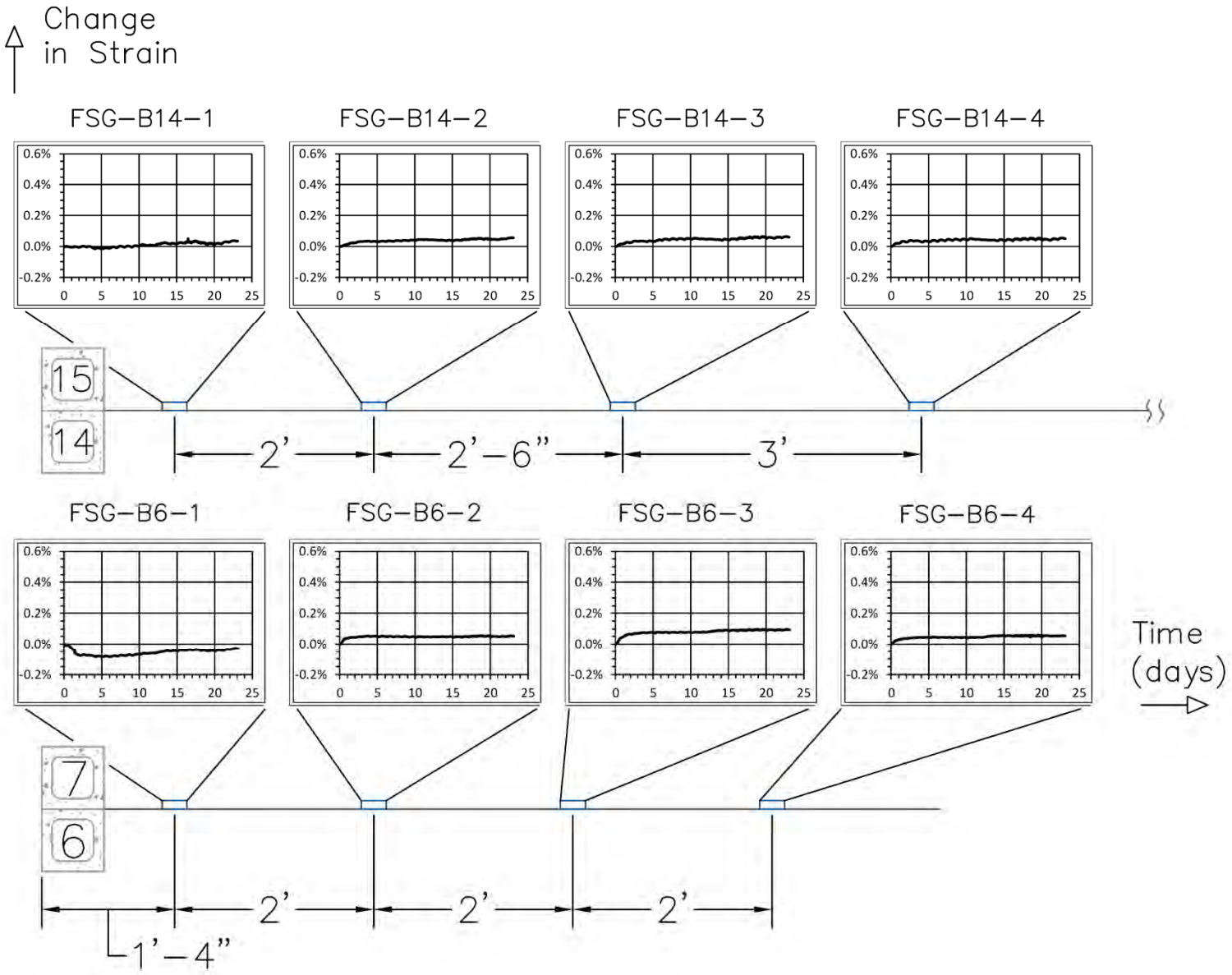

Figure 91. Strain Data for Side B Gages Oriented Perpendicular to the Wall Face During Test B1

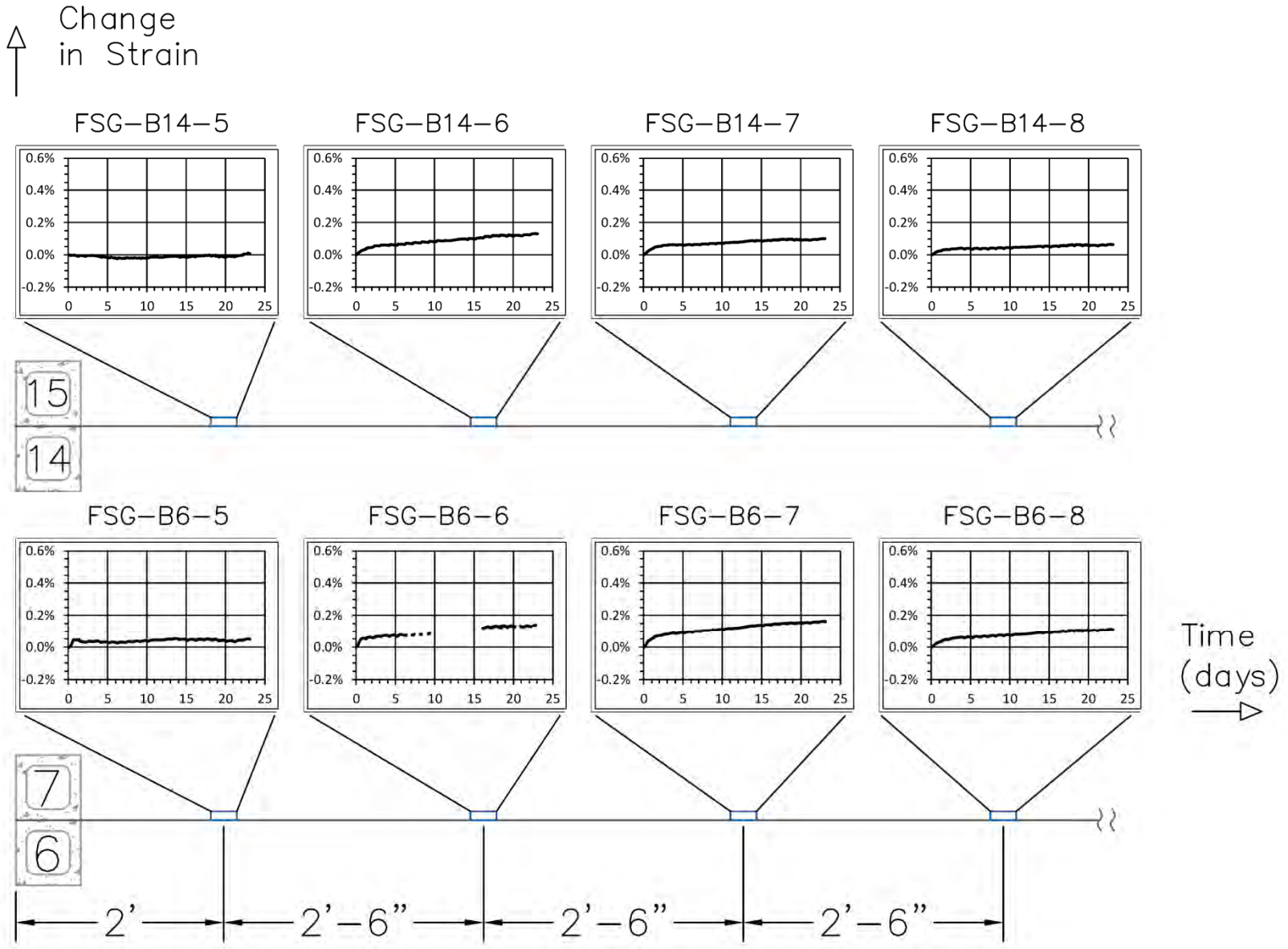

Figure 92. Strain Data for Side B Gages Oriented Parallel to the Wall Face During Test B1

In Figure 92, the strains for gages parallel to the face varied with gage location. FSG-B14-5 showed slight negative strains, consistent with previous tests. As previously discussed, the behavior of FSG-B6-5 also follows this behavior after the re-start of Test B1. The other three gages at Level 14 show trends that are similar to each other, with the magnitude of strain generally decreasing with distance from the wing wall. At Level 6, the strain was nearly identical at FSG-B6-6 and FSG-B6-7, but decreased slightly at FSG-B6-8. Strains tended to be larger at Level 6 than Level 14 for the gages oriented parallel to the face.

Overall, strains were less than 0.2% during Test B1. Comparing Figures 91 and 92, strains tended to be larger in the direction parallel to the abutment face.

It is difficult to compare the strain gage data with the DWE data in Figure 74 since much of the DWE data are believed to be influenced by large settlements of the fill. However, the strains recorded by the DWEs for the rear third of the reinforcement are believed to be accurate. The strain recorded at the end of the test was approximately 0.08%, which is reasonable when compared with Figure 91. Additionally, even though the strain values recorded in the front two thirds of the reinforcement by the DWEs are suspect, they record strain changes over Days 12 and 13 that are consistent with the changes recorded by the strain gages.

Test B2

The change in strain at each gage location for Test B2 is plotted as a function of time in Figures 93 and 94. Many but not all strains were larger than the strains measured in Test B1. Even so, the largest strain observed was 0.31%. Most gages reached a state of relative stability by the end of the test, which was nearly 14 days. Several gages, particularly those in Level 14, again recorded a shift in strain level beginning around Day 4. This time coincides with the beginning of another heavy rainfall event in which the test site received 0.88 in of rainfall over 24 hours. EPC data were examined to determine if corresponding stress changes had occurred. While some small stress changes occurred, these changes are not inconsistent with variations observed in previous tests that did not produce shifts in strain levels.

In Figure 93, which shows the strains as a function of time for gages oriented perpendicular to the face, FSG-B6-1 showed particularly irregular strain changes over the course of the test. While difficult to distinguish due to the horizontal scale of Figure 93, in the first 24 hours of the test the strain decreased slightly, rapidly increased to 0.29%, rapidly decreased to 0.10%, and then increased to 0.23% net change in strain. After this point, the strain decreased steadily until it began to approach an asymptotic value around Day 10. Due to the precarious position of the corner CMUs at the end of the testing, as seen in Figure 33, the frictional connection at the corner between the CMUs and the reinforcement may have slipped, contributing to this erratic behavior. The strains at the three other gages at Level 6 were small, relatively uniform and nearly identical to those observed in Test B1. Strain gages at Level 14 recorded strains that were generally a factor of three greater than those recorded at Level 6 during Test B2, although the strains still did not exceed 0.3%.

When compared with the strains that occurred during Test B1, the strains at Level 6 gages were approximately the same for both Test B1 and Test B2 for all gages except FSG-B6-1. Strains at Level 14 were significantly larger during Test B2 than Test B1 for all four gages.

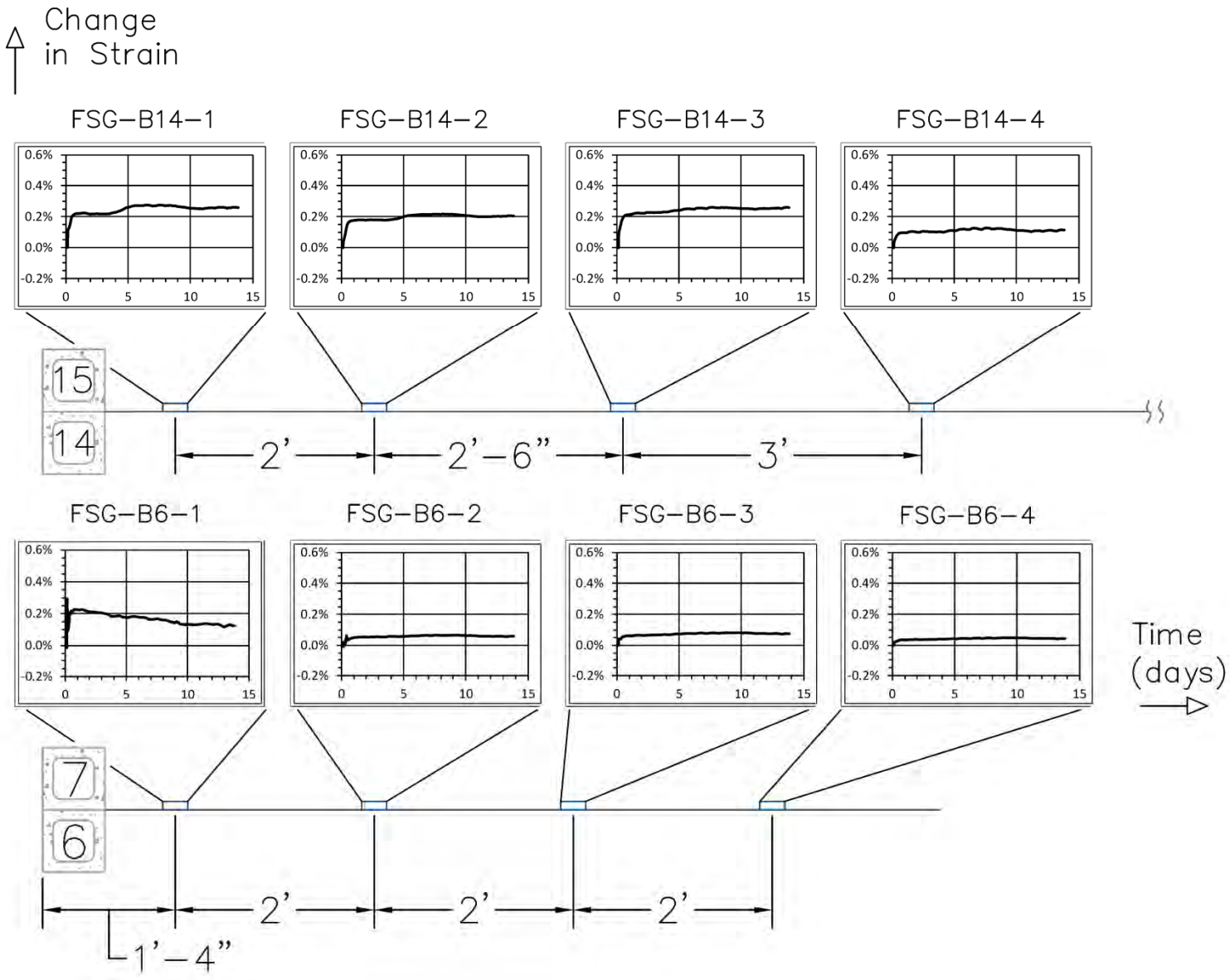

Figure 93. Strain Data for Side B Gages Oriented Perpendicular to the Wall Face During Test B2

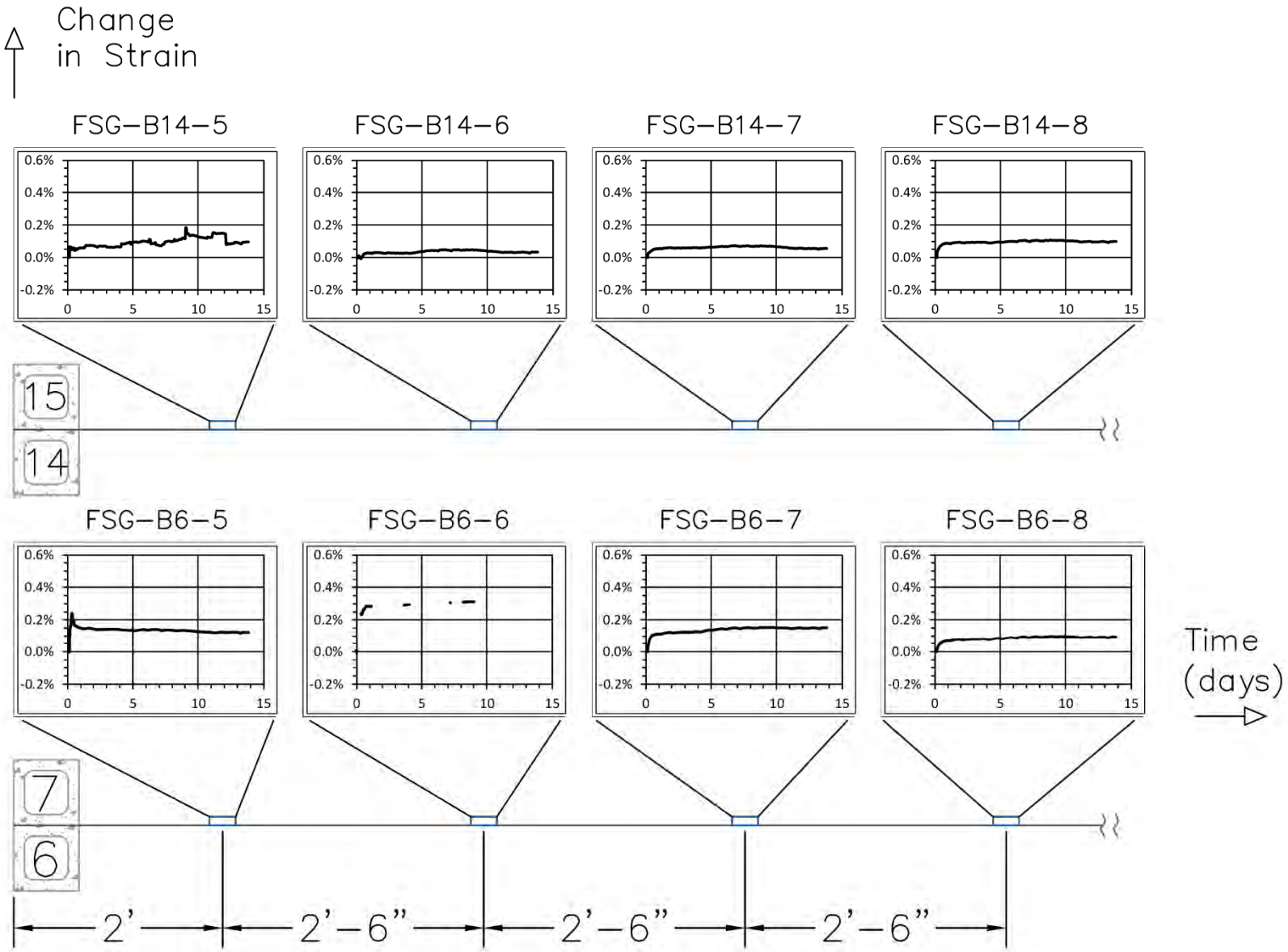

Figure 94. Strain Data for Side B Gages Oriented Parallel to the Wall Face During Test B2

Figure 94 presents the strain data as a function of time for the gages oriented parallel to the abutment face during Test B2. Somewhat similar to the behavior of FSG-B6-1, FSG-B6-5 shows a rapid increase in strain and then declines for the remainder of the test. This behavior also may have been due to slipping at the frictional connection at the corner, suggesting that the strain may have further increased had this not occurred. The corresponding gage at Level 14, FSG-B14-5, also showed erratic behavior, although the final magnitudes are similar to the strains at other gages at Level 14 oriented in this direction. The strain changes at Level 14 at the end of testing were relatively small, not exceeding 0.1%. In contrast with the behavior of Level 14 gages during Test B1, the strain tended to increase with distance from wing wall. The average strain at Level 14 gages during Test B2 was slightly larger than the average strain during Test B1, although the difference is small. Level 6 gages showed larger strains (up to 0.31%, if FSG-B6-6 is trusted) that decreased with distance from the wing wall. When compared with the strains during Test B1, FSG-B6-5 and FSG-B6-6 showed significantly larger strains in Test B2, while FSG-B6-7 and FSG-B6-8 showed nearly identical strains for both tests.

Comparing Figures 93 and 94, strains in the direction perpendicular to the face during Test B2 tended to be larger at Level 14. Strains in the direction parallel to the face tended to be larger at Level 6. Comparison with the DWE data was not possible since accurate strains could not be determined from the extensometer data for Test B2 because of the effects of large settlements of the CMUs.

Comparison of Results from Side A and Side B

Figures 95 through 98 permit comparison of the strain changes occurring on Sides A and B of the abutment during testing. These figures show the strain change at the end of the testing sequence versus position. Because Test B1 was significantly longer than the other tests, and because many gages continued to show small strain increases throughout the test, the strains at a time of 12 days were selected for comparison. This time is similar to the lengths of other tests and does not include the influence of the rainfall event, which began at approximately 12 days. All figures are plotted with the same vertical scale.

Figure 95 presents the strain levels at the end of Tests A1 and B1 for gages oriented perpendicular to the abutment face. On both sides and at both levels, the strain changes are similar, with slight relaxation of tensile strain near the face and slight increase in tensile strain farther back from the face. Level 14 during Test B1 is a slight exception in that no relaxation of the fabric was observed at the gage location nearest the face, although the remainder of the strain profile is consistent with other tests. As discussed previously, some of these apparent changes in strain could be due to curvature of the reinforcement and the top-side location of the strain gages. Figure 96 presents the strain levels at the end of Tests A1 and B1 for gages oriented parallel to the face. The horizontal axis of this graph is position, measured from the nearest wing wall. For example, FSG-A6-5 and FSG-B6-5 are plotted with the same x-coordinate. In this case, the strain increments were either negligible or slightly increased the tensile strain, and tensile strains were slightly higher on Side B, although the difference is not large. Consequently, when considering a small area of support loss, removing a greater depth of support from beneath the abutment did not result in appreciably larger strains in the reinforcement at the locations monitored by strain gages.

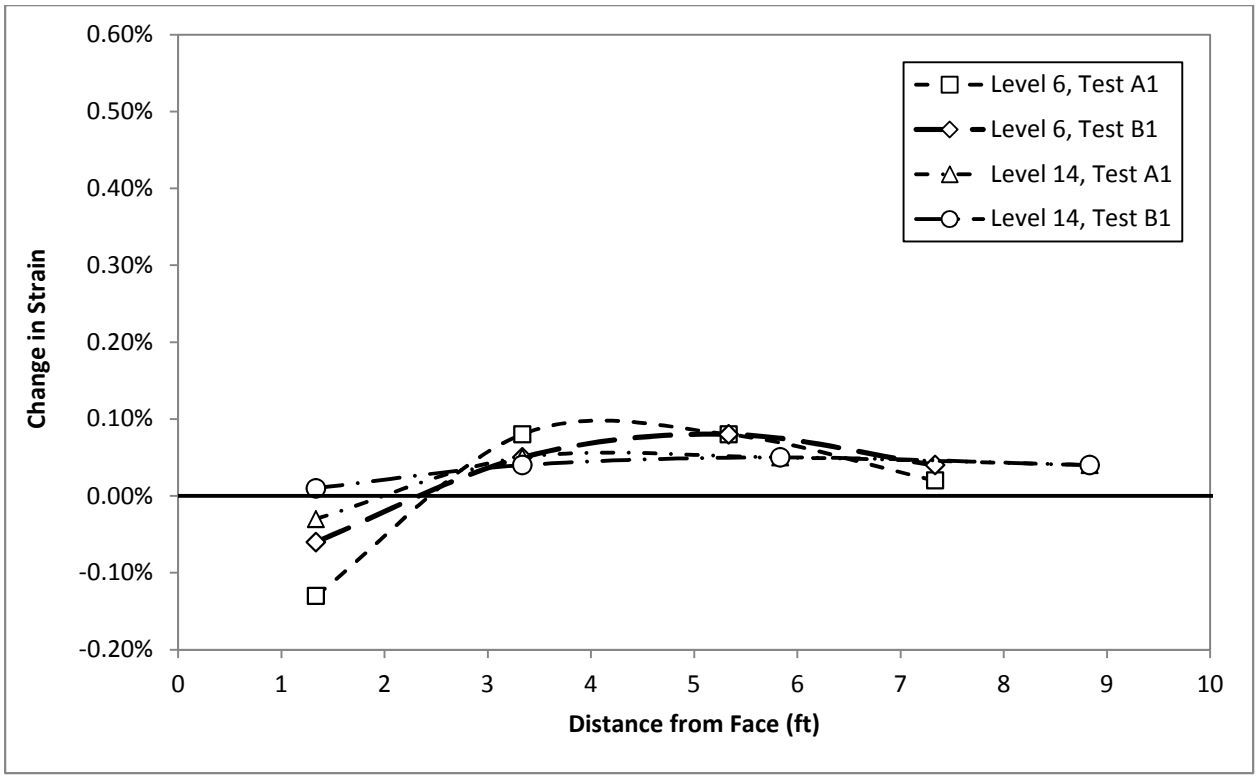

Figure 95. Strain Changes at Completion of Tests A1 and B1 for Gages Oriented Perpendicular to the Wall Face

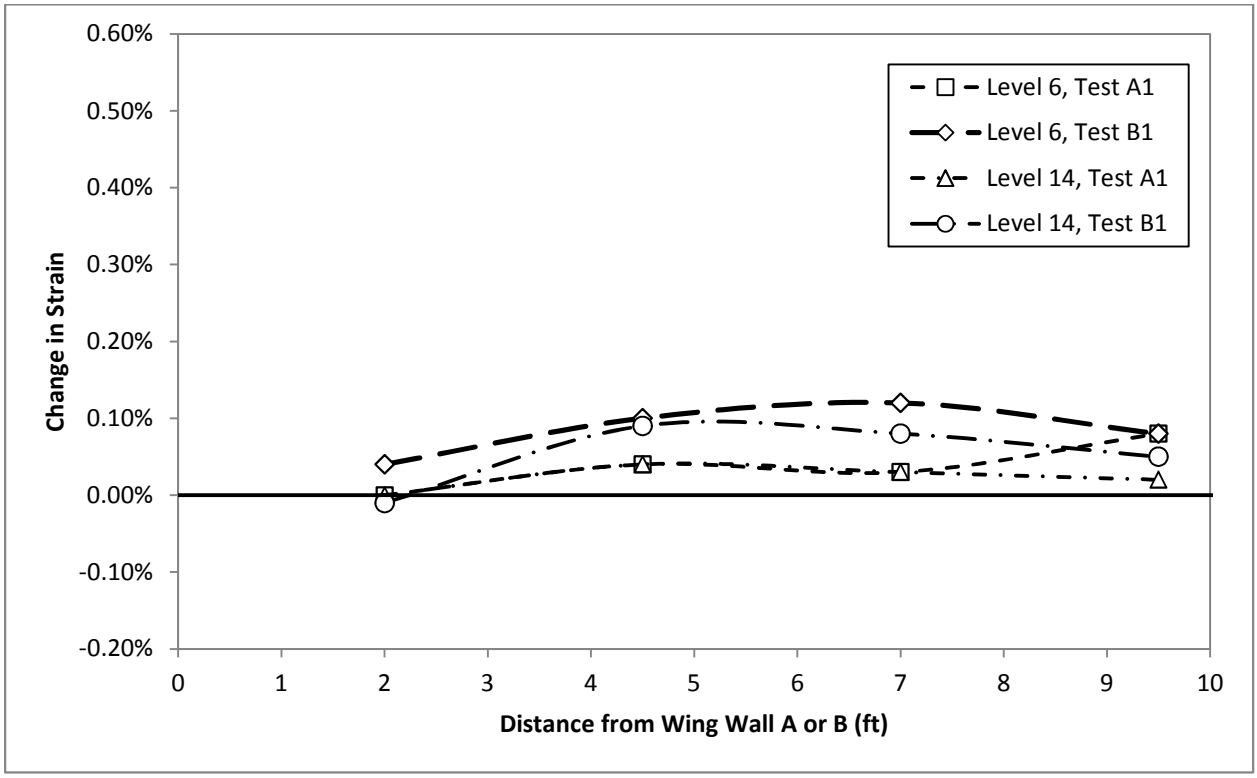

Figure 96. Strain Changes at Completion of Tests A1 and B1 for Gages Oriented Parallel to the Wall Face

Figure 97 presents the cumulative strain changes at the end of Tests A2 and B2 for gages oriented perpendicular to the face; that is, the change in strain reflects changes occurring during both Tests A1 and A2 for gages on Side A, and Tests B1 and B2 for gages on Side B. While the behavior of some gages at Level 6 appears a bit erratic after Test A2, the figure shows that the strains at Level 14 were generally significantly higher when the larger areas of support were removed. Additionally, with the exception of the gage closest to the face, the strains were not appreciably different between Side A and Side B at this level. For the gages at these two levels oriented perpendicular to the abutment face, the strains appear to be primarily influenced by the area of support lost rather than the magnitude.

Figure 98 presents the cumulative strain changes at the end of Test A2 and Test B2 for gages oriented parallel to the face. The horizontal axis of this graph is position, measured from the nearest wing wall. Strain changes at Level 14 were consistent for tests on both Sides A and B. Strains were appreciably higher at Level 6 for gages oriented parallel to the face. The strain distribution is significantly different for the two sides; however, the average strain change is about the same. Therefore, it is difficult to say to what extent the difference in the depth of support removed (i.e., the settlement magnitude) influenced the observed strains at Level 6.

Figures 97 and 98 show that, when large areas of support were removed in Tests A2 and B2, strains perpendicular to the abutment face were larger at Level 14, while strains parallel to the abutment face were larger at Level 6. The following hypothesis is proposed to explain this observation. During testing, the facing CMUs moved forward as they settled far more than they moved to the left or to the right, away from the wing walls. This movement is believed to also reflect the movement of the reinforced fill as it settled – that is, the fill primarily moved toward the face as it settled. The Level 6 reinforcement does not extend a large distance behind the region of support removal, and settlement profiler data indicate that the fill settlement extended to a significant distance behind the face in the region of the strain gages. Therefore, when these large areas of support were removed, it is possible that the entire sheet of Level 6 reinforcement moved a small distance in the same direction as the reinforced fill, preventing large strains from developing in the direction perpendicular to the abutment face. However, the reinforcement is a continuous sheet extending from wing wall to wing wall, and this embedment will prevent it from moving in the direction parallel to the face. Consequently, it is reasonable to expect higher tension and larger tensile strains in this direction at lower levels of the abutment.

At Level 14, the reinforcement extends a significant distance behind the region of support removal and is not expected to move, even when large areas of support are removed from beneath the base. As previously noted, the abutment tended to rotate forward far more than toward either wing wall. Since the reinforcement fibers oriented perpendicular to the face will be primarily responsible for restraining movement, it is reasonable to expect larger tension and tensile strains in this direction at the upper levels of the abutment.

When the locations of the maximum strains are considered for each test, they do not appear to have any correlation with the location of support removal.

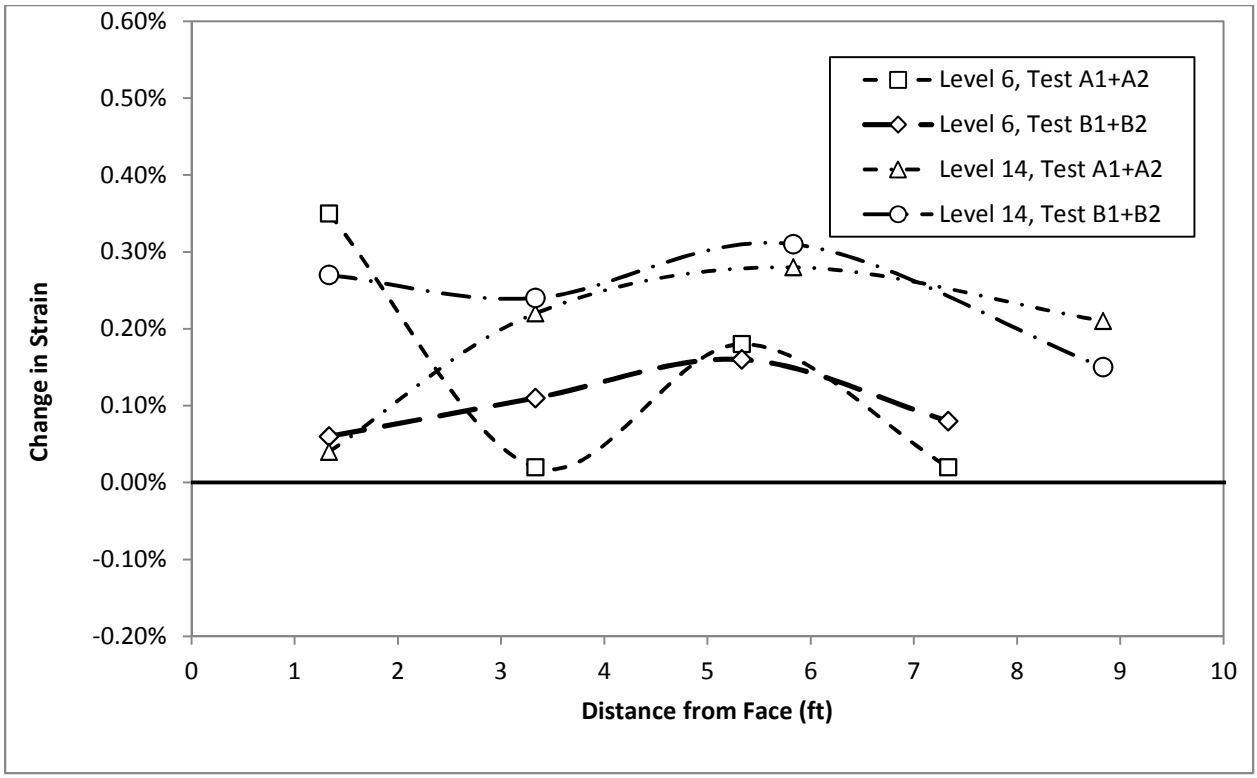

Figure 97. Cumulative Strain Changes at Completion of Tests A2 and B2 for Gages Perpendicular to Wall Face

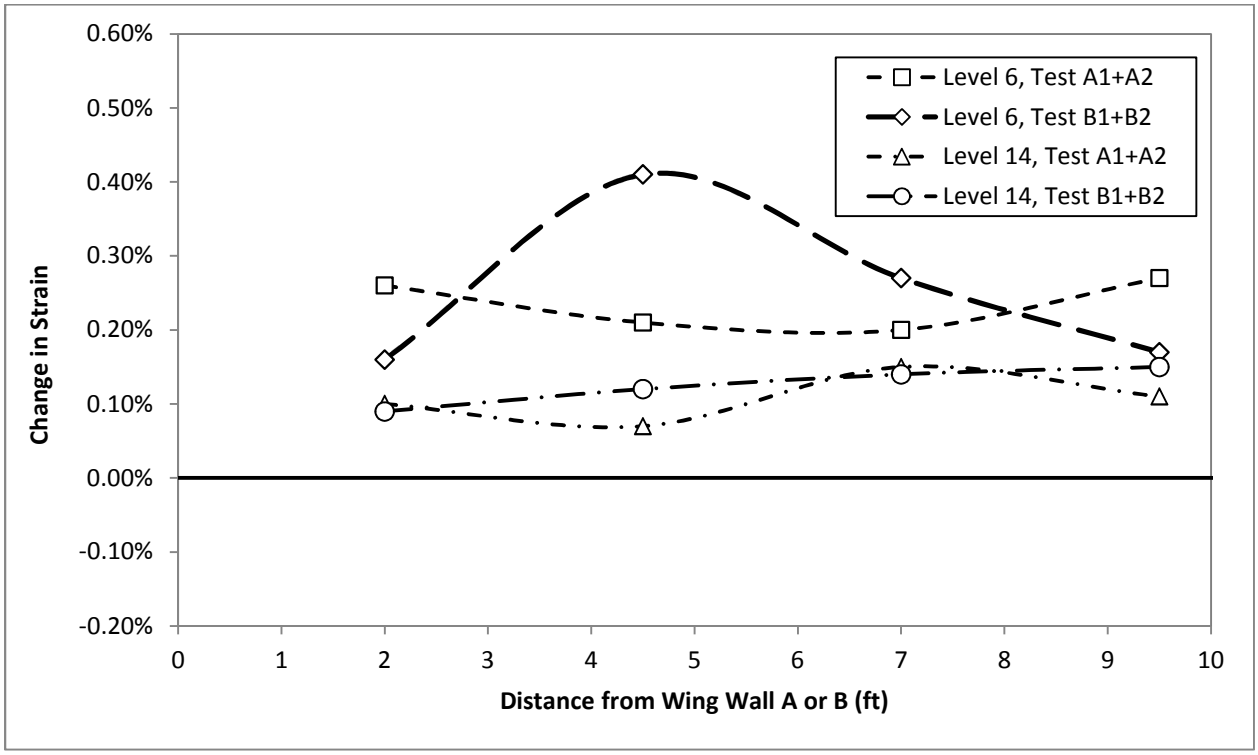

Figure 98. Cumulative Strain Changes at Completion of Tests A2 and B2 for Gages Parallel to Wall Face

Key Points

- The maximum strain observed at Levels 6 and 14 on Side A during construction and placement of the surcharge load was 0.8%. The maximum strain increase observed during placement of the surcharge load alone was 0.14%.

- The FHWA procedure for calculating lateral strains due to placement of the surcharge load gave a reasonable, if slightly conservative, estimate.

- The maximum strain observed at Levels 6 and 14 on Side A after construction, Test A1, and Test A2 was 1.0%. Despite large differential settlements beneath the foundation imposing a severe loading condition, observed strains remained well within the acceptable range.

- With the exception of the corner gages, strain increases were relatively uniform, indicating that the increased demand was well-distributed along the reinforcement.

- The significant variability in the response of the corner gages showed that they were likely influenced by curvature of the reinforcement, and perhaps by connection slipping in some cases. It also suggests that stress concentrations are most likely to develop near the face and wing walls of the abutment.

- Test A1 and Test B1, which removed two different depths of support from a smaller area beneath the foundation, resulted in similar strain increases on each side.

- Test A2 and Test B2, which removed two different depths of support from a larger area beneath the foundation, resulted in higher strains at Level 6 in the direction parallel to the abutment face and higher strains at Level 14 in the direction perpendicular to the abutment face. One possible explanation for this behavior was offered based on the abutment geometry and the area of support removed.

Potential Mitigation Measures

The large settlements of some CMU facing blocks created gaps between the blocks that would make the blocks vulnerable to removal during periods of elevated stream flow. Three possible measures to provide additional robustness to the GRS abutment are presented and discussed in this section. Determining the appropriateness of implementing these suggestions at a given site is the responsibility of the designer.

Performance of Protective Wrap

The lightweight filtration geotextile proved to be effective at containing and protecting the fill when gaps formed between facing units. Figure 99 compares the exposure of the fill when gaps opened between two levels of blocks near Corner B. The photograph on the left shows loose, exposed fill from Level 5 when a gap opened between the Level 4 and Level 5 blocks. The scattered particles in the foreground of the photograph are likely particles that fell

into the hollow cores of the CMU during construction rather than fill from behind the block. The photograph on the right shows the corresponding gap between Level 5 and Level 6, just above the block shown on the left. The black geotextile is visible, along with the thin layer of aggregate used to increase the interface friction angle with the reinforcement. The geotextile is effective at containing the fill.

Figure 100 also compares the exposure of the fill when vertical gaps opened between two adjacent blocks near Corner A. In Figure 100(a), a vertical gap between two adjacent blocks at Level 5 of Wing Wall A allowed reinforced fill to spill through to the front of the CMU face. In Figure 100(b), the black geotextile is visible through a vertical gap located at Level 6, just above and to the left (closer to the corner) of the gap in Figure 100(a). The fill is effectively contained by the geotextile, with only a few particles of the aggregate used to increase the interface friction visible.

These observations suggest that the protective wrap can provide effective restraint of the fill when gaps form between the facing units. The performance of the wrap when exposed to water action was not evaluated; however, the authors are optimistic that its performance would be satisfactory. The thin layer of aggregate may be susceptible to erosion for a short distance back from the face, but the authors believe this distance is small and unlikely to impact the performance of the wrap or the GRS wall. The performance of the wrap with an entire facing block removed could not be evaluated during the test due to stability concerns associated with attempting to remove an entire CMU block.

Overall, the protective wrap appears to be a low-cost, easily installed measure that may offer an additional layer of protection for the fill. Including such a wrap is a worthwhile consideration for sites located along waterways.

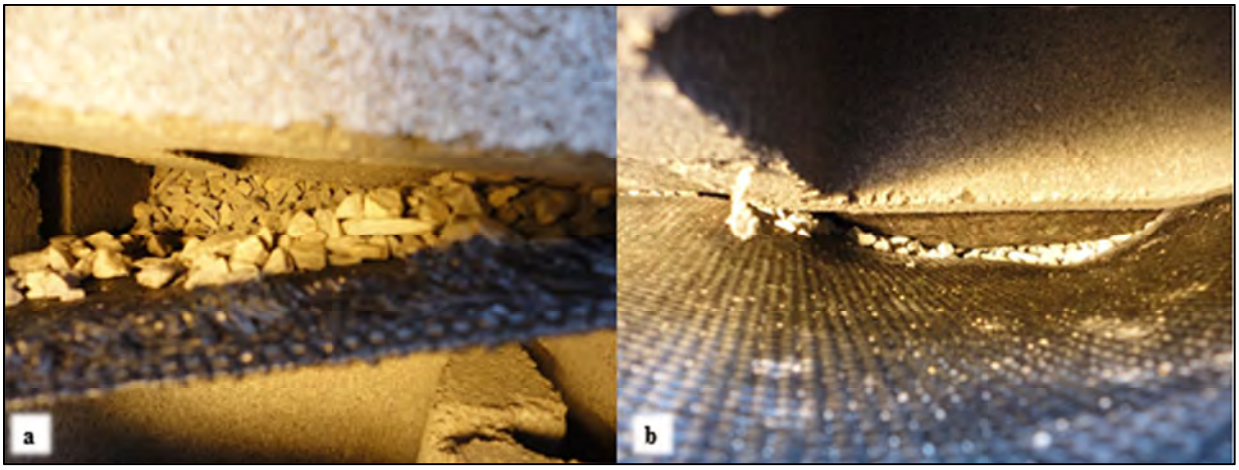

Figure 99. Comparison of Unwrapped and Wrapped Fill. (a) Unwrapped Fill at Level 5 Near Corner b; (b) Wrapped Fill at Level 6, Above Block Pictured at Left

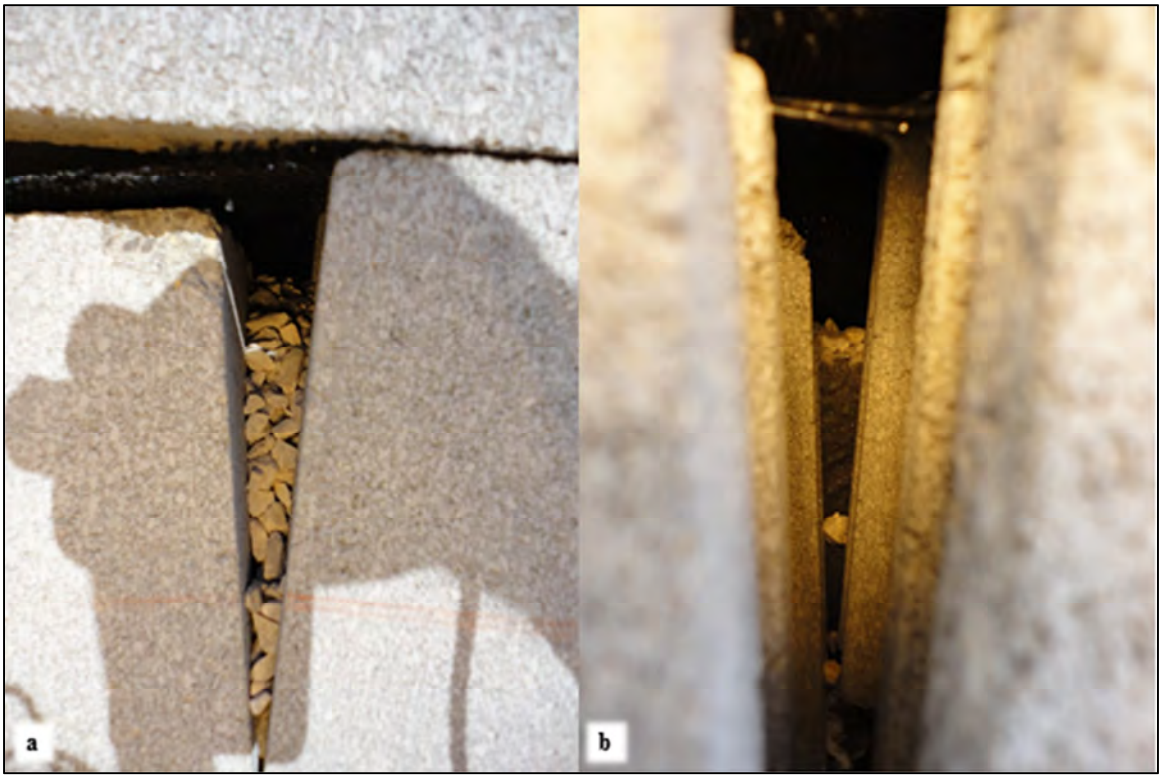

Figure 100. Second Comparison of Unwrapped and Wrapped Fill. (a) Unwrapped Fill at Wing Wall A, Level 5 Near Corner A; (b) Wrapped Fill at Level 6, Above and to the Left of the Vertical Gap in (a).

Pinning of Corner Blocks

The authors noted that the corners of the abutment appeared particularly vulnerable to dislodgement after settling. One method to mitigate this exposure would be to fill the blocks near the corner with concrete or grout and pin them together using vertical lengths of rebar, similar to way that the upper three courses were pinned together. Adams et al. (2011) describe a similar process for joining the wing wall and face of the abutment when the joint is not a right angle, and they note that such a process can be used to add strength to the wall corners. Pinning these blocks together would reduce the possibility of losing a facing block in the event of combined settlements and water action. This process could also be used to reinforce the corners if impact loads are a concern for the site.

Figure 101 provides an example of a possible configuration for the rebar elements used to pin the corner blocks together. This figure shows the middle section of a reinforced abutment corner; the short lengths of rebar at the top and bottom of the figure indicate that the rebar reinforcing will continue to the top and bottom of the abutment. The exact details, including the length of the rebar and the number of block columns adjacent to the corner to be pinned, are left to the designer.

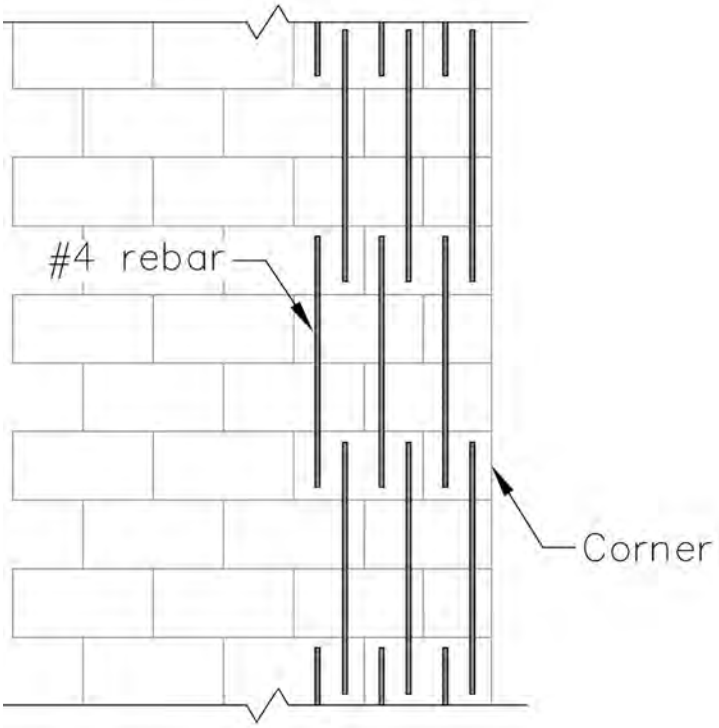

Figure 101. Illustration of Pinning the Corner Blocks

In GRS systems, the frictional connection with the reinforcement allows the facing elements to move forward a small distance during construction, relieving much of the stress acting on the back of the face. Therefore, in GRS systems, the facing elements are not considered structural elements. However, if a significant portion of the hollow CMUs were filled with concrete and pinned together, the increased rigidity of the resulting wall may result in higher stresses on the back of the wall. Therefore, the designer must balance the need for protecting the corners with the desire to incorporate some flexibility in the abutment facing system. However, the authors believe that pinning the corner blocks together would not produce large enough increases in stress from the GRS fill to harm the wall face in typical GRS-IBS applications.

When the blocks near the corner are pinned together and connected with the top three levels of blocks, which are also pinned together, these blocks may behave similar to a rigid frame. It is possible that these corner blocks may not settle noticeably in the event that differential settlements occur at that corner, due to the support provided by the upper three levels, thereby masking the effects of foundation settlement or scour. It is the responsibility of the designer to consider whether implementing this detail is appropriate for a particular site. This potential concern could be mitigated by regular and careful inspection.

Increasing the Base Width of Abutment

When the area of support removal was large, as in Tests A2 and B2, the lower levels of reinforcement over the area of support removal likely lost much of their capacity to restrain the abutment in the direction perpendicular to the abutment face. As previously discussed, displacement data and strain gage data suggest that the Level 6 reinforcement moved downward

with the fill settlement, reducing normal stresses on the reinforcement, and preventing development of significant increases in tensile forces in the reinforcement. This loss of embedment capacity decreases the restraint that the reinforcement can provide to the fill and the facing units.

Stability of the wall could be increased by increasing the base width of the abutment. This measure will prevent the reinforcement from losing embedment in the case of settlements beneath a large area of the foundation. Additionally, if this measure is combined with the suggestion to pin the corner blocks of the abutment, the authors believe that a synergistic effect may occur, producing an overall more robust abutment. However, increasing the base width will also increase the overall cost of the abutment by increasing the volume of fill and reinforcement required to construct the abutment, and in many cases increasing the volume of native soil that must be excavated. This measure is expected to offer the most significant benefits to abutments that would otherwise have a small base width, and the stability improvements it offers will likely decrease as the minimum required base width increases.

Investigation of Repairs

Following the four testing sequences, the authors considered whether any measures could be taken to repair the abutment. Pressure grouting was the primary method considered for repairs. Allen Sehn at Hayward Baker, Inc. spoke with the authors over the telephone and, after hearing a description of the problem, expressed his opinion that the likelihood of a successful repair using this or another ground improvement method was low. The primary concern Sehn mentioned is that the confining pressures in front of and beside the wall would not be large enough to contain grout applied with large enough pressures to lift blocks back to elevations close to their original configuration.

If a GRS abutment were to experience small differential settlements that did not result in structural distress but created gaps between the facing blocks, the authors believe that these gaps could be patched effectively using concrete without significantly affecting the structural behavior of the abutment. Such repairs might not be attractive.

Recommendations for Future Research

This project is, to the authors' knowledge, the first substantial investigation into the effects of differential settlement on GRS abutments. The large scale of the project has produced a sizeable and unique data set, which presents a singular opportunity for further exploration of this subject. The data set can allow for calibration and validation of a numerical model that can be used to perform parametric studies and identify the influence of different abutment geometries, different bridge loads, different areas of support loss, and different depths of support loss. For example, the effect of support removal beneath the center of the abutment, rather than the corners, can be investigated. The numerical model can also be used to improve upon the predictive equation for settlement of the abutment that is presented in this report. Although the major focus of this research was on the effect of foundation settlements beneath a GRS abutment, much data were also obtained during GRS abutment construction and bridge loading. Hence, the numerical model could be used to reliably perform many numerical experiments at

much lower cost than large-scale experiments. The results could then be compared with existing analysis procedures, e.g., Adams et al. (2011), to investigate the validity of those procedures.

A protective wrap consisting of a lightweight filtration geotextile was placed behind the facing blocks at Level 6. The purpose of this trial wrap was to examine its effectiveness in protecting and containing the reinforced fill should gaps form between the facing blocks. While the wrap was effective to this end, an evaluation of its performance when water action is applied was not performed at that time. If VDOT is considering implementing this wrap in a GRS structure that may be subjected to water action, further evaluation of its performance under these conditions would be prudent. The effects of removing one or more facing blocks could also be examined. This evaluation could be performed on a small GRS mass and would not constitute a large undertaking. The authors also placed a thin layer of aggregate between the filtration geotextile and the reinforcing geotextile to increase the interface friction angle. However, it is possible that maintaining adequate quality control oversight of this component would be challenging. Research could also be conducted to examine the interface friction of these two geotextiles to determine whether the thin layer of aggregate is necessary.

CONCLUSIONS

- *A testing concept was developed to induce carefully controlled differential settlements beneath a field-scale GRS abutment.* This testing concept was adapted from previous column-supported embankment tests and used geofoam blocks as temporary support inclusions within the subgrade, which could later be dissolved using an environmentally friendly solvent.

- *The FHWA manual by Adams et al. (2011) was a very useful resource for design and construction of the GRS abutment.* The authors found the FHWA manual to be a helpful and relatively comprehensive reference.

- *Construction of the abutment was simple and efficient.* The abutment was completed in 35 working days by two or three unskilled laborers who were inexperienced with GRS construction techniques, using a small utility vehicle and hand-operated equipment.

- *The GRS abutment demonstrated robust behavior in response to large differential settlements.* While the large magnitude and area of settlement at the base represented an extreme loading condition for this abutment, the settlements expressed at the surface of the abutment were small. Stresses were redistributed within a relatively small height above the foundation following support loss beneath the corners, maintaining support capability at upper levels of the abutment. Strain increases in the reinforcement due to this bridging action were not large and were generally well-distributed along the length of the reinforcement.

- *Settlement of the CMU facing blocks over the areas of support loss followed a consistent pattern that could be represented by a normalized predictive equation that was developed to fit the data for the conditions of the GRS test abutment.* The equation was calibrated using

data from the lower 11 levels (7 ft) of the abutment, and it is best-suited for use in this range. Although an attempt was made to formulate the predictive equation in normalized terms, it is not yet known if this normalization would apply to other configurations. So, at present, the predictive equation is specific to the conditions of this test set-up.

- *The performance of a GRS abutment is expected to be excellent when subjected to normal levels of differential settlement due to compressible soils beneath the foundation.* The robust response of the model GRS abutment to large settlements suggests excellent performance at settlement magnitudes that would normally occur in field applications.

- *The performance of a GRS abutment may be severely compromised when exposed to scour-induced settlements, if steps are not taken to protect the fill from erosion.* Scour-induced settlements imply that water will also be flowing along the face of the abutment. Even after experiencing small settlements, the facing CMUs near the corner were in a very loose condition, and they would be susceptible to removal due to water action. The fill would then be exposed to erosion by the water, potentially impacting the structural integrity of the abutment.

RECOMMENDATIONS

1. *VDOT's Structure and Bridge Division should consider GRS-IBS as a viable option for new bridges and bridge replacements.* While GRS-IBS has limitations, it is shown in this experiment to be a robust, flexible system that can be constructed efficiently and at low cost.

2. *For bridges crossing over water, VDOT's Structure and Bridge Division should consider GRS-IBS only if scour issues can be appropriately addressed according to the guidelines provided by Adams et al. (2011).* Placing the top of the RSF below the calculated scour depth and/or implementing appropriate scour countermeasures are two possible means of managing scour concerns. If scour cannot be addressed in a constructible and economical manner, GRS-IBS should not be used.

3. *When GRS-IBS is selected for a water crossing, VDOT's Structure and Bridge Division should include additional measures to protect the fill in the event of a facing element becoming dislodged, depending on the designer's consideration of site-specific risk factors.* Three such measures considered in this study are placing a protective wrap behind the face, joining the corner blocks with vertical lengths of rebar and grout or concrete, and increasing the width of the base. The authors recognize that this study was not designed to comprehensively examine these mitigation measures but are confident of their utility after observing the performance of the test abutment.

4. *VDOT's Structure and Bridge Division should inspect in-service GRS-IBS bridges on a regular schedule to identify and mitigate the effects of differential settlements early.* GRS-IBS bridges crossing over water should also be inspected after severe flooding events, according to FHWA guidelines (Adams et al, 2011). If differential settlements introduce gaps between the facing blocks that are severe enough to allow a block to be removed, the

gap should be repaired immediately. One repair measure discussed in this report is to patch the gap with concrete.

5. *VDOT's Structure and Bridge Division should use the FHWA manual by Adams et al. (2011) for the design and construction of GRS-IBS bridges.* Until further research validates or updates its recommendations and design procedures, this manual best represents the current state of the practice, and it was useful to the authors in designing and constructing this experimental abutment. For the one performance criterion that could be compared with the values predicted by the FHWA manual – tensile strains in the geosynthetic reinforcement due to bridge loading – the FHWA procedure gave somewhat conservative results.

6. *VCTIR should consider authorizing additional research into the performance of GRS-IBS bridges that are subjected to differential settlements.* While the field-scale abutment performed well under severe differential settlements, in many cases such settlements may represent the greatest threat to the performance of a GRS abutment near a waterway because of the potential for loosening the frictional connection between blocks. The data set compiled in this field-scale experiment provides an excellent opportunity to improve understanding of the behavior of GRS abutments by developing a numerical model, which can be used to thoroughly investigate the influence of a range of parameters.

BENEFITS AND IMPLEMENTATION

This research showed that the experimental GRS abutment offered robust performance when subjected to severe differential settlements and maintained an acceptable level of performance for the surcharge load. However, the abutment also appeared vulnerable if scour undermining were to induce settlements of the facing blocks. This understanding underscores the importance of complying with FHWA recommendations for managing scour potential, and it allows VDOT to make informed policy and design decisions regarding the implementation of GRS-IBS. GRS-IBS bridges can offer real cost and time savings, and the recommendations presented in this report can be used to target the most appropriate sites for GRS-IBS. Simple, low-cost measures to provide additional protection to GRS abutments along waterways were introduced. Finally, a predictive equation was developed that allows a designer to estimate the settlement of facing blocks when subjected to base settlements of known magnitude and area.

VDOT is implementing GRS-IBS technology through construction projects in its engineering districts, the first of which is the Towlston Road Bridge in Fairfax County. Recommendations from this study are being incorporated by Structure and Bridge division into designs for these structures.

ACKNOWLEDGMENTS

The authors gratefully acknowledge the organizations and individuals who contributed funding, time, skills, and expertise to make this project successful. The funding for this project was provided by VCTIR under the supervision of Michael Brown, and by the Via Foundation of Virginia Tech. Mike Adams and Jennifer Nicks of FHWA and Ed Hoppe of VCTIR provided valuable comments in the early stages of designing these experiments. Andy Zickler of VDOT suggested a trial of the protective wrap that was included at one level of this abutment.

Jon Wooge and Dwight Paulette of Virginia Tech's Kentland Farm allowed extended use of the testing site at the farm and frequently offered their resources to ensure the smooth progression of the project. Joel Sloan shared his experience conducting column-supported embankment testing, which formed the basis of the testing methods for this experiment, and also answered many instrumentation questions. Brett Farmer and Dennis Huffman also contributed their extensive expertise to many aspects of the design and construction of this experiment. Randy Dymond and the Civil Engineering Department at Virginia Tech loaned a total station for the duration of the field work. Bonnie Franklin's assistance in securing materials for the experiments was especially valuable.

Many students contributed their time to this project. Aaron Klingshirn assisted with much of the early stages of construction and with the installation of the strain gages, and he was instrumental in developing the Appendix of this report. Alex Reeb, Mike Nolden, Adam Depoy, Karla Santacruz, Russ Gatermann, and Erin Murphy also generously volunteered their time assisting with construction and taking survey data of the abutment during testing. Brandyn Turley, Keaton Scanlan, and Matthew Amonette logged many hours of work as undergraduate assistants, and their help was greatly appreciated.

The geotextiles used in this experiment were generously donated by TenCate thanks to the efforts of Bruce Lacina. Herb Roy of Vishay Micro-Measurements shared his expertise in selecting the appropriate strain gages and provided advice on installation methods. Allen Sehn of Hayward Baker offered his time and extensive experience to discuss possible methods for repairing the GRS abutment.

Many individuals from VDOT, FHWA, and other firms took a day of their time to visit the testing site. The authors appreciated their interest and trust that it was an educational experience for all.

Finally, the authors would like to thank the individuals who provided helpful comments on the drafts of this report, including Mike Adams, Jennifer Nicks, Ed Hoppe, and David Shiells.

REFERENCES

Abu-Hejleh, N., Zornberg, J.C., Wang, T., and Watcharamonthein, J. Monitored Displacements of Unique Geosynthetic-Reinforced Soil Bridge Abutments. *Geosynthetics International*, Vol. 9, No. 1, 2002, pp. 71-95.

Adams, M., Ketchart, K., Ruckman, A., DiMillio, A.F., Wu, J.T.H., and Satyanarayana, R. Reinforced Soil for Bridge Support Applications on Low-volume Roads. In *Transportation Research Record: Journal of the Transportation Research Board*, No. 1652. Transportation Research Board of the National Academies, Washington, DC, 1999, pp. 150-160.

Adams, M., Nicks, J., Stabile, T., Wu, J.T.H., Schlatter, W., and Hartmann, J. *Geosynthetic Reinforced Soil Integrated Bridge System—Interim Implementation Guide*. FHWA-HRT-11-026. Federal Highway Administration, McLean, VA, 2011.

Brandon, T.L., Al-Qadi, I.L., Lacina, B.A., and Bhutta, S.A. Construction and Instrumentation of Geosynthetically Stabilized Secondary Road Test Sections. In *Transportation Research Record: Journal of the Transportation Research Board*, No. 1534. Transportation Research Board of the National Academies, Washington, DC, 1996, pp. 50-57.

Coduto, D.P. Serviceability Requirements. In *Foundation Design: Principles and Practices*. Prentice Hall, Upper Saddle River, NJ, 2001, pp. 14-46.

Cuelho, E.V., Christopher, B.R., and Perkins, S.W. Small Strain and Displacement Monitoring Methods for Geosynthetics under Monotonic and Cyclic Loading. In *Proceedings of the First Pan American Geosynthetics Conference and Exhibition*, R.J. Bathurst and E. Palmeira (Eds.). Industrial Fabrics Association International, Cancun, Mexico, 2008, pp. 734-743.

Daigle, L., and Zhao, J.Q. *Assessing Temperature Effects on Pressure Cells.* IRC-RR-131. National Research Council Canada, Ottawa, 2003.

Sloan, J.A., Filz, G.M., and Collin, J.G. Field-Scale Column-Supported Embankment Test Facility. *Geotechnical Testing Journal*, Vol. 36, No. 6, November 2013, pp. 891-902.

Warren, K.A., and Howard, I.L. Sensor Selection, Installation, and Survivability in a Geosynthetic-Reinforced Flexible Pavement. *Geosynthetics International*, Vol. 14, No. 5, 2007, pp. 298-315.

Warren, K.A., Brooks, J.A., and Howard, I.L. Survivability of Foil Strain Gages Mounted on Geosynthetics Under Full-Scale Construction Loads. In *Geosynthetics Research and Development in Progress (GSP 130)*, R. M. Koerner, G. R. Koerner, Y. G. Hsuan, and M. V. Ashley (Eds.). American Society of Civil Engineers, Reston, VA, 2005, pp. 4085-4090.

Warren, K.A., Christopher, B., and Howard, I.L. Geosynthetic Strain Gage Installation Procedures and Alternative Strain Measurement Methods for Roadway Applications. *Geosynthetics International*, Vol. 17, No. 6, 2010, pp. 403-430.

Wu, J.T.H., Lee, K.Z.Z., Helwany, S.M.B., and Ketchart, K. *Design and Construction Guidelines for Geosynthetic-Reinforced Soil Bridge Abutments with a Flexible Facing*. NCHRP Report No. 556. Transportation Research Board of the National Academies, Washington, DC, 2006.

APPENDIX

STRAIN GAGE INSTALLATION AND CALIBRATION PROCEDURES

INTRODUCTION

This Appendix documents the installation and calibration of strain gages on a biaxial geotextile for use in a field-scale GRS test abutment. This Appendix describes the selection of materials, the installation of the strain gages in the laboratory, the calibration technique, and installation of the gages in the field-scale model. The installation procedure for the gages in the laboratory described in this Appendix has been adopted with minor modifications from Warren et al. (2010) due to the high success rate on projects utilizing this procedure.

MATERIALS

Vishay EP-08-10CBE-120 gages were selected for this application. These gages offer high-elongation performance and are compatible with existing 120-ohm data acquisition equipment owned by Virginia Tech. The 1-in gage length complies with the recommendation by Warren et al. (2010) that the gages should span at least 10 fibers of the geotextile.

The strain gages were installed on TenCate Mirafi HP570, which is a biaxial, woven polypropylene geotextile. Early in the project, Vishay Micro Measurements assisted the authors in testing the performance of two different epoxy adhesives with this geotextile using two different application techniques. M-Bond AE-10 is a general-purpose epoxy that cures in 24 to 48 hours, and M-Bond A-12 is a specialized, high-elongation epoxy that requires an extended curing time of two weeks at room temperature. The effect of short-term exposure to ultraviolet light, which oxidizes the surface of the geotextile and may create a more bondable surface, was also investigated. In the end, for this small sample size, no combination of adhesive and surface treatment provided significantly better performance than the others. The M-Bond AE-10 adhesive with no ultraviolet light treatment was selected as the simplest application with a more rapid cure time.

Standard 22 AWG wire connected the gages to the bridge completion module using a fine MEM solder with high flux content. After the gages were adhered to the geotextile, they were protected by a high quality, high elasticity, low modulus silicone—in this case, RTV 3145 manufactured by Dow Corning.

Other miscellaneous materials used for gage installation included rubber gasket material, plywood, parchment paper, and CMU blocks.

INSTALLATION

Wiring the Strain Gages

Step 1: An index card covered with a piece of clear packaging tape was used to secure the gages during wiring and subsequently transfer it to the fabric. The strain gages were taped to the packaging tape on the index card using a short length of residue-free tape to protect the resistivity grid during soldering, leaving only the solder tabs exposed. One small drop of solder was then placed on each of the nodes on a tab, as illustrated in Figure A-1.

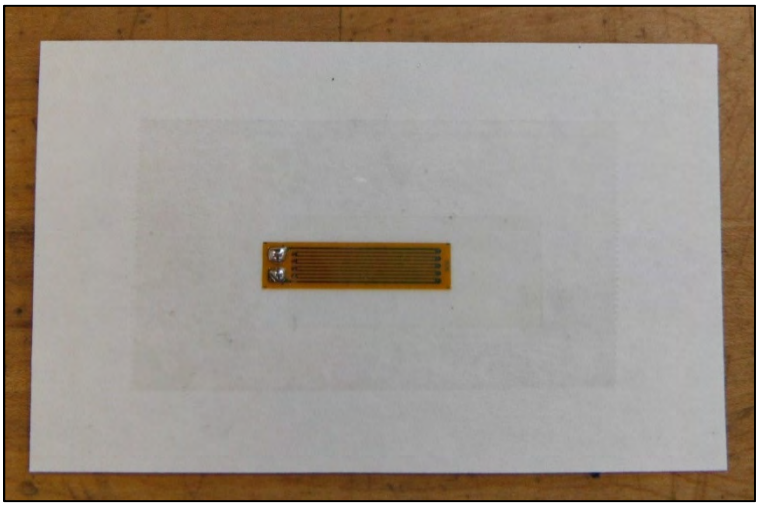

Figure A-1. Strain Gage Secured to Index Card With Solder Applied to Both Solder Tabs on Left

Step 2: Three-wire 22 AWG wire was selected to connect the strain gages to the data collection unit in the field. The wire was cut to the proper length in the laboratory and stripped, as shown in Figure A-2.

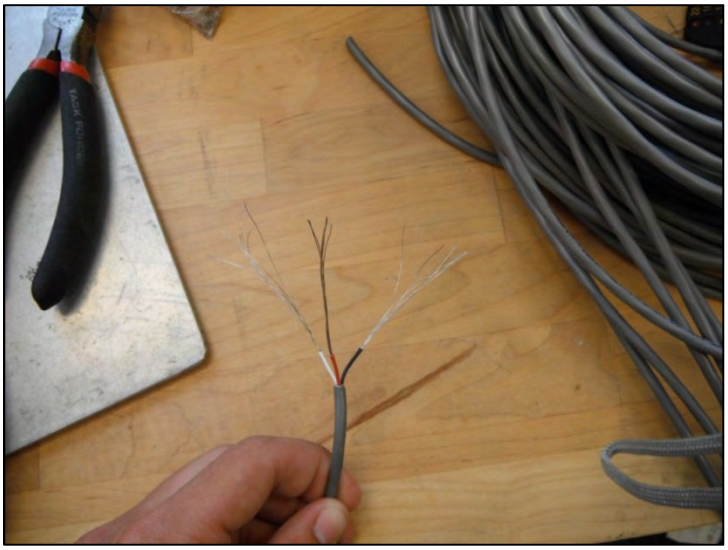

Figure A-2. Stripped 22 AWG Wire

Step 3: The stripped wire was then trimmed down to one inner strand for soldering to the tabs on the strain gages, as shown in Figure A-3. This was done to minimize the amount of solder required to connect the wire to the gages. Too much solder will increase the local stiffness of the tabs and may cause the foil grid to break at the tabs during elongation. A small amount of solder was added to the base of the exposed wire, where the remaining strands had been cut, to ensure proper conductance through all strands. The black and white wires, which will be connected to the same gage tab, were twisted together and joined with a small amount of solder, as shown in Figure A-3.

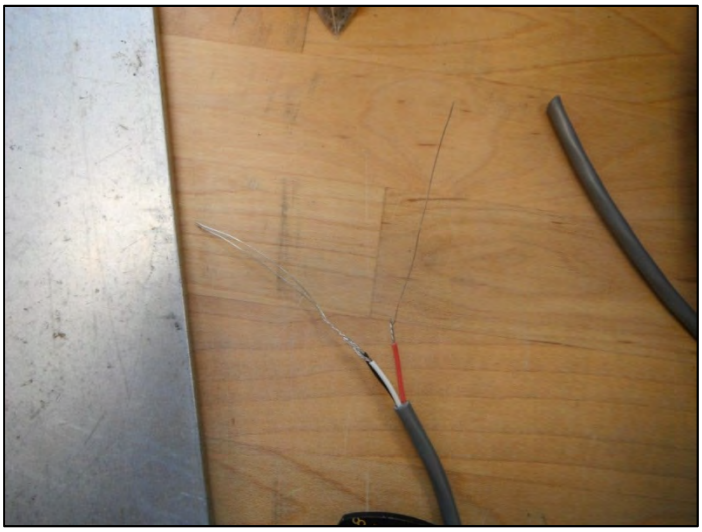

Figure A-3. Wire Cut to One Inner Strand

Step 4: The wires were bent in a serpentine fashion to provide adequate strain relief for the wire in the field, as shown in Figure A-4. This prevents the connection between the wire and gage from breaking as the fabric elongates.

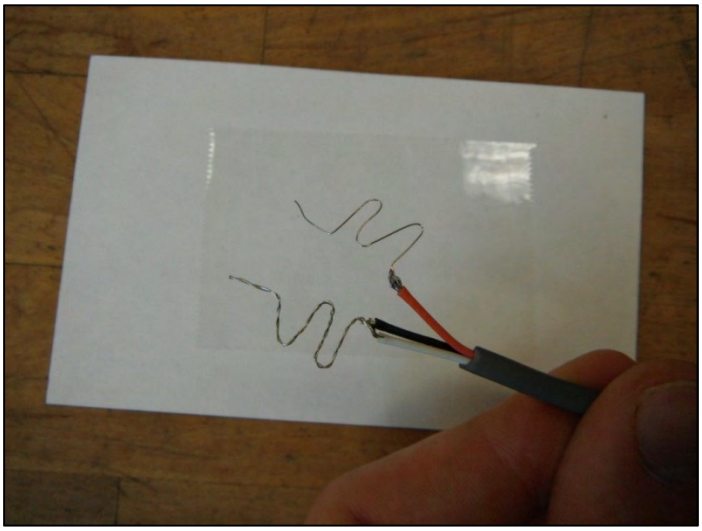

Figure A-4. Wire Bent to Provide Strain Relief

Step 5: The final step was to solder the wires to the strain gage. In some instances, it was necessary to apply more solder than the drop previously placed on the tab. Figure A-5 illustrates a gage that has been wired and is ready for installation on the geotextile.

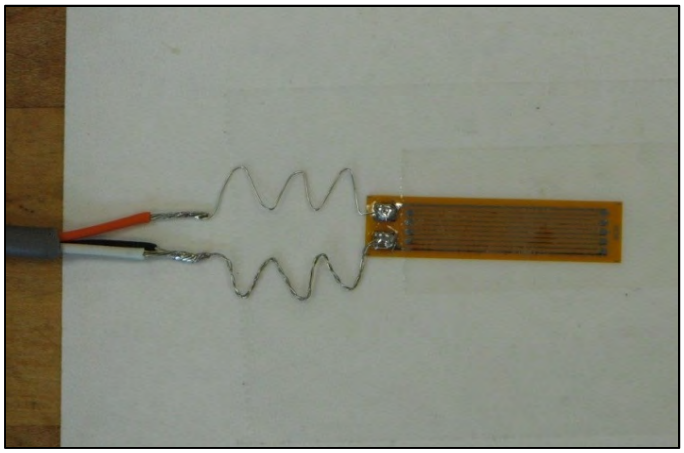

Figure A-5. Strain Gage With Wiring Complete

Installation of the Gages on the Geotextile

Installation of the strain gages on the geotextile was performed at Virginia Tech's W.C. English Geotechnical Laboratory. The geotextile would later be transported to the site of the field experiments.

Step 1: Strain gage locations were first marked on the geotextile. The geotextile used for this research project is black, so a silver marker was best for marking on the fabric. Figure A-6 shows the fabric with a solid line marking the longitudinal axis of the gage and a dashed line marking the centerline of the gage. The line marking the longitudinal axis follows a single polypropylene fiber through the weave. The gage in the foreground of the photograph is ready to install.

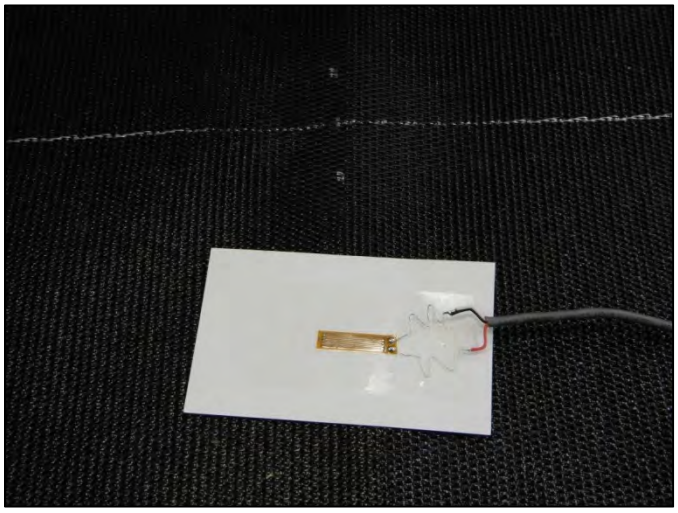

Figure A-6. Geotextile Marked for Gage Installation

Step 2: The surface of the geotextile was thoroughly cleaned to remove oils from the manufacturing process. First, a circular area approximately two inches in diameter was thoroughly cleaned using rubbing alcohol and gauze pads. The area was then lightly abraded using fine (400-grit) sandpaper and again wiped clean with another rubbing alcohol treatment.

Step 3: Once the fabric was clean, the strain gages were epoxied into place. Due to available work space in the laboratory, eight strain gages were applied at once. The epoxy can seep through the fabric, so a sheet of parchment paper was placed under each strain gage location prior to epoxy application.

The epoxy was mixed according to the manufacturer's specifications. For this application, a two-part Vishay M-bond AE-10 epoxy was used. The components were mixed for five minutes before application, and the epoxy was only in use for a maximum of 15 minutes before the batch became too thick and was disposed. Epoxy was applied to the back of the gage and to an area of about 1.5 in by 0.5 in of the fabric. Enough epoxy was used to impregnate the fibers of the geotextile in the vicinity of the gage, but care was taken not to apply too much epoxy, which would lead to a large zone of stiffened material. The exact amount of epoxy used for each strain gage was not carefully measured, but in general, a 10 gram jar was sufficient to attach eight gages. The epoxy application is shown in Figure A-7.

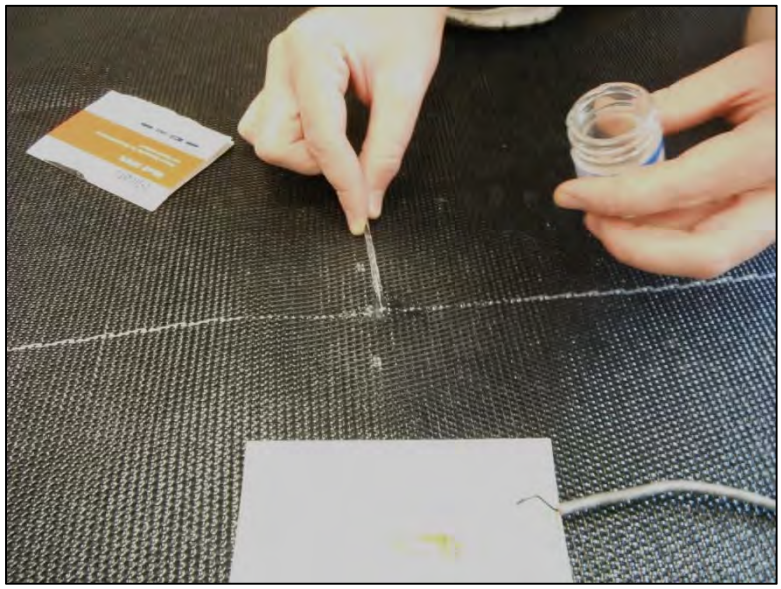

Figure A-7. Epoxy Application

Step 4: Using the tape that had secured the gage to the index card, the strain gage was then lifted from the index card, a thin layer of adhesive was applied to the back, and the gage was positioned on the fabric in line with the guide marks, as shown in Figure A-8. A small piece of parchment paper was placed over the strain gage (Figure A-9). On top of the parchment paper, a piece of rubber gasket material was placed to allow a uniform bonding pressure (Figure A-10). Finally, a 1.5 in by 2 in piece of plywood was placed on top of the gasket, a length of dimensional framing lumber was placed over two adjacent gages, and a 42-lb CMU block was positioned on top to apply the bonding pressure (Figures A-11 through A-13). Note that in

Figure A-12, the small pieces of plywood positioned beneath the center of the CMU were placed there in case the CMU began to tip, and the small pieces of plywood were never in contact with the block.

Figure A-8. Positioning the Strain Gage on the Geotextile

Figure A-9. Placing the Parchment Paper Over the Epoxied Gage

The epoxy required a curing pressure in the range of 5 to 20 psi. In this setup, the curing pressure was controlled by the size of the rubber gasket material placed over the gage. The weight of the block was distributed over two gages, and so the curing pressure for each gage could be calculated as half the weight of the block (21 lb) divided by the area of the gasket.

Two different curing pressures have been used for this project. This change was made on the recommendation of the manufacturer after discussing the installation procedure. The curing pressure for the first 16 gages installed was approximately 9.3 psi using a 1.5 in by 1.5 in piece of gasket material. The second curing pressure was approximately 7.0 psi using a 1.5 in by 2.0 in piece of gasket material. Note that the rubber gasket was not placed over the top of the solder tabs. This would have caused a non-uniform curing pressure and possibly damaged the solder connection.

The weight remained in place for 24 to 48 hours. After this time, the weights, plywood blocks, rubber gaskets, parchment paper and non-residue tape were removed. Figure A-14 shows an installed strain gage.

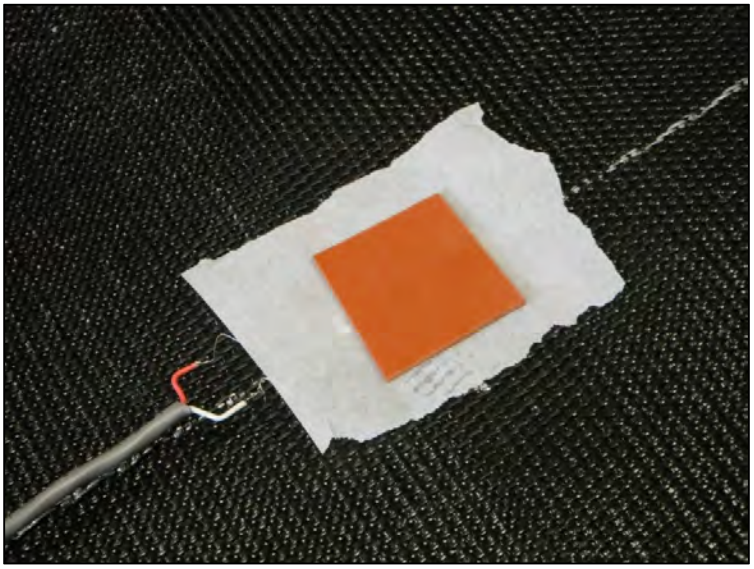

Figure A-10. Placing the Rubber Gasket Material

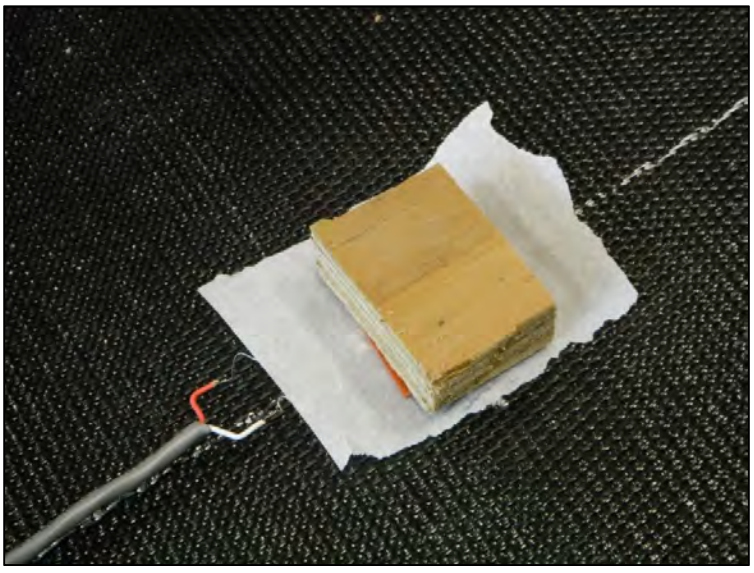

Figure A-11. Placing the Plywood Block Directly Over the Rubber Gasket Material

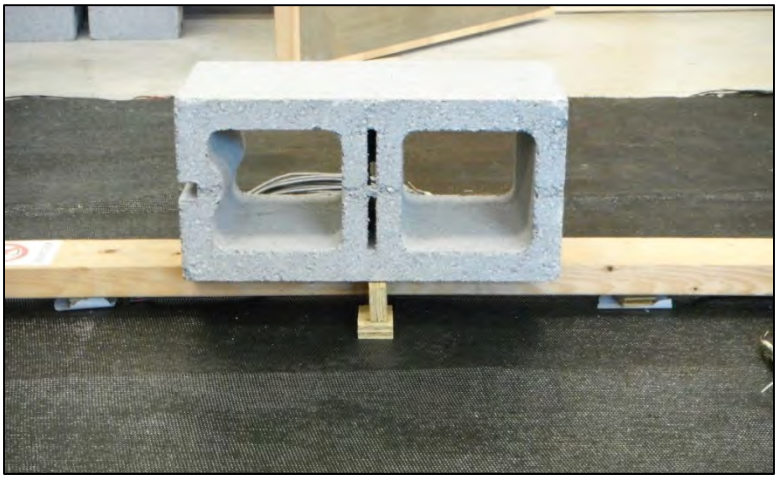

Figure A-12. CMU Block Spanning Two Strain Gages Using a 2 in by 4 in Piece of Dimensional Lumber

Figure A-13. Spacing and Configuration of 8 Strain Gages Installed at One Time

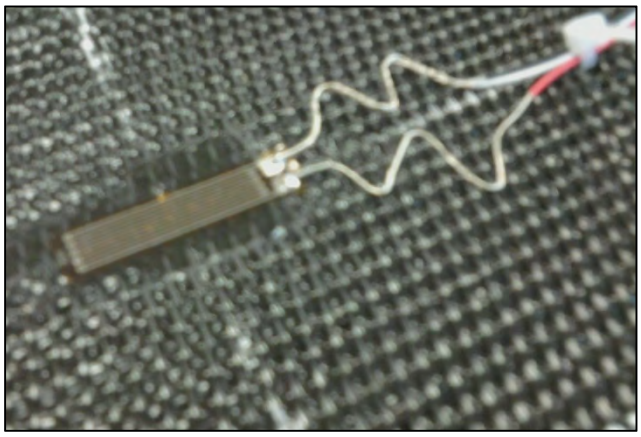

Figure A-14. Finished Strain Gage After Curing for 24+ Hours

Step 5: After the epoxy had cured, RTV was applied liberally around the wires and over the gage. The purpose of the RTV is to protect the strain gages and wires in the field. Since gravel is placed directly on top of the fabric, these stones could easily tear the resistivity grids, rendering the strain gage useless. The RTV also protects the gage and wires from water intrusion.

When applying the RTV, the exposed wires were not in contact with one another, and the strain relief bends were maintained. A toothpick was used to lift the wires while RTV is placed between the wires and the fabric. The wires were then lowered into the RTV. Additional RTV was placed over of the exposed wires and over the strain gage itself. At least 0.25 in of cover was provided over the gage and wires, extending approximately 0.5 in around the gage and beyond the unstripped wires over the gray protective wiring sheath.

The RTV was allowed to set for at least 24 hours before proceeding to the next step. Figure A-15 shows a gage after it has been protected with a coating of RTV.

Figure A-15. Finished Strain Gage Protected by RTV

Step 6: After the epoxy had cured, small wire ties were then used to secure the wires to the fabric. The ties were passed through at least two fibers in the woven geotextile fabric to prevent the ties from sliding and were fastened down tightly by hand. The first tie was placed approximately 0.5 in to 1 in back from the RTV coating. The grey wire was then secured to the geotextile at 1 ft to 3 ft spacing.

CALIBRATION

The epoxy used to attach the strain gages to the geosynthetic fabric stiffens the fabric in the locality of the gage. Consequently, the strain measured by the gage is smaller than the strain experienced by the unstiffened geosynthetic. The strain gages must be calibrated in order to

provide accurate readings. In this case, a linear relationship was assumed between the strain measured by the gage and the strain of the unstiffened fabric.

Calibration of the strain gage generally damages the gage through exposure to high strains, preventing direct calibration of the gages installed in the field-scale model. For these experiments, gages were installed on samples of the geosynthetic and tested in the laboratory, and these calibrations were applied to the field case. Eight gages were installed on 4-in-wide by 8-in-long samples of the same geosynthetic used for the field-scale abutment using the same procedure previously described. Four of these gages were oriented in the cross-machine direction of the fabric, and four were oriented in the machine direction of the fabric.

After installation, the fabric samples were subjected to a constant rate of strain test at a rate of one percent per minute using an Instron 4411 load frame. The load was applied in the direction of the gage axis. Displacement and strain readings were taken simultaneously from the load frame and datalogger, respectively, with an interval of 5 to 10 seconds. The strain data from the load frame and gages were plotted and compared. A linear calibration factor was determined for each calibration test that minimized the difference between the strain recorded by the Instron machine and that recorded by the strain gage over the range of interest. For the field scale tests, the range of interest was determined to be between 0% and 1.5% strain. The calibration factors for negative values of strain (shortening of the fabric) were assumed to be equal to the factor for the corresponding positive value of strain.

One calibration test could not be used to determine a calibration factor due to irreconcilable differences between the two sources of strain data. The results of the remaining seven calibration tests are shown in Figures A-16 through A-22. Calibration tests on gages oriented in the cross-machine direction yielded calibration factors of 2.46, 2.59, 2.85, and 2.58. Tests on gages oriented in the machine direction yielded calibration factors of 3.38, 3.25, and 2.81. From these results, calibration factors of 2.6 and 3.2 were selected for the cross-machine and machine directions, respectively.

FIELD INSTALLATION

After the strain gages were installed on a full sheet of reinforcement in the laboratory, the fabric was carefully folded and transported to the site of the field-scale abutment. The fabric was placed using the same procedure that was used for non-instrumented layers of reinforcement, and a small groove was cut into the facing CMUs at each location where the wire passed through the CMUs. Figure A-23 shows the fabric placed and rolled back to permit placement of fill close to the face without driving over the fabric. Only 16 of the 32 gages installed in the test abutment were connected at one time, due to the constraint of using a 16- channel multiplexer. The 16 gages on Side A of the abutment were the first to be spliced to the bridge completion modules and connected to the multiplexer. Zero readings were obtained for these gages. The ends of the wires for the sixteen gages on Side B were wrapped tightly with electrical tape to protect against moisture. After completion of testing on Side A, these gages were disconnected and the gages on Side B were connected to the multiplexer.

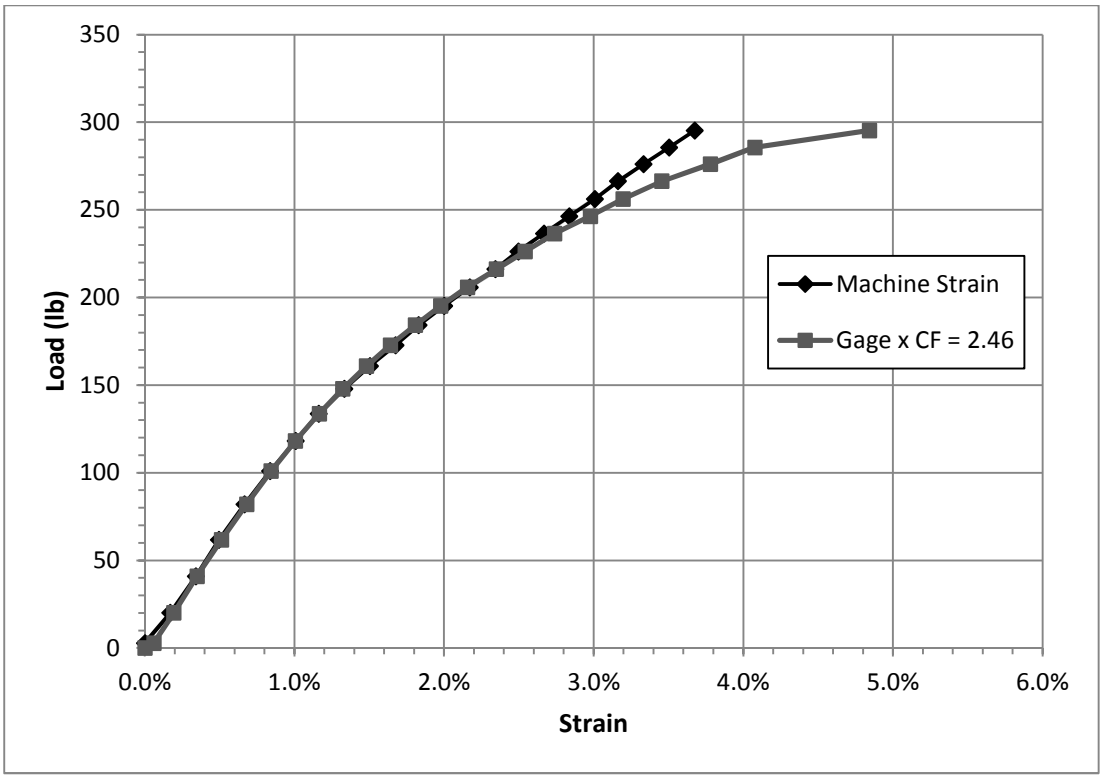

Figure A-16. Calibration 1, in Cross-Machine Direction

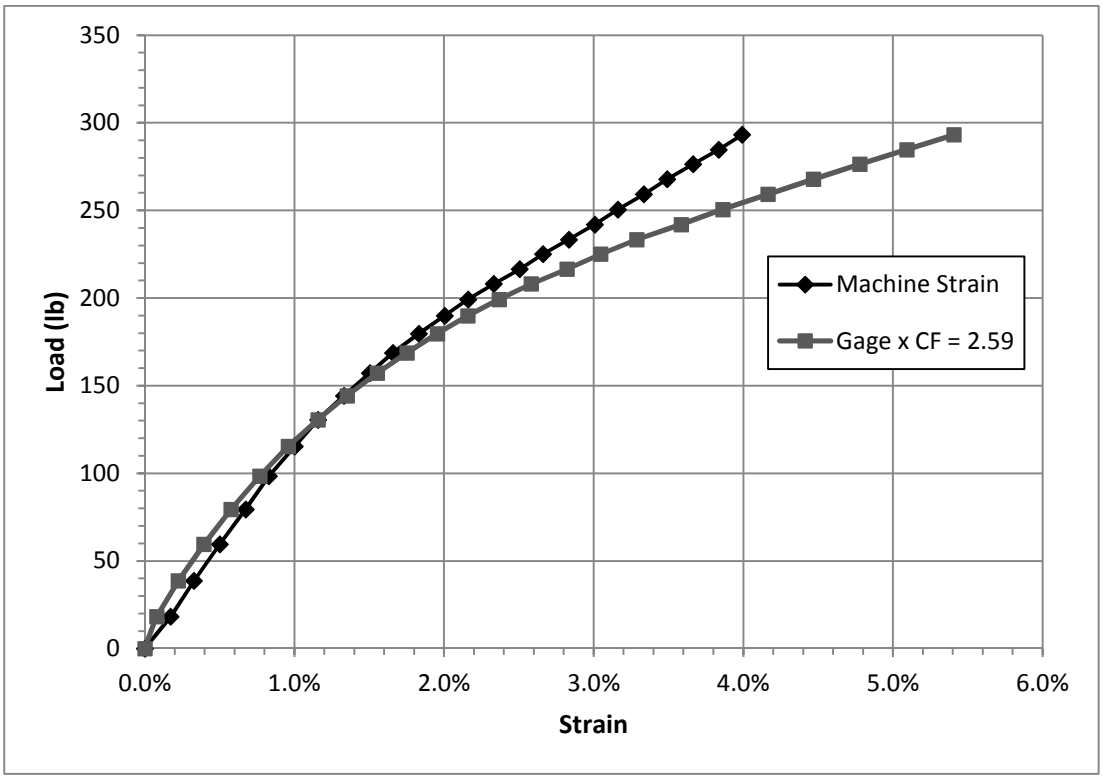

Figure A-17. Calibration 2, in Cross-Machine Direction

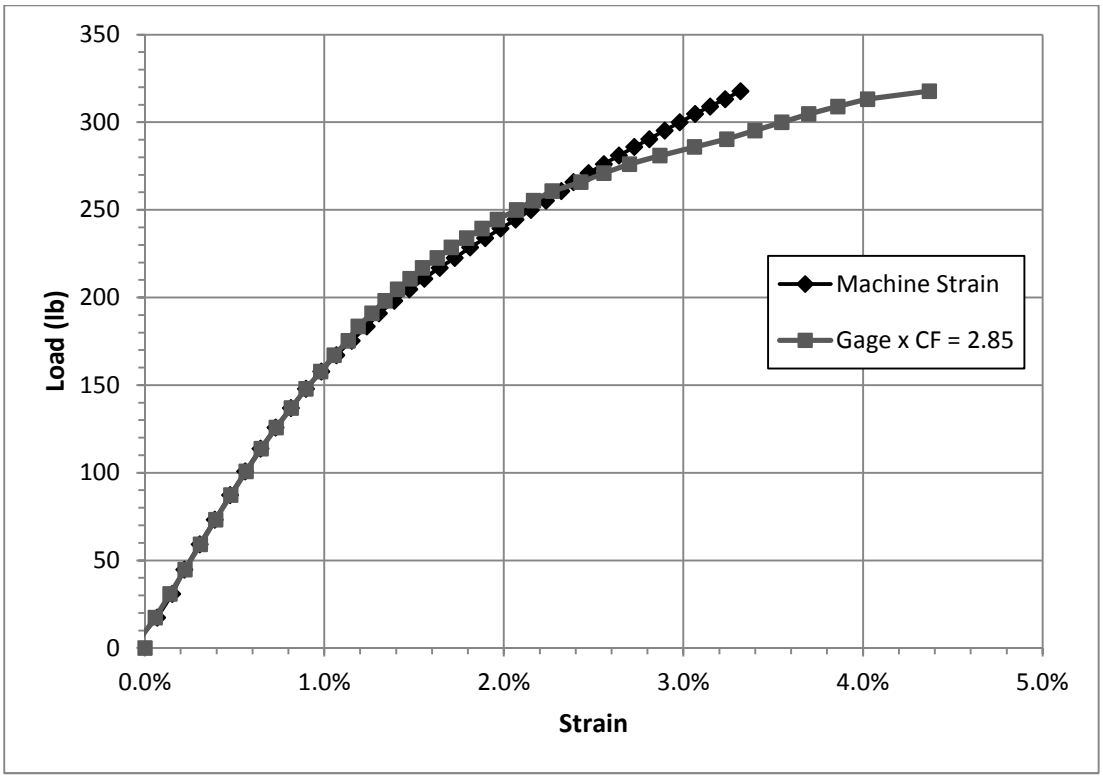

Figure A-18. Calibration 3, in Cross-Machine Direction

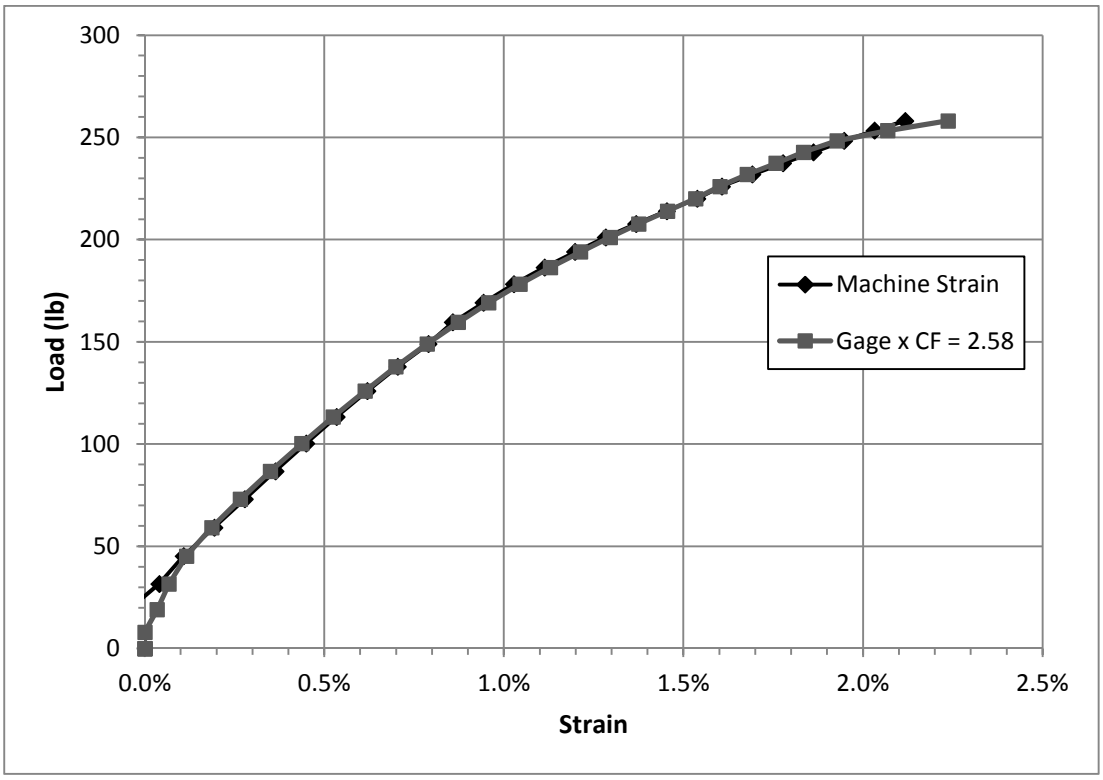

Figure A-19. Calibration 4, in Cross-Machine Direction

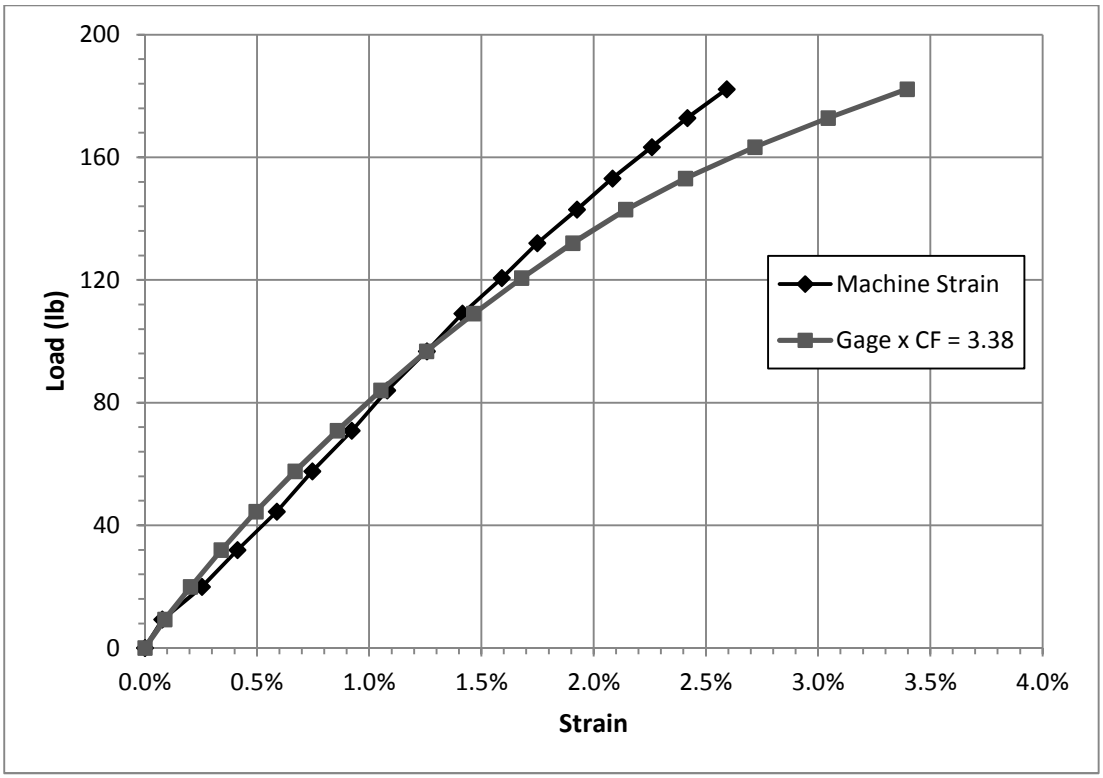

Figure A-20. Calibration 5, in Machine Direction

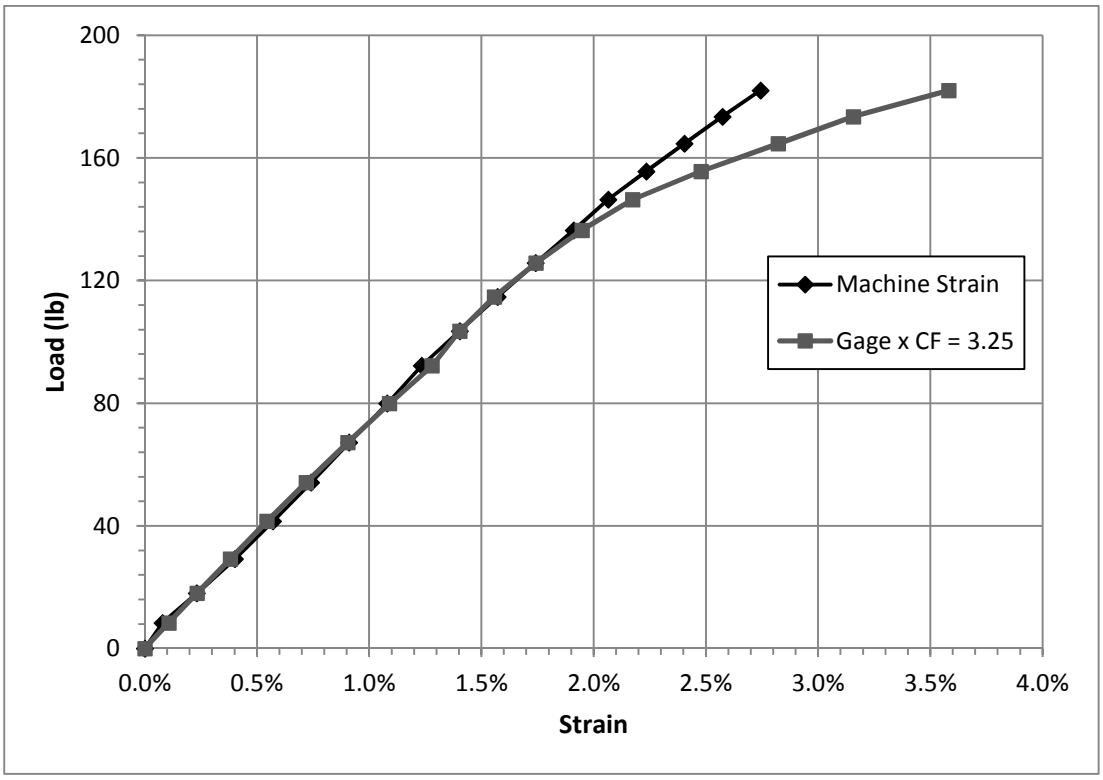

Figure A-21. Calibration 6, in Machine Direction

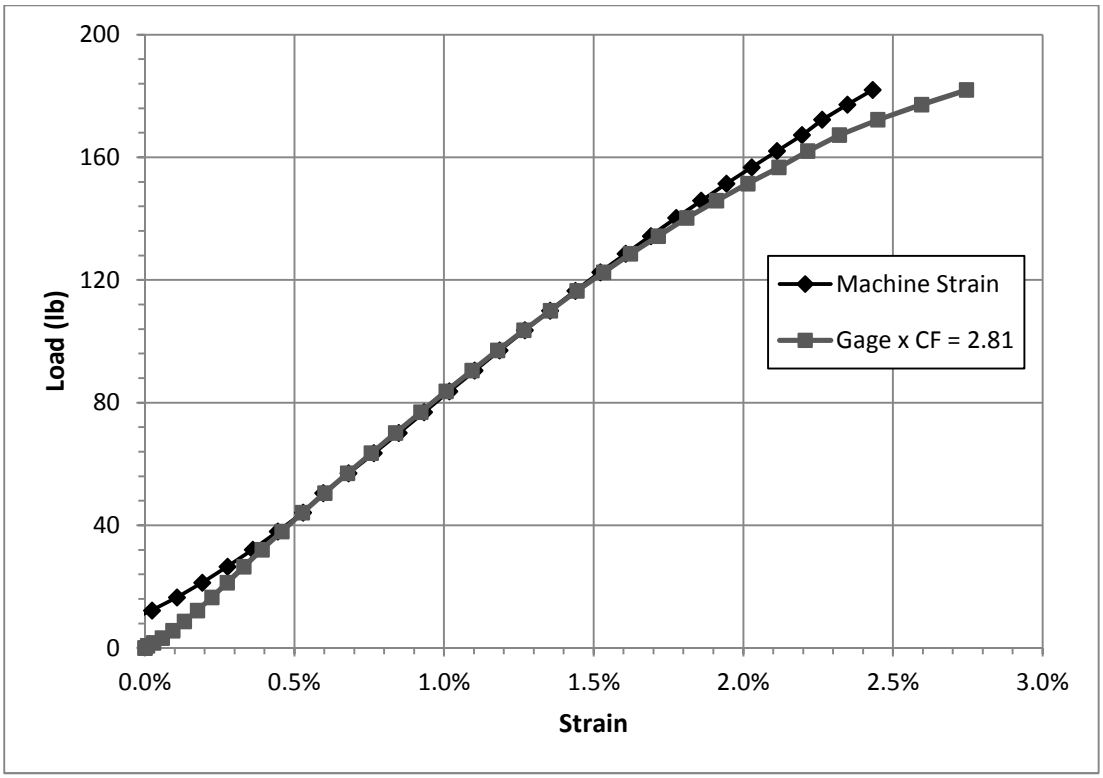

Figure A-22. Calibration 7, in Machine Direction

Figure A-23. Installing Geotextile Fabric With Attached Strain Gages

After the fabric was placed, the gages were connected, and zero readings were obtained. A small shovel of the No. 8 fill was placed over each gage for additional protection while placing the fill for the lift. The No. 8 fill was subsequently placed and compacted using the standard placement procedure discussed previously in the "Methods" section. During this compaction

process, the gages were monitored for any signs of distress or impending damage; no distress was evident.

PERFORMANCE OF STRAIN GAGES

All 32 gages survived construction and exhibited no evidence of drift. The gages on Side A were monitored for approximately 7 weeks through construction and testing. All 16 gages remained functional over this time period. The gages on side B were monitored for approximately 5 weeks during testing. Fifteen of 16 gages remained fully functional over this period; one gage began providing intermittent readings a few days into Test B1. Data provided by all functional gages were consistent and reasonable, giving no indication of drift or other abnormalities.

Overall, the gages had a 100% survival rate after construction and a 97% survival rate at the conclusion of testing approximately two months after the completion of construction. This survival rate compares favorably with other studies that reported on survival rates of strain gages installed on geosynthetic fabrics using similar installation techniques. Warren et al. (2005) reported a post-construction survival rate of 95% for 20 gages, and Warren and Howard (2007) reported a post-construction survival rate of 81% for 16 gages. Neither study reported long-term performance. In contrast, Brandon et al. (1996) reported that only 1 of 18 gages (6%) survived 8 months, with the majority of failures occurring during or shortly after construction.

The authors attribute the high survival rate of these strain gages to careful selection of the gage type and adhesive materials in collaboration with Vishay Micro Measurements; careful, consistent, and rehearsed installation procedures; and careful field installation with the use of hand-operated compaction equipment. Field installation was performed by the authors, facilitating careful installation practices.